Immuno-PET enlightening the path to optimized antibody-targeted radiotherapy

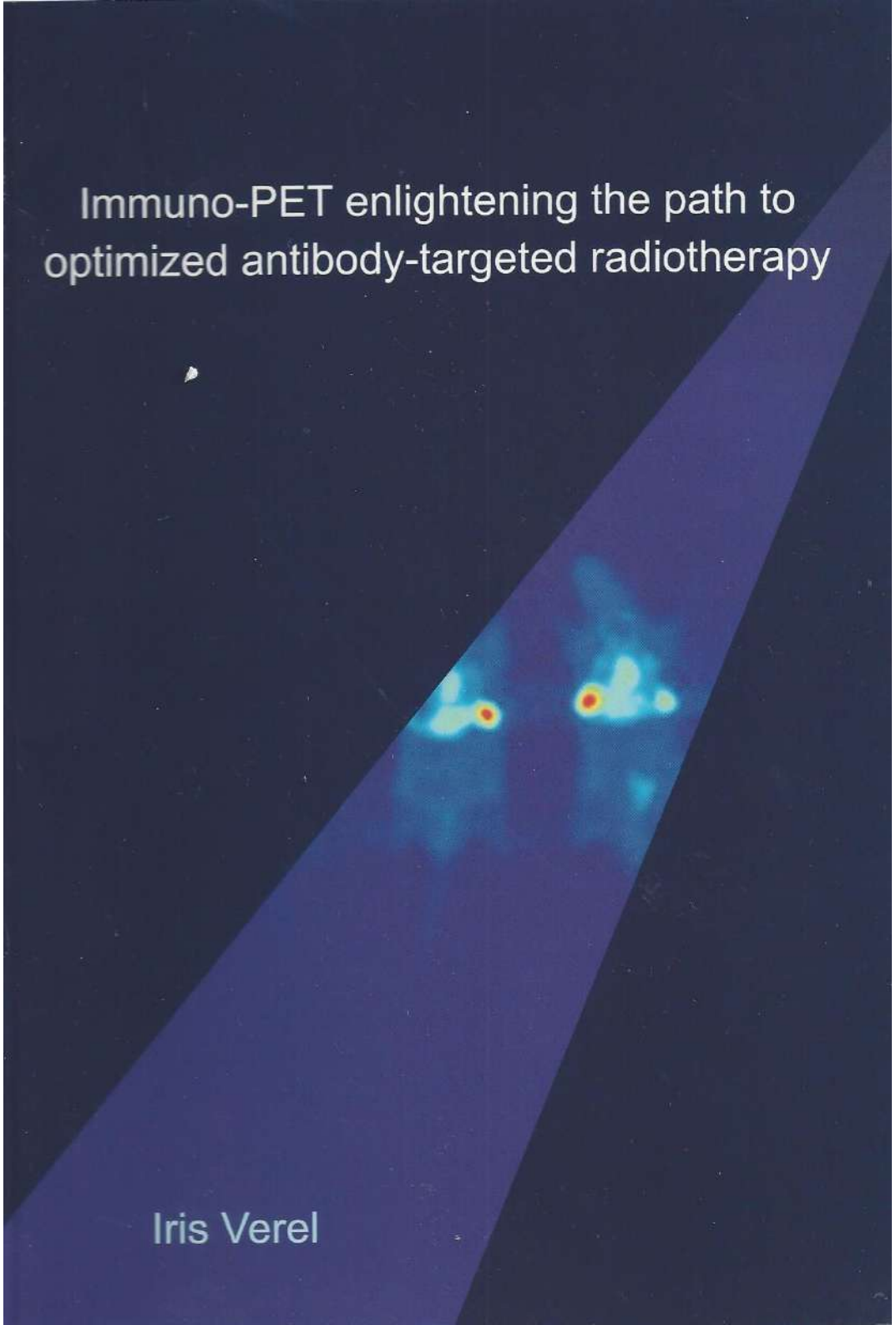

Iris Verel

Immuno-PET enlightening the path to optimized antibody-targeted radiotherapy

The research described in this thesis was performed at the Section Tumor Biology of the Department of Otolaryngology/Head and Neck Surgery, VU University Medical Center, in collaboration with the Radionuclide Center, VU University, Amsterdam, The Netherlands.

Cover: HRRT PET coronal image of HNSCC xenograft-bearing nude mice, 72 h after injection of cMAb U36-*N*-sucDf-^{89}Zr.

Thesis Vrije Universiteit, Amsterdam
ISBN 90-6464-844-1

Printed by Ponsen & Looijen bv, Wageningen

VRIJE UNIVERSITEIT

Immuno-PET enlightening the path to optimized antibody-targeted radiotherapy

ACADEMISCH PROEFSCHRIFT

ter verkrijging van de graad van doctor aan
de Vrije Universiteit Amsterdam,
op gezag van de rector magnificus
prof.dr. T. Sminia,
in het openbaar te verdedigen
ten overstaan van de promotiecommissie
van de faculteit der Geneeskunde
op donderdag 18 december 2003 om 13.45 uur
in de aula van de universiteit,
De Boelelaan 1105

door

Iris Verel

geboren te Curaçao

promotoren:	prof.dr. A.A.M.S. van Dongen
	prof.dr. G.B. Snow
copromotor:	dr. G.W.M. Visser

Aan mijn ouders
Aan Henk

CONTENTS

chapter

1

General introduction

CONTENTS

1 Tumor-targeting with radiolabeled monoclonal antibodies (MAbs)

About a century ago, Ehrlich postulated the concept of the "magic bullet" [1]. A magic bullet should consist of a compound with specific affinity to microorganisms, enabling the destruction of that organism without harmful effects to the rest of the body. He envisioned that antibodies could act as such. If antibodies could be developed that recognize tumor cells, and tumor cells alone, the same principle would then be applicable to detect and kill cancer. The introduction of the hybridoma technology for the production of monoclonal antibodies (MAbs) by Köhler and Milstein [2] in the mid 1970s turned the magic bullet concept of Ehrlich into a realistic option. With the hybridoma technology, an unlimited range of MAbs could be developed against any particular cellular antigen. The MAbs can have effector functions of their own, but therapeutic efficacy can be enhanced by arming MAbs with "warheads" such as toxins, drugs, enzymes or radionuclides. Due to a "cross-fire" effect, radionuclides are especially attractive as warheads since, in order to be effective, not all tumor cells have to be targeted by radiolabeled MAbs. Nowadays, radiolabeled MAbs can be used for detection of primary tumors and metastases throughout the body with radioimmunoscintigraphy (RIS) or for systemic treatment of cancer with radioimmunotherapy (RIT).

1.1 Tumor-targeting with MAbs

A variety of cell surface proteins on tumor cells have been explored as targets for MAbs. The efficacy of antibody targeting will be determined by the characteristics of the MAb, the tumor physiology, and the nature of the antigenic target.

1.1.1 MAb

Several considerations have to be taken into account when using MAbs for the targeting of tumor cells. Factors such as origin, size, and affinity all have their impact on the *in vivo* behavior of the MAb. After a short description of the structure of MAbs and the hybridoma technology, the influence of each of these factors on tumor-targeting will be discussed.

MAb structure Antibodies, also called immunoglobulins (Ig), consist of two identical light chains and two identical heavy chains linked to each other by disulfide bonds (Fig. 1A). These chains are composed of different domains: the variable heavy (V_H) and light (V_L) chains, called the variable region (Fv), serve as the antigen-binding domains while the constant heavy (C_H) and light (C_L) chains, called the constant region (Fc), are involved in the interactions with effector cells or in the activation of the complement cascade. The small regions that directly interact with the antigen are called complementarity determining regions (CDRs). Upon binding to the target cell, most antibodies are internalized gradually or rapidly (depending on the antigen, tumor cell, and antibody) and become degraded within lysosomes [3,4]. In order to generate MAbs via the hybridoma technology, mice are immunized with the desired target antigen or antigen-expressing tumor cells. Subsequently, their antibody

producing B cells are fused with immortal myeloma cells and the resulting hybridoma cells can be propagated indefinitely and used for the *in vitro* production of murine MAbs (mMAbs) in unlimited quantities.

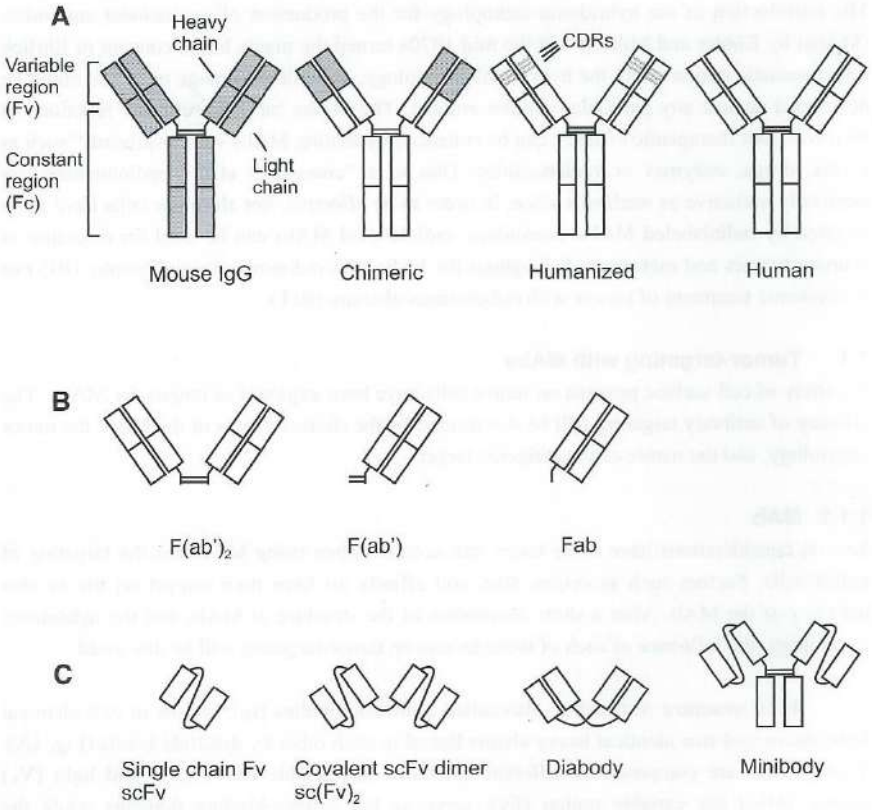

Figure 1. Schematic representation of intact MAb (A), MAb fragments (B), and single chain-based fragments (C). A, MAb of mouse (gray), chimeric (gray and white), humanized (white, only CDRs gray), and complete human origin (white). B, MAb fragments (of mouse or human origin) can be made by enzymatic cleavage of the whole MAb molecule and/or by molecular biological techniques. C, Monomeric and dimeric scFv (trimeric and tetrameric variants not shown).

MAb origin One of the first limitations encountered when using these mMAbs in patients was immunogenicity. The injection of mMAbs can induce the development of human anti-mouse antibodies (HAMA), resulting in an increased clearance of the MAb[5], allergic reactions, or even anaphylaxis[6]. Developments in recombinant DNA technology opened up an entirely new perspective for selection and production of MAbs. These techniques permit the construction of MAbs preserved for binding sites but with possible variations in subclass, origin, size, and configuration.

Besides murine MAbs, nowadays chimeric and humanized MAbs can be engineered in order to minimize the chance that the human immune system recognizes the MAb molecule as being non-self (Fig. 1A). Chimeric MAbs (cMAbs) possess murine variable domains and human constant domains[7,8]. If the immune reaction is directed against the variable domain of the mMAb, the construction of a cMAb will not solve the immunogenicity problem. For this purpose, also humanized MAbs (hMAbs) can be developed which are almost completely of human origin with only the CDRs derived from mouse. The latest achievement in MAb engineering is the fully human MAb, produced by use of phage display libraries[9-11] or by use of transgenic mice that contain human immunoglobulin gene repertoires[12-14]. During humanization, however, a considerable decrease in affinity can occur.

Recent developments in the fields of phage display library technology and expression of recombinant antibodies in heterologous systems such as microorganisms[15,16], transgenic plants[17] and transgenic animals[18] are expected to further enhance the development, production and application of MAbs in the coming years.

MAb size In humans, intact MAb molecules have a long residence time ranging from a few days to over three weeks. This results in high MAb concentrations at tumor sites, with optimal tumor-to-nontumor ratios after 2-4 days. Disadvantage is that the slow blood clearance also results in significant exposure to normal organs, especially to bone marrow. In addition, the large size of a MAb molecule (~150 kDa) limits its diffusion from the vasculature into tumor.

The use of MAb fragments increases blood clearance. This results in higher tumor-to-nontumor ratios at earlier time points, but the absolute uptake in tumor is often lower[19]. With decreasing fragment size, penetration of tumor masses will be easier and more homogeneous[20]. For many years, enzymatic digestion methods have been used for the production of smaller functional fragments out of intact MAb molecules. The resulting fragments are called $F(ab')_2$ (~100 kDa), F(ab') (~50 kDa), or Fab (~40 kDa) (Fig. 1B). Since these fragments are lacking the Fc portion, they are in general less immunogenic.

More recently, the genes encoding the IgG variable and constant domains have been used to construct a variety of recombinant antibody-based fragments. Single chain Fv (scFv, ~25 kDa) is the simplest and smallest fragment, in which the V_L and V_H chain are linked by a small peptide linker and expressed as a single protein (Fig. 1C). Due to its small size, more than 50% of monomeric scFv is cleared from the blood within 10 min[21,22], resulting in high tumor-to-nontumor ratios already within a few hours after administration. A disadvantage of

scFv, F(ab'), and Fab is that they exhibit lower avidity compared to intact MAbs or $F(ab')_2$ due to their monovalent binding[23]. The scFv can be further engineered to form a covalent dimer ($sc(Fv)_2$, ~50 kDa) or, through shortening of the linker and thus forcing noncovalent associations between two molecules, a diabody (~55 kDa). Fusion of a scFv to a constant domain and assembly into a dimer is called a minibody (~80 kDa). These dimers all exhibit high functional affinity[24,25]. It is also possible to enhance the affinity of scFv by random or site specific mutations of the selected peptide binding domains. Affinities (K_d) as high as 10^{-11} M for affinity-matured scFv have been documented[26,27]. A common characteristic of small fragments is that they are cleared from the blood pool primarily by glomerular filtration, which can cause high kidney level values[21,28,29]. The kidney uptake will be especially pronounced when residualizing radionuclides are used for RIS and RIT studies[30-32].

MAb affinity An issue that has not been settled yet, is the choice between high or low binding affinity of the MAb. At first glance, high affinity of the MAb seems desirable for the firm binding to the target antigen and for reaching high tumor concentrations. Several studies have demonstrated improved tumor delivery and therapeutic efficacy in xenograft-bearing nude mice when using MAbs with increased affinity[33-36]. Also for the scFv C6.5 (anti-HER2/neu) and two of its affinity mutants which target the same epitope, it was shown that increased affinity led to improved tumor retention[37]. On the other hand, mathematical models[38] and experimental studies[39] produced strong indications that tumor penetration by high-affinity MAb molecules was impaired and that the MAbs were only binding to the outer layers of the tumor mass, by the very fact of their successful binding to antigen. This phenomenon was called the "binding site barrier". Higher MAb affinity, higher antigen density, lower MAb dose, and faster MAb internalization and metabolism by cells were all predicted to enhance the "barrier" effect[40].

Recently, Adams *et al.*[27] demonstrated with a panel of scFv C6.5 mutants with affinities ranging from 10^{-7} to 10^{-11} M that very high affinity not only limits tumor penetration, but also the level and specificity of tumor accumulation. They showed that quantitative tumor retention did not significantly increase with enhancements in affinity beyond 10^{-9} M. At affinities of 1.2×10^{-10} to 1.5×10^{-11} M tumor retention even decreased. These data were confirmed with diabodies that were created from the same scFv[25]. In fact, the diabody with the lowest affinity exhibited the highest quantitative retention. These data are in line with the observations made in the studies with intact MAbs as described in chapter 2 of this thesis, which were performed during the same time period. Only this year, a mathematical model has been described that provides a means to predict the tumor penetration and retention of an antibody by taking several parameters, including MAb affinity, into account[41]. Comparison of the experimental scFv C6.5 data with the simulated data provided by this model showed a strong qualitative agreement.

1.1.2 Tumor

Several factors have been recognized to influence the accessibility of tumor associated antigens for MAbs such as vascularisation, interstitial pressure, the nature of the disease (e.g. solid tumors *vs.* hematological malignancies), and the tumor location in the body[19,42]. The latter can partly be explained by the natural barrier offered by normal capillary endothelial cells. This barrier can vary between tissues, from highly regulated (blood-brain barrier) to poorly permeable to macromolecules (lung and skin) to almost non existing because of the numerous gaps between the endothelial cells, fenestrations in the cells, and the lack of basement membrane (liver, spleen, and bone marrow)[43]. Tumor vasculature is in general better permeable for MAbs than blood vessels in normal tissues[42]. Because tumor vasculature consists of vessels recruited from the pre-existing network of the host vasculature, as well as of neovasculature resulting from the angiogenic host response to cancer, it is thought that the local microenvironment also has a tremendous impact on antigen accessibility[44].

Tumor vasculature is typically disordered and with a low and irregular blood flow, resulting in a failure to provide adequate and homogeneous nutritional support to tumor cells. In the end, this can lead to chronic and/or diffusion-limited hypoxic regions in the tumor. These effects are relevant for RIT, as MAb access to these sites within the tumor will be hampered, while absence of oxygen might also cause radiation resistance[45]. In addition, hypoxic tumor cells are often in a state of reduced proliferation or quiescence, another factor reducing radiation efficacy[46].

An additional barrier is formed by the extracellular matrix surrounding the tumor cells[47]. The composition of extracellular matrix is thought to be the result of an active interaction between tumor cells and stromal cells of the host organ. The diffusion rate of MAbs through the extracellular matrix might thus be largely determined by the tumor type as well as by the anatomical location[48,49]. A combination of above mentioned factors can account for variable MAb uptake among tumors and heterogeneous distribution of MAb throughout an individual tumor.

1.1.3 Antigen

The ideal target antigen shows an expression which is exclusively restricted to tumor cells. Unfortunately, until now no fully tumor-specific antigens have been found. The next best candidates are tumor-associated antigens (TAA), proteins that are present more abundantly on tumor cells then in normal tissue[50]. When the antigen is expressed in normal tissues that are poorly accessible for intravenously injected MAbs, targeting becomes "operationally" tumor selective. Preferably, a TAA is homogeneously expressed among tumors as well as within an individual tumor, with low or no expression on normal tissues. TAA on the outer cell surface will ensure accessibility of the antigen by the MAb while a high density expression of TAA will favor MAb accumulation at the tumor site. Some antigens are shed or secreted, resulting in MAb-antigen complexes in the circulation, which limits the amount of unbound MAb available for tumor binding[51]. Additionally, antigenic modulation or down-regulation of

antigen expression upon MAb administration can hamper the efficacy of the targeting procedure.

As alternative targets for anticancer MAbs, also antigens involved in angiogenesis or expressed by tumor neovasculature have been explored[52]. The potential advantages over direct targeting of tumor cells are that the vasculature is better accessible for antibodies, while many tumor cells become affected upon destruction of vasculature[53-56]. Disadvantages are that tumors with heterogeneous blood supply and tumor deposits without blood vessels such as micrometastases are less likely to be affected and that the expression of the target antigens is less restricted to tumors. At the moment, the lack of neovasculature-specific target antigens limits the potential of this approach.

Recent developments in the fields of gene and protein expression analysis by microarrays and proteomics are expected to greatly enhance the discovery of novel candidate tumor targets[57-59]. Description of the variety of TAA that are known at the moment for tumor-targeting purposes is beyond the scope of this introduction, but several comprehensive reviews have been published in which these antigens are listed[19,50,60,61].

1.2 Clinical applications of MAbs

Diagnostic applications of MAbs In order to use MAbs for diagnostic purposes, MAbs have been labeled with γ-emitting radionuclides. Until now, five radiolabeled MAbs have been approved by the U.S. Food and Drug Administration (FDA) for diagnostic imaging, among which four for imaging cancer (Table 1). The first radiolabeled MAb that received approval in 1992 was OncoScint. This agent consists of the indium-111-labeled (^{111}In-labeled) mMAb satumomab (also known as B72.3), that recognizes the tumor-associated glycoprotein-72 (TAG 72) expressed on ovarian and colorectal cancer cells. In 1996, four more diagnostic antibodies labeled with ^{111}In or technetium-99m (^{99m}Tc) were

Table 1. Diagnostic radiolabeled MAbs approved by the FDA (in order of approval date).

Trade name	Generic name	MAb type	Isotope	Antigen target	Condition	Reference
OncoScint	satumomab pendetide	Mouse, IgG	^{111}In	TAG 72	Ovarian carcinoma, colorectal carcinoma	62,63
CEA-Scan	arcitumomab	Mouse, F(ab')$_2$	^{99m}Tc	CEA	Colorectal carcinoma	64
Myoscint	imciromab pentetate	Mouse, Fab	^{111}In	myosin	Myocardial injury	65
Verluma	nofetumomab merpentan	Mouse, Fab	^{99m}Tc	EGP40	Small cell lung cancer	66,67
ProstaScint	capromab pendetide	Mouse, IgG	^{111}In	PSMA	Prostate cancer	68

approved. One of these, Myoscint, is used for myocardial injury imaging, while the other three, CEA-Scan, Verluma, and ProstaScint, are indicated for detection of several forms of cancer[69]. These diagnostic agents are mainly used for staging disease in patients suspected of recurrent or metastatic disease.

Therapeutic applications of MAbs The first therapeutic MAb receiving approval by the FDA in 1986 was mMAb orthoclone thymocyte 3 (OKT3). This MAb targets CD3 and is used to treat or prevent solid organ transplant rejection. Since then several MAbs have been approved for the treatment of conditions as diverse as transplant rejection, cardiovascular disease, virus infection, inflammatory diseases, and cancer (Table 2). All approved tumor-targeting MAbs, except Herceptin, are specific for hematologic diseases (Rituxan/Zevalin, Mylotarg, and Campath). This can be explained by the relative good accessibility of these malignant cells, in contrast to cells of solid tumors.

Radiolabeling of a MAb can enhance its action radius because radionuclides can be cytotoxic over many cell diameters. Even with a MAb that shows significant antitumor effects in unconjugated form, the coupling of a radionuclide can enhance efficacy. For example, a randomized trial has been performed in which the chimeric MAb Rituxan was compared with

Table 2. Therapeutic MAbs approved by the FDA (in order of approval date).

Trade name	Generic name	MAb type [a]	Antigen target	Condition	Reference
OKT3	muromonab	Mouse	CD3	Transplant rejection	70,71
ReoPro	abciximab	Chimeric	GPIIb/IIIa receptor	Cardiovascular disease	72
Rituxan	rituximab	Chimeric	CD20	Non-Hodgkin's lymphoma	73,74
Zenapax	daclizumab	Humanized	IL-2 receptor	Transplant rejection	75
Simulect	basiliximab	Chimeric	IL-2 receptor	Transplant rejection	76
Synagis	palivizumab	Humanized	RSV	Respitory syncytial virus	77
Remicade	infliximab	Chimeric	TNF	Rheumatoid arthritis/ Crohn's disease	78
Herceptin	trastuzumab	Humanized	ErbB2	Metastatic breast cancer	79
Mylotarg	gemtuzumab ozogamicin	Humanized, toxin-linked	CD33	Acute myeloid leukemia	80
Campath	alemtuzumab	Humanized	CD52	Chronic lymphocytic leukemia	81,82
Zevalin	ibritumomab tiuxetan	Mouse, radionuclide-linked	CD20	Non-Hodgkin's lymphoma	83
Humira	adalimumab	Human	TNF-α	Rheumatoid arthritis	84
Xolair	omalizumab	Humanized	IgE	Allergic asthma	85

[a] All the therapeutic MAbs as listed in table 2 are intact IgG.

Zevalin, the yttrium-90-labeled (^{90}Y-labeled) murine version (ibritumomab) of Rituxan (rituximab), in patients with non-Hodgkin's lymphoma. In this trial the overall response rate was in favor of Zevalin: 56% *vs.* 80%, respectively[86]. A second cancer specific radiolabeled MAb that is awaiting approval by the FDA is called Bexxar (tositumomab). This anti-CD20 mMAb labeled with iodine-131 (^{131}I) also holds promise for the treatment of non-Hodgkin's lymphoma[87].

In order to confirm tumor-targeting by the therapeutic radiolabeled MAb and to estimate the radiation dose to tumor and normal organs before applying RIT, scouting procedures with diagnostic radiolabeled MAbs can be used[88]. In the Zevalin therapeutic regimen, an imaging procedure is performed with ^{111}In-labeled mMAb ibritumomab tiuxetan prior to RIT with ^{90}Y-labeled MAb. Also in the Bexxar regimen, a dosimetric trace dose of ^{131}I-labeled MAb is used to individualize the therapeutic ^{131}I dose[89].

1.3 Radionuclides for radioimmunodetection and -therapy

As illustrated by Table 1 and 2, one of the possibilities to exploit MAbs for diagnosis and/or therapy is by the coupling of radionuclides. The choice of the radionuclide depends on the antibody used, antigen properties and application of the radiolabel: tumor detection, treatment, or treatment planning. Important characteristics of the radionuclide in this regard are its decay properties, such as its physical half-life and the type (γ-, β-, and/or α), energy, and abundance of the emitted radiation. The physical half-life should by preference be matching with the biological half-life of the MAb used. Besides that, also its chemical properties play a role, e.g. the mode of labeling needed and its fate after conjugate catabolism *in vivo*. Some radionuclides are rapidly released from the cell after internalization and catabolism, while others are known to be retained intracellularly and are thus called residualizing radionuclides[90]. The availability of a radiolabeling procedure that is simple, efficient, reproducible, and affordable is an additional requirement, especially when considering commercial application.

Radionuclides for detection and treatment planning At the moment, for radioimmunodetection mainly γ-emitters are used because photons travel far enough to be detected outside the body. Dictated by γ-camera characteristics, the γ-energy should by preference be 100-200 keV. Besides the γ-emitters ^{99m}Tc and ^{111}In, isotopes used in FDA approved diagnostic imaging immunoconjugates, also ^{131}I and ^{123}I are currently investigated in clinical imaging trials (Table 3).

^{99m}Tc has the advantages that it is widely available and that its γ-energy of 140 keV allows high quality imaging with a low radiation burden to the patient. A limitation is its short physical half-life of 6 h, making it less suitable for imaging with intact MAb molecules. Based on similar chemical properties ^{99m}Tc has been evaluated for use as matched pair radioisotope with rhenium-186 (^{186}Re), applying ^{99m}Tc-labeled MAb as a tracer to confirm tumor-targeting and to predict dosimetry for ^{186}Re-labeled MAb therapy[91,92]. In these studies quantitation with ^{99m}Tc was accurate, but not beyond 24 h. Also tracer amounts of ^{186}Re could

Table 3. Main characteristics of γ-emitting radionuclides presently used in clinical RIS studies.

Radionuclide	Half-life (h)	Main γ-energies (keV)	(%)
Technetium-99m	6.0	140	89.0
Indium-111	67.3	171	90.0
		245	94.0
Iodine-131 [a]	192.5	284	6.1
		364	81.7
		637	7.2
Iodine-123	13.2	27	70.4
		127	13.5
		159	82.8

[a] For β^--emission, see table 4

be used in such scouting procedure, but its accompanying β^--emission poses a higher radiation burden to the patient (see also Table 4).

^{111}In has good imaging qualities, whereas its physical half-life of 67 h makes it suitable for imaging intact MAbs. It is customary to use ^{111}In as a γ-emitting surrogate for tracing the biodistribution of the therapeutic radionuclide ^{90}Y in RIT trials. Comparisons between ^{111}In and ^{90}Y-labeled MAbs using DTPA derived chelates in preclinical and clinical studies, showed minor differences in biodistribution [93,94].

^{131}I is readily available, reasonable in cost, and relatively easy to couple to MAbs. However, its γ-emission of 364 keV limits its imaging qualities for a γ-camera. The half-life of ^{131}I is long (8 d). In RIT studies that use ^{131}I as the therapeutic radionuclide often an imaging study with a tracer dose of ^{131}I is included for patient selection and for dosimetry planning. Alternatively, ^{123}I has been used as it has a more suitable γ-emission of 159 keV and a relative short physical half-life.

Nowadays, positron-emitting radionuclides for detection with a positron emission tomography (PET) camera are considered as alternative for radioimmunodetection and treatment planning as will be discussed in part 2 of this General introduction.

Radionuclides for therapy For clinical RIT, β^--emitters have been most extensively studied (Table 4). The path-length of β-particles is several millimeters, i.e. 10-100 cell diameters, which permits cross-fire of poorly accessible cells or antigen-negative cells. Dependent on its energy and corresponding particle range, each β^--emitting radionuclide is associated with a certain optimal tumor size for curability [95].

Until recently, most RIT studies employed the isotope ^{131}I as the therapeutic radionuclide. Besides the previously mentioned advantages of ^{131}I (vide supra), a point of attention for its use in RIT is the occurrence of dehalogenation, which requires the blocking of

the thyroid with e.g. potassium iodide to prevent uptake of ^{131}I. Furthermore, during treatment extensive safety measures are needed to limit the radiation dose to medical personnel and relatives caused by the accompanying γ-emission. Another iodine isotope that has been studied for use in RIT is ^{125}I. This isotope, with a long half-life of 60 d, produces low-energy Auger electrons. Due to the short path length of Auger electrons (< 1 cell diameter), the isotope needs to be internalized in order to damage the nuclear DNA [96]. ^{125}I-labeled MAb 17-1A and A33 have been evaluated in RIT trials with colon cancer patients [97,98].

New developments in radionuclide production and labeling techniques have facilitated the use of other therapeutic radionuclides as well. This is particularly true for ^{90}Y. Its high β^--energy and particle range of up to 12 mm makes ^{90}Y more suitable for irradiation of larger tumors (centimeter-size [95]). Since ^{90}Y is a residualizing label, i.e. has a long residence time in the tumor cell after internalization, it can deliver a relatively large radiation dose. The absence of γ-emission minimizes external radiation exposure and enables outpatient treatment, however it also makes imaging of the *in vivo* distribution of the ^{90}Y-labeled antibody virtually impossible.

A β^--emitting radioisotope that has shown promise for RIT is ^{186}Re. This radionuclide combines a suitable half-life and β^--energy with a relatively low abundance of γ-emission suitable for high quality imaging (Table 4). Encouraging tumor responses have been achieved with antibodies labeled with ^{186}Re in patients with refractory metastatic epithelial carcinoma [99] and patients with squamous cell carcinoma of the head and neck [92]. Another rhenium isotope, the radionuclide ^{188}Re, has a relative short half-life for RIT and has been used in patients with gastrointestinal cancer [100] and for myeloablative RIT for conditioning of high-risk leukemia patients prior to stem cell transplantation [101]. Radionuclides that are also under clinical investigation are copper-67 (^{67}Cu) and lutetium-177 (^{177}Lu). In a pilot study with ^{67}Cu-labeled mMAb Lym-1, tumor regressions were observed in patients with non-Hodgkin's lymphoma [102]. Consistent production of ^{67}Cu at high specific activity is still a challenge [103]. The β^--emitter ^{177}Lu has been used in patients with advanced adenocarcinoma [104] and in patients with ovarian cancer, in the latter case intraperitoneally administered in combination with the chemotherapeutic agent taxol [105]. ^{177}Lu is similar to ^{90}Y in chemistry, but has a considerable shorter maximum particle range of 1.5 mm, making it more suitable for treatment of small tumors.

Within the approach to employ α-emitters in RIT, bismuth-213 (^{213}Bi; half-life, 0.77 h), ^{212}Bi (half-life, 1 h), astatine-211 (^{211}At; half-life, 7.2 h), and more recently actinium-225 (^{225}Ac; half-life, 10 d) have been indicated to be suitable [106-108]. Due to their short path-length, i.e. 1-10 cell diameters, and high linear energy transfer, α-particles are thought to be especially suitable for eradication of circulating tumor cells, micrometastases or minimal residual disease. The short half-life of most of these α-emitters makes them less suitable for the labeling of intact MAb molecules. Nevertheless ^{213}Bi-labeled MAbs have been used in clinical trials with patients with leukemia [109] and prostate cancer [110].

Table 4. Main characteristics of β^--emitting radionuclides presently used in clinical RIT studies.

Radionuclide	Half-life (h)	Main β^--energies (keV)[a]	(%)	Main γ-energies (keV)	(%)	Maximum particle range (mm)	Reference
Iodine-131	192	333	7	364	82	2.0	19
		606	89				
Yttrium-90	64	2284	100	----		12.0	19
Rhenium-186	89	939	21	137	10	5.0	92,99
		1077	71				
Rhenium-188	17	1965	25	155	15	11.0	100,101
		2120	71				
Copper-67	62	390	57	93	16	1.8	102
		482	22	185	49		
		575	20				
Lutetium-177	161	176	12	113	7	1.5	104
		384	9	208	11		
		497	79				

[a] Maximum β^--energy

1.4 Radiolabeling of MAbs

Initially, radiolabeling methods were focused on direct labeling because of its simplicity. These methods were relatively successful for ^{99m}Tc and the iodine radioisotopes ^{131}I, ^{125}I, and ^{123}I, but the direct coupling of ^{186}Re and ^{188}Re to MAbs appeared to lead to stability problems. For stable coupling of non-halogen radionuclides, indirect labeling methods with bifunctional chelates are mandatory. Bifunctional chelates are compounds that are able to form a stable complex with the radionuclide while containing a reactive group that can be used for coupling to the MAb. During the labeling procedure the chelate-radionuclide complex can be prepared first, followed by coupling to the MAb (prelabeling method) or the chelate can be coupled to the MAb, after which the premodified MAb is radiolabeled (postlabeling method). Advantages of the latter method are the often higher overall radiolabeling yields and the possibility to formulate labeling kits, enabling easy use in multicenter trials.

The direct labeling of iodine radioisotopes to MAbs involves the covalent attachment of radioiodine to tyrosine residues under mild oxidative conditions (Fig. 2). A consequence of using directly iodinated MAbs is that after internalization and catabolism of the MAb by the target cell, iodotyrosine is formed which is rapidly released from the cell [111,112]. In order to increase tumor retention of radioiodine, novel labeling methods have been developed using prosthetic groups that result in residualizing radiolabels [113]. This means that the catabolic products of the radioiodinated conjugates are trapped in lysosomes and thus retained intracellularly. Because of the more complex labeling procedure, low levels of radioiodine incorporation, low specific activities, and problems with MAb aggregation, the development

of residualizing iodine radiolabels still requires considerable research [114]. Until now, clinical studies have only been performed with MAbs that were directly labeled with radioiodine.

Radiometals such as ^{186}Re, ^{188}Re, and ^{99m}Tc can be bound directly to free thiol groups after reduction of S-S bonds of the MAb. This method suffers from several problems: (1) binding is non-specific with poor control of the labeling site; (2) often unstable complexes are formed with limited *in vivo* stability, and (3) cleavage of disulfide bridges can alter protein structure and impede biological integrity. The indirect labeling of Re isotopes and ^{99m}Tc can be performed with bifunctional chelates such as N_2S_2 [115] (used in the diagnostic agent Verluma, Table 1), N_3S [116], N_2S_4 [117], and S-benzoyl-MAG3 [118]. The latter chelate was originally used as precursor for ^{99m}Tc-MAG3, a tracer for measuring renal function. Based on a labeling approach described by Fritzberg *et al.* [115], a multistep procedure was developed to radiolabel MAbs with ^{99m}Tc and ^{186}Re via MAG3 (Fig. 3). Especially the formation of ^{186}Re-MAG3 proved to be different from that of ^{99m}Tc-MAG3 and required a solid-state synthesis [118].

For the coupling of the radionuclides ^{111}In, ^{90}Y, ^{177}Lu, and ^{67}Cu to MAbs, indirect labeling with a bifunctional chelate is the only option. One of the first chelates used successfully for the coupling of ^{111}In and ^{90}Y was diethylenetriaminepentaacetic acid (DTPA, Fig. 4). Examples of ^{111}In-labeled radioimmunoconjugates are the commercial imaging agents OncoScint and ProstaScint which contain the chelate GYK-DTPA [62,63,68]. Linkage of GYK-DTPA to the MAb is accomplished using one of its five carboxyl arms. An alternative approach involves the synthesis of *p*-isothiocyanatobenzyl-derivatives of DTPA (e.g. SCN-Bz-DTPA, 1B4M-DTPA and CHX-DTPA) in which the chelate is coupled via a specific linker group on the backbone ethylene carbon (Fig. 4). The latter chelate modification resulted in more stable chelate-radionuclide complexes, probably because all five carboxylate arms remain available for binding [119]. Of these derivatives, 1B4M-DTPA (also known as MX-DTPA) has been used in the Zevalin regimen and several other clinical studies for imaging and therapy with ^{111}In and ^{90}Y, respectively [93,120-122].

More recently, the macrocyclic chelate 1,4,7,10-tetraazacyclododecane-1,4,7,10-tetraacetic acid (DOTA, Fig. 5) has been developed which forms more stable ^{90}Y complexes than DTPA does [119,123,124]. This chelate has also been successfully used for coupling of ^{177}Lu to MAbs [104]. A different macroclyclic chelate, 1,4,8,11-tetraazacyclotetradecane-1,4,8,11-tetraacetic acid (TETA, Fig. 6), has been developed to couple ^{67}Cu to MAbs [102]. It is of note that one of the first clinical studies performed with DOTA-coupled MAb reported immunogenicity to DOTA [125]. However, a subsequent study did not support the view that the chelates DOTA and TETA were more immunogenic than other radiometal chelating agents [126]. It was proposed that the observed increase of immunogenicity might originate from the linker used to attach the macrocyclic chelate to the MAb [127], from a high chelate:MAb molar ratio [128,129], or from an interplay between MAb, linker, and chelate [130].

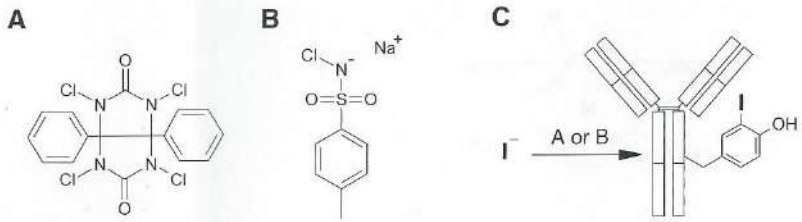

Figure 2. Chemical structures of the oxidants 1,3,4,6-tetrachloro-3α,6α-diphenylglycouril (Iodogen, used in this thesis, chapter 2, 5, and 6)(A) and *N*-chloro-*p*-toluene-sulfonamide (chloramine T)(B). These oxidants are commonly used for radiohalogenation of tyrosine residues of MAb (C).

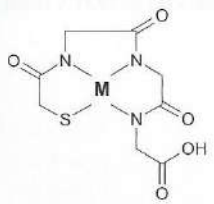

Figure 3. Chemical structure of the bifunctional chelate MAG3 (used in this thesis, chapter 2 and 6). M: radiometal.

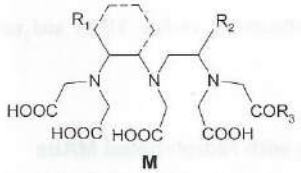

	R_1	R_2	R_3
DTPA:	H,	H,	OH
GYK-DTPA:	H,	H,	lysyl-tyrosyl-glycyl
p-SCN-Bz-DTPA:	H,	CH_2-benzyl-NCS,	OH
1B4M-DTPA/MX-DTPA:	CH_3,	CH_2-benzyl-NCS,	OH
CHX-DTPA:	cyclohexyl, (dashed line)	CH_2-benzyl-NCS,	OH

Figure 4. Chemical structure of the bifunctional chelate DTPA and several of its derivatives. M: radiometal.

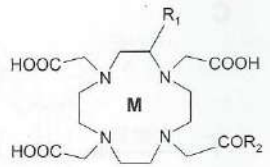

	R_1	R_2
DOTA:	H,	OH
BAD:	CH_2-benzyl-NH-CO-CH_2-Br,	OH
p-SCN-Bz-DOTA:	CH_2-benzyl-NCS,	OH
DOTA-peptide-NCS:	H,	$(NH\text{-}CH3\text{-}CO)_4$-NH-$CH_2$($CH_2$-benzyl-NCS)-CO-$NH_2$

Figure 5. Chemical structure of the bifunctional chelate DOTA (used in this thesis, chapter 4 and 6) and several of its derivatives. M: radiometal.

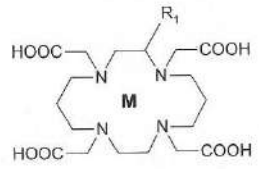

	R_1
TETA:	H
BAT:	CH_2-benzyl-NH-CO-CH_2-Br

Figure 6. Chemical structure of the bifunctional chelate TETA and one of its derivatives. M: radiometal.

1.5 Improving tumor-targeting with radiolabeled MAbs

Important variables affecting tumor response to RIT include the cumulative radiation dose delivered to the tumor, dose rate, penetration, and tumor radiosensitivity. From the studies reported so far, RIT seems to be most successful in the treatment of hematologic cancer types. Lymphomas and leukemias remain the most sensitive tumor targets for RIT, because of their intrinsic sensitivity to MAbs and radiation, and the relatively good access of the tumor cells for radioimmunoconjugates. The treatment of solid tumors with RIT still remains a challenge.

For further improvement of tumor-targeting, most attention is paid to the selection of optimal MAbs, radionuclides, and labeling methods. Other approaches focus on maximizing uptake of radiolabeled MAb in the tumor and/or reducing the amount of radiolabeled MAb in blood and normal tissues. As an interesting approach to overcome heterogeneous distribution of MAbs within tumor tissue caused by heterogeneous antigen expression, it has been suggested to apply mixtures of MAbs or a bispecific MAb directed against different antigens

or epitopes of the same tumor type [131-135]. In addition, to enhance RIT efficacy a combination of radionuclides with different energies may prove more beneficial than using a single radionuclide. For example, combining a β^--emitting radionuclide with high energy and longer tissue range, and a β^--emitter with medium energy and shorter tissue range could possibly destroy both bulky disease as well as micrometastases [95,136].

To eliminate remaining, unbound radiolabeled antibodies from the blood circulation after saturation of target sites, so-called "secondary" antibodies have been proposed as clearing agents to reduce exposure of normal tissues [137,138]. Another approach to lower the residence time of radioactivity in the body is the pretargeting strategy [139]. The concept of pretargeting is based on separate administration of the tumor-targeting MAb and a low-molecular weight radiolabeled ligand. Because the biological half-life in blood of such a ligand is short, the radiation exposure of bone marrow and other normal organs will be minimized. The binding of the radiolabeled ligand by the tumor-localized MAb can be achieved with the use of either a (strept)avidin-biotin or a bispecific MAb recognition system. Both systems have been investigated in diagnostic and therapeutic clinical trials [140-143]. Although individual dosing and timing is complicated with pretargeting because of the multiple administration steps, promising diagnostic and therapeutic results have been observed.

Several other attempts to enhance RIT efficacy have been reported. These include combined modality RIT [144], fractionated RIT [145], and bone marrow transplantation or blood stem cell reinfusion. In the case of combined modality RIT, in general RIT has been combined with chemotherapy or external beam radiation [146,147]. Clinical data on fractionated RIT, the administration of multiple-doses of radiolabeled MAb, revealed that toxicity is reduced and the maximum tolerated dose extended [148,149]. Since in most RIT trials myelotoxicity has been the dose-limiting toxicity, bone marrow transplantation or blood stem cell reinfusion may allow dose escalation [150-153].

A role for PET in improving radioimmunodetection and -therapy For optimal application of tumor-targeting MAbs in approaches for effective RIS and RIT, it must be demonstrated that the radiolabeled MAbs indeed accumulate selectively and in sufficient amounts in tumors. This can be performed by absolute quantification of tissue uptake in biopsied samples or by planar imaging with a γ-camera.

The most advanced way for visualization and quantification of radioimmunoconjugates promises to be the use of PET. Immuno-PET (PET with MAbs) combines the selective tumor-targeting properties of a MAb with the excellent sensitivity and resolution of PET. For this purpose the MAb has to be labeled with a positron emitter. Immuno-PET can be used for (1) detection of primary and metastatic tumors, (2) assessment of pharmacokinetics and biodistribution, (3) optimization of MAb scheduling, and (4) individualization of therapy [154]. As such immuno-PET might play an important role in tumor diagnosis and therapy with MAbs, as well as in research and development for the initial characterization and optimization of novel MAbs/MAb-constructs.

2 Positron Emission Tomography (PET)

2.1 General introduction imaging

Imaging techniques such as magnetic resonance imaging (MRI), X-ray computed tomography (CT), and ultrasound are of immense help in noninvasive visualization of the body[155]. These techniques are based on energy-tissue interactions and are primarily used to display anatomy. With CT and MRI, tumors can in general be recognized if their diameter is larger than 1 cm. These techniques cannot reliably distinguish between benign and malignant tumors or between post-therapeutic alterations such as scarring, inflammation, or necrosis and residual or recurrent tumors. Moreover, none of these techniques can visualize the *in vivo* behavior of new (bio-)pharmaceuticals like MAbs. For a long time, therefore, clinical testing of new medicines has been uncontrolled, with the body being a black box from which at most data from blood and urine concentrations, and the presence of metabolites, could be retrieved.

Newcomers in the area of imaging are single photon emission computerized tomography (SPECT), near infrared (NIR) optical imaging, and PET. These techniques can be used for acquiring anatomical information, as well as information at physiological and molecular levels. They require the administration of a reporter probe, consisting of a targeting component and a label, e.g. γ-emitter, fluorochrome, or positron emitter, that is detectable by a given imaging device. The targeting component might be a small molecule, peptide, enzyme substrate, or antibody.

A limitation of SPECT is that quantification with this technique is difficult, primarily on account of insufficient correction for scatter and partial absorption of γ-photons in the tissue of a patient. A disadvantage of NIR optical imaging is low penetration depth in tissue. In contrast, PET offers both accurate quantification possibilities and deep tissue imaging. In addition PET provides superior spatial and temporal resolution and sensitivity compared to SPECT.

2.2 Principles of PET

PET is based on annihilation coincidence detection and requires the administration of a positron emitter. This is a radioisotope that emits a positively charged β-particle (also called positron) and a neutrino upon conversion of a proton into a neutron ($p^+ \rightarrow n + \beta^+ + \nu$). The emitted positron will travel a distance of a few millimeters, depending on the initial positron energy and the density of the surroundings. After losing its kinetic energy, the positron combines with an electron. During this event the masses of the two particles convert into their energy equivalent according to $E=mc^2$, resulting in the formation of two 511-keV photons that are simultaneously emitted in opposite directions. This process is called annihilation (Fig 7). After administration of a positron labeled molecule to a patient, the distribution of the compound can be monitored by detection of the annihilation photon pairs. For this purpose a PET camera is used that consists of a ring of detectors placed around the body of the patient. If two photons are detected by detectors on opposite sides of the body within a very short time, it is assumed that somewhere along the line between the two detectors an annihilation

event has taken place. This line is referred to as the line of response (LOR) and is registered as a coincidence event. By calculation of the crossing of all the LORs the location of the radiation source can be determined.

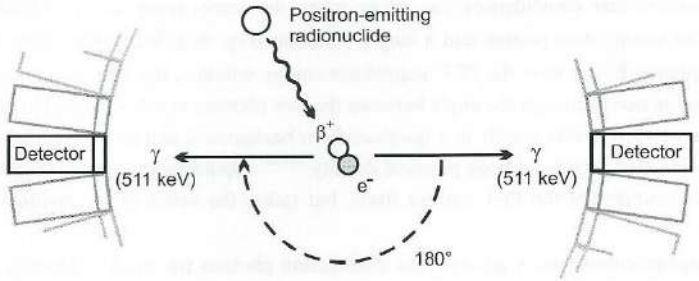

Figure 7. Positron emission, annihilation, and coincidence detection. A positron is emitted during the decay of a radionuclide, travels a short distance and combines with an electron. The positron and electron annihilate, converting their mass into two 511-keV photons emitted at 180° to each other. The two annihilation photons are electronically detected as a coincidence event when they strike opposing detectors simultaneously (detector ring schematically depicted).

2.3 Corrections applied in PET

All photon pairs that have an energy that falls within the PET acquisition energy window (typically 350 keV – 650 keV) and that are detected in coincidence within a certain time period (coincidence time window, in the order of 5-15 ns) are called coincidences. A photon pair that originates from the same annihilation event and that has no interaction with the object or object surroundings before detection, is referred to as a true coincidence (Fig. 8A). Besides that, the gross coincidence rate can consist of scatter coincidences, spurious true coincidences and random coincidences (Fig. 8B-D). In these cases the LOR is not representative of the annihilation location and degrades the image quality. Also, part of the annihilation photons will not be detected due to attenuation and dead time. To arrive at a quantitative image, a number of corrections has to be performed on the raw PET data [156,157].

Corrections. Scatter coincidences comprise of annihilation photon pairs of which one or both of the photons has undergone a Compton scatter before detection (Fig. 8B). A larger object or higher density of the material will increase the scatter rate. The use of lead or tungsten shields placed between the detector rings, called septa, can reduce the number of interplane scattered events collected. The septa, however, also reduce the number of true coincidences detected. Acquiring PET data with the septa in place is referred to as two-dimensional (2D) PET and without the septa as three-dimensional (3D) PET. For 2D PET, a commonly implemented scatter correction is described by Bergström *et al.* [158]. Scatter

correction for 3D PET still requires considerable research [159]. Several scatter correction methods have been suggested for 3D PET, such as using direct Monte Carlo-based scatter compensation approaches [160,161], simultaneous acquisition of data in two energy windows [162], model-based scatter correction methods [163,164], or non-stationary convolution subtraction scatter correction techniques [165].

Spurious true coincidences can occur when the same decay event simultaneously results in an annihilation photon and a single γ-photon (Fig. 8C). When the energy of such prompt γ-photon falls within the PET acquisition energy window, the system will accept the coincidence as true, although the angle between the two photons is not restricted to 180°. The occurrence of such events results in a quasi-uniform background and an anomalous apparent activity in inactive regions of high physical density [166,167]. Spurious true coincidences are not an intrinsic problem of the PET camera itself, but rather the result of the positron emitter used.

Random coincidences involve two annihilation photons (or single γ-photons) that do not originate from the same annihilation event but by chance are detected within the coincidence time window (Fig. 8D). Correction for random coincidences can be performed by subtraction of coincidences measured in a delayed coincidence window. In this case, one of the coincidence detectors has a delayed response relative to the other. The delay is such that the probability of detecting true coincidences is zero. The probability of detecting random coincidences will be the same, irrespective of the delay. With increasing radioactivity, the random rate will increase with the square of the activity, whereas the true coincidence rate will increase linearly. This means that at high activity levels, the occurence of randoms can be a serious problem.

Attenuation is the loss of true coincidences due to Compton processes and absorption within tissue, causing one or both of the annihilation photons not to fall within the PET acquisition energy window and/or coincidence time window (Fig. 8E). Due to attenuation, true coincidences in the center of the body have a decreased probability of detection than those on the periphery of the body. The probability of a true coincidence detection is the product of the probabilities of each of the two annihilation photons escaping the body without interaction. For this reason, the amount of attenuation along a particular LOR is the same, independent of the location of the event on the LOR. This holds true even if the event took place outside the body. This fact is used in measured attenuation correction and requires an additional transmission scan in which the body is scanned with a rotating external radioactive point or line source. In addition, a scan of the external source without the body present (a so-called blank scan) is acquired to characterize the number of counts if no attenuation loss occurs. The ratio of the blank counts divided by those in the transmission scan yields an attenuation correction factor for each emission LOR. Alternatively, calculated attenuation correction can be performed based on body outline determination, assuming that the attenuation properties are constant (i.e. a homogeneous body) [156].

Dead time losses are due to the inability of the system to process an infinite number of photons at the same time. As the rate of photons hitting a detector increases, the probability

of missing a photon due to detector dead time also increases. This problem is particular troublesome for coincidence detection, because both photons must be detected. Dead time losses can be minimized by using a system with many independent detectors, fast scintillators and fast processing electronics.

Normalization is necessary to correct for the variations in detector and LOR efficiency. Arc correction is performed to correct for the fact that due to the curved nature of the detector ring, LOR passing near the center of the gantry will be spaced farther apart than those LOR on the periphery.

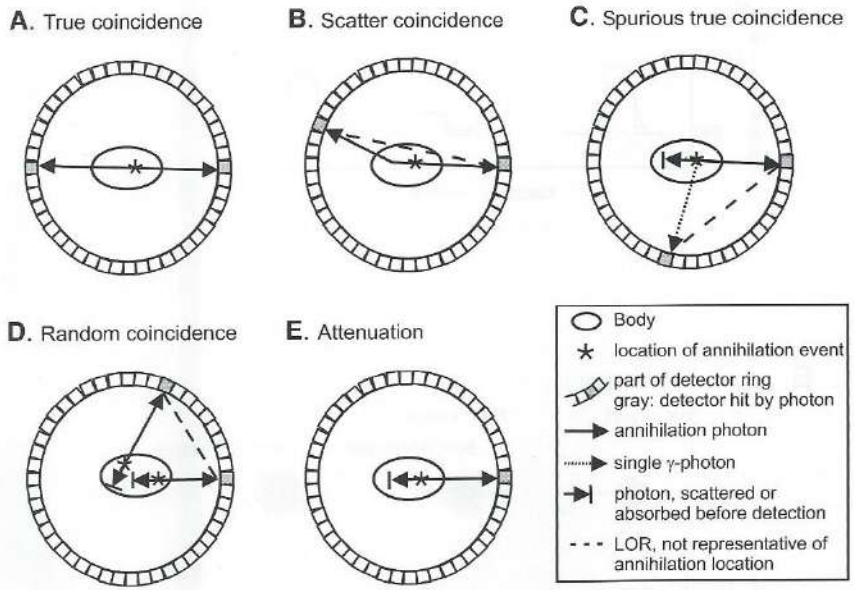

Figure 8. Schematic representation of true (A), scatter (B), spurious true (C) and random coincidences (D), and attenuation (E). A, True coincidence: two annihilation photons, emitted from the same annihilation event, travel in opposite directions without interaction with the body and are detected by opposing detectors. B, Scatter coincidence: one photon from an annihilation travels without interaction, while the other annihilation photon is deflected due to scattering in the body. C, Spurious true coincidence: a single γ-photon is detected simultaneous with an annihilation photon (or another single γ-photon), both emitted from the same decay event. D, Random coincidence: two annihilation photons (or single γ-photons), emitted from two separate decay events, are detected by chance within the coincidence time window. E, Attenuation: one or both of the annihilation photons is not detected due to scattering or absorption within the body. In the case of scatter, spurious, and random coincidences, the LOR drawn between the two detectors is not representative of the annihilation location (B-D). Three or more photons (multiples) detected in coincidence are rejected by PET coincidence electronics.

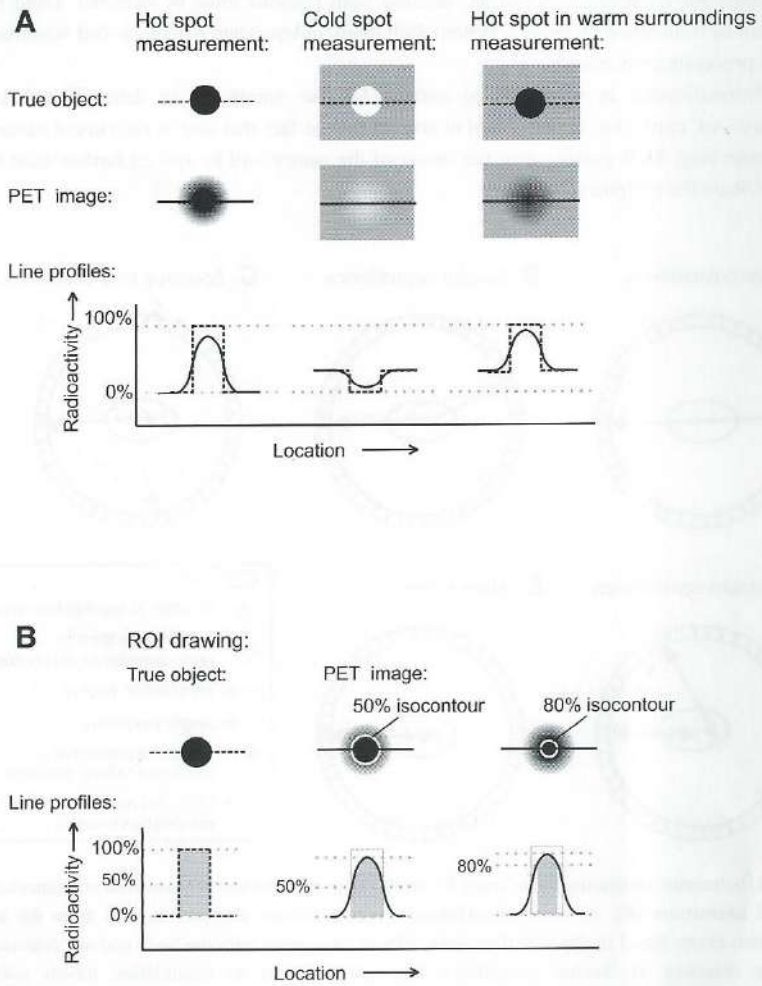

Figure 9. Schematic presentation of partial volume effects (A) and isocontour drawing (B). A, Slices through the center of the true and the PET imaged object (i.e. a sphere), and their corresponding line profiles (dashed line: true object; solid line: PET image) for three conditions of radioactivity distribution: only the object filled with radioactivity (hot spot), only the surroundings filled with radioactivity (cold spot), or the object filled with a higher concentration of radioactivity than the surroundings (hot spot in warm surroundings). B, 50% isocontour and 80% isocontour are drawn around a hot spot and line profiles are presented. Gray areas indicate the amount of radioactivity contained within the ROI.

Partial volume effects. If all the above mentioned effects are corrected for with sufficient accuracy, then the only factor influencing quantitative PET analysis of radioactivity is resolution-related. Due to limited spatial resolution, the spread of locoregional radioactivity to surrounding areas must be taken into account. The ratio of imaged activity concentration in an object to true activity concentration is called recovery coefficient (RC). With smaller objects, the RC decreases, indicating that true activity concentration has been underestimated in the PET image. Hot spot recovery coefficient (HSRC) defines the underestimation of image activity concentration of a hot object in cold surroundings, while cold spot recovery coefficient (CSRC) defines the overestimation of image activity concentration of a cold object in hot surroundings (Fig. 9A). The loss of radioactivity from the object into the surroundings and the contribution of near surroundings spillover radioactivity into the object are called partial volume effects. These errors can be corrected for if the correction factors (HSRC and CSRC) are known from a test measurement [168].

In general, for such test a cylindrical phantom is used that contains six fillable spheres with different volumes arranged in a circle. For HSRC measurements the spheres are filled with radioactivity and the cylinder with water, while for CSRC measurements the cylinder is filled with radioactivity and the spheres with water. In order to calculate RCs, the reconstructed images are analyzed by drawing regions of interest (ROIs) in the plane that includes the center of each sphere. The diameter of the ROI can be fixed (e.g. approximating the resolution of the PET system, the true sphere diameter, or an arbitrary size) or can be semi-automatically determined by drawing a 50% isocontour. The latter ROI contains all pixels with a radioactivity concentration of 50% or more of the maximum pixel radioactivity concentration (Fig. 9B). By increasing the percentage of the isocontour, the resulting ROIs will be smaller. Subsequently, the total radioactivity within the ROI will be less, but the radioactivity concentration will be higher. Alternatively, volumes of interest (VOIs, drawn across several planes) instead of ROIs can be drawn for higher accuracy. RCs are calculated by dividing the radioactivity concentration in the ROI or VOI by the true radioactivity concentration. When the true radioactivity concentration is unknown, the radioactivity concentration in the ROI of the largest sphere can be used (assuming that partial volume effects at this size can be neglected). For a linear system, CSRC should equal one minus the HSRC. The calculated RCs will depend on the diameter of the ROIs or VOIs used for data analysis [168].

2.4 Positron imaging systems and animal-PET

The potential of annihilation coincidence detection in medical imaging was recognized in the early 1950s [169], but it took at least a decade before the first positron imaging devices were developed [170-173]. These devices all made use of thallium-doped sodium iodide (NaI(Tl)) detectors and consisted of a dual-headed camera or a circular array camera. Although these devices employed the coincidence detection technique unique to positron imaging, it was not until 1975 that the first PET scanner was developed by Phelps and coworkers that could form

true computed tomographic images [174]. Since then the PET scanner has undergone several developments with respect to system design and scintillation crystals.

PET design. Over the years, the hexagonal and octagonal designs of the first systems were followed by circular designs. To reduce cost, nowadays also a rotating partial-ring system is commercially available instead of a full ring device (ECAT ART) [175]. The coincidence detection efficiency of this system, however, is reduced because of the regions of missing detectors. Also available is the "poor man's PET", a hybrid system consisting of coincidence circuits loaded onto a dual-headed γ-camera. Although this system reduces cost and is more accessible, detector sensitivity and count rate performance need improvement [176]. Recently, more sophisticated hybrid systems have been developed that make use of two layers of different detector materials [177]. The front layer is for low-energy single photon detection and the combination of the front and back detector materials are used for 511-keV detection. This approach has the potential to result in SPECT performance similar to that of standard dual-headed systems and PET performance similar to that of a mid-range clinical PET scanner. Another low-cost system consists of a full ring formed by multiple flat NaI(Tl) γ-cameras or recently developed curved detectors [178].

In order to facilitate accurate interpretation of PET images, it has been suggested to combine PET imaging with anatomical imaging by X-ray CT or MRI to provide simultaneous registration of both biological function and anatomy [179]. Combined PET/CT scanners are already commercially available [180] and although combining PET with MRI is technologically more challenging because of the strong magnetic fields restricting the use of certain electronic components, also a small MRI-compatible PET scanner has been developed [181]. The availability of anatomical data will not only provide landmarks for PET image interpretation, but can also be used for attenuation correction [182], reduction of image noise [183], and partial volume correction [184].

PET scintillation crystals. In the early years of PET, detectors were made of single crystals of NaI(Tl). Today, most PET scanners contain bismuth germanate (BGO) as scintillation material because of its much greater efficiency for detecting 511-keV photons [185]. The most widely used design is the block detector, in which the BGO block is segmented into as many as 64 elements. Each block is coupled to four photomultiplier tubes (PMT) which determine where a photon interaction occurred in the block based on Anger position logic. In this way, small size segments can be used, highly improving spatial resolution, while limiting the number of photomultiplier tubes needed. In recent years, two promising new scintillation crystals, cerium-doped gadolinium oxyorthosilicate (GSO) and cerium-doped lutetium oxyorthosilicate (LSO), have emerged. Both the excitation states of GSO and LSO have a shorter decay constant than either BGO or NaI, allowing for a short coincidence time window. Their γ-ray detection efficiency is comparable with BGO. Compared to LSO, GSO has a somewhat lower light output and cleaves easily, making detector manufacturing more difficult. LSO on the other hand has a low level of background radioactivity as a result of the

Table 5. Small animal PET systems presently in use or in development.

Commercially available Manufacturer	PET system	Special feature	Reference
Concorde Microsystems (CTI) Knoxville, TN, USA	MicroPET	*Crystal-to-detector coupling*: Optical fibers	186
Oxford Positron Systems Weston-on-the-Green, UK	Quad-HIDAC	*Detector*: High Density Avalanche Chamber	187
Hamamatsu Photonics KK Hamakita-city, Japan	Hamamatsu SHR-7700		188
Concorde Microsystems (CTI) Knoxville, TN, USA	Dual layer HRRT	*Scintillator material*: LSO *Design*: Dual layer, depth of interaction	189
Not commercially available Site of development			
Hammersmith Hospital, London, UK	RAT-PET		190
UCLA Crump Institute, Los Angeles, CA, USA	MicroPET II	*Scintillator material*: LSO *Crystal-to-detector coupling*: Optical fibers	191
University of Jülich, Jülich, Germany	TierPET	*Scintillator material*: Yttrium aluminum perovskite	192
University of Ferrara, Ferrara, Italy	YAP-PET	*Scintillator material*: Yttrium aluminum perovskite	193
Max Plank Institute, Munich, Germany	MADPET-II	*Scintillator material*: LSO *Detector*: Avalanche photodiode *Design*: Dual layer, depth of interaction	194
VU University Medical Center, Amsterdam, The Netherlands	Single layer HRRT [a]	*Scintillator material*: LSO	195
Indiana University, Indianapolis, IN, USA	IndyPET-II	*Design*: Four adjustable detector banks	196
University of Sherbrooke, Sherbrooke, Canada	Sherbrooke animal PET	*Detector*: Avalanche photodiode	197
Massachusetts General Hospital, Boston, MA, USA	Single-plane PET	*Design*: Single-ring *Scintillator material*: LSO	198
National Institutes of Health, Bethesda, MD, USA	ATLAS	*Scintillator material*: LGSO and GSO *Design*: Dual layer, depth of interaction	199

[a] In use until 2003.

presence of naturally occurring ^{176}Lu which could cause higher random event rates and influence the accuracy of the singles transmission [195,200].

Animal-PET. The use of dedicated small animal PET systems allows the careful evaluation of new tracers and of animal models of disease in an efficient and economic manner prior to human use [201-205]. The first and most obvious challenge to animal PET imaging derives from the magnitude of difference between the physical size of human subjects for which clinical PET systems have been developed and the size of small laboratory animals such as mouse and rat. To address the same biological questions in small animals as in humans, animal PET systems must have similar ratios of volumetric spatial resolution to the volume of the object of interest. Besides high resolution, the sensitivity of the system plays an important role in obtaining high quality images. Unfortunately, the former is often pursued at the expense of the latter [206].

The field of small animal PET research is relatively new and commercial systems have only been available in the last few years. Recently commercialized systems are the microPET, the Quad-HIDAC, the Hamamatsu SHR-7700, and the dual-layer high-resolution research tomograph (HRRT) PET scanner (Table 5). In addition, several institutions have continued to develop their own systems, a large selection of which is listed in Table 5. These commercial and research detectors and their predecessors have been described in detail in recently published reviews [202,203,205,207].

2.5 Positron emitters for immuno-PET

For a positron emitter to be appropriate for immuno-PET, several aspects have to be considered. The applicability of a positron emitter is dependent on the availability of methods to obtain it pure and in sufficient amounts, the time period available for transportation and labeling, the availability of procedures for its stable coupling to the MAb with maintenance of the *in vivo* biodistribution characteristics of the latter, and on the presence of undesirable components in its decay scheme that could affect image quality and quantitation accuracy. The predominant factor for a positron emitter to be suitable for immuno-PET is its physical half-life. This has to be compatible with the time needed for a MAb or MAb fragment to achieve optimal tumor-to-nontumor ratios, being typically 2-6 h for MAb fragments and 2-4 d for intact MAbs. Thusfar, the application of MAb fragments has mostly been restricted to tumor detection, while intact MAbs have found broad application for tumor detection, tumor therapy as well as for treatment planning (see paragraph 1.2). While for immuno-PET with MAb fragments also the use of short-lived positron emitters (half-life of hours) is an option, the kinetics of intact MAbs demand the use of long-lived positron emitters (half-life of days) to allow imaging at later time points for obtaining maximum information.

In relation to aforementioned considerations, application of positron emitters with a very short half-life such as the "bio-isotopes" ^{15}O, ^{13}N, and ^{11}C (half-life, 2.0, 9.7 and 20.4 min, respectively) is out of the question. The positron emitters that have been evaluated in preclinical and clinical immuno-PET studies are listed in Table 6. On basis of their half-life,

Table 6. Decay characteristics [a] of positron emitters used in preclinical or clinical RIS studies.

Positron emitter	Production	Half-life	Main β^+-energies [b]		Main γ-energies [b]		Intrinsic spatial resolution loss	Ref.
		(h)	(keV) [c]	(%)	(keV)	(%)	(mm) [d]	
Technetium-94m	^{94}Mo(p,n)	0.87	2438	67.6	871	88.5	3.2	208,209
					1869	5.4		
Gallium-68	^{68}Ge/^{68}Ga-generator	1.13	1899	87.9	---		2.4	210
Fluorine-18	^{18}O(p,n) ^{20}Ne(d,α)	1.83	634	100.0	---		0.7	211
Copper-64	^{64}Ni(d,2n) ^{64}Ni(p,n)	12.7	653	17.9	---		0.7	210,212
Yttrium-86 [e]	^{86}Sr(p,n)	14.7	1221	12.5	443	16.9	1.8	213-215
			1545	5.6	628	32.6		
					646	9.2		
					703	15.4		
					777	22.4		
					1077	82.5		
					1153	30.5		
					1854	17.2		
					1921	20.8		
Bromine-76 [e]	^{75}As(^{3}He,2n)	16.2	871	5.9	559	72.3	5.3	216,217
	^{76}Se(p,n)		990	5.1	657	15.5		
			3382	27.6	1216	8.7		
			3941	6.0	1854	14.0		
					2793	5.3		
					2951	7.6		
Zirconium-89	^{89}Y (p,n)	78.4	897	22.7	909	99.9	1.0	218,219
Iodine-124 [e]	^{124}Te(p,n)	100.3	1535	11.2	603	62.9	2.3	220,221
	^{124}Te(d,2n)		2138	11.2	723	10.1		
	^{125}Te(p,2n)				1691	10.6		

[a] Half-life, main β^+-energy keV and abundance, and main γ-energy keV and abundance as reported by ICRP [222] and the NuDat database [223].

[b] Only the energies in abundancy of $\geq$ 5% is given.

[c] Maximum β^+-energy

[d] Calculated according to Pagani *et al.* [210].

[e] Positron emitter with more than 50 γ-energies

most of these radionuclides are less suitable for use in combination with intact MAb (in particular ^{94m}Tc, ^{68}Ga, and ^{18}F, and to a lesser extent ^{64}Cu, ^{86}Y, and ^{76}Br). Other aspects that play a role in the use of these positron emitters are a complicated decay scheme with the presence of prompt single γ-photons (^{86}Y and ^{76}Br), high β^+-energy (^{94m}Tc, ^{68}Ga, and ^{76}Br), and presence of radionuclidic impurities (radioisotopes of the same element generated during cyclotron production)(^{94m}Tc, ^{64}Cu). Except for the production of ^{76}Br via the (^{3}He, 2n) reaction on ^{75}As, all these shorter-lived positron emitters require enrichment of the target material. While the positron emitters ^{68}Ga, ^{18}F, ^{64}Cu, and ^{86}Y need indirect labeling methods with bifunctional chelates, ^{94m}Tc and ^{76}Br can also be coupled directly to MAbs.

Only two positron emitters are suitable for imaging of MAb fragments as well as intact MAbs: ^{124}I (half-life, 4.18 d) and ^{89}Zr (half-life, 3.27 d). The half-life of these radionuclides offers an advantage with respect to the logistics of radiolabeling and transportation, but a disadvantage with respect to the radiation burden to the patient especially when coupled to ligands with a long biological half-life such as intact MAbs. This disadvantage might be overcome by the introduction of the latest generation of high-resolution PET scanners with a higher sensitivity, allowing lower doses of injected radioactivity for comparable images.

^{124}I emits positrons with relative high energies (β^+ = 22.4%, $E_{\beta+max}$ = 1535 and 2138 keV) and some prompt single γ-photons with energies that fall within the PET acquisition energy window. Nevertheless, quantitative PET imaging with ^{124}I has been reported to be feasible[221,224]. The production of ^{124}I requires expensive enrichment of the low abundant target material ^{124}Te or ^{125}Te and special attention to recovery of the target material. At first, the only source of ^{124}I was King Faisal Specialist Hospital, Riyadh, Saudi Arabia. Nowadays production of ^{124}I is still limited to a few centers, but several improvements on ^{124}I production have been suggested with respect to yield, recovery, and radionuclidic purity of ^{124}I, and recovery of target material[225-229]. Whether technical innovation will lead to an improvement of ^{124}I availability and cost, and broader application of ^{124}I, has to be seen. A recognized advantage of ^{124}I is that it can be directly coupled to MAbs, without the need for a multi-step labeling procedure using a bifunctional chelate. However, direct radiolabeling of MAbs with ^{124}I leaves room for improvement, as it has mostly been performed with harsh oxidants such as chloramine T, while radiolabeling yields were often low to moderate[230-233].

^{89}Zr emits positrons of medium energy (β^+ = 22.7%, $E_{\beta+max}$ = 897 keV) and has no prompt single γ-photons. Its quantitative PET imaging performance has not been evaluated yet. The production of ^{89}Zr can be performed via a (p,n) reaction on ^{89}Y, an element with a natural abundance of 100%[234-236]. Isolation of ^{89}Zr was strongly improved by the introduction of a simple and efficient hydroxamate-based method[237]. ^{89}Zr can be coupled indirectly to premodified MAbs that were obtained upon reaction of SMCC-modified MAb with the SATA-modified chelate desferrioxamine B (SMCC = succinimidyl 4-(*N*-maleimidomethyl)cyclohexane-1-carboxylate; SATA = *N*-succinimidyl *S*-acetylthioacetate)[238]. The Zr-desferrioxamine B complex itself was reported to be highly stable[239], but the applied linker chemistry creates a succinimide ring-thioether unit that might be responsible for the release of the chelate from the MAb at physiologic pH[240].

2.6 Experience with immuno-PET

Although a number of positron emitters has been suggested for MAb labeling, immuno-PET applications are still in their infancy. The immuno-PET studies that have been performed consist mostly of animal model experiments, while clinical evaluations are rare. This can be attributed mainly to limited availability of suitable positron emitters, a lack of robust labeling methods, and the relatively small number of PET cameras in operation. An issue that still needs substantial attention is the evaluation of quantitative PET imaging techniques *in vivo*. Because PET is thought to be superior to SPECT with respect to quantification, several PET isotope analogues have been suggested as substitute for γ-emitting radionuclides as used in RIS. This should, at least in theory, enable easy conversion from a SPECT to a PET imaging procedure. PET isotope analogues of therapeutic β^--emitting radionuclides as used in RIT enable the application of a PET scouting procedure prior to therapy. Examples of analogous PET/SPECT isotope pairs are ^{124}I / ^{123}I, and ^{94m}Tc / ^{99m}Tc, while examples of analogous PET/RIT isotope pairs are ^{124}I / ^{131}I, ^{86}Y / ^{90}Y and ^{64}Cu / ^{67}Cu.

In the early 1990s, research groups started labeling MAbs with the positron emitter ^{18}F[241-246]. ^{18}F has been by far the most widely available and applied positron emitter, which explains why in early days it was not only used for the labeling of MAb fragments, but also for labeling of intact MAbs in spite of its short half-life (1.83 h). ^{18}F-labeled Mel-14 $F(ab')_2$ was evaluated for biodistribution in glioma-bearing nude mice[244]. Neither maximum tumor uptake nor maximum tumor-to-nontumor ratios were achieved, however, during the first 6 h after injection. Choi *et al.*[247] labeled an anti-Tac dsFv fragment with ^{18}F, and showed a maximum accumulation of these conjugates in ATAC4 xenografts at 45-90 min after injection, indicating that the biological half-life of such small fragments is more compatible with the physical half-life of ^{18}F. No PET evaluation was performed with aforementioned conjugates. Due to the short half-life of ^{18}F and inefficient labeling, high doses of ^{18}F are needed for the preparation of the conjugate. For the preparation of 300 MBq of ^{18}F-labeled MAb fragment, Zalutsky *et al.*[245] had to start with 3.7 GBq ^{18}F for the 80-90 min taking synthesis.

Other short-lived positron emitters are ^{94m}Tc and ^{68}Ga. The approved imaging agent CEA-scan, supplied as an instant kit containing lyophilized NP-4 antibody F(ab') for labeling with ^{99m}Tc (Table 1), was used for coupling of ^{94m}Tc instead[248]. Although ^{94m}Tc and ^{99m}Tc form an analogous isotope pair, labeling results were different as NP-4-F(ab') contained much more reoxidized NP-4-$F(ab')_2$ in case of ^{94m}Tc. Ideally, for the 0.87 h half-life of ^{94m}Tc, the percentage of the biologically longer lived $F(ab')_2$ should be kept to a minimum. The authors concluded that labeling procedures had to be modified to prevent reoxidation of F(ab') thiol groups. No *in vivo* evaluation of these conjugates was performed.

Due to its short half-life of 1.13 h, the positron emitter ^{68}Ga is most suitable for the labeling of small MAb fragments (scFv) or for use in pretargeting strategies. Pretargeted PET with ^{68}Ga has been evaluated in mice bearing CD44v6- and MUC1-expressing tumors[249-251] and in patients with breast cancer[252]. In the latter study, patients received 10 mg anti-MUC1/anti-Ga-chelate bispecific antibody (Bs-MAb), followed 18 h later by 10.7 mg of a

blocker to remove residual circulating Bs-MAb from the blood, and 15 min later 9.6 μg of the chelate labeled with 230–300 MBq ^{68}Ga. PET imaging was started 60-90 min after injection of the ^{68}Ga-chelate. Average tumor-to-blood ratios and tumor-to-normal breast tissue ratios were 0.9 and 3.0 at 1 h after injection. In ten patients, 14 of 17 known breast lesions, ranging from 10–80 mm in size were clearly visualized as foci with increased activity with PET. No false-positive but three false-negative readings were obtained. Detection of axillary lymph node metastases was hampered by a high activity in blood vessels located proximately to the lymph nodes. The authors stated that PET imaging offered better sensitivity for the detection of breast cancer at low tumor contrast than conventional immunoscintigraphy. This was demonstrated by the clear visualization of tumor sites 10 mm in size, which contrasted only by a factor of 2 from surrounding normal breast tissue. Despite these promising initial results, the anti-MUC1 Bs-MAb used in this study was considered to be far from optimal due to its low affinity for the tumor antigen ($1.2x10^{-7}$ M^{-1}) and the nonspecific distribution of shed antigen.

Positron emitters suggested for immuno-PET with a half-life of several hours, but less than one day, are ^{64}Cu, ^{86}Y, and ^{76}Br. The positron emitter ^{64}Cu has been coupled to the intact anti-colorectal mMAb 1A3 and patients with suspected advanced primary or metastatic colorectal cancer were subjected to immuno-PET[253]. Intact mMAb was used for this study because previous studies had shown high renal uptake of ^{64}Cu-labeled F(ab')$_2$ fragments. After injection of the conjugate (5-20 mg mMAb, 370 MBq ^{64}Cu), PET was performed once or twice, 4 to 36 h later. All 36 patients entered in this study had CT or MRI scans, while 18 patients were also studied with ^{18}FDG-PET. In 29 patients, one or more tumor sites (40 of 56 total) were proven with immuno-PET, in 5 patients absence of tumor was confirmed and in the remaining 2 patients tumor status was not yet confirmed. All 17 primary and recurrent sites were clearly visualized, but only 23 of 39 metastatic sites (59%) were detected. The sensitivity of immuno-PET was best in abdomen and pelvis, and in these regions 11 occult small tumor lesions were detected, including 9 small foci less than 2 cm in diameter that were not detected by CT or MRI. For the detection of abdominal-pelvic tumors immuno-PET exhibited superior sensitivity in comparison with CT and MRI, while it appeared as sensitive as ^{18}FDG-PET. In contrast, detection of metastatic disease of liver and lung was difficult, due to high blood pool activity at the early time points of imaging, which were chosen because of the short half-life of ^{64}Cu (12,7 h). Detection of liver metastases was also hampered by nontarget background activity, caused by ^{64}Cu residualizing in the liver after catabolism of the conjugate. Immuno-PET and ^{18}FDG-PET appeared particularly helpful for detecting smaller tumors, those less than 2 cm in maximum diameter. Whereas CT or MRI detected just 3 of 15 of such lesions, immuno-PET and ^{18}FDG-PET detected 11 of 15 and 10 of 10, respectively.

Recently, the genetically engineered anti-CEA T84.66/GS18 minibody has been labeled with ^{64}Cu via the DOTA chelate, and PET imaging of colorectal carcinoma xenograft-bearing nude mice was performed[254]. Tumors of 25–395 mg were visualized within a few hours after injection of the tracer. Also with these ^{64}Cu-conjugates high retention of activity in the liver was observed resulting in tumor-to-liver uptake ratios less than one. As this retention

would restrict the detection of hepatic lesions, the authors started the development of alternate linker chemistry for attachment of DOTA to MAbs and MAb fragments that would allow metabolism and subsequent clearance of activity. ^{64}Cu has also been used in a pretargeting strategy, consisting of the anti-Ep-CAM MAb NR-LU-10 conjugated with streptavidin and a ^{64}Cu-DOTA-biotin ligand[255]. In mice bearing colorectal carcinoma xenografts, a maximum tumor uptake was reached with this strategy at 1 h after injection. The tumor-to-blood ratio of areas under the curves was 14 times higher for pretargeted ^{64}Cu-DOTA-biotin than for conventionally labeled ^{64}Cu-DOTA-NR-LU-10. Although no PET imaging was performed in this study, superior PET imaging contrast might be expected when using the pretargeting strategy. Also in this study increased uptake of ^{64}Cu in the liver was observed, but uptake levels were much lower than in the tumor. The positron emitter ^{86}Y has been coupled to the anti-Lewis Y hMAb hu3S193[94] and the anti-HER2 hMAb Herceptin[214] (Table 2) and their biodistributions were compared with that of their respective ^{111}In-labeled MAbs. The rational for this comparison is that PET with ^{86}Y-MAb might be better qualified for predicting ^{90}Y-MAb localization and dose delivery in RIT studies than ^{111}In-MAb SPECT. Although biodistribution data from both studies indicate that this might be the case, accurate quantitation of ^{86}Y with PET still remains a challenge due to the prompt single γ-photons emitted by this positron emitter[94]. ^{76}Br has been coupled to the anti-CEA MAb 38S1 by Lövqvist *et al.* and biodistribution studies and PET imaging were performed in colon carcinoma xenograft-bearing nude rats and pigs[256-258]. In the group of halogens, ^{76}Br and ^{124}I are the only positron emitters potentially useful for labeling of intact MAbs, and the authors hypothesized that ^{76}Br might be an interesting alternative to ^{124}I as PET isotope substitute for the iodine radionuclides used in RIS and RIT. To this end ^{76}Br-38S1 and ^{125}I-38S1 were prepared by direct labeling, and their biodistribution compared in nude rats carrying human colon xenografts. While all tumors (weighing 0.5 g or more) could be readily identified by PET imaging from 46 h after administration of ^{76}Br-38S1, the concentration of ^{76}Br radioactivity in tumor, blood and normal tissues was higher than the corresponding ^{125}I concentration at all time points. This was mainly due to catabolism of radiolabeled MAb, resulting in free radiohalides, of which $^{76}Br^-$ was retained in the blood pool in contrast to the rapidly excreted $^{125}I^-$ ion. These data indicate that ^{76}Br can not be used as a PET isotope substitute for iodine radionuclides.

Two long-lived positron emitters are ^{124}I and ^{89}Zr. In the 1990s, several studies were performed with ^{124}I-labeled MAbs in animals and patients[224,231,259-266]. Snook *et al.*[260] evaluated the biodistribution of ^{124}I-labeled H17E2 in HEp2 xenograft-bearing nude mice, without comparison with ^{131}I-labeled H17E2 and without performing PET imaging. Similar studies were performed with ^{124}I-labeled rat MAb ICR 12 for the targeting of human breast carcinoma xenografts overexpressing the c-erb B2 proto-oncogene product[262]. This time PET imaging was performed, but without quantitative analyses. Tumor xenografts of 6 mm diameter were successfully delineated with high resolution at 24, 48 and 120 h after injection. Subcutaneous ovarian cancer xenografts with a similar size (at least 7 mm) were also detected in rat using immuno-PET with the ^{124}I-labeled MAbs MX35 and MAb MH99[265]. Clinical

immuno-PET studies with ^{124}I-labeled MAbs have been performed with only small numbers of patients[231,261]. Wilson *et al.*[261] used PET with ^{124}I-labeled mMAb HMFG1 for tumor detection in 7 breast cancer patients and for quantitative measurement of conjugate uptake in the tumors. In only 2 out of 7 patients the tumor uptake of the specific antibody was greater than that seen with the non-specific antibody, while tumor-to-blood ratios were consistently much lower than one. Therefore, it can be concluded that mMAb HMFG1 is not the MAb of choice for use in immuno-PET. After almost a decade, the interest in ^{124}I MAb labeling has been renewed. The CDR-grafted hMAb A33 has been labeled with ^{124}I and colon xenograft-bearing mice were imaged[232]. Biodistribution studies revealed excellent tumor uptake of 50.0 ± 0.7 %ID/g, with maximum uptake at 4 d after injection. PET imaging detected antigen positive tumors (ranging from 0.2 to 0.7 g) by 4 h after injection, and high-resolution images were obtained by 24 h after injection. In these studies, PET was not exploited for quantitative measurements. ^{124}I-labeled MAb VG76e, a MAb directed against the vascular endothelial growth factor (VEGF), has been evaluated with PET in fibrosarcoma xenograft-bearing nude mice[233]. Results from this study are difficult to interprete, however, as the immunoreactive fraction of the conjugate obtained by evaluating three different radiolabelings strategies did not exceed 34%. The ^{124}I-labeled anti-VEGF hMAb HuMV833 has been administered to patients with progressive solid tumors, to assess the biodistribution and biological effects of HuMV833[267]. In this study, the affinity of the MAb just slightly decreased upon coupling of ^{124}I, from 1.8×10^8 M^{-1} to 1.25×10^8 M^{-1}. PET analysis revealed that MAb distribution and clearance were markedly heterogeneous between and within patients and between and within tumors. HuMV833 distribution to normal tissues also varied among patients, but the MAb was cleared from these tissues in a homogeneous fashion. The authors conclude from their results that either intrapatient dose escalation approaches or larger, more precisely defined patient cohorts would be preferable in the design of phase I studies with anti-angiogenic compounds like HuMV833. This study illustrates the potential of noninvasive molecular imaging with PET in the clinical development of new biopharmaceuticals.

The positron emitter ^{89}Zr has been coupled to the mMAbs 323/A3 and E48[238]. The biodistribution of these radioimmunoconjugates in xenograft-bearing nude mice was similar to the biodistribution of ^{99m}Tc-labeled MAbs, whereas ^{123}I-labeled MAbs showed lower tumor uptake. Liver uptake was in all experiments higher for ^{89}Zr-labeled MAb. A preliminary PET study with ^{89}Zr-labeled mMAb 323/A3 visualized tumors as small as 50 mg at 55 h after injection. As stated before, it is questionable whether these conjugates were fully stable *in vivo*, due to the presence of a succinimide ring-thioether unit between MAb and chelate.

3 Aim and outline of the thesis

As described in the introductory **chapter 1**, the use of radiolabeled MAbs has been recognized as a realistic option for improvement of diagnosis and treatment of cancer. At our institute we are focusing on the use of radiolabeled MAbs for diagnosis and therapy of head and neck squamous cell carcinoma (HNSCC). To this end, mMAb U36 and mMAb BIWA 1 were selected as MAb candidates with high potential. Both mMAbs bind to overlapping epitopes in the variable domain v6 of the cell-surface antigen CD44. RIS with these mMAbs after labeling with ^{99m}Tc was found to be as valuable as the conventional imaging techniques CT and MRI, but the detection of tumor deposits smaller than 1 cm appeared to be a problem[268,269]. Subsequently, cMAb U36 was constructed and tested in clinical phase I dose escalation RIT trials. Although not the primary aim in phase I studies, promising anti-tumor effects were observed with ^{186}Re-cMAb U36 in inoperable HNSCC patients[92,153]. Variability was observed for ^{186}Re-cMAb U36 pharmacokinetics and tumor absorbed doses for patients treated at the same radioactivity dose level, indicating that individualization of therapy might be desirable. For all three MAbs (mMAb U36, cMAb U36, and mMAb BIWA 1) human anti-mouse or human anti-chimeric antibody responses (HAMA and HACA, respectively) were observed.

The present thesis aims the further improvement of RIS and RIT with anti-CD44v6 MAbs by engineering of anti-CD44v6 MAbs as well as by introduction of immuno-PET. Introduction of PET might improve the detection of small tumor deposits with MAbs because of its high resolution. In addition, PET has potential for quantitative imaging. These features should enable PET to provide proof of antibody targeting and dosimetric evaluations prior to RIT. For this purpose we started the exploration of the long-lived positron emitters ^{89}Zr and ^{124}I, as their physical half-life is compatible with the time needed for intact MAbs to achieve optimal tumor-to-nontumor ratios.

For clinical application of MAbs, two important parameters to consider are the MAb form and the affinity of the MAb. Due to immunogenicity of aforementioned MAbs, further reduction of the murine part of the MAb is strongly recommended. Such procedures, however, may result in MAbs with diminished affinity and affected tumor uptake. In **chapter 2**, the construction of a chimeric and two humanized derivatives of mMAb BIWA 1 is described. These MAbs were evaluated together with mMAb U36 for affinity to the antigen CD44v6 *in vitro* as well as for biodistribution and efficacy in RIT using xenograft-bearing nude mice. Such preclinical evaluation studies in animals await confirmation in patients. Confirmation in a clinical setting requires accurate noninvasive quantitation methods, one of the reasons to put effort in the improvement of immuno-PET. In these studies cMAb U36 was used as a model MAb for reasons of availability.

In order to qualify the potential of immuno-PET, robust radiolabeling procedures must be developed for the stable coupling of the long-lived positron emitters ^{89}Zr and ^{124}I to MAbs, with preservation of MAb integrity and immunoreactivity. In **chapter 3**, comprehensive procedures for reproducible isolation of highly pure ^{89}Zr and production of ^{89}Zr-labeled MAbs

are described. The *in vitro* stability of ^{89}Zr-labeled cMAb U36 was assessed and its *in vivo* behavior was evaluated by biodistribution and PET imaging studies in HNSCC xenograft-bearing nude mice.

The applicability of ^{89}Zr immuno-PET as scouting procedure prior to ^{90}Y-MAb RIT and its quantitative imaging performance was evaluated in **chapter 4**. The biodistribution of ^{89}Zr-labeled and ^{88}Y-labeled cMAb U36 (^{88}Y as substitute for ^{90}Y) was compared and ^{89}Zr phantom studies were performed to determine linearity, resolution, and recovery coefficients with a small animal high-resolution research tomograph (HRRT) PET scanner. Quantitation potential was evaluated by relating PET image-derived tumor uptake data to ^{89}Zr uptake data derived from excised tumors.

In **chapter 5**, two regeneration methods were introduced to regain ^{124}I in the iodide (I^-) form, and a procedure for radiolabeling of MAbs with ^{124}I is described. An essential aspect in this procedure is the minimizing of chemical and radiation damage to the MAb. ^{124}I-labeled cMAb U36 was evaluated in biodistribution studies and compared with ^{131}I-labeled cMAb U36, and selective uptake in HNSCC xenografts was confirmed by immuno-PET imaging.

Performing immuno-PET as a tracer imaging procedure prior to RIT enables the confirmation of tumor-targeting and the estimation of radiation dose delivery to both tumor and normal tissues. One of the requirements for such a scouting procedure is that the biodistribution of the diagnostic and therapeutic radioimmunoconjugate should be similar. To evaluate and compare the potential of ^{89}Zr and ^{124}I for scouting purposes, in **chapter 6** the *in vivo* behavior of ^{89}Zr-labeled and ^{124}I-labeled cMAb U36 was studied, together with that of cMAb U36 labeled with the therapeutic radionuclides ^{88}Y (substituting ^{90}Y), ^{131}I, and ^{186}Re in HNSCC xenograft-bearing nude mice.

REFERENCES

1. Himmelweit B (ed). *The collected papers of Paul Ehrlich*. Elmsford, NY: Pergamon Press; 1975.
2. Köhler G, Milstein C. Continuous cultures of fused cells secreting antibody of predefined specificity. *Nature*. 1975;256:495-497.
3. Kyriakos RJ, Shih LB, Ong GL, Patel K, Goldenberg DM, Mattes MJ. The fate of antibodies bound to the surface of tumor cells in vitro. *Cancer Res*. 1992;52:835-842.
4. Mattes MJ, Griffiths GL, Diril H, Goldenberg DM, Ong GL, Shih LB. Processing of antibody-radioisotope conjugates after binding to the surface of tumor cells. *Cancer*. 1994;73:787-793.
5. Khazaeli MB, Conry RM, LoBuglio AF. Human immune response to monoclonal antibodies. *J Immunother*. 1994;15:42-52.
6. DeNardo GL, Bradt BM, Mirick GR, DeNardo SJ. Human antiglobulin response to foreign antibodies: therapeutic benefit? *Cancer Immunol Immunother*. 2003;52:309-316.
7. Morrison SL, Johnson MJ, Herzenberg LA, Oi VT. Chimeric human antibody molecules: mouse antigen-binding domains with human constant region domains. *Proc Natl Acad Sci USA*. 1984;81:6851-6855.
8. Jones PT, Dear PH, Foote J, Neuberger MS, Winter G. Replacing the complementarity-determining regions in a human antibody with those from a mouse. *Nature*. 1986;321:522-525.
9. Marks JD, Hoogenboom HR, Bonnert TP, McCafferty J, Griffiths AD, Winter G. By-passing immunization. Human antibodies from V-gene libraries displayed on phage. *J Mol Biol*. 1991;222:581-597.
10. Griffiths AD, Williams SC, Hartley O, Tomlinson IM, Waterhouse P, Crosby WL, Kontermann RE, Jones PT, Low NM, Allison TJ. Isolation of high affinity human antibodies directly from large synthetic repertoires. *EMBO J*. 1994;13:3245-3260.
11. Vaughan TJ, Williams AJ, Pritchard K, Osbourn JK, Pope AR, Earnshaw JC, McCafferty J, Hodits RA, Wilton J, Johnson KS. Human antibodies with sub-nanomolar affinities isolated from a large non-immunized phage display library. *Nat Biotechnol*. 1996;14:309-314.
12. Fishwild DM, O'Donnell SL, Bengoechea T, Hudson DV, Harding F, Bernhard SL, Jones D, Kay RM, Higgins KM, Schramm SR, Lonberg N. High-avidity human IgG kappa monoclonal antibodies from a novel strain of minilocus transgenic mice. *Nat Biotechnol*. 1996;14:845-851.
13. Mendez MJ, Green LL, Corvalan JRF, Jia X-C, Maynard-Currie CE, Yang X-D, Gallo ML, Louie DM, Lee DV, Erickson KL, Luna J, Roy CM-N, Abderrahim H, Kirschenbaum F, Noguchi M, Smith DH, Fukushima A, Hales JF, Klapholz S, Finer MH, Davis CG, Zsebo KM, Jakobovits A. Functional transplant of megabase human immunoglobulin loci recapitulates human antibody response in mice. *Nat Genet*. 1997;15:146-156.
14. Kellermann S-A, Green LL. Antibody discovery: the use of transgenic mice to generate human monoclonal antibodies for therapeutics. *Curr Opin Biotechnol*. 2002;13:593-597.
15. Frenken LGJ, Hessing JGM, Van den Hondel CAMJJ, Verrips CT. Recent advances in the large-scale production of antibody fragments using lower eukaryotic microorganisms. *Res. Immunol*. 1998;149:589-599.
16. Verma R, Boleti E, George AJT. Antibody engineering: comparison of bacterial, yeast, insect and mammalian expression systems. *J Immunol Methods*. 1998;216:165-181.

17. Hood EE, Woodard SL, Horn ME. Monoclonal antibody manufacturing in transgenic plants – myths and realities. *Curr Opin Biotechnol.* 2002;13:630-635.
18. Houdebine L-M. Antibody manufacture in transgenic animals and comparisons with other systems. *Curr Opin Biotechnol.* 2002;13:625-629.
19. Goldenberg DM. Targeted therapy of cancer with radiolabeled antibodies. *J Nucl Med.* 2002;43:693-713.
20. Yokota T, Milenic DE, Whitlow M, Schlom J. Rapid tumor penetration of a single-chain Fv and comparison with other immunoglobulin forms. *Cancer Res.* 1992;15:3402-3408.
21. Milenic DE, Yokota T, Filpula DR, Finkelman MA, Dodd SW, Wood JF, Whitlow M, Snoy P, Schlom J. Construction, binding properties, metabolism, and tumor targeting of a single-chain Fv derived from the pancarcinoma monoclonal antibody CC49. *Cancer Res.* 1991;51:6363-6371.
22. Colcher D, Pavlinkova G, Beresford G, Booth BJ, Batra SK. Single-chain antibodies in pancreatic cancer. *Ann NY Acad Sci.* 1999;880:263-280.
23. Kortt AA, Dolezal O, Power BE, Hudson PJ. Dimeric and trimeric antibodies: high avidity scFvs for cancer targeting. *Biomol Eng.* 2001;18:95-108.
24. Hu S, Shively L, Raubitschek A, Sherman M, Williams LE, Wong JY, Shively JE, Wu AM. Minibody: A novel engineered anti-carcinoembryonic antigen antibody fragment (single-chain Fv-CH3) which exhibits rapid, high-level targeting of xenografts. *Cancer Res.* 1996;56:3055-3061.
25. Nielsen UB, Adams GP, Weiner LM, Marks JD. Targeting of bivalent anti-ErbB2 diabody antibody fragments to tumor cells is independent of the intrinsic antibody affinity. *Cancer Res.* 2000;60:6434-6440.
26. Osbourn JK, Field A, Wilton J, Derbyshire E, Earnshaw JC, Jones PT, Allen D, McCafferty J. Generation of a panel of related human scFv antibodies with high affinities for human CEA. *Immunotechnology.* 1996;2:181-196.
27. Adams GP, Schier R, McCall AM, Simmons HH, Horak EM, Alpaugh RK, Marks JD, Weiner LM. High affinity restricts the localization and tumor penetration of single-chain Fv antibody molecules. *Cancer Res.* 2001;61:4750-4755.
28. Jackson H, Bacon L, Pedley RB, Derbyshire E, Field A, Osbourn J, Allen D. Antigen specificity and tumour targeting efficiency of a human carcinoembryonic antigen-specific scFv and affinity-matured derivatives. *Br J Cancer.* 1998;78:181-188
29. Kang NV, Hamilton S, Sanders R, Wilson GD, Kupsch JM. Efficient in vivo targeting of malignant melanoma by single-chain Fv antibody fragments. *Melanoma Res.* 1999;9:545-556.
30. Schott ME, Milenic DE, Yokota T, Whitlow M, Wood JF, Fordyce WA, Cheng RC, Schlom J. Differential metabolic patterns of iodinated versus radiometal chelated anticarcinoma single-chain Fv molecules. *Cancer Res.* 1992;52:6413-6417.
31. Yokota T, Milenic DE, Whitlow M, Wood JF, Hubert SL, Schlom J. Microautoradiographic analysis of the normal organ distribution of radioiodinated single-chain Fv and other immunoglobulin forms. *Cancer Res.* 1993;53:3776-3783.
32. Yazaki PJ, Wu AM, Tsai SW, Williams LE, Ikler DN, Wong JY, Shively JE, Raubitschek AA. Tumor targeting of radiometal labeled anti-CEA recombinant T84.66 diabody and T84.66 minibody: comparison to radioiodinated fragments. *Bioconjug Chem.* 2001;12:220-228.

33. Colcher D, Minelli MF, Roselli M, Muraro R, Simpson-Milenic D, Schlom J. Radioimmunolocalization of human carcinoma xenografts with B72.3 second generation monoclonal antibodies. *Cancer Res.* 1988;48:4597-4603.
34. Schlom J, Eggensperger D, Colcher D, Molinolo A, Houchens D, Miller LS, Hinkle G, Siler K. Therapeutic advantage of high-affinity anticarcinoma radioimmunoconjugates. *Cancer Res.* 1992;52:1067-1072.
35. Velders MP, Van Rhijn CM, Briaire IH, Fleuren GJ, Warnaar SO, Litvinov SV. Immunotherapy with low and high affinity monoclonal antibodies 17-1A and 323/A3 in a nude mouse xenograft carcinoma model. *Cancer Res.* 1995;55:4398-4403.
36. Kievit E, Pinedo HM, Schlüper HMM, Haisma HJ, Boven E. Comparison of the monoclonal antibodies 17-1A and 323/A3: the influence of the affinity on tumour uptake and efficacy of radioimmunotherapy in human ovarian cancer xenografts. *Br J Cancer.* 1996;73:457-464.
37. Adams GP, Schier R, Marshall K, Wolf EJ, McCall AM, Marks JD, Weiner LM. Increased affinity leads to improved selective tumor delivery of single-chain Fv antibodies. *Cancer Res.* 1998;58:485-490.
38. Fujimori K, Covell DG, Fletcher JE, Weinstein JN. A modeling analysis of monoclonal antibody percolation through tumors: a binding-site barrier. *J Nucl Med.* 1990;31:1191-1198.
39. Juweid M, Neumann R, Paik C, Perez-Bacete MJ, Sato J, van Osdol W, Weinstein JN. Micropharmacology of monoclonal antibodies in solid tumors: direct experimental evidence for a binding site barrier. *Cancer Res.* 1992;52:5144-5153.
40. Sung C, Shockley TR, Morrison PF, Dvorak HF, Yarmush ML, Dedrick RL. Predicted and observed effects of antibody affinity and antigen density on monoclonal antibody uptake in solid tumors. *Cancer Res.* 1992;52:377-384.
41. Graff CP, Wittrup KD. Theoretical analysis of antibody targeting of tumor spheroids: importance of dosage for penetration, and affinity for retention. *Cancer Res.* 2003;63:1288-1296.
42. Jain RK. Transport of molecules, particles, and cells in solid tumors. *Annu Rev Biomed Eng.* 1999;1:241-263.
43. Cobb LM. Intratumour factors influencing the access of antibody to tumour cells. *Cancer Immunol Immunother.* 1989;28:235-240.
44. Roberts WG, Delaat J, Nagane M, Huang S, Cavenee WK, Palade GE. Host microvasculature influence on tumor vascular morphology and endothelial gene expression. *Am J Pathol.* 1998;153:1239-1248.
45. Gray LH, Conger AD, Ebert M, Hornsey S, Scott OC. Concentration of oxygen dissolved in tissues at the time of irradiation as a factor in radiotherapy. *Br J Radiol.* 1953;26:638-648.
46. Brown JM, Giaccia AJ. The unique physiology of solid tumors: opportunities (and problems) for cancer therapy. *Cancer Res.* 1998;58:1408-1416.
47. Netti PA, Berk DA, Swartz MA, Grodzinsky AJ, Jain RK. Role of extracellular matrix assembly in interstitial transport in solid tumors. *Cancer Res.* 2000;60:2497-2503.
48. Pluen A, Boucher Y, Ramanujan S, McKee TD, Gohongi T, di Tomaso E, Brown EB, Izumi Y, Campbell RB, Berk DA, Jain RK. Role of tumor-host interactions in interstitial diffusion of macromolecules: cranial vs. subcutaneous tumors. *Proc Natl Acad Sci USA.* 2001;98:4628-4633.

49. Davies CdeL, Berk DA, Pluen A, Jain RK. Comparison of IgG diffusion and extracellular matrix composition in rhabdomyosarcomas grown in mice versus in vitro as spheroids reveals the role of host stromal cells. *Br J Cancer.* 2002;86:1639-1644.
50. Farah RA, Clinchy B, Herrera L, Vitetta ES. The development of monoclonal antibodies for the therapy of cancer. *Crit Rev Eukaryot Gene Expr.* 1998;8:321-356.
51. Peterson JA, Couto JR, Taylor MR, Ceriani RL. Selection of tumor-specific epitopes on target antigens for radioimmunotherapy of breast cancer. *Cancer Res.* 1995;55:5847s-5851s.
52. Halin C, Zardi L, Neri D. Antibody-based targeting of angiogenesis. *News Physiol Sci.* 2001;16:191-194.
53. Dvorak HF, Nagy JA, Dvorak AM. Structure of solid tumors and their vasculature: implications for therapy with monoclonal antibodies. *Cancer Cells.* 1991;3:77-85.
54. Burrows FJ, Thorpe PE. Eradication of large solid tumors in mice with an immunotoxin directed against tumor vasculature. *Proc Natl Acad Sci USA.* 1993;90:8996-9000.
55. Huang X, Molema G, King S, Watkins L, Edgington TS, Thorpe PE. Tumor infarction in mice by antibody-directed targeting of tissue factor to tumor vasculature. *Science.* 1997;275:547-550.
56. Nilsson F, Kosmehl H, Zardi L, Neri D. Targeted delivery of tissue factor to the ED-B domain of fibronectin, a marker of angiogenesis, mediates the infarction of solid tumors in mice. *Cancer Res.* 2001;61:711-716.
57. Mathiassen S, Lauemoller SL, Ruhwald M, Claesson MH, Buus S. Tumor-associated antigens identified by mRNA expression profiling induce protective anti-tumor immunity. *Eur J Immunol.* 2001;31:1239-1246.
58. Le Naour F. Contribution of proteomics to tumor immunology. *Proteomics.* 2001;1:1295-1302.
59. Nelson PS. Identifying immunotherapeutic targets for prostate carcinoma through the analysis of gene expression profiles. *Ann NY Acad Sci.* 2002;975:232-246.
60. Allen TM. Ligand-targeted therapeutics in anticancer therapy. *Nat Rev Cancer.* 2002;2:750-763.
61. Von Mehren M, Adams GP, Weiner LM. Monoclonal antibody therapy for cancer. *Annu Rev Med.* 2003;54:343-369.
62. Gallup DG. Multicenter clinical trial of ^{111}In-CYT-103 in patients with ovarian cancer. *Targeted Diagn Ther.* 1992;6:111-124.
63. Abdel-Nabi HH, Doerr RJ. Multicenter clinical trials of monoclonal antibody B72.3-GYK-DTPA ^{111}In (^{111}In-CYT-103; OncoScint CR103) in patients with colorectal carcinoma. *Targeted Diagn Ther.* 1992;6:73-88.
64. Moffat FL Jr, Pinsky CM, Hammershaimb L, Petrelli NJ, Patt YZ, Whaley FS, Goldenberg DM. Clinical utility of external immunoscintigraphy with the IMMU-4 technetium-99m Fab' antibody fragment in patients undergoing surgery for carcinoma of the colon and rectum: results of a pivotal, phase III trial. *J Clin Oncol.* 1996;14:2295-2305.
65. Bhattacharya S, Lahiri A. Clinical role of indium-111 antimyosin imaging. *Eur J Nucl Med.* 1991;18:889-895.
66. Balaban EP, Walker BS, Cox JV, Bordlee RP, Salk D, Abrams PG, Sheehan RG, Frenkel EP. Detection and staging of small cell lung carcinoma with a technetium-labeled monoclonal antibody. A comparison with standard staging methods. *Clin Nucl Med.* 1992;17:439-445.

67. Vansant JP, Johnson DH, O'Donnell DM, Stewart JR, Sonin AH, McCook BM, Powers TA, Salk DJ, Frist WH, Sandler MP. Staging lung carcinoma with a Tc-99m labeled monoclonal antibody. *Clin Nucl Med.* 1992;17:431-438.
68. Lamb HM, Faulds D. Capromab pendetide. A review of its use as an imaging agent in prostate cancer. *Drugs Aging.* 1998;12:293-304.
69. Zuckier LS, DeNardo GL. Trials and tribulations: oncological antibody imaging comes to the fore. *Semin Nucl Med.* 1997;27:10-29.
70. Kamath S, Dean D, Peddi VR, Schroeder TJ, Alexander JW, Cavallo T, First MR. Primary therapy with OKT3 for biopsy-proven acute renal allograft rejection. *Transplant Proc.* 1998;30:1178-1180.
71. Henry ML, Pelletier RP, Elkhammas EA, Bumgardner GL, Davies EA, Ferguson RM. A randomized prospective trial of OKT3 induction in the current immunosuppression era. *Clin Transplant.* 2001;15:410-414.
72. Ibbotson T, McGavin JK, Goa KL. Abciximab: an updated review of its therapeutic use in patients with ischaemic heart disease undergoing percutaneous coronary revascularisation. *Drugs.* 2003;63:1121-1163.
73. Bosly A, Keating MJ, Stasi R, Bradstock K. Rituximab in B-cell disorders other than non-Hodgkin's lymphoma. *Anticancer Drugs.* 2002;13:S25-S33.
74. Plosker GL, Figgitt DP. Rituximab: a review of its use in non-Hodgkin's lymphoma and chronic lymphocytic leukaemia. *Drugs.* 2003;63:803-843.
75. Carswell CI, Plosker GL, Wagstaff AJ. Daclizumab: a review of its use in the management of organ transplantation. *BioDrugs.* 2001;15:745-773.
76. Onrust SV, Wiseman LR. Basiliximab. *Drugs.* 1999;57:207-214.
77. Romero JR. Palivizumab prophylaxis of respiratory syncytial virus disease from 1998 to 2002: results from four years of palivizumab usage. *Pediatr Infect Dis J.* 2003;22:S46-54.
78. Braun J, Sieper J. Overview of the use of the anti-TNF agent infliximab in chronic inflammatory diseases. *Expert Opin Biol Ther.* 2003;3:141-168.
79. Lewis R, Bagnall AM, Forbes C, Shirran E, Duffy S, Kleijnen J, Riemsma R, ter Riet G. The clinical effectiveness of trastuzumab for breast cancer: a systematic review. *Health Technol Assess.* 2002;6:1-71.
80. Berger MS, Leopold LH, Dowell JA, Korth-Bradley JM, Sherman ML. Licensure of gemtuzumab ozogamicin for the treatment of selected patients 60 years of age or older with acute myeloid leukemia in first relapse. *Invest New Drugs.* 2002;20:395-406.
81. Osterborg A, Mellstedt H, Keating M. Clinical effects of alemtuzumab (Campath-1H) in B-cell chronic lymphocytic leukemia. *Med Oncol.* 2002;19:S21-S26.
82. Rai K, Hallek M. Future prospects for alemtuzumab (MabCampath). *Med Oncol.* 2002;19:S57-S63.
83. Wiseman GA, White CA, Sparks RB, Erwin WD, Podoloff DA, Lamonica D, Bartlett NL, Parker JA, Dunn WL, Spies SM, Belanger R, Witzig TE, Leigh BR. Biodistribution and dosimetry results from a phase III prospectively randomized controlled trial of Zevalin™ radioimmunotherapy for low-grade, follicular, or transformed B-cell non-Hodgkin's lymphoma. *Crit Rev Oncol Hematol.* 2001;39:181-194.
84. Rau R. Adalimumab (a fully human anti-tumour necrosis factor α monoclonal antibody) in the treatment of active rheumatoid arthritis: the initial results of five trials. *Ann Rheum Dis.* 2002;61:ii70-ii73.

85. Buhl R, Soler M, Matz J, Townley R, O'Brien J, Noga O, Champain K, Fox H, Thirlwell J, Della Cioppa G. Omalizumab provides long-term control in patients with moderate-to-severe allergic asthma. *Eur Respir J.* 2002;20:73-78.

86. Witzig TE, Gordon LI, Cabanillas F, Czuczman MS, Emmanouilides C, Joyce R, Pohlman BL, Bartlett NL, Wiseman GA, Padre N, Grillo-López AJ, Multani P, White CA. Randomized controlled trial of yttrium-90-labeled ibritumomab tiuxetan radioimmunotherapy versus rituximab immunotherapy for patients with relapsed or refractory low-grade, follicular, or transformed B-cell non-Hodgkin's lymphoma. *J Clin Oncol.* 2002;20:2453-2463.

87. Vose JM, Wahl RL, Saleh M, Rohatiner AZ, Knox SJ, Radford JA, Zelenetz AD, Tidmarsh GF, Stagg RJ, Kaminski MS. Multicenter phase II study of iodine-131 tositumomab for chemotherapy-relapsed/refractory low-grade and transformed low-grade B-cell non-Hodgkin's lymphomas. *J Clin Oncol.* 2000;18:1316-1323.

88. DeNardo GL, Juweid ME, White CA, Wiseman GA, DeNardo SJ. Role of radiation dosimetry in radioimmunotherapy planning and treatment dosing. *Crit Rev Oncol Hematol.* 2001;39:203-218.

89. Seldin DW. Techniques for using Bexxar for the treatment of non-Hodgkin's lymphoma. *J Nucl Med Technol.* 2002;30:109-114.

90. Press OW, Shan D, Howell-Clark J, Eary J, Appelbaum FR, Matthews D, King DJ, Haines AMR, Hamann P, Hinman L, Shochat D, Bernstein ID. Comparative metabolism and retention of iodine-125, yttrium-90, and indium-111 radioimmunoconjugates by cancer cells. *Cancer Res.* 1996;56:2123-2129.

91. Breitz HB, Fisher DR, Weiden PL, Durham JS, Ratliff BA, Bjorn MJ, Beaumier PL, Abrams PG. Dosimetry of rhenium-186-labeled monoclonal antibodies: methods, prediction from Technetium-99m-labeled antibodies and results of phase I trials. *J Nucl Med.* 1993;34:908-917.

92. Colnot DR, Quak JJ, Roos JC, van Lingen A, Wilhelm AJ, van Kamp GJ, Huijgens PC, Snow GB, van Dongen GAMS. Phase I therapy study of ^{186}Re-labeled chimeric monoclonal antibody U36 in patients with squamous cell carcinoma of the head and neck. *J Nucl Med.* 2000;41:1999-2010.

93. Carrasquillo JA, White JD, Paik CH, Raubitschek A, Le N, Rotman M, Brechbiel MW, Gansow OA, Top LE, Perentesis P, Reynolds JC, Nelson DL, Waldmann TA. Similarities and differences in ^{111}In- and ^{90}Y-labeled 1B4M-DTPA antiTac monoclonal antibody distribution. *J Nucl Med.* 1999;40:268-276.

94. Lövqvist A, Humm JL, Sheikh A, Finn RD, Koziorowski J, Ruan S, Pentlow KS, Jungbluth A, Welt S, Lee FT, Brechbiel MW, Larson SM. PET imaging of ^{86}Y-labeled anti-Lewis Y monoclonal antibodies in a nude mouse model: comparison between ^{86}Y and ^{111}In radiolabels. *J Nucl Med.* 2001;42:1281-1287.

95. O'Donoghue JA, Bardiès M, Wheldon TE. Relationships between tumor size and curability for uniformly targeted therapy with beta-emitting radionuclides. *J Nucl Med.* 1995;36:1902-1909.

96. Behr TM, Béhé M, Löhr M, Sgouros G, Angerstein C, Wehrmann E, Nebendahl K, Becker W. Therapeutic advantages of Auger electron- over β-emitting radiometals or radioiodine when conjugated to internalizing antibodies. *Eur J Nucl Med.* 2000;27:753-765.

97. Meredith RF, Khazaeli MB, Plott WE, Spencer SA, Wheeler RH, Brady LW, Woo DV, LoBuglio AF. Initial clinical evaluation of iodine-125-labeled chimeric 17-1A for metastatic colon cancer. *J Nucl Med.* 1995;36:2229-2233.

98. Welt S, Scott AM, Divgi CR, Kemeny NE, Finn RD, Daghighian F, Germain JS, Richards EC, Larson SM, Old LJ. Phase I/II study of iodine 125-labeled monoclonal antibody A33 in patients with advanced colon cancer. *J Clin Oncol.* 1996;14:1787-1797.

99. Breitz HB, Weiden PL, Vanderheyden J-L, Appelbaum JW, Bjorn MJ, Fer MF, Wolf SB, Ratliff BA, Seiler CA, Foisie DC, Fisher DR, Schroff RW, Fritzberg AR, Abrams PG. Clinical experience with rhenium-186-labeled monoclonal antibodies for radioimmunotherapy: results of phase I trials. *J Nucl Med.* 1992;33:1099-1109.

100. Juweid M, Sharkey RM, Swayne LC, Griffiths GL, Dunn R, Goldenberg DM. Pharmacokinetics, dosimetry and toxicity of rhenium-188-labeled anti-carcinoembryonic antigen monoclonal antibody, MN-14, in gastrointestinal cancer. *J Nucl Med.* 1998;39:34-42.

101. Buchmann I, Bunjes D, Kotzerke J, Martin H, Glatting G, Seitz U, Rattat D, Buck A, Dohner H, Reske SN. Myeloablative radioimmunotherapy with Re-188-anti-CD66-antibody for conditioning of high-risk leukemia patients prior to stem cell transplantation: biodistribution, biokinetics and immediate toxicities. *Cancer Biother Radiopharm.* 2002;17:151-163.

102. DeNardo SJ, DeNardo GL, Kukis DL, Shen S, Kroger LA, DeNardo DA, Goldstein DS, Mirick GR, Salako Q, Mausner LF, Srivastava SC, Meares CF. ^{67}Cu-2IT-BAT-Lym-1 pharmacokinetics, radiation dosimetry, toxicity and tumor regression in patients with lymphoma. *J Nucl Med.* 1999;40:302-310.

103. Novak-Hofer I, Schubiger PA. Copper-67 as a therapeutic nuclide for radioimmunotherapy. *Eur J Nucl Med.* 2002;29:821-830.

104. Mulligan T, Carrasquillo JA, Chung Y, Milenic DE, Schlom J, Feuerstein I, Paik C, Perentesis P, Reynolds J, Curt G. Phase I study of intravenous Lu-labeled CC49 murine monoclonal antibody in patients with advanced adenocarcinoma. *Clin Cancer Res.* 1995;1:1447-1454.

105. Meredith RF, Alvarez R, Khazaeli MB, LoBuglio A. Intraperitoneal radioimmunotherapy for refractory epithelial ovarian cancer with ^{177}Lu-CC49. *Min Biotechnol.* 1998;10:100-107.

106. McDevitt MR, Sgouros G, Finn RD, Humm JL, Jurcic JG, Larson SM, Scheinberg DA. Radioimmunotherapy with alpha-emitting nuclides. *Eur J Nucl Med.* 1998;25:1341-1351.

107. Andersson H, Palm S, Lindegren S, Back T, Jacobsson L, Leser G, Horvath G. Comparison of the therapeutic efficacy of ^{211}At- and ^{131}I-labelled monoclonal antibody MOv18 in nude mice with intraperitoneal growth of human ovarian cancer. *Anticancer Res.* 2001;21:409-412.

108. McDevitt MR, Ma D, Lai LT, Simon J, Borchardt P, Frank RK, Wu K, Pellegrini V, Curcio MJ, Miederer M, Bander NH, Scheinberg DA. Tumor therapy with targeted atomic nanogenerators. *Science.* 2001;294:1537-1540.

109. Sgouros G, Ballangrud AM, Jurcic JG, McDevitt MR, Humm JL, Erdi YE, Mehta BM, Finn RD, Larson SM, Scheinberg DA. Pharmacokinetics and dosimetry of an alpha-particle emitter labeled antibody: ^{213}Bi-HuM195 (anti-CD33) in patients with leukemia. *J Nucl Med.* 1999;40:1935-1946.

110. McDevitt MR, Barendswaard E, Ma D, Lai L, Curcio MJ, Sgouros G, Ballangrud ÅM, Yang W-H, Finn RD, Pellegrini V, Geerlings MW Jr, Lee M, Brechbiel MW, Bander NH, Cordon-Cardo C, Scheinberg DA. An α-particle emitting antibody ([^{213}Bi]J591) for radioimmunotherapy of prostate cancer. *Cancer Res.* 2000;60:6095-6100.

111. Geissler F, Anderson SK, Press O. Intracellular catabolism of radiolabeled anti-CD3 antibodies by leukemic T cells. *Cell Immunol.* 1991;137:96-110.

112. Shih LB, Thorpe SR, Griffiths GL, Diril H, Ong GL, Hansen HJ, Goldenberg DM, Mattes MJ. The processing and fate of antibodies and their radiolabels bound to the surface of tumor cells in vitro: a comparison of nine radiolabels. *J Nucl Med.* 1994;35:899-908.

113. Zalutsky MR, Garg PK, Narula AS. Labeling monoclonal antibodies with halogen nuclides. *Acta Radiol Suppl.* 1990;374:141-145.

114. Stein R, Govindan SV, Chen S, Reed L, Richel H, Griffiths GL, Hansen HJ, Goldenberg DM. Radioimmunotherapy of a human lung cancer xenograft with monoclonal antibody RS7: evaluation of ^{177}Lu and comparison of its efficacy with that of ^{90}Y and residualizing ^{131}I. *J Nucl Med.* 2001;42:967-974.

115. Fritzberg AR, Abrams PG, Beaumier PL, Kasina S, Morgan AC, Rao TN, Reno JM, Sanderson JA, Srinivasan A, Wilbur DS, Vanderheyden J-L. Specific and stable labeling of antibodies with technetium-99m with a diamide dithiolate chelating agent. *Proc Natl Acad Sci USA.* 1988;85:4025-4029.

116. Goldrosen MH, Biddle WC, Pancook J, Bakshi S, Vanderheyden J-L, Fritzberg AR, Morgan AC Jr, Foon KA. Biodistribution, pharmacokinetic, and imaging studies with Re-186-labeled NR-LU-10 whole antibody in LS174T colonic tumor-bearing mice. *Cancer Res.* 1990;50:7973-7978.

117. Najafi A, Alauddin MM, Sosa A, Ma GQ, Chen DC, Epstein AL, Siegel ME. The evaluation of ^{186}Re-labeled antibodies using N_2S_4 chelate in vitro and in vivo using tumor-bearing nude mice. *Int J Rad Appl Instrum B.* 1992;19:205-212.

118. Visser GWM, Gerretsen M, Herscheid JDM, Snow GB, van Dongen GAMS. Labeling of monoclonal antibodies with ^{186}Re using the MAG3 chelate for radioimmunotherapy of cancer: a technical protocol. *J Nucl Med.* 1993;34:1953-1963.

119. Harrison A, Walker CA, Parker D, Jankowski KJ, Cox JPL, Craig AS, Sansom JM, Beeley NRA, Boyce RA, Chaplin L, Eaton MAW, Farnsworth APH, Millar K, Millican AT, Randall AM, Rhind SK, Secher DS, Turner A. The in vivo release of ^{90}Y from cyclic and acyclic ligand-antibody conjugates. *Int J Rad Appl Instrum B.* 1991;18:469-476.

120. Chinn PC, Leonard JE, Rosenberg J, Hanna N, Anderson DR. Preclinical evaluation of ^{90}Y-labeled anti-CD20 monoclonal antibody for treatment of non-Hodgkin's lymphoma. *Int J Oncol.* 1999;15:1017-1025.

121. DeNardo SJ, Kramer EL, O'Donnell RT, Richman CM, Salako QA, Shen S, Noz M, Glenn SD, Ceriani RL, DeNardo GL. Radioimmunotherapy for breast cancer using indium-111/yttrium-90 BrE-3: results of a phase I clinical trial. *J Nucl Med.* 1997;38:1180-1185.

122. Pai-Scherf LH, Carrasquillo JA, Paik C, Gansow O, Whatley M, Pearson D, Webber K, Hamilton M, Allegra C, Brechbiel M, Willingham MC, Pastan I. Imaging and phase I study of ^{111}In- and ^{90}Y-labeled anti-Lewis^{Y} monoclonal antibody B3. *Clin Cancer Res.* 2000;6:1720-1730.

123. Cox JPL, Jankowski KJ, Kataky R, Parker D, Beeley NRA, Boyce BA, Eaton MAW, Millar K, Millican AT, Harrison A, Walker CA. Synthesis of a kinetically stable yttrium-90 labelled macrocycle-antibody conjugate. *J Chem Soc Chem Commun.* 1989;12:797-798.

124. Camera L, Kinuya S, Garmestani K, Wu C, Brechbiel MW, Pai LH, McMurry TJ, Gansow OA, Pastan I, Paik CH, Carrasquillo JA. Evaluation of the serum stability and in vivo

biodistribution of CHX-DTPA and other ligands for yttrium labeling of monoclonal antibodies. *J Nucl Med.* 1994;35:882-889.

125. Kosmas C, Snook D, Gooden CS, Courtenay-Luck NS, McCall MJ, Meares CF, Epenetos AA. Development of humoral immune responses against a macrocyclic chelating agent (DOTA) in cancer patients receiving radioimmunoconjugates for imaging and therapy. *Cancer Res.* 1992;52:904-911.
126. DeNardo GL, Mirick GR, Kroger LA, O'Donnell RT, Meares CF, DeNardo SJ. Antibody responses to macrocycles in lymphoma. *J Nucl Med.* 1996;37:451-456.
127. Lewis MR, Raubitschek A, Shively JE. A facile, water-soluble method for modification of proteins with DOTA. Use of elevated temperature and optimized pH to achieve high specific activity and high chelate stability in radiolabeled immunoconjugates. *Bioconjug Chem.* 1994;5:565-576.
128. Li M, Meares CF, Zhong G-R, Miers L, Xiong C-Y, DeNardo SJ. Labeling monoclonal antibodies with ^{90}Yttrium- and ^{111}Indium-DOTA chelates: a simple and efficient method. *Bioconjug Chem.* 1994;5:101-104.
129. DeNardo SJ, Zhong G-R, Salako Q, Li M, DeNardo GL, Meares CF. Pharmacokinetics of chimeric L6 conjugated to indium-111- and yttrium-90-DOTA-peptide in tumor-bearing mice. *J Nucl Med.* 1995;36:829-836.
130. Perico ME, Chinol M, Nacca A, Luison E, Paganelli G, Canevari S. The humoral immune response to macrocyclic chelating agent DOTA depends on the carrier molecule. *J Nucl Med.* 2001;42:1697-1703.
131. Blumenthal RD, Kashi R, Stephens R, Sharkey RM, Goldenberg DM. Improved radioimmunotherapy of colorectal cancer xenografts using antibody mixtures against carcinoembryonic antigen and colon-specific antigen-p. *Cancer Immunol Immunother.* 1991;32:303-310.
132. Song YQ, Wang GF, Dai XL, Xie H. Enhanced radioimmunotherapeutic efficacy of a monoclonal antibody cocktail against SMMC-7721 human hepatocellular carcinoma. *Cell Res.* 1998;8:241-247.
133. Robert B, Dorvillius M, Buchegger F, Garambois V, Mani J-C, Pugnières M, Mach J-P, Pèlegrin A. Tumor targeting with newly designed biparatopic antibodies directed against two different epitopes of the carcinoembryonic antigen (CEA). *Int J Cancer.* 1999;81:285-291.
134. Dorvillius M, Garambois V, Pourquier D, Gutowski M, Rouanet P, Mani JC, Pugniere M, Hynes NE, Pelegrin A. Targeting of human breast cancer by a bispecific antibody directed against two tumour-associated antigens: ErbB-2 and carcinoembryonic antigen. *Tumour Biol.* 2002;23:337-347.
135. Kim JC, Roh SA, Koo KH, Ryu JH, Hong HK, Oh SJ, Ryu JS, Kim HJ, Bodmer WF. Enhancement of colorectal tumor targeting using a novel biparatopic monoclonal antibody against carcinoembryonic antigen in experimental radioimmunoguided surgery. *Int J Cancer.* 2002;97:542-547.
136. Mattes MJ. Radionuclide-antibody conjugates for single-cell cytotoxicity. *Cancer.* 2002;94:s1215-s1223.
137. Ullen A, Ahlstrom KR, Heitala S, Nilsson B, Arlestig L, Stigbrand T. Secondary antibodies as tools to improve tumor to non tumor ratio at radioimmunolocalisation and radioimmunotherapy. *Acta Oncol.* 1996;35:281-285.

138. Casey JL, King DJ, Pedley RB, Boden JA, Boden R, Chaplin LC, Dorning M, Begent RH. Clearance of yttrium-90-labelled anti-tumour antibodies with antibodies raised against the 12N4 DOTA macrocycle. *Br J Cancer.* 1998;78:1307-13012.

139. Boerman OC, van Schaijk FG, Oyen WJG, Corstens FHM. Pretargeted radioimmunotherapy of cancer: progress step by step. *J Nucl Med.* 2003;44:400-411.

140. Magnani P, Fazio F, Grana C, Songini C, Frigerio L, Pecorelli S, Mangili G, Colombo N, Mariani CD, Paganelli G. Diagnosis of persistent ovarian carcinoma with three-step immunoscintigraphy. *Br J Cancer.* 2000;82:616-620.

141. Cremonesi M, Ferrari M, Chinol M, Stabin MG, Grana C, Prisco G, Robertson C, Tosi G, Paganelli G. Three-step radioimmunotherapy with yttrium-90 biotin: dosimetry and pharmacokinetics in cancer patients. *Eur J Nucl Med.* 1999;26:110-120.

142. Vuillez JP, Moro D, Brichon PY, Rouvier E, Brambilla E, Barbet J, Peltier P, Meyer P, Sarrazin R, Brambilla C. Two-step immunoscintigraphy for non-small-cell lung cancer staging using a bispecific anti-CEA/anti-indium-DTPA antibody and an indium-111-labeled DTPA dimer. *J Nucl Med.* 1997;38:507-511.

143. Weiden PL, Breitz HB. Pretargeted radioimmunotherapy (PRIT^{TM}) for treatment of non-Hodgkin's lymphoma (NHL). *Crit Rev Oncol Hematol.* 2001;40:37-51.

144. DeNardo GL, O'Donnell RT, Kroger LA, Richman CM, Goldstein DS, Shen S, DeNardo SJ. Strategies for developing effective radioimmunotherapy for solid tumors. *Clin Cancer Res.* 1999;5:3219s-3223s.

145. DeNardo GL, Schlom J, Buchsbaum DJ, Meredith RF, O'Donoghue JA, Sgouros G, Humm JL, DeNardo SJ. Rationales, evidence, and design considerations for fractionated radioimmunotherapy. *Cancer.* 2002;94:1332-1348.

146. Welt S, Ritter G, Williams C Jr, Cohen LS, Jungbluth A, Richards EA, Old LJ, Kemeny NE. Preliminary report of a phase I study of combination chemotherapy and humanized A33 antibody immunotherapy in patients with advanced colorectal cancer. *Clin Cancer Res.* 2003;9:1347-1353.

147. Buchegger F, Allal AS, Roth A, Papazyan JP, Dupertuis Y, Mirimanoff RO, Gillet M, Pelegrin A, Mach JP, Slosman DO. Combined radioimmunotherapy and radiotherapy of liver metastases from colorectal cancer: a feasibility study. *Anticancer Res.* 2000;20:1889-1896.

148. Meredith RF, Khazaeli MB, Liu T, Plott G, Wheeler RH, Russell C, Colcher D, Schlom J, Shochat D, LoBuglio AF. Dose fractionation of radiolabeled antibodies in patients with metastatic colon cancer. *J Nucl Med.* 1992;33:1648-1653.

149. DeNardo GL, DeNardo SJ, Goldstein DS, Kroger LA, Lamborn KR, Levy NB, McGahan JP, Salako Q, Shen S, Lewis JP. Maximum-tolerated dose, toxicity, and efficacy of ^{131}I-Lym-1 antibody for fractionated radioimmunotherapy of non-Hodgkin's lymphoma. *J Clin Oncol.* 1998;16:3246-3256.

150. Press OW, Eary JF, Appelbaum FR, Martin PJ, Nelp WB, Glenn S, Fisher DR, Porter B, Matthews DC, Gooley T, Bernstein ID. Phase II trial of ^{131}I-B1 (anti-CD20) antibody therapy with autologous stem cell transplantation for relapsed B cell lymphomas. *Lancet.* 1995;346:336-340.

151. Richman CM, DeNardo SJ, O'Grady LF, DeNardo GL. Radioimmunotherapy for breast cancer using escalating fractionated doses of ^{131}I-labeled chimeric L6 antibody with peripheral blood progenitor cell transfusions. *Cancer Res.* 1995;55:5916s-5920s.

152. Wong JY, Somlo G, Odom-Maryon T, Williams LE, Liu A, Yamauchi D, Wu AM, Yazaki P, Wilczynski S, Shively JE, Forman S, Doroshow JH, Raubitschek AA. Initial clinical experience evaluating yttrium-90-chimeric T84.66 anticarcinoembryonic antigen antibody and autologous hematopoietic stem cell support in patients with carcinoembryonic antigen-producing metastatic breast cancer. *Clin Cancer Res.* 1999;5:3224s-3231s.
153. Colnot DR, Ossenkoppele GJ, Roos JC, Quak JJ, de Bree R, Börjesson PK, Huijgens PC, Snow GB, van Dongen GAMS. Reinfusion of unprocessed, granulocyte colony-stimulating factor-stimulated whole blood allows dose escalation of ^{186}Re-labeled chimeric monoclonal antibody U36 radioimmunotherapy in a phase I dose escalation study. *Clin Cancer Res.* 2002;8:3401-3406.
154. Eary JF. PET imaging for planning cancer therapy. *J Nucl Med.* 2001;42:770-771.
155. Weissleder R. Scaling down imaging: molecular mapping of cancer in mice. *Nature Rev Cancer.* 2002;2:11-18.
156. Turkington TG. Introduction to PET instrumentation. *J Nucl Med Technol.* 2001;29:4-11.
157. Fahey FH. Positron emission tomography instrumentation. *Radiol Clin North Am.* 2001;39:919-929.
158. Bergström M, Eriksson L, Bohm C, Blomqvist G, Litton J. Correction for scattered radiation in a ring detector positron camera by integral transformation of the projections. *J Comput Assist Tomogr.* 1983;7:42-50.
159. Zaidi H. Scatter modelling and correction strategies in fully 3-D PET. *Nucl Med Comm.* 2001;22:1181-1184.
160. Levin CS, Dahlbom M, Hoffman EJ. A Monte Carlo correction for the effect of Compton scattering in 3-D PET brain imaging. *IEEE Trans Nucl Sci.* 1995;42:1181-1185.
161. Zaidi H. Comparative evaluation of scatter correction techniques in 3D positron emission tomography. *Eur J Nucl Med.* 2000;27:1813-1826.
162. Grootoonk S, Spinks TJ, Sashin D, Spyrou NM, Jones T. Correction for scatter in 3D brain PET using a dual energy window method. *Phys Med Biol.* 1996;41:2757-2774.
163. Ollinger JM. Model-based scatter correction for fully 3D PET. *Phys Med Biol.* 1996;41:153-176.
164. Watson CC. New, faster, image-based scatter correction for 3D PET. *IEEE Trans Nucl Sci.* 2000;47:1587-1594.
165. Bentourkia M, Lecomte R. Energy dependence of nonstationary scatter subtraction-restoration in high resolution PET. *IEEE Trans Med Imaging.* 1999;18:66-73.
166. Pentlow KS, Finn RD, Larson SM, Erdi YE, Beattie BJ, Humm JL. Quantitative imaging of yttrium-86 with PET: the occurrence and correction of anomalous apparent activity in high density regions. *Clin Positron Imaging.* 2000;3:85-90.
167. Buchholz HG, Herzog H, Forster GJ, Reber H, Nickel O, Rösch F, Bartenstein P. PET imaging with yttrium-86: comparison of phantom measurements acquired with different PET scanners before and after applying background subtraction. *Eur J Nucl Med Mol Imaging.* 2003;30:716-720.
168. Geworski L, Knoop BO, de Cabrejas ML, Knapp WH, Munz DL. Recovery correction for quantitation in emission tomography: a feasibility study. *Eur J Nucl Med.* 2000;27:161-169.
169. Wrenn FR, Good ML, Handler P. The use of positron-emitting radioisotopes for the localization of brain tumors. *Science.* 1951;113:525-527.
170. Anger H. Gamma-ray and positron scintillation cameras. *Nucleonics.* 1963;21:56-59.

171. Burnham C, Brownell G. A multi-crystal positron camera. *IEEE Trans Nucl Sci.* 1972;19:201-205.
172. Robertson J, Marr R, Rosenblum B. Thirty-two crystal positron transverse section detector. In: Freedman G, ed. *Tomographic imaging in nuclear medicine.* New York: Society of Nuclear Medicine; 1973:151-153.
173. Muehllehner G, Buchin M, Dudek J. Performance parameters of a positron imaging camera. *IEEE Trans Nucl Sci.* 1976;23:528-537.
174. Phelps ME, Hoffman EJ, Mullani NA, Ter-Pogossian MM. Application of annihilation coincidence detection to transaxial reconstruction tomography. *J Nucl Med.* 1975;16:210-224.
175. Townsend DW, Wensveen M, Byars LG, Geissbuhler A, Tochon-Danguy HJ, Christin A, Defrise M, Bailey DL, Grootoonk S, Donath A. A rotating PET scanner using BGO block detectors: design, performance and applications. *J Nucl Med.* 1993;34:1367-1376.
176. Phelps ME, Cherry SR. The changing design of positron imaging systems. *Clin Positron Imaging.* 1998;1:31-45.
177. Dahlbom M, MacDonald L, Eriksson L, Paulus M, Andreaco M, Casey M, Moyers C. Performance of a YSO/LSO phoswich detector for use in a PET/SPECT system. *IEEE Trans Nucl Sci.* 1997;44:1114-1119.
178. Adam L-E, Karp JS, Daube-Witherspoon ME, Smith RJ. Performance of a whole-body PET scanner using curve-plate NaI(Tl) detectors. *J Nucl Med.* 2001;42:1821-1830.
179. Townsend DW, Cherry SR. Combining anatomy and function: the path to true image fusion. *Eur Radiol.* 2001;11:1968-1974.
180. Beyer T, Townsend DW, Blodgett TM. Dual-modality PET/CT tomography for clinical oncology. *Q J Nucl Med.* 2002;46:24-34.
181. Marsden PK, Strul D, Keevil SF, Williams SCR, Cash D. Simultaneous PET and NMR. *Br J Radiol.* 2002;75:S53-S59.
182. Kinahan PE, Townsend DW, Beyer T, Sashin D. Attenuation correction for a combined 3D PET/CT scanner. *Med Phys.* 1998;25:2046-2053.
183. Comtat C, Kinahan PE, Fessler JA, Beyer T, Townsend DW, Defrise M, Michel C. Clinically feasible reconstruction of 3D whole-body PET/CT data using blurred anatomical labels. *Phys Med Biol.* 2002;47:1-20.
184. Hasegawa BH, Iwata K, Wong KH, Wu MC, Da Silva AJ, Tang HR, Barber WC, Hwang AH, Sakdinawat AE. Dual-modality imaging of function and physiology. *Acad Radiol.* 2002;9:1305-1321.
185. Melcher CL. Scintillation crystals for PET. *J Nucl Med.* 2000;41:1051-1055.
186. Tai C, Chatziioannou A, Siegel S, Young J, Newport D, Goble RN, Nutt RE, Cherry SR. Performance evaluation of the microPET P4: a PET system dedicated to animal imaging. *Phys Med Biol.* 2001;46:1845-1862.
187. Jeavons AP, Chandler RA, Dettmar CAR. A 3D HIDAC-PET camera with sub-millimetre resolution for imaging small animals. *IEEE Trans Nucl Sci.* 1999;46:468-473.
188. Watanabe M, Okada H, Shimizu K, Omura T, Yoshikawa E, Kosugi T, Mori S, Yamashita T. A high resolution animal PET scanner using compact PS-PMT detectors. *IEEE Trans Nucl Sci.* 1997;44:1277-1282.
189. Wienhard KSM, et al. The ECAT HRRT: performance and first clinical applications of a new High Resolution Research Tomograph. *IEEE Trans Nucl Sci.* 2002;49:104-110.

190. Bloomfield PM, Myers R, Hume SP, Spinks TJ, Lammertsma AA, Jones T. Three-dimensional performance of a small-diameter positron emission tomograph. *Phys Med Biol.* 1997;42:389-400.

191. Tai YC, Chatziioannou AF, Yang Y, Silverman RW, Meadors K, Siegel S, Newport DF, Stickel JR, Cherry SR. MicroPET II: design, development and initial performance of an improved microPET scanner for small-animal imaging. *Phys Med Biol.* 2003;48:1519-1537.

192. Weber S, Herzog H, Cremer M, Engels R, Hamacher K, Kehren F, Muehlensiepen H, Ploux L, Reinartz R, Reinhart P, Rongen F, Sonnenberg F, Coenen HH, Halling H. Evaluation of the TierPET system. *IEEE Nucl Sci.* 1999;46:1177-1183.

193. Del Guerra A, Di Domenico G, Scandola M, Zavattini G. High spatial resolution small animal YAP-PET. *Nucl Instrum Meth Phys Res Sect A.* 1998;409:508-510.

194. Rafecas M, Boning G, Pichler BJ, Lorenz E, Schwaiger M, Ziegler SI. Inter-crystal scatter in a dual layer, high resolution LSO-APD positron emission tomograph. *Phys Med Biol.* 2003;48:821-848.

195. Boellaard R, Buijs F, de Jong HWAM, Lenox M, Gremillion T, Lammertsma AA. Characterization of a single LSO crystal layer high resolution research tomograph. *Phys Med Biol.* 2003;48:429-448.

196. Rouze NC, Stantz KM, Hutchins GD. Design of IndyPET-II, a high resolution, high-sensitivity dedicated research scanner. *J Nucl Med.* 2001;42:364s.

197. Lecomte R, Cadorette J, Richard P, Rodrigue S, Rouleau D. Design and engineering aspects of a high resolution positron tomograph for small animal imaging. *IEEE Trans Nucl Sci.* 1994;41:1446-1452.

198. Correia JA, Burnham CA, Kaufman D, Fishman AJ. Development of a small animal PET imaging device with resolution approaching 1mm. *IEEE Trans Nucl Sci.* 1999;46:631-635.

199. Seidel J, Vaquero JJ, Green MV. Resolution uniformity and sensitivity of the NIH ATLAS small animal PET scanner: comparison to simulated LSO scanners without depth-of-interaction capability. In *Conference Proceedings IEEE NSS-MIC*. San Diego, CA: IEEE; 2001.

200. Huber JS, Moses WW, Jones WF, Watson CC. Effect of ^{176}Lu background on singles transmission for LSO-based PET cameras. *Phys Med Biol.* 2002;47:3535-3541.

201. Lammertsma AA, Hume SP, Myers R, Ashworth S, Bloomfield PM, Rajeswaran S, Spinks T, Jones T. PET scanners for small animals. *J Nucl Med.* 1995;36:2391-2392.

202. Chatziioannou AF. Molecular imaging of small animals with dedicated PET tomographs. *Eur J Nucl Med.* 2002;29:98-114.

203. Lewis JS, Achilefu S, Garbow JR, Laforest R, Welch MJ. Small animal imaging: current technology and perspectives for oncological imaging. *Eur J Cancer.* 2002;38:2173-2188.

204. Pomper MG. Can small animal imaging accelerate drug development? *J Cell Biochem Suppl.* 2002;39:211-220.

205. Rowland DJ, Lewis JS, Welch MJ. Molecular imaging: the application of small animal positron emission tomography. *J Cell Biochem Suppl.* 2002;39:110-115.

206. Hume SP, Gunn RN, Jones T. Pharmacological constraints associated with positron emission tomographic scanning of small laboratory animals. *Eur J Nucl Med.* 1998;25:173-176.

207. Myers R, Hume S. Small animal PET. *Eur Neuropsychopharmacol.* 2002;12:545-555.

208. Qaim SM. Production of high purity ^{94m}Tc for positron emission tomography studies. *Nucl Med Biol.* 2000;27:323-328.

209. Smith MF, Daube-Witherspoon ME, Plascjak PS, Szajek LP, Carson RE, Everett JR, Green SL, Territo PR, Balaban RS, Bacharach SL, Eckelman WC. Device-dependent activity estimation and decay correction of radionuclide mixtures with application to Tc-94m PET studies. *Med Phys.* 2001;28:36-45.

210. Pagani M, Stone-Elander S, Larsson SA. Alternative positron emission tomography with non-conventional positron emitters: effects of their physical properties on image quality and potential clinical applications. *Eur J Nucl Med.* 1997;24:1301-1327.

211. Glaser M, Luthra SK, Brady F. Applications of positron-emitting halogens in PET oncology (Review). *Int J Oncol.* 2003;22:253-267.

212. McCarthy DW, Shefer RE, Klinkowstein RE, Bass LA, Margeneau WH, Cutler CS, Anderson CJ, Welch MJ. Efficient production of high specific activity ^{64}Cu using a biomedical cyclotron. *Nucl Med Biol.* 1997;24:35-43.

213. Rösch F, Qaim G, Stöcklin G. Production of the positron emitting radioisotope ^{86}Y for nuclear medical applications. *Appl Radiat Isot.* 1993;44:677-681.

214. Garmestani K, Milenic DE, Plascjak PS, Brechbiel MW. A new and convenient method for purification of ^{86}Y using a Sr(II) selective resin and comparison of biodistribution of ^{86}Y and ^{111}In labeled Herceptin™. *Nucl Med Biol.* 2002;29:599-606.

215. Walrand S, Jamar F, Mathieu I, Camps J, Lonneux M, Sibomana M, Labar D, Michel C, Pauwels S. Quantitation in PET using isotopes emitting prompt single gammas: application to yttrium-86. *Eur J Nucl Med.* 2003;30:354-361.

216. Ribeiro MJ, Almeida P, Strul D, Ferreira N, Loc'h C, Brulon V, Trébossen R, Mazière B, Bendriem B. Comparison of fluorine-18 and bromine-76 imaging in positron emission tomography. *Eur J Nucl Med.* 1999;26:758-766.

217. Lubberink M, Schneider H, Bergstrom M, Lundqvist H. Quantitative imaging and correction for cascade gamma radiation of ^{76}Br with 2D and 3D PET. *Phys Med Biol.* 2002;47:3519-3534.

218. Verel I, Visser GWM, Boellaard R, Stigter-Van Walsum M, Snow GB, Van Dongen GAMS. ^{89}Zr immuno-PET: comprehensive procedures for the production of ^{89}Zr-labeled monoclonal antibodies. *J Nucl Med.* 2003;44:1271-1281.

219. Verel I, Visser GWM, Boellaard R, Boerman OC, van Eerd J, Snow GB, Lammertsma AA, van Dongen GAMS. Quantitative ^{89}Zr immuno-PET for in vivo scouting of ^{90}Y-labeled monoclonal antibodies in xenograft-bearing nude mice. *J Nucl Med.* 2003;44:1663-1670.

220. Pentlow KS, Graham MC, Lambrecht RM, Daghighian F, Bacharach SL, Bendriem B, Finn RD, Jordan K, Kalaigian H, Karp JS, Robeson WR, Larson SM. Quantitative imaging of iodine-124 with PET. *J Nucl Med.* 1996;37:1557-1562.

221. Herzog H, Tellmann L, Qaim SM, Spellerberg S, Schmid A, Coenen HH. PET quantitation and imaging of the non-pure positron-emitting iodine isotope ^{124}I. *Appl Radiat Isot.* 2002;56:673-679.

222. Sowby FD, ed. *Radionuclide Transformations: Energy and Intensity of Emissions.* ICRP publication 38, vol 11-13. Oxford, England: Pergamon Press; 1983:14,74, 90, 144, 202, 218, 249, 444.

223. Kinsey RR. *The NuDat Program for Nuclear Data on the Web, version 2.5, http://www.nndc.bnl.gov/nndc/nudat/.* Upton, NY: National Nuclear Data Center, Brookhaven National Laboratory; 1996.

224. Pentlow KS, Graham MC, Lambrecht RM, Cheung NK, Larson SM. Quantitative imaging of I-124 using positron emission tomography with applications to radioimmunodiagnosis and radioimmunotherapy. *Med Phys.* 1991;18:357-366.
225. Knust EJ, Dutschka K, Weinreich R. Preparation of ^{124}I solutions after thermodistillation of irradiated $^{124}TeO_2$ targets. *Appl Radiat Isot.* 2000;52:181-184.
226. Bastian Th., Coenen HH, Qaim SM. Excitation functions of $^{124}Te(d,xn)^{124,125}I$ reactions from threshold up to 14 MeV: comparative evaluation of nuclear routes for the production of ^{124}I. *Appl Radiat Isot.* 2001;55:303-308.
227. Hohn A, Nortier FM, Scholten B, van der Walt TN, Coenen HH, Qaim SM. Excitation functions of $^{125}Te(p,xn)$-reactions from their respective thresholds up to 100 MeV with special reference to the production of ^{124}I. *Appl Radiat Isot.* 2001;55:149-156.
228. Kudelin BK, Gromova EA, Gavrilina LV, Solin LM. Purification of recovered tellurium dioxide for re-use in iodine radioisotope production. *Appl Radiat Isot.* 2001;54:383-386.
229. Qaim SM, Hohn A, Bastian Th, El-Azoney KM, Blessing G, Spellerberg S, Scholten B, Coenen HH. Some optimisation studies relevant to the production of high-purity ^{124}I and ^{120g}I at a small-sized cyclotron. *Appl Radiat Isot.* 2003;58:69-78.
230. Finn R, Cheung N-KV, Divgi C, St Germain J, Graham M, Pentlow K, Larson SM. Technical challenges associated with the radiolabeling of monoclonal antibodies utilizing short-lived, positron emitting radionuclides. *Int J Rad Appl Instrum B.* 1991;18:9-13.
231. Larson SM, Pentlow KS, Volkow ND, Wolf AP, Finn RD, Lambrecht RM, Graham MC, Di Resta G, Bendriem B, Daghighian F. PET scanning of iodine-124-3F8 as an approach to tumor dosimetry during treatment planning for radioimmunotherapy in a child with neuroblastoma. *J Nucl Med.* 1992;33:2020-2023.
232. Lee FT, Hall C, Rigopoulos A, Zweit J, Pathmaraj K, O'Keefe GJ, Smyth FE, Welt S, Old LJ, Scott AM. Immuno-PET of human colon xenograft-bearing BALB/c nude mice using ^{124}I-CDR-grafted humanized A33 monoclonal antibody. *J Nucl Med.* 2001;42:764-769.
233. Collingridge DR, Carroll VA, Glaser M, Aboagye EO, Osman S, Hutchinson OC, Barthel H, Luthra SK, Brady F, Bicknell R, Price P, Harris AL. The development of [^{124}I]Iodinated-VG76e: a novel tracer for imaging vascular endothelial growth factor in vivo using positron emission tomography. *Cancer Res.* 2002;62:5912-5919.
234. Link JM, Krohn KA, Eary JF, Kishore R, Lewellen TK, Johnson MW, Badger CC, Richter KY, Nelp WB. ^{89}Zr for antibody labeling and positron emission tomography. *J Label Comp Radiopharm.* 1986;23:1297 (Abstract).
235. Dejesus OT, Nickles RJ. Production and purification of ^{89}Zr, a potential PET antibody label. *Appl Radiat Isot.* 1990;41:789-790.
236. Zweit J, Downey S, Sharma HL. Production of no-carrier-added zirconium-89 for positron emission tomography. *Appl Radiat Isot.* 1991;42:199-201.
237. Meijs WE, Herscheid JDM, Haisma HJ, Wijbrandts R, van Langevelde F, van Leuffen PJ, Mooy R, Pinedo HM. Production of highly pure no-carrier-added zirconium-89 for the labeling of antibodies with a positron emitter. *Appl Radiat Isot.* 1994;45:1147-1147.
238. Meijs WE, Haisma HJ, Klok RP, van Gog FB, Kievit E, Pinedo HM, Herscheid JDM. Zirconium-labeled monoclonal antibodies and their distribution in tumor-bearing nude mice. *J Nucl Med.* 1997;38:112-118.

239. Meijs WE, Herscheid JDM, Haisma HJ, Pinedo HM. Evaluation of desferal as a bifunctional chelating agent for labeling antibodies with Zr-89. *Int J Rad Appl Instrum A.* 1992;43:1443-1447.

240. Lewis MR, Shively JE. Maleimidocysteineamido-DOTA derivatives: new reagents for radiometal chelate conjugation to antibody sulfhydryl groups undergo pH-dependent cleavage reactions. *Bioconjug Chem.* 1998;9:72-86.

241. Garg PK, Garg S, Zalutsky MR. Fluorine-18 labeling of monoclonal antibodies and fragments with preservation of immunoreactivity. *Bioconjug Chem.* 1991;2:44-49.

242. Otsuka FL, Welch MJ, Kilbourn MR, Dence CS, Dilley WG, Wells SA Jr. Antibody fragments labeled with fluorine-18 and gallium-68: in vivo comparison with indium-111 and iodine-125-labeled fragments. *Int J Rad Appl Instrum B.* 1991;18:813-816.

243. Garg PK, Garg S, Bigner DD, Zalutsky MR. Localization of fluorine-18-labeled Mel-14 monoclonal antibody $F(ab')_2$ fragment in a subcutaneous xenograft model. *Cancer Res.* 1992;52:5054-5060.

244. Vaidyanathan G, Bigner DD, Zalutsky MR. Fluorine-18-labeled monoclonal antibody fragments: a potential approach for combining radioimmunoscintigraphy and positron emission tomography. *J Nucl Med.* 1992;33:1535-1541.

245. Zalutsky MR, Garg PK, Johnson SH, Utsunomiya H, Coleman RE. Fluorine-18-antimyosin monoclonal antibody fragments: preliminary investigations in a canine myocardial infarct model. *J Nucl Med.* 1992;33:575-580.

246. Page RL, Garg PK, Garg S, Archer GE, Bruland OS, Zalutsky MR. PET imaging of osteosarcoma in dogs using a fluorine-18-labeled monoclonal antibody Fab fragment. *J Nucl Med.* 1994;35:1506-1513.

247. Choi CW, Lang L, Lee JT, Webber KO, Yoo TM, Chang HK, Le N, Jagoda E, Paik CH, Pastan I. Biodistribution of ^{18}F- and ^{125}I-labeled anti-Tac disulfide-stabilized Fv fragments in nude mice with interleukin 2 alpha receptor-positive tumor xenografts. *Cancer Res.* 1995;55:5323-5329.

248. Griffiths GL, Goldenberg DM, Roesch F, Hansen HJ. Radiolabeling of an anti-carcinoembryonic antigen antibody Fab' fragment (CEA-scan) with the positron-emitting radionuclide Tc-94m. *Clin Cancer Res.* 1999;5:3001s-3003s.

249. Schuhmacher J, Klivenyi G, Matys R, Stadler M, Regiert T, Hauser H, Doll J, Maier-Borst W, Zoller M. Multistep tumor targeting in nude mice using bispecific antibodies and a gallium chelate suitable for immunoscintigraphy with positron emission tomography. *Cancer Res.* 1995;55:115-123.

250. Klivényi G, Schuhmacher J, Patzelt E, Hauser H, Matys R, Moock M, Regiert T, Maier-Borst W. Gallium-68 chelate imaging of human colon carcinoma xenografts pretargeted with bispecific anti-CD44V6/anti-gallium chelate antibodies. *J Nucl Med.* 1998;39:1769-1776.

251. Schuhmacher J, Klivényi G, Kaul S, Henze M, Matys R, Hauser H, Clorius J. Pretargeting of human mammary carcinoma xenografts with bispecific anti-MUC1/anti-Ga chelate antibodies and immunoscintigraphy with PET. *Nucl Med Biol.* 2001;28:821-828.

252. Schuhmacher J, Kaul S, Klivényi G, Junkermann H, Magener A, Henze M, Doll J, Haberkorn U, Amelung F, Bastert G. Immunoscintigraphy with PET: Ga-68 chelate imaging of breast cancer pretargeted with bispecific anti-MUC1/anti-Ga chelate antibodies. *Cancer Res.* 2001;61:3712-3717.

253. Philpott GW, Schwarz SW, Anderson CJ, Dehdashti F, Connett JM, Zinn KR, Meares CF, Cutler PD, Welch MJ, Siegel BA. RadioimmunoPET: detection of colorectal carcinoma with positron-emitting copper-64-labeled monoclonal antibody. *J Nucl Med.* 1995;36:1818-1824.

254. Wu AM, Yazaki PJ, Tsai S, Nguyen K, Anderson A-L, McCarthy DW, Welch MJ, Shively JE, Williams LE, Raubitschek AA, Wong JYC, Toyokuni T, Phelps ME, and Gambhir SS. High-resolution microPET imaging of carcinoembryonic antigen-positive xenografts by using a copper-64-labeled engineered antibody fragment. *Proc Natl Acad Sci USA.* 2000;97:8495-8500.

255. Lewis MR, Wang M, Axworthy DB, Theodore LJ, Mallet RW, Fritzberg AR, Welch MJ, Anderson CJ. In vivo evaluation of pretargeted ^{64}Cu for tumor imaging and therapy. *J Nucl Med.* 2003;44:1284-1292.

256. Lövqvist A, Sundin A, Alström H, Carlsson J, Lundqvist H. Pharmacokinetics and experimental PET imaging of a bromine-76-labeled monoclonal anti-CEA antibody. *J Nucl Med.* 1997;38:395-401.

257. Lövqvist A, Sundin A, Roberto A, Ahlstrom H, Carlsson J, Lundqvist H. Comparative PET imaging of experimental tumors with bromine-76-labeled antibodies, fluorine-18-fluorodeoxyglucose and carbon-11-methionine. *J Nucl Med.* 1997;38:1029-1035.

258. Lövqvist A, Lundqvist H, Lubberink M, Tolmachev V, Carlsson J, Sundin A. Kinetics of ^{76}Br-labeled anti-CEA antibodies in pigs; Aspects of dosimetry and PET imaging properties. *Med Phys.* 1999;26:249-258.

259. Lambrecht RM, Woodhouse N, Phillips R, Wolczak D, Qureshi A, Reyes ED, Graser C, Al-Yanbawi S, Al-Rabiah A, Meyer W, Marlais W, Syed R, Banjar F, Rifai A, Miliebari S. Investigational study of iodine-124 with a positron camera. *Am J Physiol Imaging.* 1988;3:197-200.

260. Snook DE, Rowlinson-Busza G, Sharma HL, Epenetos AA. Preparation and in vivo study of ^{124}I-labelled monoclonal antibody H17E2 in a human tumour xenograft model. A prelude to positron emission tomography (PET). *Br J Cancer Suppl.* 1990;10:89-91.

261. Wilson CB, Snook DE, Dhokia B, Taylor IA, Lammertsma AA, Lambrecht R, Waxman J, Jones T, Epenetos AA. Quantitative measurement of monoclonal antibody distribution and blood flow using positron emission tomography and ^{124}Iodine in patients with breast cancer. *Int J Cancer* 1991;47:344-347.

262. Westera G, Reist HW, Buchegger F, Heusser CH, Hardman N, Pfeiffer A, Sharma HL, von Schulthess GK, Mach JP. Radioimmuno positron emission tomography with monoclonal antibodies: a new approach to quantifying in vivo tumour concentration and biodistribution for radioimmunotherapy. *Nucl Med Comm.* 1991;12:429-437.

263. Bakir MA, Eccles SA, Babich JW, Aftab N, Styles JM, Dean CJ, Lambrecht RM, Ott RJ. c-erbB2 Protein overexpression in breast cancer as a target for PET using iodine-124-labeled monoclonal antibodies. *J Nucl Med.* 1992;33:2154-2160.

264. Daghighian F, Pentlow KS, Larson SM, Graham MC, Di Resta GR, Yeh SDJ, Macapinlac H, Finn RD, Arbit E, Cheung N-KV. Development of a method to measure kinetics of radiolabelled monoclonal antibody in human tumour with applications to microdosimetry: positron emission tomography studies of iodine-124 labelled 3F8 monoclonal antibody in glioma. *Eur J Nucl Med.* 1993;20:402-409.

265. Kairemo KJA. Positron emission tomography of monoclonal antibodies. *Acta Oncol.* 1993;32:825-830.

266. Rubin SC, Kairemo KJA, Brownell A-L, Daghighian F, Federici MG, Pentlow KS, Finn RD, Lambrecht RM, Hoskins WJ, Lewis JL Jr, Larson SM. High-resolution positron emission tomography of human ovarian cancer in nude rats using ^{124}I-labeled monoclonal antibodies. *Gynecol Oncol.* 1993;48:61-67.

267. Jayson GC, Zweit J, Jackson A, Mulatero C, Julyan P, Ranson M, Broughton L, Wagstaff J, Hakannson L, Groenewegen G, Bailey J, Smith N, Hastings D, Lawrance J, Haroon H, Ward T, McGown AT, Tang M, Levitt D, Marreaud S, Lehmann FF, Herold M, Zwierzina H. Molecular imaging and biological evaluation of HuMV833 anti-VEGF antibody: implications for trial design of antiangiogenic antibodies. *J Natl Cancer Inst.* 2002;94:1484-1493.

268. de Bree R, Roos JC, Quak JJ, den Hollander W, Snow GB, van Dongen GAMS. Radioimmunoscintigraphy and biodistribution of technetium-99m-labeled monoclonal antibody U36 in patients with head and neck cancer. *Clin Cancer Res.* 1995;1:591-598.

269. Stroomer JW, Roos JC, Sproll M, Quak JJ, Heider KH, Wilhelm BJ, Castelijns JA, Meyer R, Kwakkelstein MO, Snow GB, Adolf GR, van Dongen GAMS. Safety and biodistribution of ^{99m}Technetium-labeled anti-CD44v6 monoclonal antibody BIWA 1 in head and neck cancer patients. *Clin Cancer Res.* 2000;6:3046-3055.

chapter

2

Tumor-targeting properties of monoclonal antibodies with different affinity for target antigen CD44v6 in nude mice bearing head and neck cancer xenografts

Iris Verel, Karl-Heinz Heider, Miranda Siegmund, Elinborg Ostermann, Erik Patzelt, Marlies Sproll, Gordon B. Snow, Günther R. Adolf, Guus A.M.S. van Dongen

International Journal of Cancer **2002;99:396-402.**

ABSTRACT

The CD44 protein family consists of isoforms with tissue-specific expression, which are encoded by standard exons and up to nine alternatively spliced variant exons (v2-v10) of the same gene. The murine MAbs U36 and BIWA 1, directed against overlapping epitopes within the v6 region of CD44, have previously been shown to efficiently target HNSCC. We herein report on the construction of one chimeric (BIWA 2) and two humanized (BIWA 4 and BIWA 8) derivatives of BIWA 1. Together with U36 and BIWA 1, these new antibodies were evaluated for affinity to the antigen *in vitro* as well as for biodistribution and efficacy in RIT using nude mice bearing the HNSCC xenograft line HNX-OE. As determined by surface plasmon resonance, the MAbs bound to CD44v6 with an up to 46-fold difference in affinity (K_d ranging from $1.1x10^{-8}$ to $2.4x10^{-10}$ M) with the following ranking: mMAb U36 < hMAb BIWA 4 < hMAb BIWA 8 < mMAb BIWA 1 ~ cMAb BIWA 2. To evaluate their *in vivo* tumor-targeting properties, two MAbs with identical murine or human isotype were labeled with either ^{131}I or ^{125}I and administered simultaneously (50 µg/0.37 MBq each) as pairs showing a stepwise decrease in the difference in affinity: U36 *vs.* BIWA 1 (35.0-fold difference), BIWA 4 *vs.* BIWA 2 (14.0-fold), and BIWA 4 *vs.* BIWA 8 (4.0-fold). Biodistribution was assessed at 1, 2, 3 or 4 and 7 d after injection. Remarkably, for all three MAb pairs tested, the lower-affinity MAb showed a higher degree and specificity of tumor localization. The difference in tumor localization was more pronounced when the difference in affinity was larger. For example, 3 d after injection, the lower-affinity mMAb U36 showed a 50% higher tumor uptake than the higher-affinity mMAb BIWA 1, while blood levels and uptake in organs were similar. After labeling with ^{186}Re (11.1 or 14.8 MBq), the same MAb pairs showed RIT efficacy consistent with the biodistribution data: ^{186}Re-U36 was more effective than ^{186}Re-BIWA 1, ^{186}Re-BIWA 4 was slightly more effective than ^{186}Re-BIWA 2 and ^{186}Re-BIWA 4 and ^{186}Re-BIWA 8 demonstrated similar efficacy. Based on these data, we conclude that antibodies with markedly lower affinity to a given target antigen (e.g., U36, BIWA 4) may show superior tumor-targeting in comparison with higher-affinity versions of these antibodies.

INTRODUCTION

The use of radiolabeled monoclonal antibodies (MAbs) has been recognized as a realistic option for improvement of diagnosis and treatment of cancer. While in the last decade MAbs have been administered to thousands of patients with various types of tumor for both diagnostic and therapeutic purposes, the application of MAbs in head-and-neck oncology has not kept pace. One of the main reasons for this slow progress has been the lack of MAbs with a high specificity for head and neck cancer, in particular for head and neck squamous cell carcinoma (HNSCC), which accounts for approximately 90% of the head and neck tumors.

In recent years, a panel of MAbs has been developed that is capable of selective HNSCC targeting, as was demonstrated in clinical radioimmunoscintigraphy (RIS)/biodistribution studies with HNSCC patients. Among the best-qualified antibodies are the murine MAbs (mMAbs) U36 and BIWA 1 (formerly VFF-18) [1,2]. U36 and BIWA 1 bind to overlapping epitopes in the variable domain v6 of the cell-surface antigen CD44 and have been characterized extensively [3,4]. CD44 isoforms, which arise from differential splicing of up to 9 variant exons, show a tissue-specific expression pattern. Homogenous expression of v6-containing CD44 isoforms has been observed in squamous cell carcinoma of the head and neck, lung, skin, oesophagus and cervix, while heterogeneous expression was found in several other tumor types, including adenocarcinomas of the breast, lung, colon, pancreas and stomach [4]. Among normal tissues, CD44v6 isoform expression has been observed only in a subset of epithelial tissues, such as breast and prostate myoepithelium and skin and bronchial epithelium [4]. Soluble v6-containing CD44 fragments have been detected in the blood of cancer patients as well as of healthy individuals [5].

The physiological role of CD44 variants has been the subject of many investigations. Evidence has been found for involvement in adhesion [6], signal transduction [7], cell migration [8], growth factor binding [9], and tumor metastasis formation [10]. With respect to the latter, especially v6-containing CD44 isoforms have attracted much attention since they appear to be capable of conferring metastatic potential to tumor cells originally not able to metastasize [10], while outgrowth of metastases was inhibited by MAbs directed against the v6 domain [11]. Overexpression of CD44v6 in tumors has been correlated with reduced survival of patients with breast and colon cancer and with non-Hodgkin's lymphoma [12-14].

These data indicate that CD44v6 is an attractive target for MAb-based therapy, especially for the treatment of HNSCC in which the level of expression is very favourable. Since HNSCCs are intrinsically radiosensitive, radioimmunotherapy (RIT) might be particularly suitable. For the development of optimal RIT, several parameters must be considered. An important one is the radionuclide to be used. Since rhenium-186 (^{186}Re) is a promising candidate radionuclide for RIT, we have put effort into the production of optimal ^{186}Re-MAb conjugates [15]. Other parameters that can be considered for optimizing RIT are the MAb form (e.g., murine *vs.* chimeric *vs.* humanized constructs) and the affinity of the MAb. Administration of mMAbs to patients usually induces human anti-mouse antibody (HAMA) responses, as observed for U36 [1] and BIWA 1 [2]. HAMA responses can lead to rapid clearance

of the injected MAb from the body, thus reducing MAb uptake by the tumor [16], and eventually to anaphylactic reactions. One possibility to reduce HAMA responses is the use of human-mouse chimeric antibodies (cMAbs), which are composed of the variable regions of the murine MAb fused to the heavy and light chain constant region of the human immunoglobulin or of humanized antibodies (hMAbs) that retain only a small fraction of the original murine protein sequence required for antigen binding. These modifications, however, may result in MAbs with lower affinity. Decrease of affinity is generally considered to be undesirable, based on animal studies in which it was shown that tumor uptake of low-affinity MAbs is less than that of high-affinity MAbs [17-21]. Whether these results are generally applicable remains to be determined, especially because the MAbs used in many of these comparative studies were unrelated and directed against different epitopes on the same antigen [17-20]. Since the accessibility of such epitopes might be different, data on the relationship between MAb affinity and tumor uptake should be interpreted with caution.

In the present study we describe the construction of one chimeric and two humanized derivatives of BIWA 1. Together with mMAbs U36 and BIWA 1, these antibodies were evaluated for their affinity to the target antigen *in vitro*, while biodistribution and therapeutic efficacy were studied in nude mice bearing human HNSCC xenografts.

MATERIALS AND METHODS

MAbs

mMAb BIWA 1 (formerly VFF 18, IgG1) was generated by immunizing BALB/c mice with glutathione S-transferase fusion protein containing the human CD44 domains v3-v10 [4]. The epitope recognized by BIWA 1 has been mapped to amino acids 360-370 in domain v6 of CD44 (numbering according to Kugelman *et al.* [22]). The batch used for the present studies was obtained after purification on protein-G-Sepharose and dialysis against phosphate buffered saline (PBS).

mMAb U36 (IgG1) was derived after immunization of mice with the HNSCC cell line UM-SCC-22B. The epitope recognized by U36 was mapped to the amino acids 365-376 of CD44v6, indicating that U36 and BIWA 1 recognize overlapping epitopes [3]. The batch used for the current studies was supplied by Centocor Inc. U36 was purified from a concentrated tissue culture supernatant by affinity chromatography on protein A-Sepharose and further purified on Q-Sepharose.

Generation of cMAbs and hMAbs

mRNA was isolated from the BIWA 1 hybridoma cell line using the QuickPrep mRNA Purification Kit (Pharmacia). cDNA from the variable heavy (V_H) and variable light (V_L) chain was generated by RT-PCR.

Fragments were cloned into the TA cloning vector pCR II (Invitrogen) and sequenced. Two expression vectors derived from the plasmid pAD CMV1 [23] were constructed, carrying

the constant region of human γ-1 and of the human κ light chain, respectively. Subsequently, the V_H and V_L fragments of BIWA 1 were cloned into the corresponding expression vectors in front of the constant regions. The chimeric antibody was named cMAb BIWA 2. Humanized versions of the BIWA 1 heavy and light chain variable regions (generated by CDR grafting) were cloned in front of the immunoglobulin constant regions of the above-mentioned expression vectors. The resulting MAb was named hMAb BIWA 4. In addition, a mutated version of BIWA 4, called hMAb BIWA 8, was constructed with the aim of improving binding affinity. This was achieved by back-mutating two amino acids of the light chain framework 2 and keeping the humanized heavy chain unchanged.

Recombinant MAbs were stably expressed in dihydrofolate reductase-deficient Chinese hamster ovary cells by electroporation with heavy and light chain expression plasmids. Cells were seeded into 96-well microtiter plates at densities of 500 and 100 cells/well in selection medium (α-MEM with 10% dialyzed fetal calf serum (FCS)). When colonies became visible (after approx. 14 d), culture supernatants were tested for their IgG content by ELISA and the best producers expanded. Gene amplification was performed by culturing in the presence of increasing concentrations of methotrexate (20-500 nM).

Laboratory scale production of chimeric and humanized MAbs was performed in a proprietary medium (Boehringer Ingelheim) containing 1% FCS. IgG fractions were purified from tissue culture supernatants by affinity chromatography on protein A-sepharose. Purity was tested by SDS-PAGE and high-performance size-exclusion chromatography.

Evaluation of antibody affinity

Kinetic and affinity constants were measured using recombinant antigen on a BIAcore 2000 system. A glutathione-S-transferase fusion protein containing domains v3-v10 of human CD44 (GST/CD44v3-v10; 20 µg/ml) was immobilized on a CM5 sensor chip by the amine-coupling method according to the manufacturer's instructions, using 10 mM sodium acetate (pH 5.0) as coupling buffer. MAb (35 µl) at various concentrations (8-67 nM) in HBS [10 mM HEPES, (pH 7.4), 150 mM NaCl, 3.4 mM EDTA, 0.05% BIAcore surfactant P20) were injected over the antigen-coated surface at a flow rate of 5 µl/min. Dissociation of the MAb was assessed for 5 min in buffer flow (HBS). Between two analyses, the surface of the chip was regenerated with a single pulse of 15 µl of 30 mM HCl. Analysis of the data and calculation of kinetic constants were performed with the BIAcore BIAevaluation software, version 2.1. Association rates (k_a), dissociation rates (k_d), and dissociation constants (K_d) were assessed for all antibodies.

Relative binding affinities were also evaluated by competitive cell ELISA. Human A431 cells, originating from an epidermoid carcinoma of the vulva and known to express high levels of CD44v6, were seeded in 96-well tissue culture plates in 200 µl/well RPMI-1640 with 10% FCS at a density of $2.5 - 5 \times 10^5$ cells/ml. Plates were incubated overnight at 37°C in a humidified incubator with 5% CO_2 in air. After removal of the medium, cells were washed once with PBS, fixed with 96% ethanol for 1 min and washed again with PBS. cMAb BIWA 2, hMAb BIWA 4 and hMAb BIWA 8 (prediluted to 10 µg/ml) were applied in 1:2 serial

dilutions (8 steps) in 100 µl/well in PBS/0.5% bovine serum albumin (BSA)/0.05% Tween 20 (assay buffer) and incubated for 30 min at room temperature. Prediluted mMAb BIWA 1 (100 µl, 20 ng/ml) was added and plates were incubated for 2 h at room temperature on an orbital shaker. Control samples contained prediluted samples only, without BIWA 1 (0% control) or BIWA 1 only without any competing antibodies (100% control). After washing three times with PBS/0.05% Tween 20 (washing buffer), 100 µl of the secondary antibody (peroxidase-conjugated goat antimouse Fc, diluted 1:15,000 in assay buffer; DAKO) were added for detection of mMAb BIWA 1, and the plates incubated for 1 h at room temperature on an orbital shaker. After washing three times with washing buffer, plates were developed with 100 µl/well tetramethylbenzidine substrate solution (Kierkegaard and Perry). The reaction was stopped after 15 min with 50 µl/well 1 M phosphoric acid. Absorbance was measured in an ELISA plate reader at 450 nm (reference 610-690 nm).

Radioiodination of MAbs

Iodination of MAbs was performed essentially as described by Haisma *et al.*[24], using either iodine-125 (^{125}I; 3.7 GBq/ml) or ^{131}I (7.2 GBq/ml), both purchased from Amersham. One mg of MAb IgG dissolved in 500 µl PBS (pH=7.4) and 37 MBq ^{125}I or ^{131}I were mixed in a vial coated with 75 µg Iodogen (Pierce). After 5 min of incubation at room temperature, free iodine was removed by gelfiltration on a PD-10 column (Pharmacia Biotech). After removal of unbound ^{125}I or ^{131}I, the radiochemical purity always exceeded 97% as determined by TLC and HPLC procedures described previously[15]. No aggregates or fragments were formed, as assessed by HPLC analysis.

Preparation of ^{186}Re-labeled MAbs

^{186}Re-labeled MAbs were prepared according to a multistep procedure using the chelate S-benzoylmercaptoacyltriglycine (S-benzoyl-MAG3) as previously described[15]. In this procedure, a solid-state synthesis for the preparation of ^{186}Re-MAG3 is followed by esterification with 2,3,5,6-tetrafluorophenol (TFP) and conjugation of the reactive ^{186}Re-MAG3-TFP ester to the MAb. After conjugation, the ^{186}Re-labeled MAb was purified on a PD-10 column. After removal of unbound ^{186}Re, the radiochemical purity always exceeded 98%.

Binding assay for radiolabeled MAbs

In vitro binding characteristics of the labeled MAbs used in the biodistribution and therapy studies were determined in an immunoreactivity assay essentially as described previously[15]. To test the binding of iodinated or ^{186}Re-labeled MAbs, UM-SCC-11B cells (kindly provided by Dr. T.E. Carey, University of Michigan, Ann Arbor, MI) fixed in 0.1% glutaraldehyde were used. Five serial dilutions (ranging from $5x10^6$ cells/tube to $3.1x10^5$ cells/tube) were prepared with 1% BSA in PBS. Excess of unlabeled MAb IgG was added to a second tube with the lowest concentration of cells to determine nonspecific binding. IgG labeled with 10,000 cpm of ^{125}I, ^{131}I or ^{186}Re was added to each tube; and samples were incubated

overnight at 4°C. Cells were spun down, radioactivity in the pellet and supernatant was measured in a γ-counter (LKB-Wallac 1282 CompuGamma; Pharmacia) and the percentage of bound and free radioactivity was calculated. Data were graphically analyzed in a modified Lineweaver-Burk plot and the immunoreactivity was determined by linear extrapolation to conditions representing infinite antigen excess.

Biodistribution studies in HNSCC-bearing nude mice

For the biodistribution experiments, nude mice bearing subcutaneously implanted human HNSCC xenografts (HNX-OE) were used as described previously [15]. Female mice (Hsd athymic *nu/nu*, 25-32 g; Harlan CPB) were 8-10 weeks old at the time of the experiments. Three biodistribution experiments were conducted with mice bearing 1 or 2 tumors ranging 30-470 mm^3. In the first experiment, 0.37 MBq (50 μg) ^{131}I-labeled mMAb U36 were injected simultaneously with 0.37 MBq (50 μg) ^{125}I-labeled mMAb BIWA 1 in mice bearing tumors of 133 ± 28 mm^3 (n = 20 mice, 37 tumors). In the second experiment, 0.37 MBq (50 μg) ^{131}I-labeled hMAb BIWA 4 and 0.37 MBq (50 μg) ^{125}I-labeled cMAb BIWA 2 were co-injected in mice bearing tumors of 167 ± 31 mm^3 (n = 21 mice, 32 tumors). In the third experiment, 0.37 MBq (50 μg) ^{131}I-labeled hMAb BIWA 4 and 0.37 MBq (50 μg) ^{125}I-labeled hMAb BIWA 8 were coinjected in mice with tumors of 130 ± 21 mm^3 (n = 23 mice, 40 tumors). Conjugates were intravenously (i.v.) injected in a volume of 100 μl after dilution in 0.9% NaCl. To obtain a comparable blood/body clearance of the coinjected MAbs, only MAbs with an identical murine or human isotype were combined. The antibody dose (total dose 100 μg/mouse) was chosen to be high enough to prevent rapid isotype-related elimination of the MAb from the blood [25,26] and low enough to prevent antigen saturation in the tumor.

At indicated time points after injection, mice were anaesthetized, bled, killed and dissected. Besides the tumors, the following organs were removed: liver, spleen, kidney, heart, stomach, ileum, colon, bladder, sternum, muscle, lung, skin and tongue. After weighing, radioactivity in tumors, blood and organs was counted in the dual-isotope γ-counter, with automatic correction for the ^{131}I Comptons in the ^{125}I window setting. Radioactivity uptake in these tissues was calculated as the percentage of the injected dose per gram of tissue (%ID/g).

All animal experiments were performed according to the principles of laboratory animal care and the Dutch national law "Wet op de Dierproeven" (Stb 1985, 336). Until the day of MAb administration, mice were routinely housed under specific pathogen-free conditions in sterile cages in a humidity- and temperature-controlled clean room (classification 2000 according to the Federal Standard 209d). On the day of injection, mice were transported to the Radionuclide Center, VU University and sterile radioimmunoconjugates were administered under aseptic conditions in a laminar flow hood.

RIT studies in nude mice

Animal RIT studies were performed to compare the therapeutic efficacy of the different MAbs labeled with ^{186}Re. The immunoreactive fractions of the conjugates always exceeded 75%. Three therapy experiments were conducted with mice bearing 1 or 2 HNX-OE tumors ranging

45-195 mm^3. ^{186}Re doses were chosen to be the maximum tolerated dose (MTD) level (i.e., 14.8 MBq) or lower (11.1 MBq). The MTD level is defined as the dose resulting in 5-15% body weight loss. In previous studies, it has been shown that the biodistribution of ^{186}Re-labeled MAbs and iodinated MAbs is similar in this animal model [15,27,28] and that neither ^{186}Re nor iodine is retained in the tumor cell upon MAb internalisation [27]. In the first experiment, mice were given a single i.v. injection of either 11.1 MBq (100 µg) ^{186}Re-labeled mMAb U36 or 11.1 MBq (100 µg) ^{186}Re-labeled mMAb BIWA 1. In the second experiment, either 11.1 MBq (100 µg) ^{186}Re-labeled hMAb BIWA 4 or 11.1 MBq (100 µg) ^{186}Re-labeled cMAb BIWA 2 were administered. In the third experiment, either 14.8 MBq (100 µg) ^{186}Re-labeled hMAb BIWA 4 or 14.8 MBq (100 µg) ^{186}Re-labeled hMAb BIWA 8 were administered. Average tumor volumes were similar for all experimental groups: Experiment 1, 95 ± 34 mm^3 ($n = 7$ mice, 12 tumors) for the ^{186}Re-mMAb U36-treated group, 91 ± 15 mm^3 ($n = 7$ mice, 12 tumors) for the ^{186}Re-mMAb BIWA 1-treated group and 99 ± 54 mm^3 ($n = 6$ mice, 11 tumors) for the control group; experiment 2, 101 ± 35 mm^3 ($n = 7$ mice, 12 tumors) for the ^{186}Re-hMAb BIWA 4-treated group, 92 ± 43 mm^3 ($n = 7$ mice, 12 tumors) for the ^{186}Re-cMAb BIWA 2-treated group and the control group was the same as in experiment 1; experiment 3, 105 ± 43 mm^3 ($n = 8$ mice, 13 tumors) for the ^{186}Re-hMAb BIWA 4-treated group, 100 ± 42 mm^3 ($n = 8$ mice, 13 tumors) for the ^{186}Re-hMAb BIWA 8-treated group and 110 ± 46 mm^3 ($n = 7$ mice, 11 tumors) for the control group. During treatment, tumors were measured twice weekly and tumor volumes relative to the volume at the start of treatment were calculated. Toxicity was monitored by measurement of body weight twice weekly. Mice were killed when one of the tumors exceeded 1,000 mm^3.

Statistics

Differences in tissue uptake and tumor-to-blood uptake ratios between coinjected MAbs were statistically analysed for each time point using the Student *t* test for paired data. Differences in average tumor volume between the various RIT treatment groups were statistically analysed for each time point using the Student *t* test for independent samples.

RESULTS

In vitro binding characteristics of the CD44v6-specific MAbs

The binding affinities of the five MAbs were analysed using recombinant antigen as well as human tumor cell lines. Kinetic and affinity constants were evaluated by surface plasmon resonance using GST/CD44v3-v10 as immobilized antigen. Table 1 shows the k_a, k_d and K_d values. mMAb BIWA 1 and cMAb BIWA 2, containing identical variable regions, have similar k_a, k_d, and K_d values and show the highest affinity. In contrast, mMAb U36 and hMAb BIWA 4 have lower k_a and higher k_d values, resulting in markedly lower K_d values (factors 35.0 and 10.5, respectively). hMAb BIWA 8, containing back-mutations in the light chain framework region 2, showed a marked decrease of k_d, resulting in increased affinity compared to hMAb BIWA 4.

The relative binding affinities of the cMAb and the hMAbs were also evaluated in a competitive cell ELISA using human A431 tumor cells (Fig. 1). In accordance with the affinity measurements on recombinant antigen, cMAb BIWA 2 was the most effective competitor, followed by hMAb BIWA 8 and hMAb BIWA 4. Similar results (not shown) were obtained with two other human HNSCC cell lines (FaDu and LICR-LON-HN5).

Table 1. Kinetics and affinity constants of MAbs directed against CD44v6

Antibody	k_a ($M^{-1} \cdot sec^{-1}$)	k_d (sec^{-1})	K_d (M)	K_d relative to murine BIWA 1
Murine BIWA 1	$1.3x10^5$	$4.2x10^{-5}$	$3.2x10^{-10}$	1.0
Murine U36	$1.5x10^4$	$1.7x10^{-4}$	$1.1x10^{-8}$	35.0
Chimeric BIWA 2	$1.7x10^5$	$4.1x10^{-5}$	$2.4x10^{-10}$	0.7
Humanized BIWA 4	$6.5x10^4$	$2.2x10^{-4}$	$3.4x10^{-9}$	10.5
Humanized BIWA 8	$7.5x10^4$	$6.3x10^{-5}$	$8.4x10^{-10}$	2.6

Biodistribution in HNSCC-bearing nude mice

Biodistribution studies were performed in HNX-OE xenograft-bearing nude mice. Two MAbs with identical murine or human isotype were labeled with either ^{125}I or ^{131}I and injected simultaneously (50 µg, 0.37 MBq each). Each pair of MAbs was selected to provide a stepwise decrease in the difference in affinities: mMAb U36 had 35.0-fold lower affinity than mMAb BIWA 1 (experiment 1), hMAb BIWA 4 had 14.0-fold lower affinity than cMAb BIWA 2 (experiment 2) and hMAb BIWA 4 had 4.0-fold lower affinity than hMAb BIWA 8 (experiment 3). The fractions of MAb binding to $5x10^6$ cells and at infinite antigen excess were, respectively, 59.7% and 87.4% for ^{131}I-mMAb U36 and 91.1% and 91.1% for ^{125}I-mMAb BIWA 1 in experiment 1; 77.4% and 82.3% for ^{131}I-hMAb BIWA 4 and 80.5% and

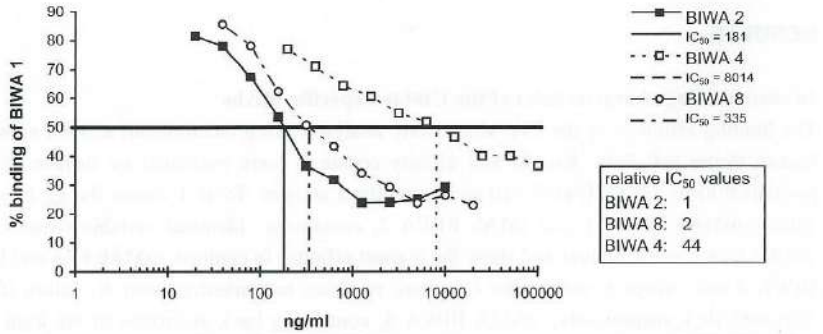

Figure 1. Evaluation of relative binding affinities tested in a competitive cell ELISA. IC_{50}, concentrations of cMAb and hMAbs at which binding of mMAb BIWA 1 to attached A431 cells is reduced by 50%. IC_{50} values relative to BIWA 2 are indicated.

79.9% for ^{125}I-cMAb BIWA 2 in experiment 2; and 77.3% and 74.5% for ^{131}I-hMAb BIWA 4 and 91.8% and 92.1% for ^{125}I-hMAb BIWA 8 in experiment 3.

The biodistributions in experiment 1 were determined at 1, 2, 3 and 7 d after injection; biodistributions in experiments 2 and 3 were determined at 1, 2, 4 and 7 d after injection (Fig. 2 and 3). The average %ID/g and SEM of tumor, blood and various organs after simultaneous injection of ^{131}I-mMAb U36 and ^{125}I-mMAb BIWA 1 were determined and tumor-to-blood ratios calculated. Tumor uptake of low-affinity U36 was significantly higher than uptake of high-affinity BIWA 1 ($P \leq 0.001$) at all time points (Fig. 2A), while no significant differences were found between the uptake values of these MAbs in blood (Fig. 2A) and normal tissues (data not shown) at 1, 2 and 3 d after injection. At 3 d, 50% higher tumor uptake of U36 compared to BIWA 1 was observed. At 7 d, BIWA 1 levels in blood and most of the organs were significantly lower than U36 levels, indicating more rapid clearance of BIWA 1 from the blood/body. Tumor-to-blood ratios were significantly higher for U36 than for BIWA 1 at all time points (Fig. 3A).

Similar relationships were found in the evaluation of the two other MAb pairs, as partly demonstrated by Figure 2B, C and 3B, C. hMAb BIWA 4, while having the lower affinity, showed significantly higher tumor uptake ($P \leq 0.01$) than cMAb BIWA 2 (Fig. 2B) and hMAb BIWA 8 (Fig. 2C) at all time points, while MAb levels in blood (Fig. 2B, C, respectively) and normal tissues (data not shown) were similar for these pairs of MAbs at 1, 2 and 4 d after injection. A 45% higher tumor uptake of BIWA 4 compared to BIWA 2 is illustrated in Figure 2B, while a 20% higher tumor uptake of BIWA 4 compared to BIWA 8 is illustrated in Figure 2C, at 4 d after injection. At 7 d after injection, BIWA 2 and BIWA 8 levels in blood and organs were mostly significantly lower than BIWA 4 levels, indicating more rapid clearance of these MAbs from the blood/body. Tumor-to-blood ratios were significantly higher for BIWA 4 than for BIWA 2 (Fig. 3B) and BIWA 8 (Fig. 3C) at all time points.

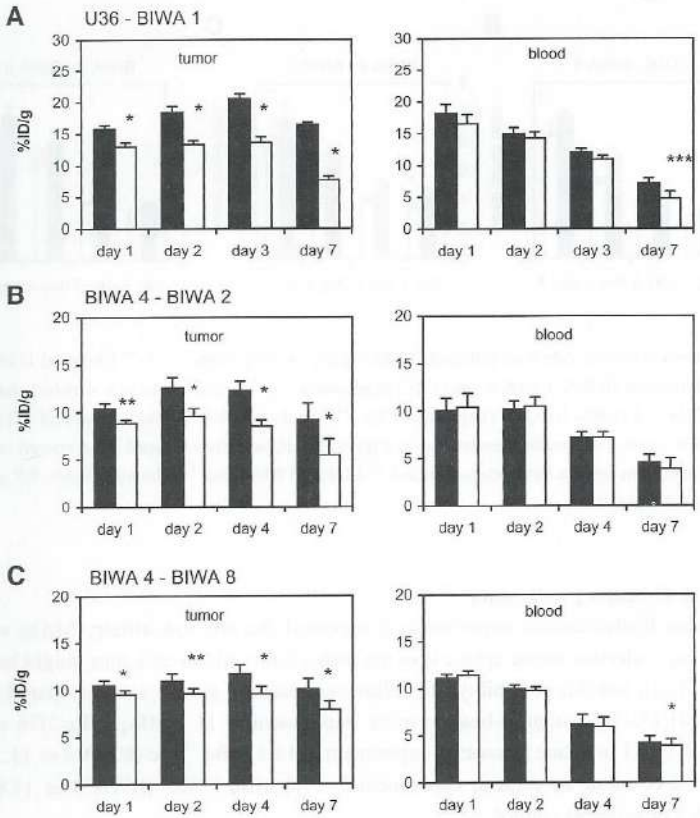

Figure 2. Tumor and blood levels of coinjected MAb pairs in HNX-OE xenograft-bearing mice ($n = 5$ or 6) at 1, 2, 3 or 4 and 7 d after injection. A (experiment 1), ^{131}I-labeled U36 (0.37 MBq, 50 µg; black bars) and ^{125}I-labeled BIWA 1 (0.37 MBq, 50 µg; white bars). B (experiment 2), ^{131}I-labeled BIWA 4 (0.37 MBq, 50 µg; black bars) and ^{125}I-labeled BIWA 2 (0.37 MBq, 50 µg; white bars). C (experiment 3), ^{131}I-labeled BIWA 4 (0.37 MBq, 50 µg; black bars) and ^{125}I-labeled BIWA 8 (0.37 MBq, 50 µg; white bars). At the indicated days after injection, mice were bled, killed and dissected and the radioactivity levels (%ID/g ± SEM) of tumor, blood and several organs (data not shown) were assessed. Significantly different uptake between coinjected ^{131}I-labeled MAb and ^{125}I-labeled MAb: $*P \leq 0.001$; $**P \leq 0.01$ and $***P \leq 0.05$.

Consistent results were obtained from an additional experiment (data not shown) in which the radiolabels were exchanged: ^{125}I-BIWA 4 *vs.* ^{131}I-BIWA 8 instead of ^{131}I-BIWA 4 *vs.* ^{125}I-BIWA 8. Data from this latter experiment rule out the possibility that the type of radiolabel had influenced the pharmacokinetic behavior of the labeled MAb.

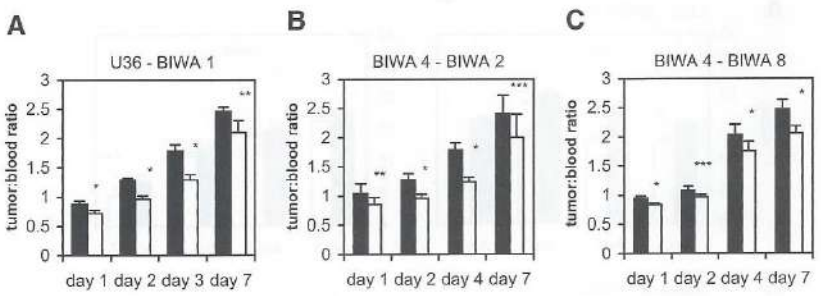

Figure 3. Tumor-to-blood ratios of coinjected MAb pairs. A (experiment 1), ^{131}I-labeled U36 (black bars) and ^{125}I-labeled BIWA 1 (white bars). B (experiment 2), ^{131}I-labeled BIWA 4 (black bars) and ^{125}I-labeled BIWA 2 (white bars). C (experiment 3), ^{131}I-labeled BIWA 4 (black bars) and ^{125}I-labeled BIWA 8 (white bars). For details, see legend to Figure 2. Ratios were obtained from paired samples. Significantly different uptake between coinjected ^{131}I-labeled MAb and ^{125}I-labeled MAb: $*P \leq 0.001$; $**P \leq 0.01$ and $***P \leq 0.05$.

RIT in HNSCC-bearing nude mice

From the three biodistribution experiments it appeared that the low-affinity MAbs showed higher and more selective tumor uptake than the high-affinity MAbs and, thus, might be better suited for RIT. To test this possibility, the following treatment groups were compared in RIT studies with HNX-OE xenograft-bearing mice: experiment 1, 11.1 MBq ^{186}Re-U36 or 11.1 MBq ^{186}Re-BIWA 1 or saline as control; experiment 2, 11.1 MBq ^{186}Re-BIWA 4 or 11.1 MBq ^{186}Re-BIWA 2 or saline as control; experiment 3, 14.8 MBq ^{186}Re- BIWA 4 or 14.8 MBq ^{186}Re-BIWA 8 or saline as control.

In Figure 4, mean relative tumor volume (as a percentage of the tumor volume at day 0) for the control and treatment groups is plotted against time. Tumors of mice in the control group in all three experiments showed exponential growth, with a tumor volume doubling time of about 7 d. In the groups treated with the ^{186}Re-labeled anti-CD44v6 MAbs, tumors stopped growing, in some cases accompanied by tumor regression, shortly after injection of conjugates. However, all tumors ultimately regrew. As a control, the nonbinding ^{186}Re-labeled hMAb F19 (directed against a human epitope on fibroblast activation protein) was evaluated in the same animal model. This radioimmunoconjugate did not induce growth cessation (data not shown).

In experiment 1, administration of 11.1 MBq ^{186}Re-BIWA 1 resulted in a decrease of the tumor growth rate but not in a reduction of the mean tumor size. Administration of 11.1 MBq ^{186}Re-U36, however, caused a reduction of the mean tumor volume from 185 mm^3 to 120 mm^3 between 7 and 17 d after injection, after which tumors started growing again. The mean relative tumor volume in the ^{186}Re-U36-treated group was significantly smaller ($P < 0.001$) than that of the ^{186}Re-BIWA 1-treated group from 14 d on.

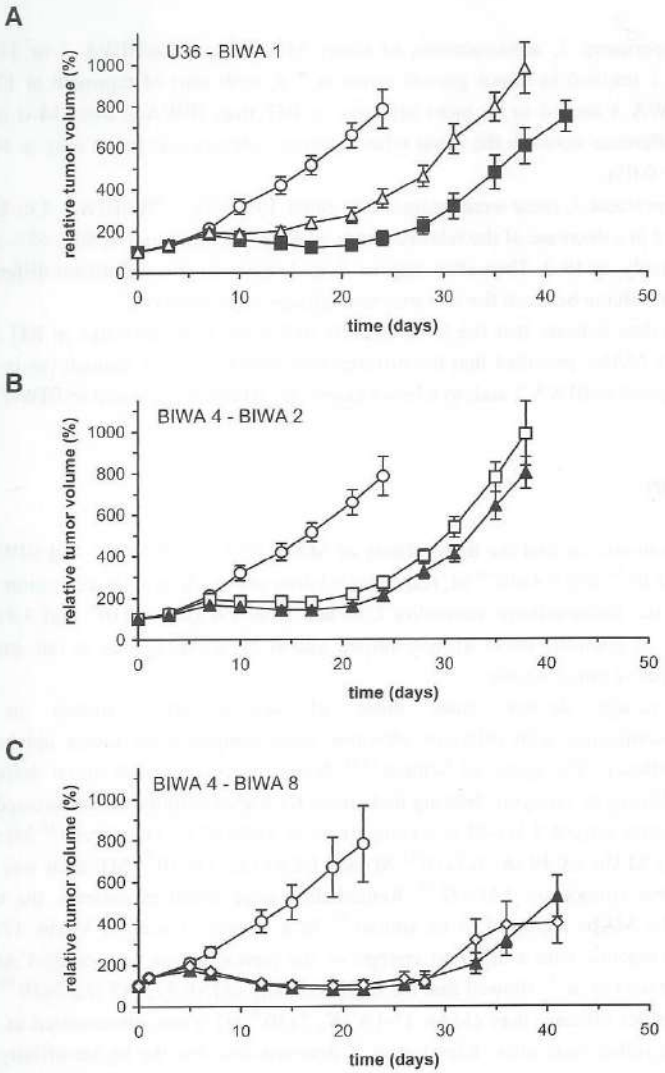

Figure 4. Therapeutic efficacy of ^{186}Re-labeled CD44v6-specific MAbs in HNX-OE xenograft-bearing nude mice. A (experiment 1), mice were injected with saline (open circles) as control, 11.1 MBq ^{186}Re-U36 (solid squares), or 11.1 MBq ^{186}Re-BIWA 1 (open triangles). B (experiment 2), mice were injected with saline (open circles), 11.1 MBq ^{186}Re-BIWA 4 (solid triangles), or 11.1 MBq ^{186}Re-BIWA 2 (open squares). C (experiment 3), mice were injected with saline (open circles), 14.8 MBq ^{186}Re-BIWA 4 (solid triangles), or 14.8 MBq ^{186}Re-BIWA 8 (open diamonds). Control groups in (A,B) are the same. Tumor size is expressed as average tumor volume (± SEM) during treatment relative to average tumor volume at the start of therapy.

In experiment 2, administration of either 11.1 MBq ^{186}Re-BIWA 4 or 11.1 MBq ^{186}Re-BIWA 2 resulted in tumor growth arrest at 7 d, with start of regrowth at 17 d after injection. BIWA 4 tended to be more effective in RIT than BIWA 2 from 14 d on, but a significant difference between the mean relative tumor volumes was found only at 14 d after injection ($P < 0.05$).

In experiment 3, mice were treated with either 14.8 MBq ^{186}Re-BIWA 4 or BIWA 8, which resulted in a decrease of the relative tumor volume to a minimum of 80 ± 62% and 98 ± 81%, respectively, at 19 d. Thereafter, tumors started regrowth. No significant differences in relative tumor volume between the two treatment groups were observed.

These data indicate that the lower-affinity MAbs are more effective in RIT than the higher-affinity MAbs, provided that the difference in affinity is large enough (as is the case for U36 compared to BIWA 1 and, to a lesser extent, for BIWA 4 compared to BIWA 2).

DISCUSSION

Our results demonstrate that the high affinity of MAbs BIWA 1, BIWA 2 and BIWA 8 (K_d $3.2x10^{-10}$, $2.4x10^{-10}$, and $8.4x10^{-10}$ M, respectively) does not result in improved tumor delivery compared to the lower-affinity antibodies U36 and BIWA 4 (K_d $1.1x10^{-8}$ and $3.4x10^{-9}$ M, respectively). In contrast, lower affinity turned out to be advantageous in our study with respect to selective tumor uptake.

Our results deviate from those of several other studies in which radioimmunoconjugates with different affinities were compared for tumor uptake and/or therapeutic efficacy. The group of Schlom [17,18] demonstrated improved tumor delivery and therapeutic efficacy in xenograft-bearing nude mice for higher-affinity MAbs directed against the pancarcinoma antigen TAG-72 in a comparison of MAb B72.3 (K_d $4.0x10^{-10}$ M) with the higher-affinity MAbs CC49 (K_d $6.2x10^{-11}$ M) and CC83 (K_d $3.6x10^{-11}$ M), each was reactive with a different epitope on TAG-72 [18]. Remarkably, once tested in patients, the targeting capacity of the MAbs appeared to be similar [29]. In a couple of studies, MAbs 17-1A and 323/A3, both reactive with a different epitope on the pancarcinoma antigen Ep-CAM, were compared. Velders *et al.* [30] showed that the higher-affinity cMAb 323/A3 (K_d $5x10^{-10}$ M) had consistently better efficacy than cMAb 17-1A (K_d $2x10^{-8}$ M) when administered as "naked" MAb to xenografted nude mice. Kievit *et al.* [20] demonstrated that the higher-affinity mMAb 323/A3 targeted better to ovarian cancer xenografts but was more heterogeneously distributed when compared to cMAb 17-1A. At equivalent radiation doses, ^{131}I-labeled mMAb 323/A3 induced better growth inhibition than ^{131}I-labeled cMAb 17-1A in 2 of 3 xenograft lines tested. Adams *et al.* [21] generated affinity mutants of the human anti-HER 2/neu single-chain Fv antibody C6.5 by site-directed mutagenesis and tested them for tumor-targeting in xenograft-bearing SCID mice. Their studies are of particular interest because all of these mutants targeted the same antigenic epitope and demonstrated a 320-fold difference in affinity ($3.2x10^{-7}$ to $1.0x10^{-9}$ M). Biodistribution studies with these scFv antibodies revealed an

increase in degree and specificity of localization with increasing affinity. During the time period our experiments were performed, the same researchers performed similar biodistribution studies but now using C6.5 mutation variants with affinities as high as 10^{-11} M [31]. They showed that quantitative tumor retention did not significantly increase with enhancements in affinity beyond 10^{-9} M. At affinities of $1.2x10^{-10}$ M to $1.5x10^{-11}$ M, tumor retention even decreased. These latter data are in line with our present observations with intact MAbs.

It is tempting to speculate that the improved therapeutic efficacy of ^{186}Re-U36 compared to ^{186}Re-BIWA 1 is due to the higher tumor uptake, as observed with the lower-affinity MAb U36. However, other factors also might play a role. On the basis of mathematical models of the distribution of MAbs throughout tumors, Fujimori *et al.* [32] postulated that the use of lower-affinity MAbs in RIT might be advantageous for antitumor effects. While high-affinity MAbs will become firmly bound to antigens located at the periphery of the tumor and, therefore, will be retarded in their penetration deeply into tumors ("binding site barrier" theory), such a phenomenon will be met to a lesser extent with low-affinity MAbs. Indeed, it has been demonstrated that, besides tumor localization (this report), tumor penetration might be restricted by the high affinity of MAbs, thus resulting in a decrease of the efficacy of MAb-targeted therapies [20,31].

In conclusion, our results demonstrate that a significant loss of affinity incurred by humanisation of BIWA 1 does not have a negative impact on the tumor-targeting properties and therapeutic efficacy of the derivatives. hMAb BIWA 4 is currently being used in tumor uptake/biodistribution studies in patients with HNSCC.

REFERENCES

1. De Bree R, Roos JC, Quak JJ, den Hollander W, Snow GB, van Dongen GAMS. Radioimmunoscintigraphy and biodistribution of ^{99m}Tc-labeled monoclonal antibody U36 in patients with head and neck cancer. *Clin Cancer Res.* 1995;1:591-598.
2. Stroomer JWG, Roos JC, Sproll M, et al. Safety and biodistribution of ^{99m}Technetium-labeled anti-CD44v6 monoclonal antibody BIWA 1 in head and neck cancer patients. *Clin Cancer Res.* 2000;6:3046-3055.
3. Van Hal NLW, van Dongen GAMS, Rood-Knippels EMC, van der Valk P, Snow GB, Brakenhoff RH. Monoclonal antibody U36, a suitable candidate for clinical immunotherapy of squamous cell carcinoma, recognizes a CD44 isoform. *Int J Cancer.* 1996;68:520-527.
4. Heider K-H, Sproll M, Susani S, et al. Characterization of a high-affinity monoclonal antibody specific for CD44v6 as candidate for immunotherapy of squamous cell carcinomas. *Cancer Immunol Immunother.* 1996;43:245-253.
5. Van Hal NLW, van Dongen GAMS, ten Brink CB, et al. Evaluation of soluble CD44v6 as a potential serum marker for head and neck squamous cell carcinoma. *Clin Cancer Res.* 1999;5:3534-3541.
6. Lesley J, Hyman R, Kincade PW. CD44 and its interaction with extracellular matrix. *Adv Immunol.* 1993;54:271-335.
7. Webb DS, Shimizu Y, van Seventer GA, Shaw S, Gerrard TL. LFA-3, CD44, and CD45: physiologic triggers of human monocyte TNF and IL-1 release. *Science.* 1990; 249:1295-1297.
8. Thomas L, Byers HR, Vink J, Stamenkovic I. CD44H regulates tumor cell migration on hyaluronate-coated substrate. *J Cell Biol.* 1992;118: 971-977.
9. Koopman G, Taher TE, Mazzucchelli I, et al. CD44 isoforms, including the CD44v3 variant, are expressed on endothelium, suggesting a role for CD44 in the immobilization of growth factors and the regulation of local immune response. *Biochem Biophys Res Commun.* 1998;7:172-176.
10. Günthert U, Hofmann M, Rudy W, et al. A new variant of glycoprotein CD44 confers metastatic potential to rat carcinoma cells. *Cell.* 1991;65:13-24.
11. Seiter S, Arch R, Reber S, et al. Prevention of tumor metastasis formation by anti-variant CD44. *J Exp Med.* 1993;177:443-455.
12. Kaufmann M, Heider K-H, Sinn HP, Von Minckwitz G, Ponta H, Herrlich P. CD44 variant exon epitopes in primary breast cancer and length of survival. *Lancet.* 1995;345: 615-619.
13. Mulder JW, Kruyt PM, Sewnath M, et al. Colorectal cancer prognosis and expression of exon-v6-containing CD44 proteins. *Lancet.* 1994;344:1470-1472.
14. Stauder R, Eistener W, Thaler J, Günther U. CD44 variant isoforms in non-Hodgkin's lymphoma: a new independent prognostic factor. *Blood.* 1995;85:2885-2890.
15. Van Gog FB, Visser GWM, Klok R, van der Schors R, Snow GB, van Dongen GAMS. Monoclonal antibodies labeled with Rhenium-186 using the MAG3 chelate: Relationship between the number of chelate groups and biodistribution characteristics. *J Nucl Med.* 1996;37:352-362.
16. Khazaeli MB, Conry R, LoBuglio AF. Human immune response to monoclonal antibodies. *J Immunother.* 1994;15:42-52.

17. Colcher D, Minelli MF, Roselli M, Muraro R, Simpson-Milenic D, Schlom J. Radioimmunolocalization of human carcinoma xenografts with 72.3 second generation monoclonal antibodies. *Cancer Res.* 1988;48:4597-4603.
18. Schlom J, Eggensperger D, Colcher D, et al. Therapeutic advantage of high-affinity anticarcinoma radioimmunoconjugates. *Cancer Res.* 1992;52:1067-1072.
19. Langmuir VK, Mendonca HL, Woo DV. Comparisons between two monoclonal antibodies that bind to the same antigen but have differing affinities: uptake kinetics and ^{125}I-antibody therapy efficacy in multicell spheroids. *Cancer Res.* 1992;52:4728-4734.
20. Kievit E, Pinedo HM, Schluper HM, Haisma HJ, Boven E. Comparison of monoclonal antibodies 17-1A and 323/A3: the influence of the affinity on tumor uptake and efficacy of radioimmunotherapy in human ovarian cancer xenografts. *Br J Cancer.* 1996;73: 457-464.
21. Adams GP, Schier R, Marshall K, et al. Increased affinity leads to improved selective tumor delivery of single-chain Fv antibodies. *Cancer Res.* 1998;58:485-490.
22. Kugelman LC, Gangluly S, Haggerty JG, Weissman SM, Milstone LM. The core protein of epican, a heparan sulfate proteoglycan on keratinocytes, is an alternative form of CD44. *J Invest Dermatol.* 1992;99:886-891.
23. Himmler A, Maurer-Fogy I, Kronke M, et al. Molecular cloning and expression of human and rat tumor necrosis factor receptor chain (p60) and its soluble derivative, tumor necrosis binding protein. *DNA & Cell Biol.* 1990;9:705-715.
24. Haisma HJ, Hilgers J, Zurawski VR Jr. Iodination of monoclonal antibodies for diagnosis and therapy using a convenient one vial method. *J Nucl Med.* 1986;27:1890-1895.
25. Sharkey RM, Natale A, Goldenberg DM, Mattes MJ. Rapid blood clearance of immunoglobulin G2a and immunoglobulin G2b in nude mice. *Cancer Res.* 1991;51: 3102-3107.
26. Van Gog FB, Brakenhoff RH, Snow GB, van Dongen GAMS. Rapid elimination of mouse/human chimeric monoclonal antibodies in nude mice. *Cancer Immunol Immunother.* 1997;44:103-111.
27. Steffens MG, Kranenborg MH, Boerman OC, et al. Tumor retention of ^{186}Re-MAG3, ^{111}In-DTPA and ^{125}I-labeled monoclonal antibody G250 in nude mice with renal cell carcinoma xenografts. *Cancer Biother Radiopharm.* 1998;13:133-139.
28. Kievit E, van Gog FB, Schluper HM, van Dongen GAMS, Pinedo HM, Boven E. Comparison of the biodistribution and the efficacy of monoclonal antibody 323/A3 labeled with either ^{131}I or ^{186}Re in human ovarian cancer xenografts. *Int J Radiat Oncol Phys.* 1997;38:813-823.
29. Gallinger S, Reilly RM, Kirsh JC, et al. Comparative dual label study of first and second generation antitumor-associated glycoprotein-72 monoclonal antibodies in colorectal cancer patients. *Cancer Res.* 1993; 53:271-278.
30. Velders MP, van Rhijn CM, Briaire IH, Fleuren GJ, Warnaar SO, Litvinov SV. Immunotherapy with low and high affinity monoclonal antibodies 17-1A and 323/A3 in a nude mouse xenograft carcinoma model. *Cancer Res.* 1995;55:4398-4403.
31. Adams GP, Schier R, McCall AM, et al. High affinity restricts the localization and tumor penetration of single-chain Fv antibody molecules. *Cancer Res.* 2001;61:4750-4755.
32. Fujimori K, Covell DG, Fletcher JE, Weinstein JN. A modeling analysis of monoclonal antibody percolation through tumors: a binding-site barrier. *J Nucl Med.* 1990;31:1191-1198.

chapter

3

^{89}Zr immuno-PET: comprehensive procedures for the production of ^{89}Zr-labeled monoclonal antibodies

Iris Verel, Gerard W.M. Visser, Ronald Boellaard, Marijke Stigter-van Walsum, Gordon B. Snow, Guus A.M.S. van Dongen

***Journal of Nuclear Medicine* 2003;44:1271-1281.**

ABSTRACT

The use of immuno-PET, the combination of PET with monoclonal antibodies (MAbs), is an attractive option to improve tumor detection and MAb quantification. The long-lived positron emitter ^{89}Zr has ideal physical characteristics for immuno-PET, such as a half-life of 3.27 d, which is compatible with the time needed for intact MAbs to achieve optimal tumor-to-nontumor ratios. Thus far, a major limitation in the use of ^{89}Zr has been the lack of suitable methods for its stable coupling to MAbs. In this article, practical protocols for reproducible isolation of highly pure ^{89}Zr and the production of optimal-quality MAb-^{89}Zr conjugates are provided. **Methods:** ^{89}Zr was produced by a (p,n) reaction on natural yttrium (^{89}Y), isolated with a hydroxamate column, and used for labeling of premodified MAbs. MAbs were premodified with a novel bifunctional derivative of the chelate desferrioxamine B (Df) via a new linker chemistry. To this end, Df was initially succinylated (*N*-sucDf), temporarily filled with Fe(III), esterified by use of tetrafluorophenol, and then directly coupled to MAbs. Chimeric MAb (cMAb) U36, directed against head and neck cancer, was used for *in vitro* and *in vivo* evaluation. The *in vitro* stability of cMAb U36-*N*-sucDf-^{89}Zr was assessed in human serum, and its *in vivo* behavior was evaluated by biodistribution and PET imaging studies in tumor-bearing nude mice. A cMAb U36-Df-^{89}Zr conjugate containing a previously described succinimide ring-thioether unit in the linker was used as a reference. **Results:** ^{89}Zr was produced in large batches (6.5-13.5 GBq) and isolated with improved radionuclidic purity (>99.99%) and high yield (>94%). The Df-premodified MAbs gave ^{89}Zr-labeling efficiencies of 80% within 30 min, resulting in conjugates with preserved integrity and immunoreactivity. With respect to stability, the novel cMAb U36-*N*-sucDf-^{89}Zr conjugate appeared to be superior to the reference conjugate. *In vivo*, the novel conjugate demonstrated selective tumor-targeting, and on PET images obtained at 24, 48, and 72 h after injection of this conjugate, small tumors in the range of 19-154 mg were readily visualized. **Conclusion:** Methods were developed for improved purification of the long-lived positron emitter ^{89}Zr. Moreover, a novel bifunctional Df chelate was synthesized for the reproducible coupling of ^{89}Zr to MAbs. The suitability of such conjugates to detect millimeter-sized tumors in xenograft-bearing nude mice was demonstrated.

INTRODUCTION

Radiolabeled monoclonal antibodies (MAbs) have shown considerable potential for diagnosis and treatment of cancer [1,2]. In recently performed clinical radioimmunoscintigraphy (RIS) and radioimmunotherapy (RIT) studies at our institute, the potential of the CD44v6-specific MAb U36 for these purposes has been demonstrated [3,4]. For the detection of head and neck squamous cell carcinoma (HNSCC), primary tumors as well as metastases, RIS with technetium-99m-labeled (^{99m}Tc-labeled) MAb U36 IgG was found to be as valuable as the conventional imaging techniques CT and MRI, but the detection of tumor deposits smaller than 1 cm appeared to be a problem [3]. Introduction of PET might further improve tumor detection because of its high resolution. In addition, PET has potential for quantitative imaging. These features should enable PET to provide proof of principle of antibody targeting and dosimetric determinations prior to RIT. For this purpose, we are focusing on the coupling of positron emitters to MAbs and the use of these radiolabeled MAbs in immuno-PET.

For a positron emitter to be appropriate for immuno-PET, it has to fulfill several requirements. Its physical half-life has to be compatible with the time needed for a MAb to achieve optimal tumor-to-nontumor ratios. For intact MAbs used for targeting solid tumors, this time is generally 2-4 d. Therefore, commonly used positron emitters such as carbon-11 (^{11}C) and fluorine-18 (^{18}F) (half-life, 20 and 110 min, respectively) are not suitable for labeling of MAbs. With respect to decay characteristics, the positron-emitting isotope should by preference have no prompt γ-photons with an energy near 511 keV to optimize quantitative accuracy, and the β^+-energy should be as low as possible to obtain a high resolution. Besides this, production of the positron emitter should be easy (by preference with a medium-to-small cyclotron), reproducible, and at low cost. Finally, procedures should be available for stable coupling of the positron emitter to the MAb, with maintenance of the *in vivo* biodistribution characteristics of the latter.

Regarding the required half-life of several days, the two positron emitters iodine-124 (^{124}I; half-life, 4.18 d) and zirconium-89 (^{89}Zr; half-life, 3.27 d) are most suitable. The low natural abundance of the target material for the production of ^{124}I, however, requires enrichment into tellurium-124 (^{124}Te) for a (p,n) or a (d,2n) reaction or into ^{125}Te for a (p,2n) reaction. At the current stage of development, production of ^{124}I is too expensive to allow routine clinical application. With respect to the latter, ^{89}Zr can be produced by a (p,n) reaction on yttrium-89 (^{89}Y), an element that does not require enrichment because of its natural abundance of 100%. Taking the aforementioned considerations into account, we regard ^{89}Zr ($\beta^+ = 22.7\%$, $E_{\beta+max} = 0.897$ MeV)(see Table 1) to be a promising candidate for immuno-PET.

The bifunctional chelate desferrioxamine B (Df) (Fig. 1) is the ideal chelate for binding of ^{89}Zr because of the stable bond formation of ^{89}Zr with the three hydroxamate groups of this chelate [6]. For the coupling of this chelate to MAbs, Meijs *et al.* [7] modified the chelate into *N*-(*S*-acetyl)mercaptoacetyldesferrioxamine B (SATA-Df), and the lysine groups of the MAb were modified into maleimide groups. Upon reaction of these two, a linker was formed containing a succinimide ring-thioether unit. At physiologic pH, the latter unit,

however, might be responsible for the release of the chelate from the MAb as has, for example, been shown by Lewis and Shively[8] for their dodecanetetraacetic acid (DOTA)-conjugated MAbs. It can be anticipated that such instability will result in suboptimal delivery of ^{89}Zr to the tumor.

Table 1. γ-Spectroscopic analysis of ^{89}Zr and its purification by hydroxamate column

	Half-life	Main γ-energies		Crude ^{89}Zr solution [a]	Waste fractions [b]	Purified ^{89}Zr solution [c]
Isotope	(d)	MeV	% Abundance	(% activity ± SD)	(% activity ± SD)	(% activity ± SD)
^{89}Zr [d]	3.27	0.511 [e]	45.3	99.98 ± 0.0045	1.0 ± 1.0	97.0 ± 3.3
		0.909	99.9			
		1.202	0.014 [f]			
		1.622	0.070 [f]			
		1.657	0.100			
		1.713	0.769			
		1.744	0.130			
^{88}Zr	83.4	0.393	100	$1.5 \pm 1.8 \times 10^{-4}$	$1.2 \pm 2.3 \times 10^{-6}$	$2.2 \pm 2.2 \times 10^{-4}$
^{88}Y	106.64	0.898	93.4	$6.0 \pm 5.1 \times 10^{-5}$	$6.2 \pm 5.5 \times 10^{-5}$	ND
		1.836	99.3			
^{48}V	16.24	0.511	100	$2.9 \pm 0.3 \times 10^{-3}$	$3.1 \pm 0.3 \times 10^{-3}$	ND
		0.984	100			
		1.312	97.5			
^{56}Co	78.76	0.511	39.7	$8.9 \pm 4.4 \times 10^{-4}$	$9.7 \pm 4.3 \times 10^{-4}$	ND
		0.847	99.9			
		1.238	67.0			
^{65}Zn	243.9	0.511	2.92	$7.1 \pm 4.1 \times 10^{-3}$	$6.9 \pm 5.3 \times 10^{-3}$	ND
		1.116	50.7			
^{156}Tb	5.34	0.199	37.4	$2.6 \pm 0.5 \times 10^{-3}$	$3.3 \pm 0.5 \times 10^{-3}$	ND
		0.534	61.2			
		1.222	29.4			

[a] Total amount of activity found in crude solution is set at 100%; data are mean ± SD of five productions.

[b] Consisting of flow-through (after loading crude ^{89}Zr solution onto hydroxamate column), HCl fraction, and water fraction.

[c] Consisting of five 1 M oxalic acid fractions of 0.5 ml.

[d] Complete list of found γ-energies of ^{89}Zr

[e] Resulting from 22.7% β^+ abundance, $E_{\beta+\,max}$ = 0.897 MeV.

[f] These data are from this study; γ-energies with abundance of 0.1% or higher were found to be in full accordance with γ-energies reported by International Commission on Radiological Protection[5].

ND = not detectable, i.e., below 10 Bq.

In our group, good results have been obtained with a conjugation method based on the reaction of an active 2,3,5,6-tetrafluorophenol-chelate ester (TFP-chelate ester) with the lysine moieties of the MAb, resulting in a stable amide bond as the linker unit. This method gives optimal control over the number of groups conjugated to the MAb and has been used for the production of radioimmuno- and photoimmunoconjugates [9,10].

In the present report, we describe the use of this TFP ester approach for the improved purification of ^{89}Zr as well as for the coupling of a novel bifunctional derivative of Df to MAbs. The *in vitro* stability of these ^{89}Zr-conjugates and their biodistribution in xenograft-bearing nude mice were determined and compared with succinimide ring-thioether linked Df-^{89}Zr conjugates. The feasibility of visualizing millimeter-sized tumors was demonstrated in HNSCC-bearing nude mice.

MATERIALS AND METHODS

Monoclonal antibodies

Selection, production, and characterization of chimeric MAb (cMAb) U36, as well as of the control murine MAbs (mMAbs) 425 and E48, have been described elsewhere [10].

^{89}Zr production and purification

^{89}Zr was produced by a (p,n) reaction on natural yttrium (^{89}Y). For this purpose, an ^{89}Y-target was bombarded with 14-MeV protons [11] for 2-3 h (65-80 μA) while the target support was cooled with water (AVF cyclotron; Philips). ^{89}Y targets were prepared by sputtering an ^{89}Y layer (35 μm, Highways International) on a copper support (Mallinckrodt Medical) as described by Meijs *et al.* [12]. After irradiation, the ^{89}Y layer was slowly dissolved in four successive 0.5-ml portions of 1 M HCl (Sigma-Aldrich). Then, ^{89}Zr was oxidized to the IV-oxidation state with 0.1 ml hydrogen peroxide (30% v/v; Mallinckrodt Baker), and 0.22 ml of 12 M HCl was added to set the final HCl concentration at 2 M. After 1 h, ^{89}Y and radionuclidic impurities were removed using a hydroxamate column.

Hydroxamate column material for purification of ^{89}Zr was prepared from Accell Plus CM cation exchange media (300 Å, 0.35 mmol/g ligand density; Waters). To ensure a reproducible high level of hydroxamate function, a new two-step ester-mediated method was developed. In the first reaction step, the carboxylic acid groups of the cation exchange medium were esterified using an excess of TFP (Acros Organics) and 1-ethyl-3-(3-dimethylaminopropyl)-carbodiimide (EDC; Acros Organics). For an optimal conversion of carboxylic acid groups into ester groups, the TFP and EDC were added in two successive portions. In short: To 1 g of Accell, suspended in 8 ml of water for injection (Baxter), 75 μl of 3 M HCl, 1 ml of a TFP solution (200 mg/ml in MeCN, 1.2 mmol) and 384 mg of solid EDC (2 mmol) were added (final pH 5.7-6.0). The suspension was mixed end over end for 1 h. Afterward, 105 μl of 3 M HCl were added, along with a new 1-ml portion of TFP and a new

384-mg portion of EDC (final pH 5.7-6.0). After 1 h of mixing, the material was washed with 30 ml of MeCN to remove EDC, its corresponding urea-reaction product, and unreacted TFP.

In the second reaction step, hydroxamate groups were introduced on the resin via the reaction of the ester groups with an excess of hydroxylamine hydrochloride (Aldrich). The hydroxylamine hydrochloride solution was prepared by adding 690 mg (10 mmol) hydroxylamine hydrochloride to a mixture of 1 ml of 1 M NaOH and 2 ml of MeOH, followed after 5 min by the addition of 1 ml of 1 M NaOH to bring the pH to 5.3-5.4. This solution was added to the esterified resin (final pH 5.1-5.2) and mixed overnight at room temperature. The column material was washed thoroughly with 140 ml of water for injection and 70 ml of MeCN, respectively, and dried *in vacuo* (freeze-drying). The material can be stored for at least four months without any decrease of ^{89}Zr-binding capacity (extended storage periods are under investigation). For the preparation of a hydroxamate column, an Extract-Clean tube (1.5 ml; Alltech) with a frit placed at the bottom (pore size, 20 µm) was packed with a suspension of 100 mg of hydroxamate column material in 0.9% NaCl (Baxter). After applying the ^{89}Zr-target solution and the eluting solvents, the flow of solvents was initiated by connecting vacuum tubes (vacutainers without additives; Becton Dickinson) to the column with a needle (0.6x25 mm).

Before use, a hydroxamate column was equilibrated with 5 ml of MeCN, followed by 10 ml of 0.9% NaCl and, finally, 2 ml of 2 M HCl. After loading of the ^{89}Zr-target solution onto the column, the column was rinsed with 6 ml of 2 M HCl and 6 ml of sterile water for injection, respectively. Under these conditions, ^{89}Zr and the trace amount of ^{88}Zr remained bound to the resin, whereas ^{89}Y and the radionuclidic metal impurities were eluted. The zirconium isotopes were eluted with five successive 0.5 ml-portions of 1 M oxalic acid (Aldrich). In general, the oxalic acid fractions contained successively 40%, 40%, 10%, 5%, and 2% of the applied radioactive zirconium.

Preparation of MAb-*N*-succinyldesferrioxamine B-^{89}Zr

MAbs were premodified with a novel bifunctional derivative of the chelate Df (*N*-sucDf) via an amide linkage and subsequently labeled with ^{89}Zr (Fig. 1).

The chelate Df was converted into *N*-succinyldesferrioxamine B (*N*-sucDf) in step 1 according to a modified procedure of Herscheid *et al.* [13]. In short: 1.7 g of succinic anhydride (17 mmol; Baker Chemicals) were added to 7.5 ml of pyridine (Sigma-Aldrich Chemie) containing 0.5 g of Df (0.76 mmol; Novartis). The solution was stirred for 24 h at room temperature and added to 120 ml of 0.15 M NaOH. After additional stirring for 16 h at room temperature, the pH was adjusted to 2 with 12 M HCl and cooled for 2 h at 4°C. The precipitate was thoroughly washed with 500 ml of 0.01 M HCl, and the white product was dried *in vacuo* (freeze-drying).

Coupling of *N*-sucDf to MAbs and labeling with ^{89}Zr is schematically represented in steps 2 through 6 of Figure 1. In short, the hydroxamate groups of *N*-sucDf were temporarily blocked with iron (Fe(III)) in step 2, *N*-sucDf-Fe was esterified with TFP in step 3, and TFP-*N*-sucDf-Fe was coupled to MAbs in step 4. Thereafter, Fe(III) was removed by transchelation

to ethylenediaminetetraacetic acid (EDTA) (formation of $[Fe(III)EDTA]^{-}$ [14]) in step 5, and MAb-*N*-sucDf was labeled with ^{89}Zr in step 6.

Preparation of MAb-SMCC-SATA-Df-^{89}Zr

As reference to the new method for ^{89}Zr labeling (as depicted in Fig.1), Df was also coupled to MAbs via a thioether linkage as previously described by Meijs *et al.* [7]. In short, the amine group of Df was reacted with *N*-succinimidyl *S*-acetylthioacetate (SATA; Pierce). Modification of MAb-lysine groups into maleimide groups was performed by reaction with sulfosuccinimidyl 4-(*N*-maleimidomethyl)cyclohexane-1-carboxylate (sulfo-SMCC; Pierce); the number of maleimide groups per MAb molecule was 0.8-0.9 as determined chemically with Ellman's reagent [7]. MAb-SMCC was purified by the use of a 10DG column (Bio-Rad). After incubation of the purified MAb-SMCC sample with SATA-Df (activated in 0.1 M Na_2CO_3) for 90 min, unreacted maleimide groups were quenched with an excess of hydroxylamine for 15 min. Purification and labeling of the thus modified MAb with ^{89}Zr and the subsequent purification of the conjugate were performed essentially the same as described for the novel procedure (Fig. 1, step 5 and 6).

Analyses

A Ge(Li) detector coupled to a multichannel analyzer was used to quantify ^{89}Zr, to monitor ^{89}Zr purification, and (after decay of most of ^{89}Zr) to identify and quantify radionuclidic impurities (Table 1). For quantification of ^{89}Zr activities in a dose calibrator, the ^{54}Mn mode was used, multiplying the displayed amount of activity by a factor of 0.67. Quantification in a γ-counter (LKB-Wallac 1282 CompuGamma; Pharmacia) was performed on the 909-keV γ-energy of ^{89}Zr (efficiency, 21.7%). Samples of the ^{89}Zr oxalic acid fractions and of the purified MAb-^{89}Zr solution were analyzed for the presence of any remaining ^{89}Y by particle-induced x-ray emission (PIXE) according to the method described by Vis *et al.* [15].

High–performance liquid chromatography (HPLC) was performed to monitor the Df derivatives, the chemically modified MAbs, and the radiolabeled MAbs. *N*-sucDf, *N*-sucDf-Fe, and TFP-*N*-sucDf-Fe were analyzed with a Chromspher 5 C18 column (250x4.6 mm; Chrompack) with a gradient elution. Solvent A consisted of 10 mM sodium phosphate, pH 6, and solvent B of 100% MeCN. The gradient was as follows (flow rate, 1 ml/min): 5 min of 100% A, linear increase of eluent B to 35% during 25 min, 10 min of 35% B. HPLC analysis of the chemically modified MAbs and the radiolabeled MAbs was performed as described before[10]. MAb compounds were monitored by UV absorbance at 280 nm, Df compounds at 215 nm, and Df-Fe(III) complexes at 430 nm, whereas radiolabeled compounds were monitored either by continuous radioanalytical detection or by measurement of collected fractions. The equipment used has been described before [10].

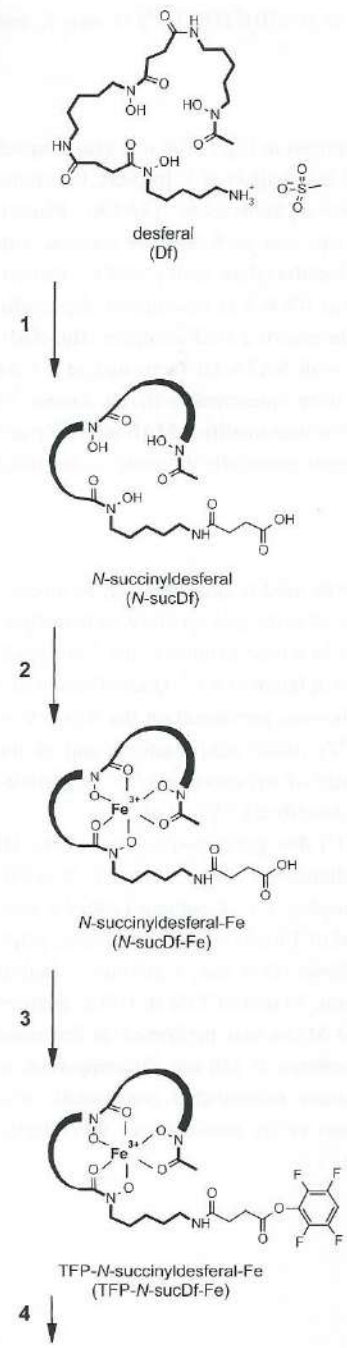

Figure 1. Schematic representation of premodification and postlabeling of MAbs with ^{89}Zr.

Bold arches represent $-(CH_2)_2CONH(CH_2)_5-$
The term *desferal* (Df) (Novartis) is used instead of desferrioxamine B and *Df-Fe* is used to represent the corresponding iron(III) complex (ferrioxamine).

Step 1 is synthesis of *N*-sucDf, as described in Materials and Methods.

Step 2 is complexation of *N*-sucDf with Fe(III).
- *N*-sucDf (9 mg, 13.6 μmol) is dissolved in 3 ml of 0.9% NaCl, containing 60 μl of 0.1 M Na_2CO_3 (final pH 6.5-7.0). To this solution, 0.3 ml (14.8 μmol) of $FeCl_3$ solution (8 mg/ml in 0.1 M HCl) is added.

Step 3 is esterification of *N*-sucDf-Fe.
- After 10 min, to *N*-sucDf-Fe solution are added 300 μl (0.36 mmol) of TFP solution (200 mg/ml in MeCN) and 120 mg (0.63 mmol) of solid EDC (final pH 5.8-6.0).
- After 45 min of incubation, reaction mixture is loaded onto conditioned Sep-Pak C_{18} cartridge (Waters), followed by washing with 60 ml of sterile water for injection. TFP-*N*-sucDf-Fe is eluted from Sep-Pak cartridge with 1.5 ml of MeCN.

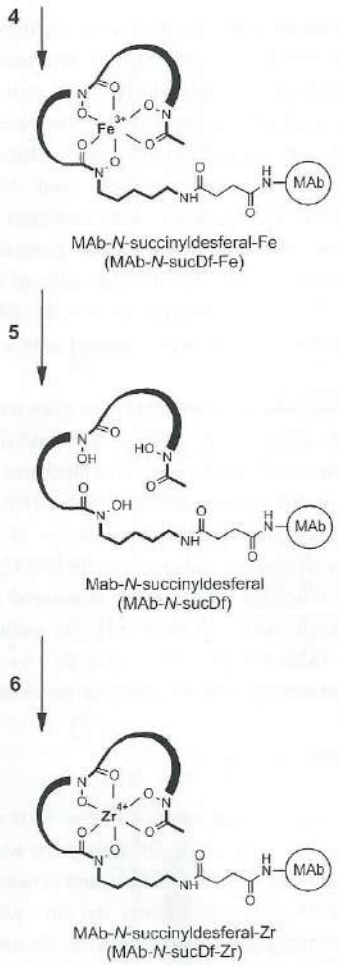

Step 4 is conjugation of TFP-*N*-sucDf-Fe to MAb.

- To 1 ml (33 nmol) of MAb solution (5 mg/ml), pH 9.5-9.8 (adjusted with 0.1 M Na_2CO_3), 20 µl (63 nmol) of TFP ester solution (2.5 mg/ml in MeCN) are added to obtain final chelate:MAb ratio of 1:1 (based on 54% reaction efficiency).
- After 30 min, two times 25 µl of gentisic acid solution (100 mg/ml in 0.32 M Na_2CO_3) are added to reaction mixture and pH is adjusted to 4.3-4.5 with four times 6 µl of 0.25 M H_2SO_4.

Step 5 is removal of Fe(III) from MAb-*N*-sucDf-Fe.

- To reaction mixture, 50 µl (3.3 µmol) of an EDTA solution (25 mg/ml) is added and solution is incubated for 30 min at 35°C (final pH 4.3-4.5).
- After 30 min, EDTA, TFP, iron (as $[Fe(III)EDTA]^-$), and unreacted hydrolyzed ester (*N*-sucDf) are removed by gel filtration using PD-10 column (eluent: 0.9% NaCl/gentisic acid [5 mg/ml], pH 5): First 2.6 ml (containing reaction volume and first 1.5 ml) are discarded, and modified MAb is collected in next 2 ml.

Step 6 is labeling of MAb-*N*-sucDf with ^{89}Zr.

- To 600 µl of ^{89}Zr oxalic acid solution (1 M oxalic acid), 130 µl of 0.9% NaCl, 270 µl of 2 M Na_2CO_3, and 3 ml of 0.5 M HEPES (pH 7.2-7.4) are added, followed by 2 ml (33 nmol) of modified MAb solution (2.5 mg/ml in 0.9% NaCl/gentisic acid [5 mg/ml], pH 5), final pH 7.2-7.4. Reaction volume can be varied provided amounts of oxalic acid, Na_2CO_3, and HEPES buffer are adjusted accordingly.
- After 30 min, reaction mixture (6 ml) is divided over three PD-10 columns (eluent: 0.9% NaCl/gentisic acid [5 mg/ml], pH 5): First 2.5 ml (2-ml sample volume and first 0.5 ml) are discarded, and radiolabeled MAb is collected in next 3 ml.

HPLC analyses of PD-10 column (Pharmacia Biotech) elution profiles were performed as described before [16]. Profiles of EDTA, *N*-sucDf, and TFP (Fig. 1, step 5) were determined with a gradient elution by UV absorbance at 210 nm. Solvent A consisted of 10 mM sodium phosphate, pH 6, and solvent B of 100% MeCN. The gradient was as follows (flow rate, 1 ml/min): 2 min of 100% A, linear increase of eluent B to 40% during 13 min, 5 min of 40% B (retention time of 2.9, 12.3, and 15.6 min, respectively). Oxalic acid and *N*-2-hydroxyethylpiperazine-*N*'-2-ethanesulfonic acid (HEPES) (Fig. 1, step 6) were analyzed by HPLC with 10 mM sodium phosphate, pH 6, as eluent, a flow rate of 0.4 ml/min (retention time of 6.2 and 7.8 min, respectively), and a wavelength of 210 nm. For determination of the PD-10 column elution profile of $[Fe(III)EDTA]^-$, ^{59}Fe (370 MBq/ml in 0.5 M HCl; Amersham Pharmacia Biotech) was used as tracer and the fractions were counted with a γ-counter.

For the measurement of the serum stability of radioimmunoconjugates, samples were incubated in freshly prepared human serum (1:1 v/v dilution) at 37°C in a humidified incubator maintained at 5% CO_2 and 95% air. Radioimmunoconjugates were also incubated in heat-inactivated serum (treated for 40 min at 56°C); in 20% human serum albumin (HSA; Sanquin), pH 7.2 and 9.0; and in 20% HSA, pH 9.0, supplemented with an excess of L-cysteine (9 μmol/ml). At various time intervals, samples were taken and analyzed by HPLC.

Radiochemical purity and integrity of the radiolabeled MAbs were monitored by instant thin-layer chromatography (ITLC) (eluent: citric acid, 20 mM, pH 5), sodium dodecylsulfate-polyacrylamide gel electrophoresis (SDS-PAGE) and analysis by a PhosphorImager (Molecular Dynamics), and immunoreactivity determination as previously described [9,10].

Animal studies

For the biodistribution and PET studies, female nude mice (athymic nu/nu, 23-32 g, 8-10 wk old; Harlan CPB) bearing human HNX-OE xenografts were used. HNX-OE xenografts were established after subcutaneous injection of HNSCC cell-line VU-SCC-OE [17] and repeated transplantation as xenograft in nude mice. Two to three wk after implantation, the mice were used for experiments. All animal experiments were performed according to the U.S. National Institutes of Health principles of laboratory animal care [18] and the Dutch national law "Wet op de Dierproeven" (Stb 1985, 336).

For the biodistribution study, mice (tumor size, 30-200 mg) were anaesthetized with ether, and 0.37 MBq cMAb U36-*N*-sucDf-^{89}Zr (100 μl, 100 μg MAb) or 0.37 MBq of the reference conjugate cMAb U36-SMCC-SATA-Df-^{89}Zr (100 μl, 100 μg MAb) was injected into the retroorbital plexus. The specific activities of the radioimmunoconjugates were 41 MBq/mg and 39 MBq/mg, respectively, and unlabeled MAb was added to bring the total MAb dose at 100 μg per mouse. At indicated time points after injection, the mice were anaesthetized, bled, killed, and dissected. After blood, tumor, normal tissues, and gastrointestinal contents were weighed, the amount of radioactivity in each was measured in a γ-counter. Radioactivity uptake was calculated as the percentage of the injected dose per gram

of tissue (%ID/g). Differences in tissue uptake between groups were statistically analyzed with the Student *t* test for unpaired data. Differences were considered significant for $P < 0.05$.

PET studies were performed using a prototype single-crystal-layer HRRT three-dimensional PET scanner (CTI). The axial field of view (FOV) of the PET scanner is 25.5 cm, and the transaxial FOV is 31.2 cm; radial and transaxial resolution are 2.6 mm in full width at half maximum (FWHM) at the center of the field. Transmission scans for attenuation correction were obtained in two-dimensional mode (consisting of 52 scans, using a 740-MBq ^{137}Cs point source), and emission scans were obtained in three-dimensional mode. Images were reconstructed by filtered backprojection and consisted of 207 image planes of 256x256 pixels, and each voxel equaled 1.21x1.21x1.21 mm.

Mice bearing HNX-OE xenografts (19-154 mg) were anaesthetized with ether and injected with 3.7 MBq cMAb U36-*N*-sucDf-^{89}Zr (109 MBq/mg, 250 µl, 100 µg MAb). Before scanning, the mice were anaesthetized with sodium pentobarbital (75 mg/kg, intraperitoneal) and positioned in the PET scanner. A transmission scan of 380 s was followed by a 60-min emission scan. Mice were scanned and then immediately dissected at 24 ($n = 2$), 48 ($n = 2$), and 72 h ($n = 6$) after injection. In addition, 2 mice were scanned three times: at 24, 48, and 72 h after injection; after 72 h these mice were dissected. Activity in tumors at the time of scanning was quantified by Ge(Li) and in a γ-counter together with a standard.

RESULTS

Production and purification of ^{89}Zr

After irradiation, the ^{89}Y-layer was dissolved and the amount of ^{89}Zr was determined, as well as that of contaminating radionuclides (Table 1). The crude yield of ^{89}Zr was between 6.5 GBq and 13.5 GBq (110-190 min of irradiation), with less than 1.3-2.7 MBq (0.02%) of radionuclidic impurities. A small amount (0.00015%) of ^{88}Zr was observed, being the result of a (p,2n) reaction on ^{89}Y. The isotope ^{88}Y is formed as daughter product from ^{88}Zr and possibly from a (p,pn) reaction on ^{89}Y. The isotope zinc-65 (^{65}Zn) is formed by a (p,n) reaction on the copper support, whereas vanadium-48 (^{48}V), cobalt-56 (^{56}Co), and terbium-156 (^{156}Tb) are formed on titanium, iron, and gadolinium impurities, respectively, in the ^{89}Y-target. Removal of the bulk nonradioactive ^{89}Y and of the radionuclidic impurities ^{88}Y, ^{48}V, ^{56}Co, ^{65}Zn, and ^{156}Tb (except ^{88}Zr) was achieved with a hydroxamate column (Table 1). As a result, more than 99.99% pure ^{89}Zr was obtained in 1 M oxalic acid, with an overall yield of 97.0 ± 3.3%. PIXE analysis of the isolated ^{89}Zr oxalate revealed the absence of nonradioactive ^{89}Y.

Preparation of MAb-*N*-sucDf-^{89}Zr.

Step 1 in the preparation of MAb-*N*-sucDf via the TFP ester approach, as depicted in Figure 1, is the carboxylation of the primary amine of Df. After isolation of the product, *N*-sucDf was obtained in a yield of 68-73%. After temporary blocking of the hydroxamate groups of *N*-sucDf with Fe(III) in step 2 (^{59}Fe was used as a tracer to facilitate analytic monitoring) and nearly quantitative esterification (Fig. 2A and 2B), TFP-*N*-sucDf-Fe was isolated by a Sep-Pak (Waters) procedure in yields of about 80% in step 3. The TFP ester could be stored for at least 8 wk in MeCN at –70°C (data not shown).

Conjugation conditions selected for the technical protocol comprised the addition of 63 nmol of ester to 33 nmol of MAb in step 4. For cMAb U36, mMAb E48, and mMAb 425, these conditions resulted in a reproducible conjugation efficiency of 54 ± 5% (Fig. 2C) and, consequently, in a reproducible chelate:MAb substitution ratio of about 1:1. After removal of Fe(III) by transchelation to EDTA in step 5, less than 5% Fe remained complexed by MAb-*N*-sucDf after 30 min (Fig. 2D). Isolation of the MAb-*N*-sucDf on a PD-10 column efficiently removed more than 97% of EDTA, $[Fe(III)EDTA]^-$, TFP and *N*-sucDf (data not shown).

In step 6, MAb-*N*-sucDf was labeled with ^{89}Zr in HEPES buffer (final concentration, 0.25 M) at pH 7.2-7.4. After 30 min at this pH optimum, the amount of ^{89}Zr transchelated from oxalate to MAb-*N*-sucDf is always more than 80%, even in the presence of 0.1 M oxalic acid. A similar transchelation rate was found in reaction volumes of 1-9 ml, that is, enabling the use of 100-900 µl of 1 M oxalic acid, provided the MAb concentration was more than 0.5 mg/ml. Below pH 6 and above pH 8, less than 15% labeling was obtained under the same conditions. The use of phosphate buffer instead of HEPES strongly affected the kinetics: at pH 7.3, the labeling efficiency was less than 30% after 30 min. Labeling efficiency was not influenced by the amount of ^{89}Zr used, in the range of 0.0037-1.5 GBq. Radioimmunoconjugates could be prepared with a specific activity from 10 to 550 MBq/mg MAb. Assessment of the PD-10

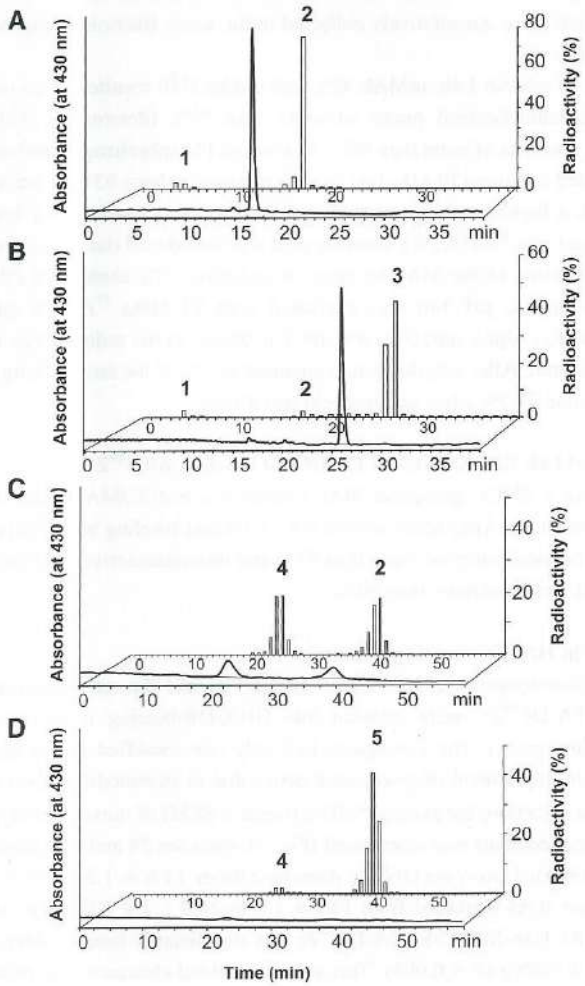

Figure 2. HPLC profiles (absorbance at 430 nm and radioactivity after fraction collection) during synthesis of TFP-*N*-sucDf ester and preparation of MAb-*N*-sucDf. Analysis after reaction of *N*-sucDf with ^{59}Fe-$FeCl_3$ (A), after esterification of *N*-sucDf-^{59}Fe-Fe (B), after reaction of TFP-*N*-sucDf-^{59}Fe-Fe with MAb (C), and after removal of iron from MAb-*N*-sucDf-^{59}Fe-Fe with EDTA (D). Analyses were performed with Chromspher (Chrompack) 5 C18 column (A and B) or Superdex (Pharmacia Biotech) 200 HR column (C and D). Peak 1 = unreacted ^{59}Fe-$FeCl_3$ (retention time, 3.3 min; reaction performed with an excess of 1.1 to 1); peak 2 = *N*-sucDf-^{59}Fe-Fe (retention time, 16.7 min for A and B and 39 min for C); peak 3 = TFP-*N*-sucDf-^{59}Fe-Fe (retention time, 25.9 min); peak 4 = MAb-*N*-sucDf-^{59}Fe-Fe (retention time, 23 min); peak 5 = $[^{59}$Fe-Fe(III)EDTA$]^-$ (retention time, 38 min).

column elution profile of unreacted ^{89}Zr, oxalic acid, and HEPES buffer by HPLC revealed that the compounds were quantitatively collected in the waste fractions eluted after the MAb-containing fraction.

Labeling of mMAb E48, mMAb 425, and cMAb U36 resulted in an overall yield of 80% (± 6%), a radiochemical purity of more than 95% (determined with ITLC), and immunoreactive fractions of more than 90%. In general, PhosphorImager analysis of the SDS-PAGE gel revealed a major 150-kDa IgG band containing at least 93% of the radioactivity, a minor band with a higher molecular weight (≤ 3%), a minor band with a lower molecular weight (≤ 2%), and free ^{89}Zr (≤ 2%). Gentisic acid was introduced during labeling and storage to prevent deterioration of the MAb integrity by radiation. The chemoprotective potency of gentisic acid (5 mg/ml, pH 5.0) was evaluated with 93 MBq ^{89}Zr per milliliter as the challenging condition. Upon storage at 4°C for 2 h, 95.3% of the radioactivity was present in the 150-kDa IgG band. After 2 d, this band contained 88.7% of the radioactivity when gentisic acid was present and 79.7% when gentisic acid was absent.

Preparation of cMAb U36-SMCC-SATA-Df and labeling with ^{89}Zr

To arrive at about 1 SMCC group per MAb molecule, a SMCC/MAb molar ratio of 2 was used during the reaction. After reaction with SATA-Df and labeling with ^{89}Zr, the conjugates showed a radiochemical purity of more than 95% and immunoreactive fractions of more than 90%. The overall yield was more than 80%.

Biodistribution in HNSCC-bearing nude mice

Both radioimmunoconjugates, cMAb U36-*N*-sucDf-^{89}Zr and the reference conjugate cMAb U36-SMCC-SATA-Df-^{89}Zr, were injected into HNX-OE-bearing nude mice (n = 4 per conjugate per time point). The conjugates had only one modified lysine group per MAb molecule to avoid impairment of pharmacokinetics due to overmodification (*19-21*). At 24, 48, and 72 h after injection, the average %ID/g (mean ± SEM) of tumor, blood, normal tissues and gastrointestinal contents was determined (Fig. 3). Between 24 and 72 h after injection, the blood level of cMAb U36-*N*-sucDf-^{89}Zr decreased from 14.6 ± 1.2 to 12.3 ± 0.7 %ID/g, whereas the tumor level increased from 14.1 ± 1.0 to 26.0 ± 1.9 %ID/g ($p < 0.005$). Blood clearance of cMAb U36-SMCC-SATA-Df-^{89}Zr was significantly faster: a decrease from 10.7 ± 0.8 to 5.1 ± 0.6 %ID/g ($P < 0.005$). This enhanced blood clearance was reflected in lower tumor levels (not exceeding 10 %ID/g), lower levels in most organs, but significantly increased levels in colon content at 24 and 48 h after injection (4.8 ± 0.8 *vs.* 1.7 ± 0.2 %ID/g, $P < 0.05$, and 5.3 ± 1.8 *vs.* 1.2 ± 0.2 %ID/g, $P < 0.05$, respectively) and in ileum content at 24 h after injection (1.5 ± 0.3 *vs.* 0.5 ± 0.2 %ID/g, $P < 0.05$).

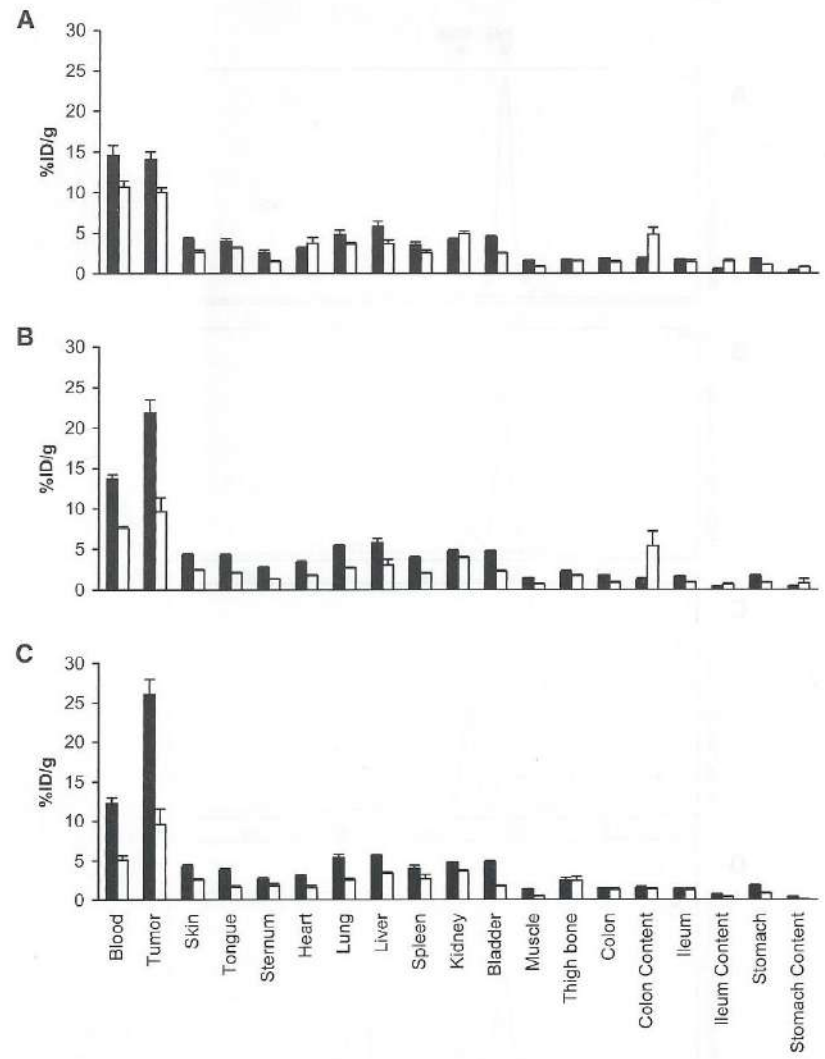

Figure 3. Biodistribution of cMAb U36-*N*-sucDf-^{89}Zr (black bars, n = 4) and cMAb U36-SMCC-SATA-Df-^{89}Zr (white bars, n = 4). Each conjugate (100 µg of MAb; 0.37 MBq) was injected into retroorbital plexus of HNX-OE-bearing nude mice. At 24 (A), 48 (B), and 72 h (C) after injection, mice were bled, sacrificed, and dissected, and radioactivity levels (%ID/g ± SEM) of blood, tumor, organs, and gastrointestinal contents were assessed.

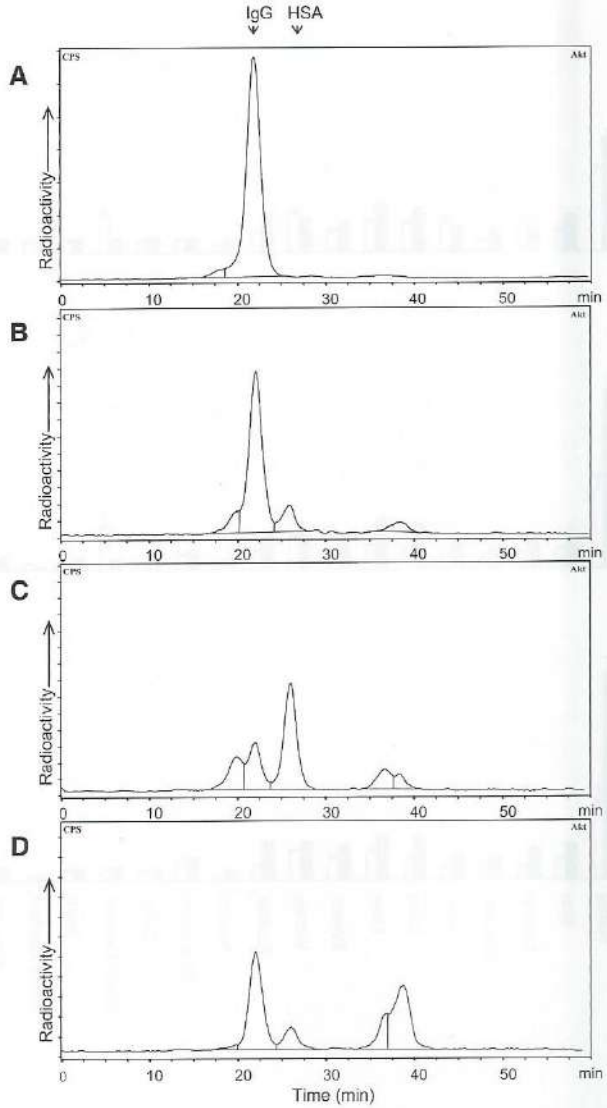

Figure 4. *In vitro* stability of cMAb U36-*N*-sucDf-^{89}Zr and cMAb U36-SMCC-SATA-Df-^{89}Zr, monitored by HPLC. Conjugates were incubated for 24 h at 37°C: cMAb U36-*N*-sucDf-^{89}Zr in human serum (A), cMAb U36-SMCC-SATA-Df-^{89}Zr in human serum (B), cMAb U36-SMCC-SATA-Df-^{89}Zr in HSA, at pH 9 (C), and cMAb U36-SMCC-SATA-Df-^{89}Zr in HSA, at pH 9 with an excess of L-cysteine (D). Retention times of IgG and HSA are indicated.

In vitro serum stability of cMAb U36-*N*-sucDf-^{89}Zr and cMAb U36-SMCC-SATA-Df-^{89}Zr

The enhanced blood clearance of the reference conjugate cMAb U36-SMCC-SATA-Df-^{89}Zr, as observed *in vivo*, was found to be related to the succinimide ring-thioether unit in the linker. Whereas HPLC analysis of cMAb U36-*N*-sucDf-^{89}Zr showed no loss of radiolabel on incubation during 24 h at 37°C in human serum (Fig. 4A), the reference conjugate cMAb U36-SMCC-SATA-Df-^{89}Zr gave an increased shoulder at 20 min; elution of radioactivity at 26 min, which corresponds to the HPLC retention time of albumin; and a broad radioactivity peak at 36-40 min (Fig. 4B). In a series of experiments, the nature of this phenomenon was evaluated. Incubation in heat-inactivated serum gave the same results as in serum, excluding enzyme-induced instability. To verify the possible transfer of a ^{89}Zr-chelate fragment to serum proteins, HSA (which contains one –SH group per molecule) was chosen as a representative protein. Incubation in HSA gave a pattern (data not shown) closely resembling that in Fig. 4B. Increasing the pH of the HSA incubation solution to 9 resulted in a more extensive transfer of radioactivity from the monomeric MAb peak to the HSA peak, an enhanced shoulder at 20 min, and an increased peak at 36-40 min (Fig. 4C). The presence of L-cysteine reduced the transfer to HSA, with a concomitant increase in radioactivity at 39 min and a decrease in the shoulder at 20 min (Fig. 4D). Under the same conditions, MAb-*N*-sucDf-^{89}Zr, as produced by the novel coupling method, did not show these instability phenomena (data not shown).

PET studies

To determine the feasibility of visualizing small tumors with the novel radiolabeled cMAb U36-*N*-sucDf-^{89}Zr, 12 HNX-OE-bearing nude mice were subjected to immuno-PET. In the coronal as well as transaxial images obtained at 24 (4 mice imaged), 48 (4 mice imaged), and 72 h (8 mice imaged) after injection, all tumors could be clearly seen as hot spots (Fig. 5). Tumors as small as 19 mg, containing about 17 kBq at the time of the scanning (72 h), could be visualized with the HRRT PET scanner. From the nontarget tissues, only the blood pool in the heart and the liver area (and nose at 24 h) was visible.

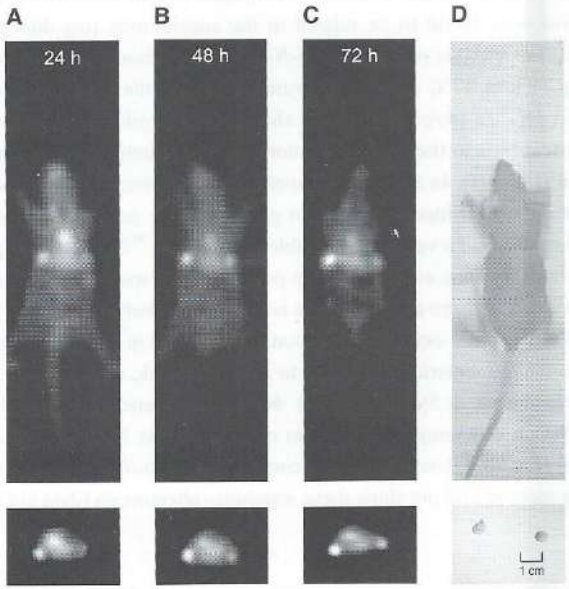

Figure 5. HNX-OE-bearing nude mouse, injected with cMAb U36-*N*-sucDf-^{89}Zr (100 µg of MAb; 3.7 MBq). Coronal (upper) and transaxial (lower) PET images were obtained from same mouse at 24 (A), 48 (B), and 72 h (C). Image planes are those for which both tumors of same animal were visible. D, Photographs of imaged mouse and excised tumors (left, 47 mg; right, 45 mg).

DISCUSSION

The assessment of tumor localizations may be improved by combining the selective tumor-targeting properties of a MAb with the excellent sensitivity and contrast resolution of PET. In the present report, we have described a novel method for labeling MAbs with the long-lived positron emitter ^{89}Zr via amide bond (-NH-CO-) coupled Df, taking all the requirements for clinical application into account. Radioimmunoconjugates produced by this method were stable in serum *in vitro* and showed high accumulation in tumors in nude mice. The feasibility of visualizing small tumors was shown with ^{89}Zr-immuno-PET. The required ^{89}Zr was produced in high amounts and efficiently isolated in a consistent way.

The chelate Df has frequently been used for radiolabeling of MAbs. However, a diversity of problems was met in getting chemical control over the coupling process and the quality of the resulting final product [22-24]. In the MAb-Df-^{89}Zr labeling method developed by Meijs *et al.* [7], which was used as the reference method in the present study, lysine groups of the MAb were modified into maleimide groups, giving a succinimide ring-thioether unit in the linkage on reaction with SATA-Df. Evaluation of cMAb U36-SMCC-SATA-Df-^{89}Zr prepared according to the latter method, however, revealed instability in serum *in vitro*, with the transfer of the ^{89}Zr-chelate complex to serum proteins. *In vivo* experiments in tumor-bearing nude mice demonstrated such instability under physiological conditions. Lewis and Shively [8] described comparable transfer phenomena for their ^{90}Y-DOTA-labeled MAb, containing a linker with two succinimide ring-thioether units. They argued a succinimide ring cleavage, possibly Y catalyzed, to be responsible for release of chelate from the MAb. Our *in vitro* results with HSA strongly suggest that on opening of the succinimide ring, the chelate can break off at either side of the sulfur atom (-S-). In case the S-containing Df-^{89}Zr fragment is formed, coupling with HSA takes place, while cleavage at the other side of the S-bond leaves the reactive S-atom at the MAb side, making the MAb susceptible to aggregation (Fig. 4C). These reactions could be counteracted by quenching reactive S-atoms with L-cysteine (Fig. 4D).

To circumvent adverse *in vivo* instability of the MAb-Df linker, we have here described a novel coupling method based on the use of an active TFP ester. This method creates a chemically stable amide bond between the chelator Df and MAb and gives good control over the number of groups to be coupled to the MAb. To allow conjugation, the amine group present on Df was converted into a carboxylic acid functionality. For the synthesis of the corresponding TFP-*N*-sucDf ester, it was necessary to temporarily protect the three hydroxamate groups of Df against reactions with EDC. Without blocking of the hydroxamate groups, intractable results were obtained that were not further analyzed. Interestingly, blocking with ^{89}Zr did not yield the required TFP ester. Therefore, direct conjugation of MAbs with TFP-*N*-sucDf-^{89}Zr was not possible. Blocking with iron proved adequate, enabling the development of a postconjugation labeling method. After reaction of this TFP-*N*-sucDf-Fe ester with MAb, the iron was efficiently detached from Df with the aid of EDTA, under conditions that did not affect the integrity of the MAb.

For the labeling of the premodified MAb with ^{89}Zr, reaction conditions were established that enabled efficient labeling in the presence of oxalic acid, the solution in which ^{89}Zr is isolated. Therefore, the very time-consuming sublimation step, as proposed by Meijs *et al.* [12] for the removal of the potent ^{89}Zr-chelating agent oxalic acid, is not required any longer. The transchelation of ^{89}Zr from oxalate to Df appeared to take place efficiently within a narrow pH range (7.2-7.4). This observed sharp pH-optimum required the presence of a strong but indifferent buffer. HEPES was found to fulfill the latter requirements.

The need for protection of the MAb against radiation damage has been shown in previous MAb studies [9,25-28]. Ascorbic acid as an antioxidant could not be used because this reagent causes detachment of ^{89}Zr from Df by reducing Zr^{4+} to Zr^{2+}. The presence of gentisic acid during labeling, purification, and storage proved to be beneficial and, as such, has been made part of the protocol.

Because the novel labeling procedure for ^{89}Zr described in this report uses lysine residues of the MAb for the stable coupling of the Df moiety, the method is applicable to each intact MAb (as confirmed by labeling of MAbs E48 and 425), as well as to MAb fragments or peptides that contain a lysine group. The labeling of the conjugate is based on the postlabeling of a premodified MAb, which makes it possible to centrally produce sterile batches of MAb-*N*-sucDf, with easy coupling of ^{89}Zr at the user's site. By our strongly modified ^{89}Zr isolation, it is now possible to obtain large batches of ^{89}Zr (on the order of 10 GBq) in a reproducible way, at low cost, and with a radionuclidic purity of more than 99.99%.

The feasibility of visualizing small tumors with radiolabeled cMAb U36-*N*-sucDf-^{89}Zr with an HRRT PET scanner was demonstrated in xenograft-bearing nude mice. After injection of the conjugate, HNSCC xenografts in the range of 19-154 mg were detected after 24 h. Target-to-background ratios improved when imaging was performed after prolonged periods, and none of the normal organs showed an adverse high uptake. Similar results were obtained with an ECAT EXACT HR$^+$ positron scanner (CTI) (data not shown).

Sensitive detection of small tumors in nude mice was recently also observed for the positron emitter copper-64 (^{64}Cu; half-life, 12.7 h) using a ^{64}Cu-DOTA-minibody of T84.66 (molecular weight, 80 kDa), albeit with a high accumulation of ^{64}Cu in the liver (32.4 %ID/g after 4 h) [28]. With regard to ^{124}I, a more suitable candidate for use in combination with whole IgG [29,30], recently the capacity of ^{124}I-CDR-grafted humanized A33 for detection of colon carcinoma xenografts in nude mice was evaluated [31,32]. In this case, high-resolution images of tumors ranging from 200 to 700 mg were obtained 24 h after injection. In ongoing studies at our laboratory, we are evaluating how ^{124}I compares with ^{89}Zr with respect to radiopharmacokinetic behavior, tumor retention, and suitability for PET imaging of small tumors.

A direct practical clinical application of immuno-PET would be its combination with radioimmunotherapy. In this way, imaging can be used for the selection of, for example, rhenium-186- (^{186}Re-), ^{131}I- or ^{90}Y-radioimmunotherapy candidates by confirmation of tumor-targeting with additional estimation of radiation delivery to tumor and normal organs. The possibility of using PET with a ^{89}Zr-labeled MAb to predict and quantify targeting of a ^{90}Y-

labeled MAb during treatment for more extended periods would be of special interest because of the lack of γ-emission of ^{90}Y.

Because of the encouraging results presented here, the ^{89}Zr-labeled cMAb U36 IgG is currently evaluated for its capacity to detect primary tumors and metastases in operable HNSCC patients. To this end, results from ^{89}Zr-immuno-PET are being compared with results from CT, MRI, ^{18}FDG-PET, and histopathological evaluation.

CONCLUSION

This study provided practical protocols for reproducible isolation of the long-lived positron emitter ^{89}Zr and its coupling to MAbs via the chelate Df using new linker chemistry. Resulting MAb-^{89}Zr conjugates appeared optimal with respect to radiochemical purity, integrity, immunoreactivity, and stability. Moreover, specific targeting and sensitive detection (with a PET camera) of head and neck cancer xenografts were demonstrated. These achievements justify clinical evaluation of MAbs-^{89}Zr conjugates.

ACKNOWLEDGMENTS

The authors thank the staff of the BV Cyclotron (VU University) for performing the irradiations, Jan H. Rector (Solid State Physics, VU University) for sputtering ^{89}Y on copper supports, and Fred L. Buijs (Radionuclide Center, VU University) for the PET analyses.

REFERENCES

1. Goldenberg DM, Larson SM, Reisfeld RA, Schlom, J. Targeting cancer with radiolabeled antibodies. *Immunol Today.* 1995;16:261-264.
2. DeNardo SJ, Kroger LA, DeNardo GL. A new era for radiolabeled antibodies in cancer? *Curr Opin Immunol.* 1999;11:563-569.
3. De Bree R, Roos JC, Quak JJ, den Hollander W, Snow GB, van Dongen GAMS. Radioimmunoscintigraphy and biodistribution of ^{99m}Tc-labeled monoclonal antibody U36 in patients with head and neck cancer. *Clin Cancer Res.* 1995;1:591-598.
4. Colnot DR, Quak, JJ, Roos JC, et al. Phase I therapy study of ^{186}Re-labeled chimeric monoclonal antibody U36 in patients with squamous cell carcinoma of the head and neck. *J Nucl Med.* 2000;41:1999-2010.
5. Sowby FD, ed. *Radionuclide transformations: Energy and intensity of emissions*; ICRP publication 38, volumes 11-13. Oxford, England: Pergamon Press; 1983:44, 58, 79, 205, 217, 218, 668.
6. Meijs WE, Herscheid JDM, Haisma HJ, Pinedo HM. Evaluation of desferal as a bifunctional chelating agent for labelling antibodies with zirconium-89. *Appl Radiat Isot.* 1992;43:1443-1447.
7. Meijs WE, Haisma HJ, Klok RP, et al. Zirconium-88/89 labelled monoclonal antibodies: distribution in tumour-bearing nude mice. *J Nucl Med.* 1997;38:112-118.
8. Lewis MR, Shively JE. Maleimidocysteineamido-DOTA derivatives: new reagents for radiometal chelate conjugation to antibody sulfhydryl groups undergo pH-dependent cleavage reactions. *Bioconjug Chem.* 1998;9:72-86.
9. Visser GWM, Gerretsen M, Herscheid JDM, Snow GB, van Dongen GAMS. Labeling of monoclonal antibodies with ^{186}Re using the MAG3 chelate for radioimmunotherapy of cancer: a technical protocol. *J Nucl Med.* 1993;34:1953-1963.
10. Vrouenraets MB, Visser GWM, Stigter M, Oppelaar H, Snow GB, van Dongen GAMS. Targeting of aluminum (III) phthalocyanine tetrasulfonate by use of internalizing monoclonal antibodies: improved efficacy in photodynamic therapy. *Cancer Res.* 2001;61:1970-1975.
11. Mustafa MG, West HI, O'Brien Jr. H, Lanier RG, Benhamou M, Tamura T. Measurements and a direct-reaction-plus-Hauser-Feshbach analysis of ^{89}Y(p,n)^{89}Zr, ^{89}Y(p,2n)^{88}Zr, and ^{89}Y(p,pn)^{88}Y reactions up to 40 MeV. *Physical Review C.* 1988;38:1624-1637.
12. Meijs WE, Herscheid JDM, Haisma HJ, et al. Production of highly pure no-carrier-added zirconium-89 for the labelling of antibodies with a positron emitter. *Appl Radiat Isot.* 1994;45:1143-1147.
13. Herscheid JDM, Hoekstra A, Vos C. *N*-succinyldesferrioxamine B: A potential radiopharmaceutical for assessing renal function. *Eur J Nucl Med.* 1984;9:508-510.
14. Monzyk B, Crumbliss AL. Factors that influence siderophore-mediated iron bioavailability: catalysis of interligand iron(III) transfer from ferrioxamine B to EDTA by hydroxamic acids. *J Inorg Biochem.* 1983;19:19-39.
15. Vis RD, Kramer JLAM, Tros GHJ, van Langevelde F, Mars L. The upgraded Amsterdam nuclear microprobe. *Nucl Instr Meth.* 1993;B77:41-44.
16. Van Gog FB, Visser GWM, Stroomer JWG, Roos JC, Snow GB, van Dongen GAMS. High dose rhenium-186-labeling of monoclonal antibodies for clinical application: pitfalls and solutions. *Cancer.* 1997;80:2360-2370.

17. Hermsen MAJA, Joenje H, Arwert F, Welters MJP, Braakhuis BJM, Bagnay M, Westerveld A and Slater R. Centromeric breakage as a major cause of cytogenetic abnormalities in oral squamous cell carcinoma. *Genes Chromos Cancer.* 1996;15:1-9.
18. *Guide for the Care and Use of Laboratory Animals.* Washington, DC: Government Printing Office; 1985. NIH publication 86-23.
19. Pelegrin A, Folli S, Buchegger F, Mach JP, Wagnieres G, van den Bergh H. Antibody-fluorescein conjugates for photoimmunodiagnosis of human colon carcinoma in nude mice. *Cancer.* 1991;67:2529-2537.
20. Kukis DL, DeNardo GL, DeNardo SJ, et al. Effect of the extent of the chelate substitution on the immunoreactivity and biodistribution of 2IT-BAT-Lym-1 immunoconjugates. *Cancer Res.* 1995;55:878-884.
21. Van Gog FB, Visser GMW, Klok R, van der Schors R, Snow GB, van Dongen GAMS. Monoclonal antibodies labeled with rhenium-186 using the MAG3 chelate: relationship between the number of chelated groups and biodistribution characteristics. *J Nucl Med.* 1996;37:352-362.
22. Koizumi M, Endo K, Kunimatsu M, et al. ^{67}Ga-labeled antibodies for immunoscintigraphy and evaluation of tumor targeting of drug-antibody conjugates in mice. *Cancer Res.* 1988;48:1189-1194.
23. Pochon S, Buchegger F, Pélegrin A, et al. A novel derivative of the chelon desferrioxamine for site-specific conjugation to antibodies. *Int J Cancer.* 1989;43:1188-1194.
24. Arano Y, Inoue T, Mukai T, et al. Discriminated release of a hippurate-like radiometal chelate in nontarget tissues for target-selective radioactivity localization using pH-dependent dissociation of reduced antibody. *J Nucl Med.* 1994;35:326-333.
25. Chakrabarti MC, Le N, Paik CH, De Graff WG, Carrasquillo JA. Prevention of radiolysis of monoclonal antibody during labeling. *J Nucl Med.* 1996;37:1384-1388.
26. Visser GW, Klok RP, Klein Gebbinck JW, ter Linden T, van Dongen GA, Molthoff CF. Optimal quality ^{131}I-monoclonal antibodies on high-dose labeling in a large reaction volume and temporarily coating the antibody with IODO-GEN. *J Nucl Med.* 2001;42:509-519.
27. Liu S, Edwards DS. Stabilization of ^{90}Y-labeled DOTA-biomolecule conjugates using gentisic acid and ascorbic acid. *Bioconjug Chem.* 2001;12:554-558.
28. Wu AM, Yazaki PJ, Tsai S, et al. High-resolution microPET imaging of carcinoembryonic antigen-positive xenografts by using a copper-64-labeled engineered antibody fragment. *Proc Natl Acad Sci.* 2000;97:8495-8500.
29. Wilson CB, Snook DE, Dhokia B, et al. Quantitative measurement of monoclonal antibody distribution and blood flow using positron emission tomography and ^{124}Iodine in patients with breast cancer. *Int J Cancer.* 1991;47:344-347.
30. Larson SM, Pentlow KS, Volkow ND, et al. PET scanning of iodine-124-3F9 as an approach to tumor dosimetry during treatment planning for radioimmunotherapy in a child with neuroblastoma. *J Nucl Med.* 1992;33:2020-2023.
31. Lee FT, Hall C, Rigopoulos A, et al. Immuno-PET of human colon xenograft-bearing BALB/c nude mice using ^{124}I-CDR-grafted humanized A33 monoclonal antibody. *J Nucl Med.* 2001;42:764-769.
32. Eary JF. PET imaging for planning cancer therapy. *J Nucl Med.* 2001;42:770-771.

chapter

4

Quantitative ^{89}Zr immuno-PET for *in vivo* scouting of ^{90}Y-labeled monoclonal antibodies in xenograft-bearing nude mice

Iris Verel, Gerard W.M. Visser, Ronald Boellaard, Otto C. Boerman, Julliette E.M. van Eerd, Gordon B. Snow, Adriaan A. Lammertsma, Guus A.M.S. van Dongen

***Journal of Nuclear Medicine* 2003;44:1663-1670.**

ABSTRACT

Immuno-PET as a scouting procedure before radioimmunotherapy (RIT) aims at the confirmation of tumor-targeting and the accurate estimation of radiation dose delivery to both tumor and normal tissues. Immuno-PET with ^{89}Zr-labeled monoclonal antibodies (MAbs) and ^{90}Y-MAb RIT might form such a valuable combination. In this study, the biodistribution of ^{89}Zr-labeled and ^{88}Y-labeled MAb (^{88}Y as substitute for ^{90}Y) was compared and the quantitative imaging performance of ^{89}Zr immuno-PET was evaluated. **Methods:** Chimeric MAb (cMAb) U36, directed against an antigen preferentially expressed in head and neck cancer, was labeled with ^{89}Zr using the bifunctional chelate *N*-succinyldesferrioxamine B (*N*-sucDf) and with ^{88}Y using the bifunctional chelate *p*-isothiocyanatobenzyl-1,4,7,10-tetraazacyclododecane-1,4,7,10-tetraacetic acid (*p*-SCN-Bz-DOTA). The radioimmunoconjugates were coinjected in xenograft-bearing nude mice, and biodistribution was determined at 3, 24, 48, 72, and 144 h after injection. ^{89}Zr was evaluated and compared with ^{18}F in phantom studies to determine linearity, resolution, and recovery coefficients, using a high-resolution research tomograph (HRRT) PET scanner. The potential of PET to quantify cMAb U36-*N*-sucDf-^{89}Zr was evaluated by relating image-derived tumor uptake data (noninvasive method) to ^{89}Zr uptake data derived from excised tumors (invasive method). **Results:** ^{89}Zr-*N*-sucDf-labeled and ^{88}Y-*p*-SCN-Bz-DOTA-labeled cMAb U36 showed a highly similar biodistribution, except for sternum and thigh bone at later time points (72 and 144 h after injection). Small differences were found in kidney and liver. Imaging performance of ^{89}Zr approximates that of ^{18}F, whereas millimeter-sized (19-154 mg) tumors were visualized in xenograft-bearing mice after injection of cMAb U36-*N*-sucDf-^{89}Zr. After correction for partial volume effects, an excellent correlation was found between image-derived ^{89}Zr tumor radioactivity and γ-counter ^{89}Zr values of excised tumors (R^2 = 0.79). **Conclusion:** The similar biodistribution and the favorable imaging characteristics make ^{89}Zr a promising candidate for use as a positron-emitting surrogate for ^{90}Y.

INTRODUCTION

The use of radiolabeled monoclonal antibodies (MAbs) for the improvement of diagnosis and treatment of cancer continues to be an expanding area of research [1]. The potential of this approach was demonstrated by, among others, ibritumomab tiuxetan (Zevalin; IDEC Pharmaceuticals), the first radioimmunotherapy (RIT) procedure that received approval by the U.S. Food and Drug Administration (FDA), in 2002 [2]. Initially, the ibritumomab tiuxetan regimen (for treating non-Hodgkin's lymphoma) consisted of an imaging procedure for which the chelate-coupled MAb ibritumomab tiuxetan was labeled with indium-111 (^{111}In), followed one week later by a RIT procedure for which the same conjugate was labeled with yttrium-90 (^{90}Y).

^{90}Y has a physical half-life of 64.1 h and emits high-energy β^--particles (100% β^-, E_{β^-max} = 2.28 MeV). The absence of γ-ray emission minimizes dose radiation burden for medical personnel and relatives and enables outpatient treatment. Whereas these characteristics make ^{90}Y attractive for therapy, the lack of associated photon emission does not allow external imaging of the *in vivo* distribution of the ^{90}Y-labeled antibody. Attempts have been made to use the ^{90}Y-associated bremsstrahlung for these purposes, but because of low bremsstrahlung photon counts, high amounts of ^{90}Y would be needed for quantitative imaging [3,4]. For this reason, the method was judged to be of limited practical value for tracer imaging procedures. In practice, it is customary to use ^{111}In (half-life, 67.3 h; E_γ = 171 and 245 keV) as a γ-emitting surrogate for tracing the biodistribution of ^{90}Y in RIT trials [5-7]. For coupling to MAbs, the DOTA chelator is generally used because it binds these three-valent radionuclides with a very high stability [8].

Performing radioimmunoscintigraphy (RIS) as a tracer imaging procedure before RIT enables the confirmation of tumor-targeting and the estimation of radiation dose delivery to both tumor and normal tissues. At least three requirements need to be met for optimal use of an imaging radioimmunoconjugate as a predictor of a therapeutic radioimmunoconjugate. First, imaging and RIT conjugates should have similar biodistribution. Second, radionuclides used for imaging and RIT should have similar physical half-lives, preferably matching the biological half-lives of MAbs. Third, procedures for quantification of uptake and subsequent dose calculations should be reasonably accurate. With respect to the last requirement, MAb distribution has been estimated using planar γ-camera imaging and SPECT. These procedures, however, have intrinsic limitations with respect to quantification, primarily on account of scatter and partial absorption of γ-photons in the tissue of a patient. Because of more accurate scatter and attenuation corrections, PET is better qualified for tracer quantification. Besides, PET provides superior spatial and temporal resolution for imaging.

In our search for candidate positron emitters for PET with MAbs (immuno-PET), we set up the production, purification and antibody labeling of zirconium-89 (^{89}Zr; half-life, 78.4 h) and iodine-124 (^{124}I; half-life, 100.3 h), as these tracers have physical half-lives that are compatible with the time needed for MAbs to achieve optimal tumor-to-nontumor ratios

(typically 2-4 d for intact MAbs). Of these isotopes, ^{89}Zr (22.7% β^+, $E_{\beta+max}$ = 0.897 MeV; Fig. 1) can be obtained with high radionuclidic purity by a (p,n) reaction on ^{89}Y, an element that is an ideal target material because of its 100% natural abundance. Recently, stable coupling of ^{89}Zr to MAbs was accomplished using the chelate *N*-succinyldesferrioxamine B (*N*-sucDf) and new linker chemistry based on amide bond formation[10]. In addition, preliminary *in vitro* data indicated residualization of the radionuclide after internalization of ^{89}Zr-labeled MAbs by tumor cells, a phenomenon also observed with ^{111}In and ^{90}Y but not with ^{131}I and rhenium-186 (^{186}Re) (I. Verel *et al.*, unpublished data).

Taking these considerations into account, it was postulated that immuno-PET with ^{89}Zr-labeled MAbs might be a useful scouting procedure for ^{90}Y-MAb RIT. In the present study, the potential of this approach was evaluated by studying the biodistribution of both conjugates on coinjection and by assessing the quantitative imaging performance of ^{89}Zr immuno-PET. For this purpose, nude mice with head and neck squamous cell carcinoma (HNSCC) xenografts were used as an *in vivo* model, chimeric MAb (cMAb) U36 was used for HNSCC targeting, a high-resolution research tomograph (HRRT) three-dimensional (3D) PET scanner was used for imaging, and ^{88}Y (half-life, 107 d) was used instead of ^{90}Y to enable counting in a γ-counter. Biodistribution of cMAb U36-*N*-sucDf-^{89}Zr and cMAb U36-*p*-SCN-Bz-DOTA-^{88}Y conjugates was studied up to 6 d after injection. In addition, the potential of PET to quantify cMAb U36-*N*-sucDf-^{89}Zr was evaluated by relating image-derived tumor uptake data (noninvasive method) to ^{89}Zr data derived from excised tumors (invasive method).

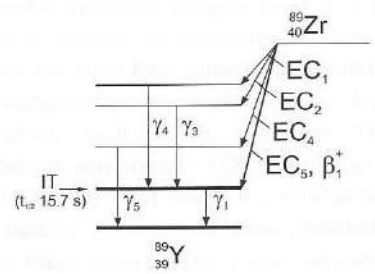

Transition		Energy (MeV)	Abundance (%)
β^+	1	0.897	22.7
EC	5		76.2
γ	1	0.909	99.9
	3	1.657	0.10
	4	1.713	0.77
	5	1.744	0.13

Figure 1. Simplified ^{89}Zr decay scheme (modified from ICRP publication[9]). Only transitions in excess of 0.1% abundance are shown. EC = electron capture; IT = isomeric transition; $t_{1/2}$ = half-life.

MATERIALS AND METHODS

MAb

Selection, production and characterization of cMAb U36 have been described elsewhere [11].

Production and isolation of ^{89}Zr

The improved procedure for ^{89}Zr production and isolation has been described recently in detail [10]. Briefly, ^{89}Zr was produced via a (p,n) reaction on natural ^{89}Y by irradiating an ^{89}Y-layer on a copper support (14-MeV protons). The irradiated ^{89}Y-layer was dissolved in 2 M HCl and, after addition of hydrogen peroxide, loaded onto a hydroxamate column. This column was washed with 2 M HCl and sterile water to remove radionuclidic impurities and the bulk nonradioactive ^{89}Y and eluted with 1 M oxalic acid to obtain 99.99% pure ^{89}Zr.

Radiolabeling

Preparation of ^{89}Zr-labeled cMAb U36 cMAb U36 was premodified with the chelate desferrioxamine B mesylate (Df) (desferal; Novartis) via an amide linkage and labeled with ^{89}Zr according to recently described novel procedures [10]. Df was succinylated (*N*-sucDf), temporarily filled with iron (Fe(III)), and coupled to MAbs by means of a tetrafluorophenol-*N*-sucDf ester. On average, one Df-chelate per MAb molecule was conjugated. After premodification of the MAb, as well as after labeling of the premodified MAb with ^{89}Zr, the MAb solution was purified using a PD-10 column (Pharmacia Biotech), eluting with 5 mg/ml gentisic acid (pH 5). For biodistribution studies, cMAb U36-*N*-sucDf was labeled with 155 MBq ^{89}Zr and 2.2 mg MAb in a volume of 2.3 ml. For PET imaging studies, the reaction conditions were 3.6 mg premodified cMAb U36, 460 MBq ^{89}Zr, and a reaction volume of 6 ml.

Preparation of ^{88}Y-labeled cMAb U36 cMAb U36 was conjugated with *p*-isothiocyanatobenzyl-1,4,7,10-tetraazacyclododecane-1,4,7,10-tetraacetic acid (*p*-SCN-Bz-DOTA; Macrocyclics), essentially as described by Hnatowich *et al.* [12]. All steps were performed under strict metal-free conditions. A 50-fold molar excess of *p*-SCN-Bz-DOTA was added to cMAb U36 (10 mg/ml) in 0.1 M $NaHCO_3$ buffer, pH 8.2, and incubated for 30 min at room temperature. Approximately two *p*-SCN-Bz-DOTA moieties were conjugated per MAb molecule. Nonconjugated chelator was removed by extensive dialysis against metal-free 0.25 M NH_4OAc, pH 5.4. After dialysis, the chelated MAb was diluted in 0.25 M NH_4OAc, pH 5.4, to a concentration of 1 mg/ml and stored at –20°C. cMAb U36-*p*-SCN-Bz-DOTA was labeled with ^{88}Y ($E_{main\ \gamma}$ = 898 keV and 1836 keV, 93.4% and 99.3% abundance, respectively) (74 MBq/ml, Isotope Products Europe Blaseg) by adding 5.6 MBq $^{88}YCl_3$ to 100 µg premodified cMAb U36 in 0.25 M NH_4OAc, pH 5.4. After incubation for 60 min at 45°C, unbound ^{88}Y was removed using a PD-10 column eluted with phosphate-buffered saline (PBS), 0.5% bovine serum albumin.

Analyses

All conjugates were analyzed by instant thin-layer chromatography (ITLC) and high-performance liquid chromatography (HPLC) (for ^{89}Zr-conjugates) or fast-protein liquid chromatography (FPLC) (for ^{88}Y-conjugates) for radiochemical purity, by sodium dodecylsulfate-polyacrylamide gel electrophoresis (SDS-PAGE) for integrity, and by a cell-binding assay for immunoreactivity.

ITLC analysis of radiolabeled MAbs was performed on silica gel-impregnated glass fiber sheets (Gelman Sciences Inc.). As the mobile phase, a citrate buffer concentration of 20 mM, pH 5.0, was used for ^{89}Zr-labeled MAbs, and a concentration of 0.15 M, pH 6.0, was used for ^{88}Y-labeled MAbs.

HPLC monitoring of the synthesis of cMAb U36-*N*-sucDf-^{89}Zr was performed as described previously [10]. FPLC was performed with a Biosep Sec S3000 column (300x7.8 mm, Phenomenex) with PBS, pH 7.4, as eluent.

A germanium(lithium) detector coupled to a multichannel analyzer was used for absolute quantification of ^{89}Zr and for calibration of other detectors. Routine single-isotope radioactivity measurements of ^{88}Y and ^{89}Zr were performed with a dose calibrator or a γ-counter (LKB-Wallac, 1282 CompuGamma; Pharmacia). For quantification in a dose calibrator, the manganese-54 (^{54}Mn) mode was used, multiplying the displayed amount of activity by a factor of 0.67 when measuring ^{89}Zr, and multiplying by a factor of 0.43 when measuring ^{88}Y. Quantification in a γ-counter was performed on the 909-keV γ-energy of ^{89}Zr and on the 898-keV γ-energy of ^{88}Y. For the dual-isotope counting of biodistribution studies, the 511-keV γ-energy of ^{89}Zr and the 1837-keV γ-energy of ^{88}Y were used. Crossover corrections from one radionuclide into the alternate window were performed using a standard of each radionuclide.

The integrity of the radioimmunoconjugates was monitored by electrophoresis on a Phastgel System (Pharmacia Biotech) using preformed 7.5% SDS-PAGE gels under nonreducing conditions. Analysis and quantification of the radioactivity in the bands was performed with Phosphor Imager (B&L-Isogen Service Laboratory) screens and subsequent scanning by a Phosphor Imager.

In vitro binding characteristics of radiolabeled MAbs were determined in an immunoreactivity assay essentially described by Lindmo *et al.* [13], using UM-SCC-11B cells fixed in 0.1% glutaraldehyde.

Biodistribution

Nude mice bearing subcutaneously implanted human xenografts of the cell line HNX-OE were used. Female mice (athymic nu/nu, 21-31 g, Harlan CPB) were 10-14 wk old at the time of the experiments. All animal experiments were performed according to National Institutes of Health principles of laboratory animal care [14] and Dutch national law ("wet op de Dierproeven", Stb 1985, 336).

The mice (n = 20) were injected in the retroorbital plexus with a mixture of 0.37 MBq cMAb U36-*N*-sucDf-^{89}Zr, 0.13 MBq cMAb U36-*p*-SCN-Bz-DOTA-^{88}Y, and

unlabeled cMAb U36 (total of 100 μg MAb). At indicated time points after injection, mice were anaesthetized, bled, killed, and dissected. After blood, tumor (weight, 35-370 mg), normal tissues, and gastrointestinal contents were weighed, the amount of radioactivity in each was measured in a γ-well counter. Radioactivity uptake was calculated as the percentage of the injected dose per gram of tissue (%ID/g). Differences in tissue uptake between coinjected conjugates were statistically analyzed for each time point with SPSS 10.0 software (SPSS Inc.) using the Student *t* test for paired data. Two-sided significance levels were calculated, and $P < 0.05$ was considered statistically significant.

PET studies

PET scanner Measurements were performed using a prototype single-crystal-layer HRRT 3D PET scanner (CTI PET Systems) [15]. The HRRT consists of 8 flat-panel detector heads, arranged in an octagon. The distance between two opposing heads is 46.9 cm. Each head contains 9x13 lutetium oxyorthosilicate crystal blocks of 7.5-mm thickness, which are cut into 8x8 crystals, resulting in 7,488 individual crystal elements per head and 59,904 crystals for the entire gantry.

Transmission scans for attenuation correction were routinely obtained with each scan in two-dimensional (2D) mode (consisting of 52 scans with a total duration of 360 s) using a single point source of 740 MBq ^{137}Cs and an energy window of 550-800 keV. Emission data can be acquired in 3D mode only. For the present study, acquisition was performed with an energy window of 400-650 keV, and emission data were rebinned (compressed) online into 32-bit list mode using a span of 9 and a ring difference of 67. Random subtraction was applied online by a delayed window technique. The 32-bit list mode file was subsequently converted into a single-frame histogram online.

For image reconstruction purposes, the transmission scan was first reconstructed and the resulting transmission (Tx)-image was scaled to correct for the difference in photon energy between emission (511 keV) and transmission (662 keV) counts using a histogram-based method [15]. After attenuation correction and normalization (without correction for dead time losses), the gaps in the resulting 3D emission sinogram were corrected by angular and transaxial interpolation. The fully corrected 3D emission scan was than Fourier rebinned into 207 image planes of 1.21 mm, which were subsequently reconstructed by 2D filtered backprojection with a Hanning 0.5 filter. The reconstructed volume consisted of 207 image planes of 256x256 voxels, with each voxel equaling 1.21x1.21x1.21 mm. For the present study, no scatter correction was applied because evaluation studies with the HRRT scanner showed that the scatter fraction was below 0.05 for small-animal scans and no accurate scatter-correction algorithm was available at the moment for HRRT scans [15].

Phantom studies Three basic phantoms were used. For linearity measurements, a phantom consisting of a cylinder (4.5 cm in diameter x 11.9 cm long) filled with 200 MBq ^{89}Zr was scanned for 30 min at several time points during the decay of ^{89}Zr. Two line sources were used for determination of spatial resolution, one filled with ^{89}Zr and the other with fluorine-18 (^{18}F) as a reference. The two sources were inserted in the central axis of a

water-filled cylinder (20 cm in diameter x 20 cm long) and located transaxial, 5 cm off center. For determination of recovery coefficients, a Jaszczak phantom was used. This phantom consists of a water-filled cylinder, containing 6 spheres with inner diameters ranging from 4.4 to 28 mm (0.05 to 11.5 cm^3). The spheres were filled with either ^{89}Zr or ^{18}F and scanned for 30 min.

Animal studies Mice bearing HNX-OE xenografts were injected with 3.7 MBq cMAb U36-*N*-sucDf-^{89}Zr (100 μg), and up to 4 mice were scanned simultaneously. The total activity within the field of view of the scanner stayed well within the region of linearity. Before being scanned, the mice were anaesthetized with sodium pentobarbital (75 mg/kg, intraperitoneally) and positioned in the PET scanner. A transmission scan of 360 s was performed, followed by a 60-min emission scan. At 24 and 48 h after injection 2 mice were scanned, and at 72 h after injection 8 mice were scanned. The mice were killed immediately after scanning, and tumors (weight, 19-154 mg) were excised and counted with both a germanium(lithium) detector and a γ-counter.

PET data analysis

Phantom studies The calibration factor to convert region-of-interest (ROI) counts/pixel/s to Bq/ml was determined by drawing an ROI in the image of the scanned cylinder. For the determination of the count rate linearity, the observed counts were subsequently converted with the aid of this calibration factor and plotted as a function of known radioactivity concentration.

Spatial resolution of ^{89}Zr, expressed as full width at half maximum (FWHM), was calculated by linear interpolation of horizontal and vertical line profiles, averaged over 5 adjacent image planes. For comparison, the same was performed for ^{18}F.

Hot spot recovery coefficients (HSRCs) of ^{89}Zr were determined by drawing an ROI for each sphere of the Jaszczak phantom, using a 50% isocontour (ROI including pixels with ≥50% of the maximum pixel radioactivity concentration). Subsequently, the HSRC was calculated for each sphere by dividing the measured radioactivity concentration in the ROI ($A_{m,\ sphere}$) by the measured radioactivity concentration in the ROI of the largest sphere ($A_{m,\ largest\ sphere}$). The ROI areas derived from this experiment were compared with the true sphere sizes to assess the accuracy of size prediction using a 50% isocontour. For comparison, the same was performed for ^{18}F.

Animal studies For the quantification of radioactivity in millimeter-sized tumors, 3D volumes of interest (VOIs) were drawn semiautomatically using software kindly provided by J. Nuyts (Katholieke Universiteit Leuven). The radioactivity concentration in these VOIs was corrected for partial volume effects starting from the following equation:

$$A_{u,\ tumor} = (HSRC \bullet A_{c,\ tumor}) + (CSRC \bullet A_{m,\ surroundings}) \qquad \text{Eq. 1}$$

where $A_{u,\ tumor}$ is the uncorrected radioactivity concentration in the tumor measured by PET, consisting of a tumor self-contribution and a near-surroundings spillover contribution.

$A_{c,\,tumor}$ is the radioactivity concentration in the tumor after correction for partial volume effects, $A_{m,\,surroundings}$ is the measured radioactivity concentration in the surrounding tissue near the tumor, and CSRC is the cold spot recovery coefficient.

$A_{u,\,tumor}$ was determined by drawing an 80% isocontour VOI around the tumor. HSRCs were determined by drawing 80% isocontour VOIs around each sphere of the Jaszczak phantom and were plotted as a function of VOI volume. The relationship between hot and cold spot measurements was taken as described by Geworski *et al.* [16]:

$$CSRC = 1 - HSRC \qquad \text{Eq. 2}$$

$A_{m,\,surroundings}$ was determined for each tumor by drawing two ROIs in the plane with the maximum pixel tumor radioactivity concentration, together specifying a ring-shaped area around the tumor with a thickness of one pixel. The inner ROI (ROI_1) marked the boundary of the tumor and was established by decreasing the percentage of the isocontour until reaching the largest tumor ROI volume that did not include nearby radioactivity-containing organs. Subsequently, the second ROI (ROI_2) was drawn with 2 times the diameter of ROI_1 in the x- and y-directions. The radioactivity concentration in the ring-shaped area ($A_{m,\,surroundings}$) was determined according to the following equation:

$$A_{m,\,surroundings} = \frac{(N_2 - N_1)}{(V_2 - V_1)} \qquad \text{Eq. 3}$$

where N_1 and V_1 are the radioactivity and volume of ROI_1, respectively, and N_2 and V_2 are those of ROI_2.

Rewriting Equation 1 and substituting Equation 2 and Equation 3 gives the following equation used in this study:

$$A_{c,\,tumor} = \frac{A_{u,\,tumor}}{HSRC} - \frac{(1 - HSRC) \bullet (N_2 - N_1)}{HSRC \bullet (V_2 - V_1)} \qquad \text{Eq. 4}$$

$A_{c,\,tumor}$ values (PET assessed) were plotted against the actual radioactivity levels in the excised tumors (*ex vivo* assessed), and regression analysis was performed with SPSS 10.0.

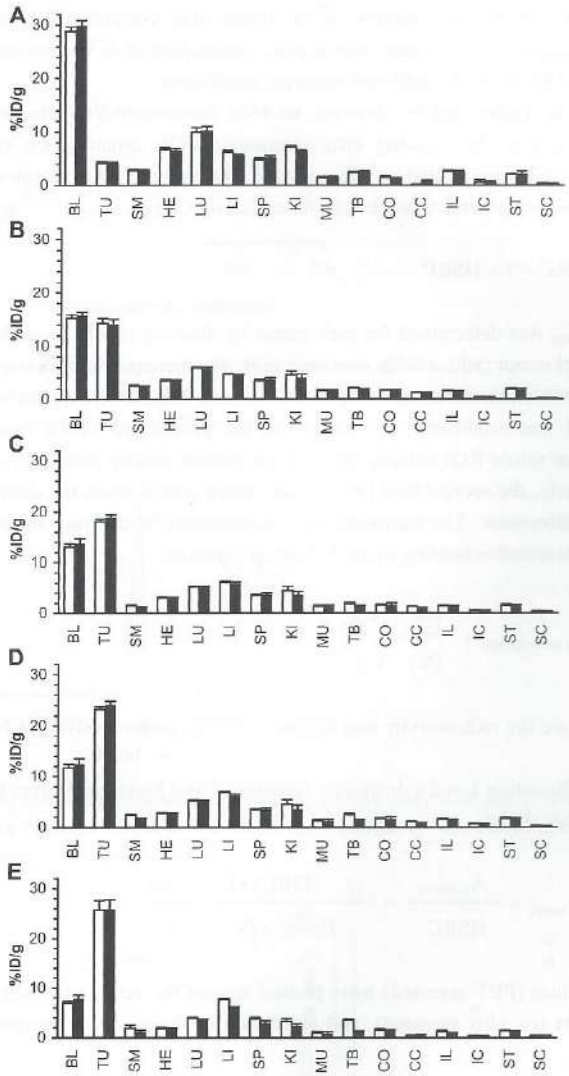

Figure 2. Biodistribution of coinjected cMAb U36-*N*-sucDf-^{89}Zr (0.37 MBq, white bars) and cMAb U36-*p*-SCN-Bz-DOTA-^{88}Y (0.13 MBq, black bars) in HNX-OE xenograft-bearing nude mice at 3, (A), 24 (B), 48 (C), 72 (D), and 144 h (E) after injection. At the indicated time points, 4 mice were bled, sacrificed, and dissected, and radioactivity levels (%ID/g ± SEM) of blood, tumor, organs, and gastrointestinal contents were assessed. BL = blood; TU = tumor; SM = sternum; HE = heart; LU = lung; LI = liver; SP = spleen; KI = kidney; MU = muscle; TB = thigh bone; CO = colon; CC = colon content; IL = ileum; IC = ileum content; ST = stomach; SC = stomach content.

RESULTS

Radiolabeling

Labeling of cMAb U36-*N*-sucDf with ^{89}Zr resulted in an overall yield of 81% ± 6%, a radiochemical purity of 97.4% ± 0.9 %, and 93% ± 2% immunoreactivity (n = 2). cMAb U36-*p*-SCN-Bz-DOTA was labeled with ^{88}Y with an overall yield of 97%, a radiochemical purity of 100%, and 96% immunoreactivity. Upon phosphor imager analysis of SDS-PAGE gels, all three radioimmunoconjugates showed more than 92% of the activity in the 150-kDa IgG band. The specific activities of cMAb U36-*N*-sucDf-^{89}Zr for biodistribution and PET studies and of cMAb U36-*p*-SCN-Bz-DOTA-^{88}Y were 50 MBq/mg, 109 MBq/mg, and 46 MBq/mg, respectively.

Biodistribution studies

For comparison of the biodistribution of ^{89}Zr-labeled and ^{88}Y-labeled MAb in tumor-bearing nude mice, cMAb U36-*N*-sucDf-^{89}Zr was coinjected with cMAb U36-*p*-SCN-Bz-DOTA-^{88}Y. At 3, 24, 48, 72, and 144 h after injection, the average uptake (%ID/g, mean ± SEM) in tumor, blood, normal tissues, and gastrointestinal contents was determined (Fig. 2). In general, ^{89}Zr-labeled MAb and ^{88}Y-labeled MAb showed similar uptake in tumor, blood and other organs at all time points. Tumor uptake increased over time, from 4.1 ± 0.3 %ID/g at 3 h to 25.7 ± 1.9 %ID/g at 144 h for the ^{89}Zr-labeled MAb and from 4.0 ± 0.3 %ID/g at 3 h to 25.9 ± 1.8 %ID/g at 144 h for the ^{88}Y-labeled MAb. Blood values decreased from 28.8 ± 0.8 %ID/g at 3 h to 6.9 ± 0.4 %ID/g at 144 h for the ^{89}Zr-labeled MAb and from 29.9 ± 0.9 %ID/g at 3 h to 7.9 ± 0.7 %ID/g at 144 h for the ^{88}Y-labeled MAb. Significant differences ($p < 0.01$) between ^{89}Zr-labeled MAb and ^{88}Y-labeled MAb were found at 72 h and 144 h after injection in liver (6.9 ± 0.8 *vs.* 6.2 ± 0.8 %ID/g and 7.7 ± 0.5 *vs.* 6.0 ± 0.4 %ID/g, respectively), sternum (2.5 ± 0.1 *vs.* 1.6 ± 0.03 %ID/g and 1.8 ± 0.2 *vs.* 1.1 ± 0.1 %ID/g, respectively), and thigh bone (2.5 ± 0.1 *vs.* 1.3 ± 0.1 %ID/g and 3.5 ± 0.4 *vs.* 1.1 ± 0.1 %ID/g, respectively). For the kidney, a significant difference was found at all time points (from 7.3 ± 0.2 *vs.* 6.5 ± 0.3 %ID/g at 3 h to 3.2 ± 0.2 *vs.* 2.4 ± 0.2 %ID/g at 144 h).

PET studies

Phantom studies ^{89}Zr phantom studies were performed to determine linearity, resolution, and recovery coefficients. Linearity (PET-assessed radioactivity concentration *vs.* the actual radioactivity concentration) was high (R^2 = 0.99) in the radioactivity range of 0.04-0.33 MBq/ml ^{89}Zr. At the highest radioactivity concentration measured, 0.75 MBq/ml, nonlinearity was observed (Fig. 3). Image resolution of ^{89}Zr, expressed as FWHM, was 4.0 mm (Fig. 4). Under the same conditions, FWHM for ^{18}F was 3.9 mm. HSRC (50% isocontour) for ^{89}Zr and ^{18}F as a function of sphere volume is shown in Figure 5A. In general, the ^{89}Zr-HSRC values were slightly lower than the ^{18}F-HSRC values. At 50% isocontour, the sphere areas were overestimated by a factor of 1.29 for ^{89}Zr and 1.07 for ^{18}F (Fig. 5B). The lower HSRC values and the higher overestimation of sphere areas of ^{89}Zr are

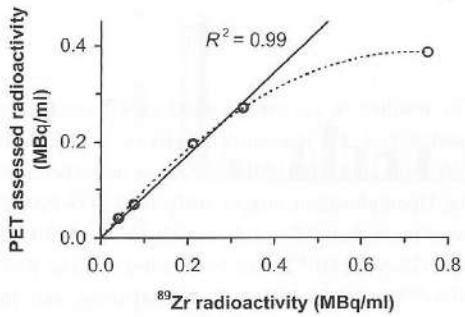

Figure 3. ^{89}Zr counting rate linearity determination with HRRT PET scanner. Plot is of PET-assessed radioactivity in cylinder phantom *vs.* radioactivity based on dose calibrator measurements. Note presence of linearity, except for highest radioactivity measurement.

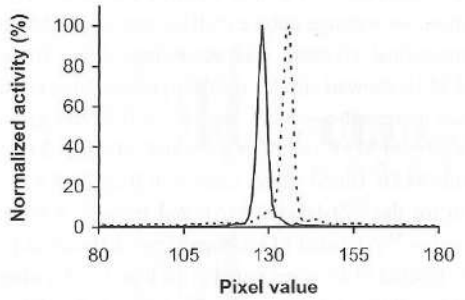

Figure 4. Spatial resolution determination for ^{89}Zr (dotted line) with HRRT PET scanner. Line profile was drawn through the image of the line source containing ^{89}Zr. For comparison, line profile for ^{18}F (solid line) is also shown.

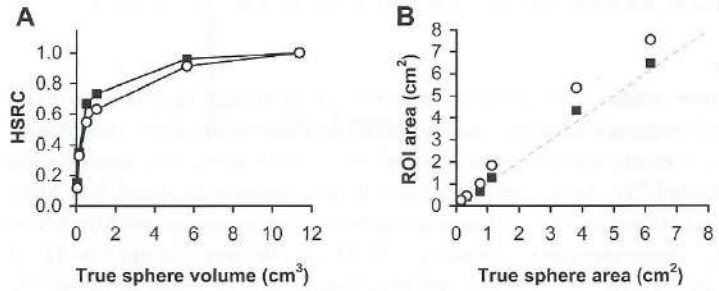

Figure 5. HSRCs (A) and sphere size estimations (B) for ^{89}Zr (white circle) with a HRRT PET scanner. For comparison, ^{18}F (black square) data are also shown. For this purpose, 50% isocontour ROIs were drawn around spheres of Jaszczak phantom.

most probably related to the higher positron energy of ^{89}Zr ($E_{\beta+max}$ = 0.897 MeV) in comparison with that of ^{18}F ($E_{\beta+max}$ = 0.634 MeV).

Animal studies Tumor imaging with ^{89}Zr-*N*-sucDf-labeled MAb was successful in 22 of 22 tumors (19-154 mg, 12 mice). Figure 6 shows a typical image of a xenograft-bearing nude mouse at 72 h after injection, with excellent visualization of tumors. The same studies were used to assess the potential of PET for quantification of tumor uptake. PET analysis, applying corrections for partial volume effects according to Equation 4, gave tumor uptake values in close agreement (R^2 = 0.79, 24 ± 17% error) with *ex vivo* tumor uptake values (Fig. 7A). Figure 7B shows this correlation to be independent of the volume and the day of imaging. The result of quantification without correction for partial volume effects is shown in Figure 7C and indicated that such correction is especially important for tumors with a small VOI.

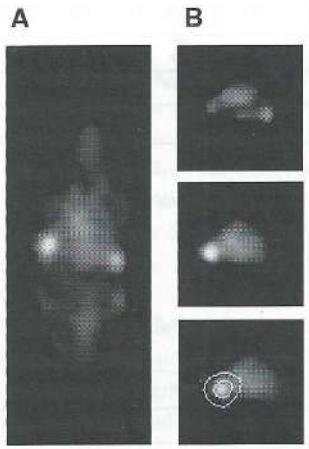

Figure 6. HRRT PET images of HNX-OE xenograft-bearing mouse injected with cMAb U36-*N*-sucDf-^{89}Zr (3.7 MBq) at 72 h after injection. A, Coronal image plane in which both tumors (left, 124 mg; right, 26 mg) were visible was chosen. B, Transaxial image planes in which right tumor was optimally visible (top) or left tumor was optimally visible (middle en bottom) were chosen. Bottom panel of B illustrates approach to arrive at ring-shaped area used for surroundings determination.

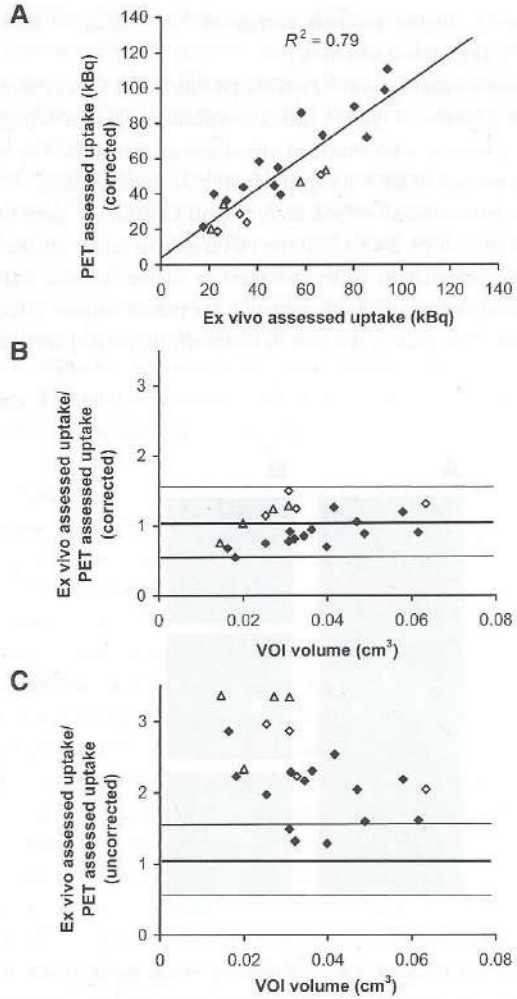

Figure 7. Correlation between PET assessed tumor uptake and *ex vivo* assessed tumor uptake. HNX-OE xenograft-bearing mice were injected with cMAb U36-*N*-sucDf-^{89}Zr (3.7 MBq) and scanned at 1 d (open diamonds, $n = 2$), 2 d (open triangles, $n = 2$) or 3 d (closed diamonds, $n = 8$) with a HRRT PET camera. Immediately after scanning the mice were dissected and the radioactivity levels in the tumors were determined with a γ-counter. After reconstruction of the images, VOIs were drawn over the tumors and radioactivity amounts were calculated. A, After correction for partial volume effects, PET assessed (image-derived) tumor radioactivity values were plotted as a function of *ex vivo* assessed (γ-counter-derived) tumor radioactivity values. The ratio of *ex vivo* assessed and PET assessed tumor radioactivity values, corrected (B) or not corrected (C) for partial volume effects, was plotted as a function of VOI volume.

DISCUSSION

Whereas ^{90}Y has attractive characteristics for therapy, imaging and the assessment of ^{90}Y biodistribution are complicated. The use of ^{111}In as an imaging analog for ^{90}Y has appeared to be suboptimal, because of the often-observed dissimilar biodistribution of these radionuclides[5]. Besides this, imaging with ^{111}In uses a γ-camera, which has intrinsic limitations with respect to quantification. In theory, PET provides better possibilities for quantification of tracer uptake, but this technique is in its infancy with respect to the availability of suitable positron emitters, tracers, and quantification techniques[17].

Recently, we described the production of large batches of highly pure ^{89}Zr by a (p,n) reaction on natural yttrium (^{89}Y), and its stable coupling to MAbs[10]. Because of the congruency in half-life of ^{89}Zr and ^{90}Y (78.4 *vs.* 64.1 h) and the fact that both radionuclides residualize upon internalization, we postulated ^{89}Zr to be a suitable positron-emitting surrogate for ^{90}Y.

The present study was performed to examine the potential of immuno-PET with ^{89}Zr-labeled MAbs as a scouting procedure in combination with ^{90}Y-MAb RIT and to assess its quantitative imaging performance in a realistic setting, that is, small tumors in a region with low object-to-background ratio. As a first evaluation, the biodistribution of cMAb U36-^{89}Zr and cMAb U36-^{88}Y was compared using the *N*-sucDf chelate for coupling of ^{89}Zr and the commonly used chelate *p*-SCN-Bz-DOTA for coupling of ^{88}Y (instead of ^{90}Y). Notwithstanding different chelators, both radionuclides showed similar uptake levels in blood, tumor, and most of the organs up to 144 h after injection. Only in kidney and, at the later time points (72 and 144 h after injection), in liver, sternum, and thigh bone was a higher uptake of ^{89}Zr than of ^{88}Y observed. The difference in bone retention was in the same range as previously observed in biodistribution studies on ^{111}In- and ^{90}Y-labeled MAbs[5]. The subtle divergence in biodistribution between ^{89}Zr and ^{88}Y is most probably due to the chemical differences between the radionuclides in combination with the chelators. With respect to the latter, investigations are ongoing to possibly find one chelate that binds both radionuclides with the same high stability.

As an alternative positron-emitting surrogate for ^{90}Y, ^{86}Y (33% β^+, $E_{\beta+max}$ = 1.2 MeV) has been receiving increasing attention[18-24]. An advantage in the use of the same element would be that deconjugation should result in identical tissue distribution. With respect to ^{86}Y-immuno-PET, the biodistribution of an ^{86}Y-labeled anti-Lewis Y MAb was recently compared with the biodistribution of the ^{111}In-labeled MAb, using CHX-diethylenetriaminepentaacetic acid (CHX-DTPA) as the chelate[23]. The uptake of ^{111}In and ^{86}Y was found to be similar in most tissues. In this study, no quantitative analysis with the authors' 2D PET system was performed, because of the difficulties met with from partial volume effects when ^{86}Y is used to image small tumors. Moreover, the authors foresaw problems with ^{86}Y quantification when using 3D PET imaging equipment. These problems concern the subtraction of coincidences, which result from a 511-keV annihilation photon with a prompt γ-photon emitted by ^{86}Y. These so-called spurious true coincidences (not

randoms) are accepted by the PET camera despite the fact that the two γ-photons have no angular correlation. As illustrated in phantom studies by Pentlow *et al.*[22], when using standard corrections on imaging of ^{86}Y with PET, such "spurious true coincidences" can introduce quantification artifacts, especially in regions of higher density. Solutions to these artifacts are under investigation[22].

Several aspects justify further development of ^{89}Zr-labeled radioimmunoconjugates in parallel to ^{86}Y-labeled conjugates. First, ^{89}Zr has no significant prompt γ-photons (see Fig. 1), which can hamper quantification. As illustrated in this article, quantitative imaging performance of ^{89}Zr was comparable to that of ^{18}F, and tumors as small as 19 mg were clearly visualized in xenograft-bearing nude mice after injection of ^{89}Zr-labeled cMAb U36. The potential of ^{89}Zr-PET for quantification was further illustrated by the good correlation between PET-assessed tumor uptake data and *ex vivo* tumor uptake data ($R^2 = 0.79$). Second, the half-life of ^{89}Zr (78.4 h) better fits the time needed for intact MAbs to achieve optimal tumor-to-nontumor ratios (typically 48–96 h) than the half-life of ^{86}Y (14.7 h). Also, the longer half-life of ^{89}Zr will evidently have advantages for logistics related to labeling and transportation.

Because of the encouraging results herein, ^{89}Zr-labeled cMAb U36 IgG is currently being evaluated for its capacity to detect primary tumors and metastases in operable HNSCC patients. Moreover, the potential of ^{89}Zr immuno-PET for quantification will be further evaluated in that clinical study.

CONCLUSION

The biodistributions of cMAb U36-*N*-sucDf-^{89}Zr and cMAb U36-*p*-SCN-Bz-DOTA-^{88}Y matched well, except for sternum and thigh bone at later time points (72 and 144 h) after injection. Small differences were found in kidney and liver. The imaging performance of ^{89}Zr was comparable to that of ^{18}F, with a similar spatial resolution and HSRC. PET imaging with ^{89}Zr-labeled MAb did reveal millimeter-sized tumors in xenograft-bearing mice, with a good correlation between image-derived and *ex vivo*-determined tumor radioactivity. Thus, ^{89}Zr appears to be a promising candidate for use as a positron-emitting surrogate for ^{90}Y.

ACKNOWLEDGMENTS

The authors thank BV Cyclotron (VU University) for performing the irradiations, Jan H. Rector (Solid State Physics VU University) for sputtering ^{89}Y on copper supports, Fred L. Buijs (Radionuclide Center, VU University) for analyzing the PET data, and Marijke Stigter, Maria J.W.D. Vosjan, and Liesbet Vervoort (VU University Medical Center) for contributing to the experiments.

REFERENCES

1. DeNardo SJ, Kroger LA, DeNardo GL. A new era for radiolabeled antibodies in cancer? *Curr Opin Immunol.* 1999;11:563-569.
2. Wagner HN, Wiseman GA, Marcus CS, et al. Administration guidelines for radioimmunotherapy of non-Hodgkin's lymphoma with ^{90}Y-labeled anti-CD20 monoclonal antibody. *J Nucl Med.* 2002;43:267-272.
3. Shen S, DeNardo GL, DeNardo SJ. Quantitative bremsstrahlung imaging of yttrium-90 using a Wiener filter. *Med Phys.* 1994;21:1409-1417.
4. Shen S, DeNardo GL, Yuan A, DeNardo DA, DeNardo SJ. Planar gamma camera imaging and quantitation of yttrium-90 bremsstrahlung. *J Nucl Med.* 1994;35:1381-1389.
5. Carrasquillo JA, White JD, Paik CH, et al. Similarities and differences in ^{111}In- and ^{90}Y-labeled 1B4M-DTPA antiTac monoclonal antibody distribution. *J Nucl Med.* 1999;40:268-276.
6. Pai-Scherf LH, Carrasquillo JA, Paik C, et al. Imaging and phase I study of ^{111}In- and ^{90}Y-labeled anti-Lewis^{Y} monoclonal antibody B3. *Clin Cancer Res.* 2000;6:1720-1730.
7. O'Donnell RT, DeNardo SJ, Yuan A, et al. Radioimmunotherapy with ^{111}In/^{90}Y-2IT-BAD-m170 for metastatic prostate cancer. *Clin Cancer Res.* 2001;7:1561-1568.
8. Meares CF, Moi MK, Diril H, et al. Macrocyclic chelates of radiometals for diagnosis and therapy. *Br J Cancer Suppl.* 1990;62:21-26.
9. Sowby FD editor. *Radionuclide transformations: Energy and intensity of emissions*; ICRP publication 38, volumes 11-13. Oxford, England: Pergamon Press; 1983.
10. Verel I, Visser GWM, Boellaard R, Stigter-van Walsum M, Snow GB, van Dongen GAMS. ^{89}Zirconium immuno-PET: comprehensive procedures for the production of ^{89}Zr-labeled monoclonal antibodies. *J Nucl Med.* 2003;44:1271-1281.
11. Schrijvers AHGJ, Quak JJ, Uyterlinde AM, et al. MAb U36, a novel monoclonal antibody successful in immunotargeting of squamous cell carcinoma of the head and neck. *Cancer Res.* 1993;53:4383-4390.
12. Hnatowich DJ, Childs RL, Lanteigne D, Najafi A. The preparation of DTPA-coupled antibodies radiolabeled with metallic radionuclides: an improved method. *J Immunol Methods.* 1983;65:147-157.
13. Lindmo T, Boven E, Luttita F, Fedorko J, Bunn PA Jr. Determination of the immunoreactive fraction of radiolabeled monoclonal antibodies by linear extrapolation to binding at infinite antigen excess. *J Immunol Methods.* 1984;72:77-89.
14. *Guide for the Care and Use of Laboratory Animals.* Washington, DC: Government Printing Office; 1985. NIH publication 86-157.
15. Boellaard R, Buijs F, de Jong HWAM, Lenox M, Gremillion T, Lammertsma AA. Characterization of a single LSO crystal layer high resolution research tomograph. *Phys Med Biol.* 2003;48:429-448.
16. Geworski L, Knoop BO, Levi de Cabrejas M, Knapp WH, Munz DL. Recovery correction for quantitation in emission tomography: a feasibility study. *Eur J Nucl Med.* 2000;27:161-169.
17. Eary JF. PET imaging for planning cancer therapy. *J Nucl Med.* 2001;42:770-771.

18. Herzog H, Rösch F, Stocklin G, Lueders C, Qaim SM, Feinendegen LE. Measurement of pharmacokinetics of yttrium-86 radiopharmaceuticals with PET and radiation dose calculation of analogous yttrium-90 radiotherapeutics. *J Nucl Med.* 1993;34:2222-2226.
19. Rösch F, Herzog H, Plag C, et al. Radiation doses of yttrium-90 citrate and yttrium-90 EDTMP as determined via analogous yttrium-86 complexes and positron emission tomography. *Eur J Nucl Med.* 1996;23:958-966.
20. Wester H-J, Brockmann J, Rösch F, et al. PET-pharmacokinetics of ^{18}F-octreotide: a comparison with ^{86}Ga-DFO- and ^{86}Y-DTPA-octreotide. *Nucl Med Biol.* 1997;24:275-286.
21. Rösch F, Herzog H, Stolz B, et al. Uptake kinetics of the somatostatin receptor ligand [^{86}Y]DOTA-DPhe^{1}-Tyr^{3}-octreotide ([^{86}Y]SMT487) using positron emission tomography in non-human primates and calculation of radiation doses of the ^{90}Y-labelled analogue. *Eur J Nucl Med.* 1999;26:358-366.
22. Pentlow KS, Finn RD, Larson SM, et al. Quantitative imaging of yttrium-86 with PET: the occurrence and correction of anomalous apperent activity in high density regions. *Clinical Positron Imaging.* 2000;3:85-90.
23. Lövqvist A, Humm JL, Sheikh A, et al. PET imaging of ^{86}Y-labeled anti-Lewis Y monoclonal antibodies in a nude mouse model: comparison between ^{86}Y and ^{111}In radiolabels. *J Nucl Med.* 2001;42:1281-1287.
24. Garmestani K, Milenic DE, Plascjak PS, Brechbiel MW. A new and convenient method for purification of ^{86}Y using a Sr(II) selective resin and comparison of biodistribution of ^{86}Y and ^{111}In labeled Herceptin™. *Nucl Med Biol.* 2002;29:599-606.

chapter

5

Efficient production of high quality ^{124}I-labeled monoclonal antibodies at patient dose level: overcoming the challenges posed by radiation chemistry

Iris Verel, Gerard W.M. Visser, Maria J.W.D. Vosjan, Ron Finn,
Ronald Boellaard, Guus A.M.S. van Dongen

Submitted.

ABSTRACT

Monoclonal antibodies (MAbs) and other (bio)pharmaceuticals containing the long-lived positron-emitting isotope ^{124}I (half-life, 100.3 h) can be used for quantitative imaging with positron emission tomography (PET). Labeling yields with this precious isotope are often low to moderate, which is in contrast to other iodine isotopes. In this study it was ascertained that not an intrinsic atom characteristic of ^{124}I, but the radiation induced deterioration of the starting ^{124}I-solution formed the prime inorganic obstacle to quantitative radiolabel yields. Regeneration methods were examined to regain ^{124}I in the iodide (I^-) form at a distant user site (receipt after several days of transportation). Subsequently, MAbs were labeled with regenerated ^{124}I under conditions that minimize chemical and radiation damage, and their quality was studied *in vitro* and *in vivo*. **Methods:** The possible involvement of an intrinsic atom characteristic of ^{124}I was evaluated by labeling MAb with a mixture of ^{124}I, ^{123}I, ^{126}I, and ^{130}I, followed by quantitative γ-spectroscopic analysis. Deterioration of the ^{124}I-iodide quality was studied by HPLC analysis and labeling experiments. An electrochemical method using a Pt/H_2 column and a new chemical method using a $NaIO_3$/NaI carrier-mix were applied to regenerate ^{124}I. The chimeric MAb (cMAb) U36, and the murine MAbs (mMAbs) 425 and E48 were radiolabeled with regenerated ^{124}I according to a mild Iodogen-based method, the so-called Iodogen-coated MAb method. For comparison, these MAbs were also labeled with ^{131}I under the same conditions. ^{124}I-labeled cMAb U36 was evaluated in biodistribution studies, upon coinjection with ^{131}I-labeled cMAb U36, and by PET imaging at 24, 48, and 72 h after injection of the conjugate in nude mice bearing the head and neck cancer xenograft line HNX-OE. **Results:** Labeling of cMAb U36 with the radioiodide-mixture resulted in exactly the same labeling yields for each isotope, excluding a different chemical reactivity of ^{124}I-iodide. At the users site, the percentage of ^{124}I in the iodide form was below 30%, resulting in labeling yields of less than 20%. However, employing either regeneration method, greater than 90% recovery as ^{124}I-iodide was accomplished. Labeling with the regenerated ^{124}I resulted in overall labeling yields of more than 70%, with a radiochemical purity of more than 95%, and with preservation of MAb integrity and immunoreactivity, also at patient dose level (85 MBq). Biodistribution studies demonstrated that tissue uptake values were fully concordant for ^{124}I-labeled and ^{131}I-labeled cMAb U36, whereas selective tumor uptake was confirmed with immuno-PET revealing visualization of 15 out of 15 tumors. **Conclusion:** At a distant user site, ^{124}I can be efficiently recovered as iodide, and high quality ^{124}I-MAbs can be produced provided radiation damage-related protective measures are taken.

INTRODUCTION

Radionuclides of iodine (I) are widely used in studies on selective tumor-targeting with monoclonal antibodies (MAbs), peptides and other (bio)pharmaceuticals. Radioiodinated tracers are used, among others, for the absolute quantification of tissue uptake in biopsied samples (e.g. ^{123}I, ^{125}I, ^{131}I), for tumor imaging (e.g. ^{123}I, ^{131}I), and for therapy (^{131}I). Iodine isotopes are reasonable in cost, readily available, and can be coupled to proteins by facile procedures. Moreover, they offer the attractive possibility to be used pair-wise e.g. (1) for a comparison of biodistribution upon co-administration, and (2) for an approach in which imaging is performed as a scouting procedure prior to ^{131}I-therapy to confirm tumor-targeting and to estimate radiation dose delivery to both tumor and normal tissues. Most nuclear medicine imaging has involved planar imaging with a γ-camera, and more recently, single photon emission computerized tomography (SPECT). For quantification, however, these procedures are not optimal, primarily as a result of scatter and the partial absorption of the γ-photons in the tissue of the patient. Positron Emission Tomography (PET) is better suited for imaging as PET provides superior temporal and spatial resolution.

In search for candidate positron emitters for PET with tumor-seeking monoclonal antibodies (immuno-PET), we are putting effort in the production of high quality MAbs labeled with ^{124}I (half-life, 100.3 h) and zirconium-89 (^{89}Zr; half-life, 78.4 h), since these positron-emitting tracers have a physical half-life which is compatible with the time needed for MAbs to achieve optimal tumor-to-nontumor ratios (2-4 d for intact MAbs). We recently reported on the development of a novel procedure for stable coupling of ^{89}Zr to MAbs via pre-modification with a new bifunctional desferal derivative, because an earlier described route appeared to suffer from an unfortunate *in vivo* instability of the succinimide ring-thioether unit linkage [1].

The present study deals with the labeling of MAb with ^{124}I. Surveying the ^{124}I-literature, in general ^{124}I-compounds are obtained in low to moderate yields suggesting an inorganic ^{124}I-problem. Moreover, there isn't any well-documented ^{124}I-technical protocol to arrive at optimal quality ^{124}I-labeled MAbs in a dose suitable for clinical studies. This relates to (1) the use of harsh oxidants like chloramine-T or *N*-bromosuccinimide, (2) the use of the not innocuous sulphite-based reducing agents to stop the labeling reaction, and (3) insufficient precautions against radiation damage during and after labeling. It also means that in the reported patient pilot studies with ^{124}I-conjugates [2-4], insight in the factors responsible for tumor uptake and retention might have been impeded. We therefore feel that quality standardizing of ^{124}I-MAbs production should have high priority to appreciate the real potential of ^{124}I-immuno-PET.

In this optimization study, we first evaluated whether the aforementioned labeling problems were related to an intrinsic atom characteristic of ^{124}I or only to radiation induced formation of ^{124}I-oxoiodo complexes with anionic Lewis bases present in the ^{124}I-solution as is the case for astatine [5]. Ascertaining that the latter "ageing" of the starting ^{124}I-solution was the main factor, we herein describe two methods to regenerate a deteriorated ^{124}I-solution, a

chemical regeneration procedure and a recently developed in-house electrochemical method. Regenerated ^{124}I and ^{131}I (as reference) were used for labeling of MAbs at low dose and at patient dose level. Labeling was performed with the aid of a 1,3,4,6-tetrachloro-3α,6α-diphenyl-glycouril (Iodogen) based protocol that minimizes chemical and radiation damage. The iodinated MAbs were characterized for MAb integrity and immunoreactivity. ^{124}I-labeled cMAb U36 was evaluated by comparison of biodistribution with ^{131}I-labeled cMAb U36 upon coinjection in xenograft-bearing nude mice and by imaging with a high-resolution research tomograph (HRRT) PET scanner.

MATERIALS AND METHODS

Monoclonal antibodies and radionuclides

Selection, production and characterization of chimeric MAb (cMAb) U36, as well as of the murine MAbs (mMAbs) 425 and E48, have been described elsewhere[6]. ^{124}I in 0.1 M phosphate buffer pH 7.0 (2.6-3.3 MBq/μl, 50-55 μl, more than 99% as iodide at the time of packaging at the supplier) was kindly provided by Dr. R. Finn (Memorial Sloan-Kettering Cancer Center, NY). Upon receiving the ^{124}I solution after 2-3 d of transport, a stock solution was prepared by transferring the radioactivity stepwise from the small delivery vial to a stock vial with the aid of 1 mM NaOH. This transfer was nearly quantitative: more than 99%. Hereafter the final radioactivity concentration was adjusted to 100 MBq/ml, resulting in a 4.5-5.0 mM phosphate buffer/1 mM NaOH stock solution (final pH 8). Test mixtures of ^{123}I, ^{124}I, ^{126}I, and ^{130}I (99.8% as carrier free iodide), freshly isolated in 1-2 MBq amounts in 10 mM NaOH were kindly provided by BV Cyclotron (VU University, Amsterdam, The Netherlands). ^{131}I was obtained from Amersham (7.4 GBq/ml).

Pretreatment of ^{124}I activity

Electrochemical regeneration Radioiodine was regenerated by adsorption on a platinum/hydrogen (Pt/H_2) column by an in-house method as recently described for several common radioiodine isotopes (up to 50 GBq) by Braker *et al.*[7]. In short, a Varian mini-column (10 x 3 mm, Varian) was filled with 360-400 mg of Pt powder (200 mesh, Alfa Aesar) and connected to a pressure system (0-1 bar). Before use, the Pt column was saturated with H_2 by means of a H_2 gas flow (10 ml/min, 10 min) and subsequently purged with a flow of N_2 gas (10 ml/min, 10 min). Aliquots of the ^{124}I stock solution were diluted with 1 mM NaOH and, after adjustment to pH 2 with 5 mM H_2SO_4, passed through the Pt/H_2 column under a flow of N_2 gas (1 ml/min). The volume of the loading sample for regeneration is not restricted (tested up to 40 ml). After loading and subsequent washing of the column with 5 ml of Millipore water, the absorbed radioiodine was eluted as iodide with an alternated flow of in total 1 ml 10 mM NaOH and H_2 gas (overall recovery more than 90%).

Chemical regeneration To aliquots of the ^{124}I stock solution, 5 µl of carrier-mix was added and incubated for 2-4 min. The carrier-mix was freshly made and consisted of 0.1 mg/ml NaI (Sigma-Aldrich) and 0.1 mg/ml $NaIO_3$ (Merck) in 1 mM NaOH.

Labeling with Iodogen-coated MAb method

The novel "Iodogen-coated MAb" method, as described by Visser *et al.* [8], is the method of choice for high dose iodination (for clinical application) as it minimizes chemical and radiation damage to the MAb, and allows the use of a large volume of iodide solution (up to 1 ml). Essential in this procedure is the implementation of ascorbic acid, as was also performed in production of rhenium-186- (^{186}Re-) [9], ^{90}Y- [10], and ^{131}I-labeled MAbs [8]. MAbs were labeled with "aged" ^{124}I and regenerated ^{124}I, with ^{131}I, and with a mixture of iodine isotopes according to this procedure. The volume of the radioiodine solution was adjusted to 1 ml with 1 mM NaOH, after which 10 µl ascorbic acid (1.41 mg/ml; Bufa) was added. After incubation for 3 min, 0.2 ml 1 M Na_2HPO_4 (pH 7.2) and 0.7 ml 0.1 M Na_2HPO_4 (pH 6.8) containing 1 mg MAb were added. Thereafter, temporarily coating of the MAb with Iodogen (Pierce) was started (t = 0 min) by adding 35 µl of a freshly prepared Iodogen/MeCN solution (1 mg/ml) and abrogated at t = 3 min by adding 0.2 ml ascorbic acid solution (25 mg/ml, pH 5). During the whole procedure the reaction vial was gently shaken on a wobbling device. At t = 8 min 50 µl 20% human serum albumin (HSA; Sanquin) was added and at t = 12 min the reaction mixture was loaded onto a PD-10 column (Amersham) and eluted with 0.9% NaCl/ascorbic acid (5 mg/ml, pH 5). The first 2.7 ml (2.2 ml sample volume and the first 0.5 ml) was discarded and the radiolabeled MAb was collected in the next 3 ml. In the labeling experiments with a mixture of iodine isotopes, an additional 2 ml was collected (containing unreacted iodine). To the MAb containing fraction an additional 0.1 ml 20% HSA solution was added to make the final concentration 1% [w/w] HSA.

For animal experiments, an amount of activity was taken which has been shown to be realistic for immuno-PET in a clinical setting [11]. To this end, labeling of 2 mg of cMAb U36 was performed with 85 MBq ^{124}I chemically regenerated using 10 µl of carrier-mix, or with 89 MBq ^{131}I. In this particular case also 10 µl of carrier-mix was added to the ^{131}I-solution to arrive at approximately the same I/MAb molar ratio.

Labeling with Iodogen-coated vial method

The Iodogen-coated vial method was implemented as this method is often used for low dose, preclinical iodination [8]. For reaction with "aged" ^{124}I or regenerated ^{124}I, with ^{131}I, or with a mixture of iodine isotopes, also MAbs were used as model substrates. In short, 20 ml β-scintillation glass vials were coated with 75 µg Iodogen in dichloromethane, dried under a stream of N_2 gas resulting in a thin coating of Iodogen on the bottom surface of the vial. The vials were stored under N_2 atmosphere. To a Iodogen-coated glass vial, successively 50 µl 0.5 M Na_2HPO_4 (pH 7.4), 0.5 mg MAb in 0.35 ml 0.1 M Na_2HPO_4 (pH 6.8), and radioiodine in 0.1 ml 1 mM NaOH were added. After gentle shaking for 4 min at room temperature, 0.1 ml ascorbic acid (25 mg/ml, pH 5) was added. After an additional 5 min, the reaction mixture

was transferred to a syringe connected to a filter (0.22 µm Acrodisc, Gelman Sciences) followed by 0.4 ml 0.1 M Na_2HPO_4 (pH 6.8), used for an additional rinsing of the reaction vial. This combined solution was filtered and purified on a PD-10 column with 0.9% NaCl/ascorbic acid (5 mg/ml, pH 5) as eluent. The first 2.5 mL (1.0 ml sample volume and the first 1.5 ml) were discarded and the radiolabeled MAb was collected in the next 1.5 ml. In the labeling experiments with a mixture of iodine isotopes, an additional 2 ml was collected (containing unreacted iodine). To the MAb containing fraction 0.075 ml 20% HSA solution was added (1% [w/w] final concentration).

Analyses

High-performance liquid chromatography (HPLC) analysis of inorganic ^{124}I, using a Lichrospher RP-Select B column (125 x 4 mm, 5 µm; Merck) was performed as described previously[8]. Before analysis, injections of 5 µl of NaI:$NaIO_3$ (1:1 v/v, 1 mg/ml each) were made for calibration/equilibration of the column. The HPLC retention times, measured by UV at 210 nm, were 2.2 min for IO_3^- and 5.1 min for I^-. The HPLC retention time measured on radioactivity was 4.8 min for $^{124}I^-$ (delay between radiodetector and UV detector is 0.3 min); identification of other ^{124}I components in the stock solution was not attempted. HPLC analysis of ^{124}I- or ^{131}I-labeled MAbs, using a Superdex 200 HR 10/30 column (Pharmacia Biotech), was performed as described previously[8].

Instant thin-layer chromatography (ITLC) analysis of radiolabeled MAbs was carried out on silica impregnated glass fiber sheets (Gelman Sciences Inc.). As mobile phase, 20 mM citric acid pH 5 was used.

A germanium(lithium) (Ge(Li)) detector coupled to a multichannel analyzer was used for absolute quantification of ^{124}I ($E_{main\ \gamma}$ = 603 keV, 62.9 % abundance). For determination of the ratio of iodine isotopes in the iodine mixture before and after labeling, Ge(Li) analysis was performed on the 159 keV γ-energy of ^{123}I, the 603 keV γ-energy of ^{124}I, the 389 keV γ-energy of ^{126}I, and the 536 keV γ-energy of ^{130}I. Routine single isotope radioactivity measurements of ^{124}I and ^{131}I were performed with a dose calibrator or a γ-counter (LKB-Wallac, 1282 CompuGamma; Pharmacia). For quantification of ^{124}I in a dose calibrator the ^{137}Cs mode was used, multiplying the displayed amount of activity by a factor 0.566. For γ-counter measurements the corresponding window settings for ^{124}I and ^{131}I were used (for the 603 keV γ-energy and the 364 keV γ-energy, respectively). In the dual isotope biodistribution studies, cross-over corrections from one radionuclide into the alternate window were performed using a standard of each radionuclide.

The integrity of the radioimmunoconjugates was monitored by electrophoresis on a Phastgel System (Pharmacia Biotech) using preformed 7.5% SDS-PAGE gels under nonreducing conditions. Analysis and quantification of the radioactivity in the bands was performed with a Phosphor Imager (B&L-Isogen Service Laboratory).

In vitro binding characteristics of radiolabeled MAbs were determined in an immunoreactivity assay essentially as described by Lindmo *et al.*[12]. For cMAb U36, mMAb

425, and mMAb E48, UM-SCC-11B cells, A431 cells and UM-SCC-22A cells fixed in 0.1% glutaraldehyde were used, respectively.

Biodistribution studies

Nude mice bearing subcutaneously implanted human xenografts of the cell line HNX-OE were used. Female mice (Athymic nu/nu, 19-29 g, Harlan CPB) were 10-14 weeks old at the time of the experiments. Thyroid uptake was blocked by the addition of potassium iodide to the drinking water (0.1%) starting one day before the experiment. All animal experiments were performed according to the principles of laboratory animal care[13] and Dutch national law ("wet op de dierproeven", Stb 1985, 336).

The mice (n = 12) were injected in the retroorbital plexus with a mixture of 0.53 MBq ^{124}I-labeled cMAb U36, 0.74 MBq ^{131}I-labeled cMAb U36, and unlabeled cMAb U36 (total of 100 µg MAb). At indicated time points after injection, mice were anaesthetized, bled, killed, and dissected. After weighing, the amount of radioactivity in tumors (size 180-820 mg), organs, blood, and gastrointestinal contents was measured in a γ-counter. Radioactivity uptake was calculated as the percentage of the injected dose per gram of tissue (%ID/g). Differences in tissue uptake of both radioiodinated MAbs were statistically analyzed with the Student t test for paired data. Two-sided significance levels were calculated and $P < 0.05$ was considered statistically significant.

PET studies

PET studies were performed using a prototype single-crystal-layer HRRT 3D PET scanner (CTI)[14], essentially as recently described for ^{89}Zr-labeled MAbs[15]. In short, transmission scans for attenuation correction were routinely obtained with each scan in two-dimensional mode using a single point ^{137}Cs source. Emission data can be acquired in three-dimensional mode only. For the present study, emission data were collected in rebinned 32bit list mode and subsequently histogrammed only into a single frame. Images were reconstructed with filtered backprojection Hanning 0.5 filter and consisted of 207 image planes of 256x256 voxels, with each voxel equaling 1.21x1.21x1.21 mm.

Mice bearing HNX-OE xenografts (size 106-777 mg) were injected with 3.7 MBq ^{124}I-labeled cMAb U36 (110 µg). Before scanning, mice (n = 8) were anaesthetized with sodium pentobarbital (75 mg/kg, intraperitoneal) and positioned in the PET scanner. A transmission scan of 360 s was performed followed by a 60 min emission scan. At 24, 48, and 72 h after injection, two mice were scanned, immediately followed by dissection. In addition, two mice were scanned three times: at 24, 48, and 72 h after injection; after 72 h these mice were dissected.

RESULTS

Radiolabeling

In a first set of experiments, it was considered whether the oxidation potential of the ^{124}I-isotope, or any other intrinsic atom characteristic, is a parameter influencing labeling efficiencies. To this end, a mixture of freshly isolated ^{123}I, ^{124}I, ^{126}I, and ^{130}I was used for a parallel labeling of cMAb U36 according to the Iodogen-coated MAb method and the Iodogen-coated vial method. This resulted in labeling yields of 87 ± 2 % (n = 3) and 84 ± 2 % (n = 3), respectively. Ge(Li) analysis showed that the ratio of iodine isotopes in the product fraction and in the unreacted iodine fraction was the same as the ratio in the starting iodide solution, eliminating the possibility that an iodine isotope effect occurs. As a typical example, starting with a ^{123}I:^{126}I:^{130}I:^{124}I iodide-solution with a netto Ge(Li) count ratio of 1.42:0.34:0.72:1, for the product fraction and its corresponding unreacted iodine fraction a ratio of 1.43:0.34:0.71:1 and 1.43:0.31:0.72:1 respectively was found for the Iodogen-coated MAb method, and 1.42:0.32:0.71:1 and 1.43:0.32:0.71:1 respectively for the Iodogen-coated vial method.

Next, the iodide quality as a parameter influencing labeling efficiencies was investigated. In a realistic end-user setting for ^{124}I, i.e. 2-3 d delay between packaging and

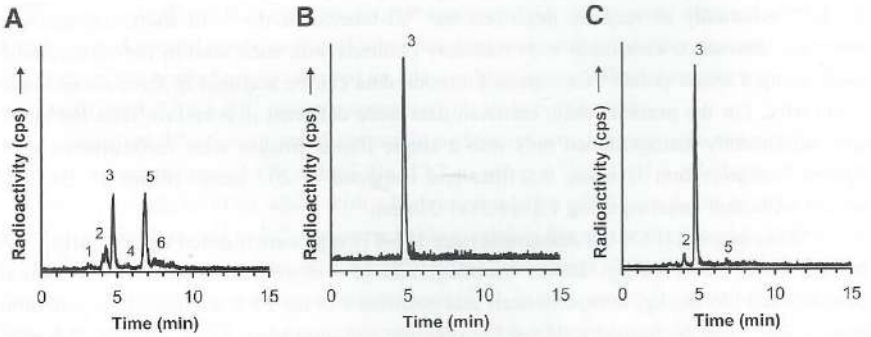

Figure 1. HPLC analysis of a ^{124}I sample after 2 d transportation and 16 h storage as a stock solution (100 MBq/ml)(A) and after regeneration with Pt/H_2 column adsorption (B) or NaI/$NaIO_3$ carrier-mix induced regeneration (C). Percentages: A, 27.2% $^{124}I^-$ (3) and 72.8% unidentified ^{124}I components (1, 2.5%; 2, 14.3%; 4, 5.1%; 5, 34.6%; 6, 16.3%); B, 99.9% $^{124}I^-$ (3); C, 91.3% $^{124}I^-$ (3) and 8.7% unidentified ^{124}I components (2, 5.8%; 5, 2.9%).

delivery, preparation of a stock solution and storage for 16 h, HPLC analysis revealed a massive deterioration of the ^{124}I-iodide as illustrated by Figure 1A. Interestingly, $^{124}IO_3^-$ was not observed. An aliquot of a ^{124}I solution of this composition (27% $^{124}I^-$) was used for labeling of cMAb U36 via the Iodogen-coated MAb method and the Iodogen-coated vial method. This resulted in overall labeling yields of 18% and 14%, respectively, indicating that the formed inorganic iodo-species did not contribute to the labeling yield.

Treatment of the deteriorated ^{124}I solution gave upon electrochemical regeneration a $^{124}I^-$ peak containing more than 98% of the radioactivity, and upon chemical regeneration containing more than 90% of the radioactivity (Fig. 1B and 1C). Labeling of cMAb U36 with electrochemical regenerated ^{124}I resulted in labeling yields comparable to those obtained with the fresh radioiodide isotope mixture. Using chemically regenerated ^{124}I-aliquots and the Iodogen-coated MAb method, the MAbs cMAb U36, mMAb 425 and mMAb E48 were labeled with overall labeling yields above 72% (Table 1). Radiochemical purity always exceeded 95%, immunoreactivity was more than 75% and integrity of the MAbs, as determined by electrophoresis and expressed as percentage of radioactivity confined to the 150-kDa band, was always more than 90%. Experiments performed with ^{131}I under the same conditions resulted in similar quality features but slightly higher overall labeling yields (Table 1). This can be attributed to the remaining lower percentage of ^{124}I-iodide in case of chemical regeneration.

Table 1. Labeling of MAbs with chemically regenerated ^{124}I and ^{131}I using the Iodogen-coated MAb method.

Isotope	Activity (MBq)	MAb	Overall labeling yield (% ± SD)	Radiochemical purity (% ± SD)	Immunoreactivity (% ± SD)	Integrity [a] (% ± SD)
^{124}I	4.5-7.8	U36 [b]	72.3 ± 2.8	97.8 ± 0.4	91.1 ± 3.9	93.4 ± 1.3
	2.9-5.7	425 [c]	79.0 ± 3.1	96.5 ± 0.4	82.6 ± 2.0	90.5 ± 1.1
	4.4-7.1	E48 [c]	72.0 ± 2.5	97.1 ± 0.5	75.4 ± 2.9	90.3 ± 1.9
^{131}I	12.2-21.1	U36 [b]	79.3 ± 2.4	98.8 ± 0.6	95.6 ± 1.2	95.0 ± 2.1
	14.6-20.4	425 [c]	85.4 ± 3.0	99.4 ± 0.3	87.6 ± 0.8	90.5 ± 0.4
	14.7-20.3	E48 [c]	76.2 ± 3.7	95.3 ± 0.2	75.0 ± 1.4	90.1 ± 0.8
^{124}I [d]	85	U36	77.8	98.3	94.5	93.1
^{131}I [d]	89	U36	90.3	99.7	96.2	92.2

[a] Determined by electrophoresis and phosphor imager analysis, percentage of radioactivity in the major 150-kDa band is given.

[b] $n = 4$, mean ± SD

[c] $n = 2$, mean ± SD

[d] Patient dose labeling experiment, used for animal studies. It is of note that in this case also carrier-mix has been added to ^{131}I activity.

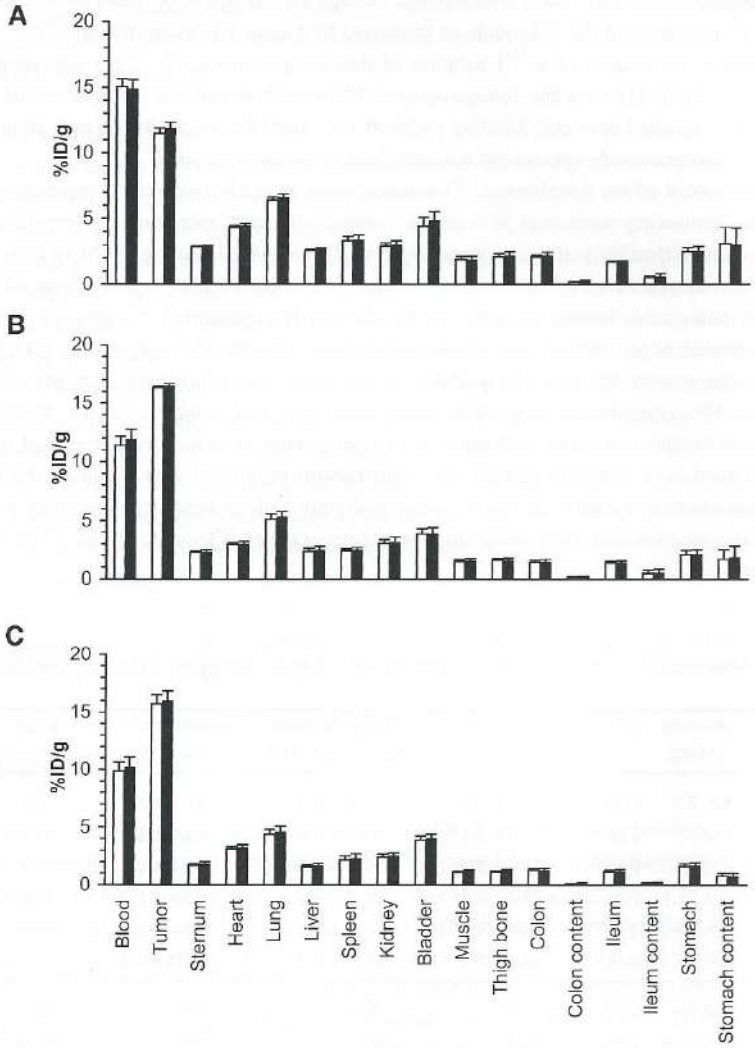

Figure 2. Biodistribution of coinjected ^{124}I-labeled cMAb U36 (0.53 MBq, black bars) and ^{131}I-labeled cMAb U36 (0.74 MBq, white bars) in HNX-OE xenograft-bearing mice at 24 (A), 48 (B), and 72 h (C) after injection. cMAb U36 was labeled using the Iodogen-coated MAb method after regeneration of ^{124}I with NaI/$NaIO_3$ carrier-mix. In order to arrive at approximately similar I/MAb ratios for both radioimmunoconjugates, the same amount of carrier-mix was added to ^{131}I. At the indicated time points 4 mice were bled, sacrificed, dissected and the radioactivity levels (%ID/g ± SE) of blood, tumor, organs and gastrointestinal contents were assessed.

Animal studies

In order to evaluate the tumor-targeting capacity of ^{124}I-labeled MAb labeled at patient dose level (85 MBq/2 mg MAb), cMAb U36 was labeled with either ^{124}I or ^{131}I, and radioiodinated MAb preparations were administrated simultaneously to HNX-OE xenograft-bearing nude mice for biodistribution assessment ($n = 4$ per time point). An overall labeling yield of 77.8% for ^{124}I-labeled and 90.3% for ^{131}I-labeled cMAb U36 was obtained with a radiochemical purity of 98.3% and 99.7%, an immunoreactivity of 94.5% and 96.2%, and an integrity of 93.1% and 92.2%, respectively. The specific radioactivities were 32.6 MBq/mg and 40.4 MBq/mg and the I/MAb molar ratios were 0.39 and 0.53, respectively. At 24, 48, and 72 h after injection, the average %ID/g (mean ± SEM) of tumor, blood, normal tissues, and gastrointestinal contents were determined (Fig. 2). At all time points, uptake values were fully congruent for ^{124}I-labeled and ^{131}I-labeled cMAb U36. Tumor uptake for ^{124}I-labeled and ^{131}labeled MAb increased in time from approx. 12 %ID/g at 24 h (11.9 ± 0.5 *vs.* 11.5 ± 0.4, respectively) to approx. 16 %ID/g at 72 h (16.0 ± 0.8 *vs.* 15.7 ± 0.8, respectively) and blood values decreased from approx. 15 %ID/g at 24 h (14.9 ± 0.7 *vs.* 15.0 ± 0.6, respectively) to approx. 10 %ID/g at 72 h (10.2 ± 0.9 *vs.* 9.9 ± 0.8, respectively).

To complete the *in vivo* evaluation, 8 HNX-OE xenograft-bearing nude mice were subjected to immuno-PET with the patient-dose labeled product used for the biodistribution studies. In the coronal as well as transaxial images, tumor imaging at 24, 48, and 72 h after injection was successful in 15 of 15 tumors (106-777 mg). Figure 3 shows the images of a xenograft-bearing nude mouse made at 24, 48, and 72 h after injection, with good visualization of tumors and improved delineation at later time points. From the non-target tissues, only the blood pool in the heart, liver, and the nose area were visible.

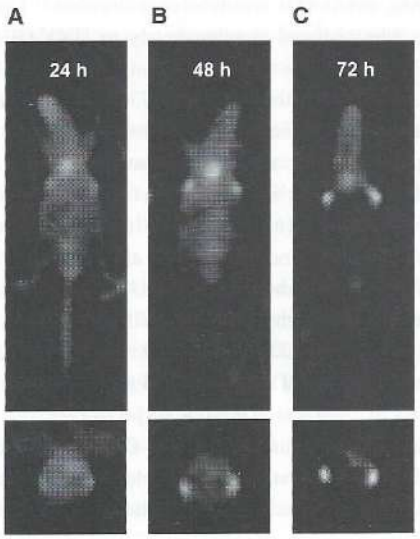

Figure 3. PET images of a HNX-OE xenograft-bearing nude mouse injected with ^{124}I-labeled cMAb U36 (3.7 MBq, 110 µg MAb, I/MAb molar ratio 0.4). Coronal (upper) and transaxial (lower) images were acquired at 24 (A), 48 (B), and 72 h (C) after injection. Image planes have been chosen where both tumors (tumor left, 110 mg; tumor right, 112 mg) were visible.

DISCUSSION

Due to its long half-life of 100.3 h, the positron emitter ^{124}I has been proposed to be suitable for immuno-PET [16-20]. Although labeling with radioiodine isotopes has been a widespread practice for decades, in several studies ^{124}I-compounds were obtained in lower yields when directly compared with other iodine isotopes [3,21-24]. In order to elucidate this phenomenon, in this study the involvement of an intrinsic chemical characteristic of $^{124}I^-$ and interference of radiolytic processes were investigated. Introduction of two regeneration methods made efficient labeling of MAbs with ^{124}I as straightforward as the labeling with ^{131}I. Moreover, by taking precautions against radiation and chemical damage to the MAb, ^{124}I-cMAb U36 labeled at patient dose level appeared to be similar to the reference conjugate ^{131}I-labeled cMAb U36 with respect to integrity, *in vitro* antigen binding as well as *in vivo* tumor-targeting. The latter was demonstrated with the aid of biodistribution studies upon coinjection in tumor-bearing nude mice, and by a PET- imaging study over a period of 3 d.

If ^{124}I is produced in-house, auto-oxidation of the ^{124}I-iodide solution will be limited when the ^{124}I is used shortly after isolation, provided the dose rate i.e. the activity concentration is not too high. Most applications of ^{124}I though are anticipated to occur at a distant user site. In that case the detrimental effects of the high-energy positrons and gammas will be considerable. Indeed, a ^{124}I-batch produced in the USA and transported for use to Europe contained a high amount of ^{124}I-oxoiodo species. In addition, this ^{124}I stock solution did not contain iodate (IO_3^-) in contrast to (alkaline) ^{131}I-batches [8]. This indicates that during the deterioration of the ^{124}I activity the phosphate ions in the stock solution are involved by means of phosphato-iodo complexes.

Regeneration of the ^{124}I activity with the use of the electrochemical method is the method of choice in studies that require carrier free ^{124}I-(bio)pharmaceuticals. Another application of the method is the possibility to recover the unreacted ^{124}I as iodide from the corresponding PD-10 purification fractions; the presence of ascorbic acid in these fractions was found to have no effect on the Pt/H_2 column absorption process. Regeneration of the ^{124}I can be best performed immediately before use, as it was found that the carrier free condition rapidly resulted in ageing of the ^{124}I-iodide solution again (data not shown).

If carrier free ^{124}I is not required, the chemical regeneration method is an easy and facile alternative. This method is based on the fact that disproportionation, a common process in inorganic halogen chemistry, does not proceed under carrier free conditions. The addition of $NaI/NaIO_3$ carrier-mix generated the required IO^- and IO_2^- species to start the disproportionation. Single addition of either NaI or $NaIO_3$ did not initiate this regeneration process, while regeneration with just ascorbic acid, as described previously for high dose ^{131}I labeling [8], proved to require too high amounts of ascorbic acid. The amount of carrier-mix was chosen to keep the iodine-to-MAb molar ratio below 1.4, as this ratio has been shown not to affect immunoreactivity and pharmacokinetics [8]. It is of note that variables such as the $NaI/NaIO_3$ ratio, the amount of carrier-mix added, and the duration of the regeneration effect as a function of the amount of radioactivity, are not studied in extenso yet. These variables

might become important when larger doses of ^{124}I are used for batch-wise production of conjugate.

Regeneration of the ^{124}I solution creates an optimal starting point for labeling MAbs with ^{124}I. Next, the preparation of radiolabeled MAbs is a critical factor in the evaluation of immuno-PET. Since direct labeling of MAbs with radioiodine isotopes such as ^{131}I is still the standard method used for clinical applications as opposed to indirect labeling methods, in this study MAbs were labeled with ^{124}I according to a direct labeling method with the use of the mild oxidant Iodogen. For an adequate ^{124}I-scouting of a ^{131}I-RIT conjugate the MAb should be labeled in exactly the same way with optimal protection against chemical and radiation damage, and by preference with the same I/MAb molar ratio load. We regard the latter parameter to be important as long as for optimal quality MAbs the influence of I/MAb molar ratio (upper limit 1.4) on e.g. the blood clearance rate and on the tumor retention has not been established. In congruency with these premises, cMAb U36 labeled with ^{124}I at patient dose level exhibited exactly the same pharmacokinetic behavior as the corresponding ^{131}I-conjugate and a feasibility to study tumor accumulation with the use of PET.

For the labeling of monoclonal antibodies, the positron emitters ^{124}I and ^{89}Zr both have ideal half-lives of several days. Based on their individual chemical and *in vivo* characteristics, this set of positron emitters offers the unique opportunity to study a variety of scouting and RIT combinations. Since ^{89}Zr is known to residualize upon internalization of the ^{89}Zr-MAb conjugate into the tumor cell, ^{89}Zr can act as imaging and quantifying surrogate isotope for e.g. ^{90}Y or lutetium-177 (^{177}Lu). The non-residualizing ^{124}I on the other hand is an ideal scouting tracer for ^{131}I and possibly for ^{186}Re. Besides MAbs, also peptides and other (bio)pharmaceuticals can be labeled with ^{124}I and ^{89}Zr for drug discovery and development. To retain the pharmacological, biological, and biochemical properties of the molecule studied, it can be anticipated that with decreasing molecule size the use of chelate-based methods, such as needed for the coupling of ^{89}Zr, might become less suitable. In that case labeling with ^{124}I could have preference. Future experiments are planned to study the scope of suitability of these two isotopes for tracing MAbs and peptides.

CONCLUSION

This study provides two regeneration methods, a chemical and an electrochemical method, to obtain the long-lived positron emitter ^{124}I as almost pure iodide at a distant user site. Achievements obtained as such will certainly also facilitate efficient use of ^{124}I in methods for indirect labeling. MAbs were labeled efficiently with thus regenerated ^{124}I via a mild Iodogen-based method. Highly similar biodistribution was demonstrated for ^{124}I-labeled cMAb U36 and ^{131}I-labeled cMAb U36, whereas selective tumor-targeting was visualized with immuno-PET in xenograft-bearing nude mice.

ACKNOWLEDGMENTS

The authors thank Anton H. Braker (Radionuclide Center, VU University) for performing radioiodine regeneration using the Pt/H_2 column, Fred L. Buijs (Radionuclide Center, VU University) for the PET analyses, Marijke Stigter (Otolaryngology/Head and Neck Surgery, VU University Medical Center) for assistance in the animal experiments, and Peter J. van Leuffen and Roel Mooy of BV Cyclotron (VU University) for supplying test mixtures of radioiodine isotopes.

REFERENCES

1. Verel I, Visser GWM, Boellaard R, Stigter-van Walsum M, Snow GB, van Dongen GAMS. ^{89}Zr immuno-PET: comprehensive procedures for the production of ^{89}Zr-labeled monoclonal antibodies. *J Nucl Med.* 2003;44:1271-1281.
2. Wilson CB, Snook DE, Dhokia B, et al. Quantitative measurement of monoclonal antibody distribution and blood flow using positron emission tomography and ^{124}Iodine in patients with breast cancer. *Int J Cancer.* 1991;47:344-347.
3. Larson SM, Pentlow KS, Volkow ND, et al. PET scanning of iodine-124-3F8 as an approach to tumor dosimetry during treatment planning for radioimmunotherapy in a child with neuroblastoma. *J Nucl Med.* 1992;33:2020-2023.
4. Daghighian F, Pentlow KS, Larson SM, et al. Development of a method to measure kinetics of radiolabelled monoclonal antibody in human tumour with applications to microdosimetry: positron emission tomography studies of iodine-124 labelled 3F8 monoclonal antibody in glioma. *Eur J Nucl Med.* 1993;20:402-409.
5. Visser GWM. Inorganic astatine chemistry. Part II: the chameleon behaviour and electrophilicity of At-species. *Radiochim Acta.* 1989;47:97-103.
6. Vrouenraets MB, Visser GWM, Stigter M, Oppelaar H, Snow GB, van Dongen GAMS. Targeting of aluminum (III) phthalocyanine tetrasulfonate by use of internalizing monoclonal antibodies: improved efficacy in photodynamic therapy. *Cancer Res.* 2001;61:1970-1975.
7. Braker AH, Moet FP, van der Zwart RE, Eersels JLH, Herscheid JDM. Adsorption of radioiodine on platinum: a fast and simple column method to obtain concentrated and pure radioiodide in either water or anhydrous solvents. *Appl Radiat Isot.* 2002;57:475-482.
8. Visser GW, Klok RP, Klein Gebbinck JW, ter Linden T, van Dongen GA, Molthoff CF. Optimal quality ^{131}I-monoclonal antibodies on high-dose labeling in a large reaction volume and temporarily coating the antibody with IODO-GEN. *J Nucl Med.* 2001;42:509-519.
9. Visser GWM, Gerretsen M, Herscheid JDM, Snow GB, van Dongen GAMS. Labeling of monoclonal antibodies with ^{186}Re using the MAG_3 chelate for radioimmunotherapy of cancer: a technical protocol. *J Nucl Med.* 1993;34:1953-1963.
10. Chakrabarti MC, Le N, Paik CH, De Graff WG, Carrasquillo JA. Prevention of radiolysis of monoclonal antibody during labeling. *J Nucl Med.* 1996;37:1384-1388.
11. Jayson GC, Zweit J, Jackson A, et al. Molecular imaging and biological evaluation of HuMV833 anti-VEGF antibody: implications for trial design of antiangiogenic antibodies. *J Natl Cancer Inst.* 2002;94:1484-1493.
12. Lindmo T, Boven E, Luttita F, Fedorko J, Bunn PA Jr. Determination of the immunoreactive fraction of radiolabeled monoclonal antibodies by linear extrapolation to binding at infinite antigen excess. *J Immunol Methods.* 1984;72:77-89.
13. *Guide for the Care and Use of Laboratory Animals*. Washington, DC: Government Printing Office; 1985. NIH publication 86-23.
14. Boellaard R, Buijs F, de Jong HWAM, Lenox M, Gremillion T, Lammertsma AA. Characterization of a single LSO crystal layer high resolution research tomograph. *Phys Med Biol.* 2003;48:429-448.
15. Verel I, Visser GWM, Boellaard R, et al. Quantitative ^{89}Zr immuno-PET for in vivo scouting of ^{90}Y-labeled monoclonal antibodies in xenograft-bearing nude mice. *J Nucl Med.* 2003;44:1663-1670.

16. Pentlow KS, Graham MC. Quantitative imaging of I-124 using positron emission tomography with applications to radioimmunodiagnosis and radioimmunotherapy. *Med Phys.* 1991;18:357-366.
17. Westera G, Reist HW, Buchegger F, et al. Radioimmuno positron emission tomography with monoclonal antibodies: a new approach to quantifying in vivo tumour concentration and biodistribution for radioimmunotherapy. *Nucl Med Comm.* 1991;12:429-437.
18. Bakir MA, Eccles SA, Babich JW, et al. c-erbB2 Protein overexpression in breast cancer as a target for PET using iodine-124-labeled monoclonal antibodies. *J Nucl Med.* 1992;33:2154-2160.
19. Rubin SC, Kairemo KJA, Brownell A-L, et al. High-resolution positron emission tomography of human ovarian cancer in nude rats using ^{124}I-labeled monoclonal antibodies. *Gyn Onc.* 1993;48:61-67.
20. Kairemo KJA. Positron emission tomography of monoclonal antibodies. *Acta Oncol.* 1993;32:825-830.
21. Finn R, Cheung N-KV, Divgi C, et al. Technical challenges associated with the radiolabeling of monoclonal antibodies utilizing short-lived, positron emitting radionuclides. *Nucl Med Biol.* 1991;18:9-13.
22. Lee FT, Hall C, Rigopoulos A, et al. Immuno-PET of human colon xenograft-bearing BALB/c nude mice using ^{124}I-CDR-grafted humanized A33 monoclonal antibody. *J Nucl Med.* 2001;42:764-769.
23. Collingridge DR, Carroll VA, Glaser M, et al. The development of [^{124}I]iodinated-VG76e: a novel tracer for imaging vascular endothelial growth factor in vivo using positron emission tomography. *Cancer Res.* 2002;62:5912-5919.
24. Glaser M, Collingridge DR, Aboagye EO, et al. Iodine-124 labelled annexin-V as a potential radiotracer to study apoptosis using positron emission tomography. *Appl Radiat Isot.* 2003;58:55-62.

chapter

6

Long-lived positron emitters ^{89}Zr and ^{124}I for scouting of therapeutic radioimmunoconjugates with PET

Iris Verel, Gerard W.M. Visser, Otto C. Boerman, Julliette E.M. van Eerd, Ron Finn, Ronald Boellaard, Maria J.W.D. Vosjan, Marijke Stigter-van Walsum, Gordon B. Snow, Guus A.M.S. van Dongen

***Cancer Biotherapy & Radiopharmaceuticals* 2003;18:655-661.**

ABSTRACT

Immuno-PET imaging might be of value for the selection of radioimmunotherapy (RIT) candidates to confirm tumor-targeting and to estimate radiation doses to tumor and normal tissues. One of the requirements to be set for such a scouting procedure is that the biodistributions of the diagnostic and therapeutic radioimmunoconjugates should be similar. In the present study we evaluated the potential of the positon emitters zirconium-89 (^{89}Zr) and iodine-124 (^{124}I) for this approach, as these radionuclides have a relatively long half-life that matches with the kinetics of MAbs *in vivo* (half-life, 3.27 and 4.18 d, respectively). **Methods:** After radiolabeling of the head and neck squamous cell carcinoma (HNSCC)-selective chimeric antibody (cMAb) U36, the biodistribution of two diagnostic (cMAb U36-*N*-sucDf-^{89}Zr and cMAb U36-^{124}I) and three therapeutic radioimmunoconjugates (cMAb U36-*p*-SCN-Bz-DOTA-^{88}Y – with ^{88}Y being substitute for ^{90}Y –, cMAb U36-^{131}I, and cMAb U36-MAG3-^{186}Re) was assessed in mice with HNSCC-xenografts, at 24, 48, and 72 h after injection. **Results:** Two patterns of biodistribution were observed, one pattern matching for ^{89}Zr- and ^{88}Y-labeled cMAb U36 and one pattern matching for ^{124}I-, ^{131}I-, and ^{186}Re-cMAb U36. The most remarkable differences between both patterns were observed for uptake in tumor and liver. Tumor uptake levels were 23.2 ± 0.5 and 24.1 ± 0.7 %ID/g for the ^{89}Zr- and ^{88}Y-cMAb U36 and 16.0 ± 0.8, 15.7 ± 0.8, and 17.1 ± 1.6 %ID/g for ^{124}I-, ^{131}I-, and ^{186}Re-cMAb U36-conjugates, respectively, at 72 h after injection. For liver these values were 6.9 ± 0.8 (^{89}Zr), 6.2 ± 0.8 (^{88}Y), 1.7 ± 0.1 (^{124}I), 1.6 ± 0.1 (^{131}I), and 2.3 ± 0.1 (^{186}Re), respectively. **Conclusion:** These preliminary data justify the further development of immuno-PET with ^{89}Zr-labeled MAbs for scouting of therapeutic doses of ^{90}Y-labeled MAbs. In such approach ^{124}I-labeled MAbs are most suitable for scouting of ^{131}I- and ^{186}Re-labeled MAbs.

INTRODUCTION

Tumor-targeting with radiolabeled monoclonal antibodies (MAbs) has become an attractive approach for diagnosis and therapy of cancer [1]. Initially, iodine-131 (^{131}I) was the radionuclide of choice for radioimmunotherapy (RIT). More recently, also other radionuclides like rhenium-186 (^{186}Re), lutetium-177 (^{177}Lu), and particularly yttrium-90 (^{90}Y) are used in RIT studies. A favorable aspect in the use of ^{90}Y-labeled conjugates is the minimal radiation burden to medical personnel and relatives, due to the lack of γ-emission. However, the *in vivo* distribution of ^{90}Y-labeled MAbs can not be visualized scintigraphically.

To optimize RIT, demonstration of specific tumor uptake and estimation of radiation doses to critical organs is important. These data can be achieved by performing radioimmunoscintigrapy (RIS) as scouting procedure prior to RIT [2]. Traditionally for imaging of radioactivity, planar imaging with a γ-camera and more recently, single photon emission computerized tomography (SPECT), have been used. These procedures, however, have intrinsic limitations for quantification, due to corrections for scatter and attenuation that have to be applied. Positron emission tomography (PET) offers the advantage of attenuation correction enabling more accurate quantification, together with a high spatial resolution and the possibility for kinetic measurements.

For the application of immuno-PET, the positron emitter used should have a physical half life of several days, compatible with the time needed for a MAb to achieve optimal tumor-to-nontumor ratios. Two positron emitters that fulfil this requirement are zirconium-89 (^{89}Zr) and iodine-124 (^{124}I) (half-life, 3.27 and 4.18 d, respectively). To justify scouting procedures based on these two positron emitters in order to predict RIT, the pharmacokinetics have to be the same for the diagnostic and the therapeutic radioimmunoconjugate. For this purpose, a preliminary study was performed to evaluate the biodistribution of MAb labeled with the diagnostic radionuclides ^{89}Zr and ^{124}I, and the three therapeutic radionuclides ^{88}Y (substituting ^{90}Y), ^{131}I, and ^{186}Re. The head and neck squamous cell carcinoma (HNSCC)-selective chimeric antibody (cMAb) U36 was labeled with these radionuclides and the biodistribution in mice with HNX-OE xenografts was assessed.

MATERIALS AND METHODS

MAb

Selection and production of murine MAb U36 and its chimeric (mouse/human) IgG_1 derivative (cMAb U36) have been decribed previously [3]. MAb U36 recognizes the v6 domain of CD44v6. The CD44 protein family consists of isoforms, encoded by standard exons and up to nine alternatively spliced variant exons (v2 – v10), which are expressed in a tissue-specific way. Homogenous expression of v6-containing CD44 isoforms has been observed in squamous cell carcinoma of the head and neck, lung, skin, esophagus and cervix, while heterogenous expression was found in adenocarcinomas of the breast, lung, colon, pancreas

and stomach. In normal tissues, expression has been found in epithelial tissues such as skin, breast and prostate myoepithelium, and bronchial epithelium [3]. The potential of cMAb U36 for selective targeting of head and neck cancer has been demonstrated in clinical radioimmunoscintigraphy and radioimmunotherapy studies [4].

Radiolabeling

cMAb U36 was labeled with five radionuclides: ^{89}Zr (2.7 GBq/ml, in-house production by a (p,n) reaction on natural ^{89}Y and isolated with the use of a hydroxamate column), ^{88}Y (74 MBq/ml, Isotope Products Europe Blaseg), ^{124}I (2.6 GBq/ml, kindly provided by Dr. R. Finn, Memorial Sloan Kettering Cancer Center), ^{131}I (7.4 GBq/ml, Amersham), and ^{186}Re (11.0 MBq/nmol, Mallinckrodt Medical) (Fig. 1).

Antibody labeling with ^{89}Zr was achieved via the chelate desferrioxamine B (Df) (desferal, Novartis) using a method published previously [5]. First, MAb was premodified with the chelate Df via an amide linkage. To this end, Df was succinylated (*N*-sucDf), temporarily filled with stable iron (Fe(III)), and coupled to MAb by means of a tetrafluorophenol-Df ester. After purification of the premodified MAb on a PD-10 column (eluent: 0.9% NaCl/gentisic acid 5 mg/ml, pH 5.0), ^{89}Zr (155 MBq) was added in order to label the MAb-*N*-sucDf conjugate (2.2 mg). Finally, purification on a PD-10 column was performed to remove any unbound ^{89}Zr (eluent: 0.9% NaCl/gentisic acid 5 mg/ml, pH 5.0).

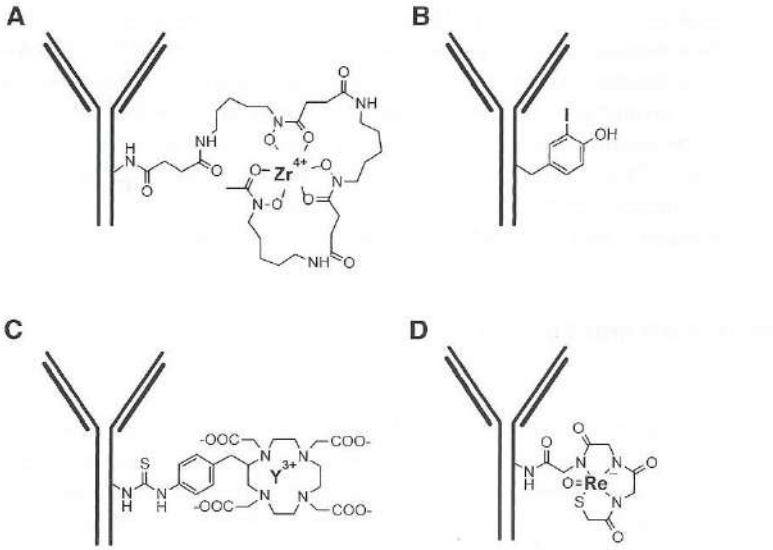

Figure 1. Schematic representation of MAb labeled with ^{89}Zr (A), $^{124/131}$I (B), ^{88}Y (C), or ^{186}Re (D).

For the labeling with ^{88}Y, cMAb U36 was conjugated with the chelate *p*-isothiocyanatobenzyl-1,4,7,10-tetraazacyclododecane-1,4,7,10-tetraacetic acid (*p*-SCN-Bz-DOTA, Macrocyclics), essentially as described by Ruegg *et al.*[6]. After conjugation, nonconjugated chelate was removed by extensive dialysis (0.25 M NH_4Ac pH 5.4). The MAb-DOTA conjugate (0.1 mg) was reacted with ^{88}Y (5.55 MBq) for 60 min. All steps were performed under strict metal-free conditions.

MAbs were labeled with ^{124}I and ^{131}I according to the so-called Iodogen-coated MAb method, as previously described by Visser *et al.*[7], with some essential modifications in the pretreatment of ^{124}I-activity (chapter 5). In short, a MAb solution (2 mg in sodium phosphate buffer) was added to the radioactivity (85 MBq ^{124}I or 89 MBq ^{131}I). Labeling with iodine was initiated by adding a freshly prepared Iodogen/MeCN solution (35 µg in 35 µl), thus coating the MAb temporarily with Iodogen, and abrogated after 3 min by adding ascorbic acid. After 8 min a 20% HSA solution was added and the reaction mixture was filtered and purified on a PD-10 column (eluent: 0.9% NaCl/ascorbic acid 5 mg/ml, pH 5.0).

^{186}Re-labeled MAb conjugates were prepared according to a multistep procedure using the chelate S-benzoylmercaptoacetyltriglycine (S-benzoyl-MAG3) as previously described[8]. In this procedure a solid-state synthesis for the preparation of ^{186}Re-MAG3 (244 MBq) is followed by esterification with 2,3,5,6-tetrafluorophenol and conjugation of the reactive ^{186}Re-MAG3-TFP ester to the MAb (1 mg). After conjugation the ^{186}Re-labeled MAb was purified on a PD-10 column (eluent: 0.9% NaCl/ascorbic acid 5 mg/ml, pH 5.0).

All conjugates were analyzed by instant thin-layer chromatography (ITLC) and high-performance liquid chromatography (HPLC) for radiochemical purity, SDS-PAGE for integrity and by a cell-binding assay for immunoreactivity. Radiochemical purity always exceeded 97%, always more than 92% of the activity was present in the 150-kDa IgG peak/band, and immunoreactivity always exceeded 93%.

Analyses

HPLC has been described previously for the monitoring of the synthesis of ^{89}Zr-labeled MAb[5], the analysis of radioiodinated MAbs[7], and the analysis of ^{186}Re-labeled MAG3, the corresponding ester and ^{186}Re-labeled MAb[8]. Analysis of ^{88}Y-labeled MAb was the same as for the ^{89}Zr-labeled MAb[5].

ITLC analysis of radiolabeled MAbs was carried out on silica gel impregnated glass fiber sheets (Gelman Sciences Inc.). As mobile phase, 20 mM citric acid, pH 5.0 was used for ^{124}I-, ^{131}I-, and ^{89}Zr-labeled MAbs, 0.1 M sodium citrate, pH 8.0 was used for ^{186}Re-labeled MAbs, and 0.15 M citric acid, pH 6.0 for ^{88}Y-labeled MAbs. R_f values were 0 for radiolabeled MAb and 1 for unbound label, irrespective the kind of mobile phase used.

The integrity of the radiolabeled MAbs was monitored by electrophoresis on a Phastgel System (Pharmacia Biotech) using preformed 7.5% SDS-PAGE gels under nonreducing conditions. Analysis and quantification of the radioactivity of the bands was performed with the use of Phosphor Imager screens and subsequent scanning by a Phosphor Imager (B&L-Isogen Service Laboratory).

In vitro binding characteristics of radiolabeled MAbs were determined in an immunoreactivity assay essentially as described by Lindmo *et al.* [9], using UM-SCC-11B cells fixed in 0.1% glutaraldehyde.

Biodistribution

Nude mice bearing subcutaneously implanted human xenografts of the cell line HNX-OE (size 30-600 mg) were used. Female mice (Athymic nu/nu, 19-32 g, Harlan CPB) were 10-14 weeks old at the time of the experiments. In the first experiment mice were injected in the retroorbital plexus with cMAb U36 (100 µg MAb) labeled with either ^{89}Zr (0.37 MBq) or ^{88}Y (0.13 MBq). In the second experiment either ^{124}I (0.53 MBq) or ^{131}I (0.74 MBq) were administered, and in the third experiment either ^{186}Re (1.85 MBq) or ^{89}Zr (0.37 MBq). In the fourth experiment mice were injected with either ^{131}I (0.74 MBq) or ^{186}Re (1.85 MBq). When the same radionuclide was used in two different experiments, one of the experiments was used as representative. Four mice per group were used with a total of 6 to 8 tumors. At 24, 48, and 72 h after injection, mice were anaesthetized, bled, killed, and dissected. After weighing, the amount of radioactivity in organs and blood was measured in a γ-counter. Radioactivity uptake was calculated as the percentage of the injected dose per gram of tissue (%ID/g).

Differences in tissue uptake between the different groups were statistically analyzed with one-way ANOVA with a Bonferroni post-test correction using SPSS 10.0 (SPSS Inc.). Differences were considered to be significant for $P < 0.05$. All animal experiments were performed according to the principles of laboratory animal care (NIH publication 85-23, revised 1985) and the Dutch national law "Wet op de Dierproeven" (Stb 1985, 336).

RESULTS

In Figure 2 biodistributions of cMAb U36 labeled with the diagnostic positron emitters ^{89}Zr and ^{124}I and the therapeutic radionuclides ^{88}Y, ^{131}I, and ^{186}Re are summarized. Blood values and values in heart and lung were similar for all radioimmunoconjugates at the time points examined (Fig. 2A, C, and D). The radioactivity levels in tumor, liver and (to a lesser degree) spleen was significant higher for ^{89}Zr and ^{88}Y as compared to ^{124}I, ^{131}I, and ^{186}Re (Fig. 2B, E, and G). Also the amount of radioactivity in the kidney was significantly higher for ^{89}Zr as compared to ^{124}I, ^{131}I and ^{186}Re, while ^{88}Y values were in between (Fig. 2F). At 72 h, the sternum value for ^{89}Zr was elevated (Fig. 2H). Radioactivity levels in all the other organs examined were similar for all conjugates, ranging at 72 h between 1.1-1.3 %ID/g (muscle), 3.8-4.2 %ID/g (bladder), 3.1-3.5 %ID/g (tongue), 1.1-2.5 %ID/g (thigh bone), 1.2-1.7 %ID/g (colon), 1.1-1.6 %ID/g (ileum) and 1.4-1.7 %ID/g (stomach) (data not shown).

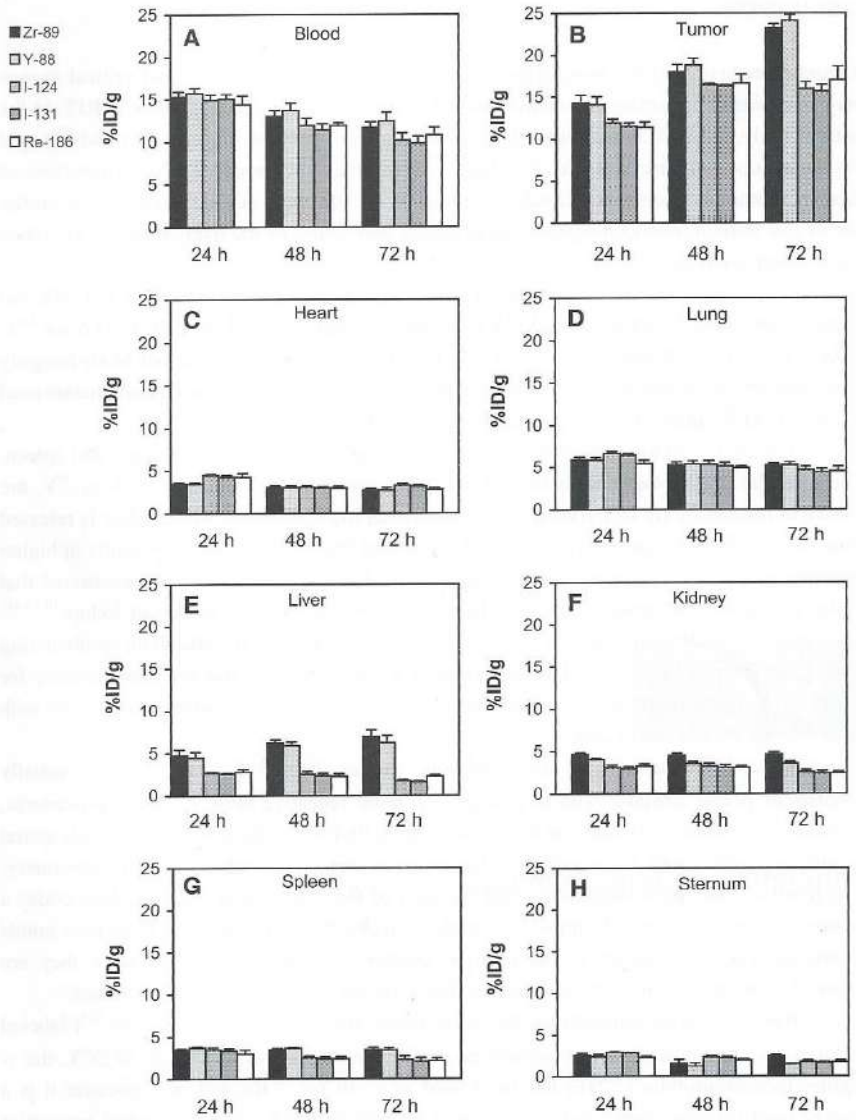

Figure 2. Biodistributions of cMAb U36 labeled with ^{89}Zr (black), ^{88}Y (light gray), ^{124}I (gray), ^{131}I (dark gray) or ^{186}Re (white) in mice (n = 4) with HNX-OE xenografts at 24, 48, and 72 h after injection. At the indicated time points after injection the mice were bled, dissected, and the radioactivity levels (%ID/g ± SEM) of blood (A), tumor (B), heart (C), lung (D), liver (E), kidney (F), spleen (G), and sternum (H) were assessed.

DISCUSSION

Accurate prediction of the biodistribution and radiation doses to tumor and critical organs may be achieved by performing an immuno-PET scouting procedure as prelude to RIT. In the present study, cMAb U36 was labeled with the long-lived positron emitters ^{89}Zr and ^{124}I, and the therapeutic radionuclides ^{88}Y, ^{131}I, and ^{186}Re in order to compare the biodistributions of these radioimmunoconjugates. Uptake levels in blood and most normal tissues were similar for all five radioimmunoconjugates. Tumor values and values of the liver, spleen, and kidney were significant higher for ^{89}Zr and ^{88}Y.

Blood clearance appeared similar for all five conjugates, despite the fact that different chelates were used for labeling the MAb with radionuclides (desferal for ^{89}Zr, DOTA for ^{88}Y, MAG3 for ^{186}Re, and none for ^{124}I and ^{131}I, Fig. 1). These data indicate that MAb integrity remained preserved during each of these labeling procedures and that the type of chelate used did not affect the pharmacokinetic behavior of the MAb.

The most striking differences were observed in the tumor, liver, kidney, and spleen. These results can be explained when taking into account that radiometals, such as ^{90}Y, are known to residualize (to be trapped) within a cell after internalization, while iodine is released from the cell [10,11]. Previous *in vivo* studies have shown that this phenomenon results in higher retention of ^{88}Y/^{90}Y in tumors, liver, kidney, and spleen [12,13]. It has been demonstrated that ^{186}Re, although a radiometal, exhibits a biodistribution more similar to that of iodine [10,14-16]. The similar biodistribution of ^{89}Zr to ^{88}Y suggests that these radiometals share residualizing properties. Even a better fit might be obtained when using one and the same chelate for coupling of both radionuclides to MAbs. Studies in this direction are currently performed with DOTA being the chelate of choice.

Scouting procedures for the therapeutic radionuclides ^{131}I, ^{186}Re, and ^{90}Y usually consists of planar imaging with a γ-camera or more recently, SPECT. These procedures, however, have intrinsic limitations for quantification. PET offers the advantage of high spatial resolution together with the possibility of attenuation correction enabling accurate dosimetry. The results of this pilot study show that for each of these three therapeutic radionuclides a positron emitter exists which shows similar pharmacokinetic behavior at the three time points examined. The combination of the positron emitter ^{124}I with ^{131}I is ideal since they are alternative isotopes of the same element, enabling the use of the same labeling method.

Based on the biodistribution data of this study, also further investigation of ^{124}I-labeled MAb as scouting procedure in combination with ^{186}Re seems worthwhile. In SPECT, the γ-emitter technetium-99m (^{99m}Tc) has been used as scout for ^{186}Re, not only because it is a widely used imaging agent, but also because Re and Tc have similar chemical properties enabling the use of the same chelator. Disadvantage of ^{99m}Tc, besides the limitations for quantification of γ-energies, is the lack of accurate prediction of dosimetry caused by its short half-life of 6.02 h [17,18]. Additional experiments with ^{124}I and ^{186}Re, evaluating their biodistributions at later time points, should determine the applicability of this combination.

Besides similar pharmacokinetics, the diagnostic and therapeutic radionuclide should exhibit a similar physical half-life. This requirement ensures that potentially important pharmacokinetic data at later time points will not be missed. Several positron emitters have been suggested to act as imaging predictor for therapeutic radioimmunoconjugates, including bromine-76 (^{76}Br; half-life, 16.2 h), copper-64 (^{64}Cu; half-life, 12.7 h), gallium-66 (^{66}Ga; half-life, 9.5 h), ^{86}Y (half-life, 14.7 h), ^{124}I (half-life, 4.18 d), and ^{89}Zr (half-life, 3.27 d) [19-24]. Due to the fact that therapeutic radionuclides generally have a half-life of several days (^{90}Y, 2.67 d; ^{131}I, 8.06 d; ^{186}Re, 3.78 d), only two positron emitters qualify: ^{124}I and ^{89}Zr (half-life, 4.18 d and 3.27 d, respectively).

CONCLUSION

In this preliminary study, the biodistributions of the positron emitters ^{124}I and ^{89}Zr have been compared with the biodistributions of the therapeutic radionuclides ^{88}Y (substituting ^{90}Y), ^{131}I, and ^{186}Re. The results described herein justify further investigation of ^{89}Zr as scouting match for ^{90}Y, and ^{124}I as match for ^{131}I or ^{186}Re.

ACKNOWLEDGMENTS

The authors thank the staff of the BV Cyclotron (VU University) for performing the irradiations, Jan H. Rector (Solid State Physics, VU University) for sputtering ^{89}Y on copper supports, and Fred L. Buijs (Radionuclide Center, VU University) for the PET analyses.

REFERENCES

1. DeNardo SJ, Kroger LA, DeNardo, GL. A new era for radiolabeled antibodies in cancer? *Curr Opin Immunol.* 1999;11:563-569.
2. DeNardo GL, Juweid ME, White CA, Wiseman GA, DeNardo SJ. Role of radiation dosimetry in radioimmunotherapy planning and treatment dosing. *Crit Rev Oncol Hematol.* 2001;39:203-218.
3. Schrijvers AHGJ, Quak JJ, Uyterlinde AM, et al. MAb U36, a novel monoclonal antibody successful in immunotargeting of squamous cell carcinoma of the head and neck. *Cancer Res.* 1993;53:4383-4390.
4. Colnot DR, Quak JJ, Roos JC, et al. Phase I therapy study of ^{186}Re-labeled chimeric monoclonal antibody U36 in patients with squamous cell carcinoma of the head and neck. *J Nucl Med.* 2000;41:1999-2010.
5. Verel I, Visser GWM, Boellaard R, Stigter-van Walsum M, Snow GB, van Dongen GAMS. ^{89}Zr immuno-PET: comprehensive procedures for the production of ^{89}Zr-labeled monoclonal antibodies. *J Nucl Med.* 2003;44:1271-1281.
6. Ruegg CL, Anderson-Berg WT, Brechbiel MW, Mirzadeh S, Gansow OA, Strand M. Improved in vivo stability and tumor targeting of bismuth-labeled antibody. *Cancer Res.* 1990;50:4221-4226.
7. Visser GW, Klok RP, Klein Gebbinck JW, ter Linden T, van Dongen GA, Molthoff CF. Optimal quality ^{131}I-monoclonal antibodies on high-dose labeling in a large reaction volume and temporarily coating the antibody with IODO-GEN. *J Nucl Med.* 2001;42:509-519.
8. Visser GWM, Gerretsen M, Herscheid JDM, Snow GB, van Dongen GAMS. Labeling of monoclonal antibodies with ^{186}Re using the MAG3 chelate for radioimmunotherapy of cancer: a technical protocol. *J Nucl Med.* 1993;34:1953-1963.
9. Lindmo T, Boven E, Luttita F, Fedorko J, Bunn PA Jr. Determination of the immunoreactive fraction of radiolabeled monoclonal antibodies by linear extrapolation to binding at infinite antigen excess. *J Immunol Methods.* 1984;72:77-78.
10. Shih LB, Thorpe SR, Griffiths GL, et al. The processing and fate of antibodies and their radiolabels bound to the surface of tumor cells in vitro: a comparison of nine radiolabels. *J Nucl Med.* 1994;35:899-908.
11. Press OW, Shan D, Howell-Clark J, et al. Comparative metabolism and retention of iodine-125, yttrium-90, and indium-111 radioimmunoconjugates by cancer cells. *Cancer Res.* 1996;56:2123-2129.
12. Sharkey RM, Motta-Hennessy C, Pawlyk D, Siegel JA, Goldenberg DM. Biodistribution and radiation dose estimates for yttrium- and iodine-labeled monoclonal antibody IgG and fragments in nude mice bearing human colonic tumor xenografts. *Cancer Res.* 1990;50:2330-2336.
13. Behr TM, Béhé M, Löhn M, et al. Therapeutic advantages of Auger electron- over β-emitting radiometals or radioiodine when conjugated to internalizing antibodies. *Eur J Nucl Med.* 2000;27:753-765.
14. Van Gog FB, Visser GWM, Klok R, van der Schors R, Snow GB, van Dongen GAMS. Monoclonal antibodies labeled with rhenium-186 using the MAG3 chelate: Relationship between the number of chelate groups and biodistribution characteristics. *J Nucl Med.* 1996;37:352-362.

15. Steffens MG, Kranenborg MH, Boerman OC, et al. Tumor retention of ^{186}Re-MAG3, ^{111}In-DTPA and ^{125}I-labeled monoclonal antibody G250 in nude mice with renal cell carcinoma xenografts. *Cancer Biother Radiopharm.* 1998;13:133-139.
16. Kievit E, van Gog FB, Schluper HM, van Dongen GAMS, Pinedo HM, Boven E. Comparison of the biodistribution and the efficacy of monoclonal antibody 323/A3 labeled with either ^{131}I or ^{186}Re in human ovarian cancer xenografts. *Int J Radiat Oncol Phys.* 1997;38:813-823.
17. Breitz HB, Fisher DR, Weiden PL, et al. Dosimetry of rhenium-186-labeled monoclonal antibodies: methods, prediction from technetium-99m-labeled antibodies and results of phase I trials. *J Nucl Med.* 1993;34:908-917.
18. Colnot DR, Wilhelm AJ, Cloos J, et al. Evaluation of limited blood sampling in a preceding ^{99m}Tc-labeled diagnostic study to predict the pharmacokinetics and myelotoxicity of ^{186}Re-cMAb U36 radioimmunotherapy. *J Nucl Med.* 2001;42:1364-1367.
19. Lövqvist A, Sundin A, Ahlström H, Carlsson J, Lundqvist H. Pharmacokinetics and experimental PET imaging of a bromine-76-labeled monoclonal anti-CEA antibody. *J Nucl Med.* 1997;38:395-401.
20. Wu AM, Yazaki PJ, Tsai S, et al. High-resolution microPET imaging of carcino-embryonic antigen-positive xenografts by using a copper-64-labeled engineered antibody fragment. *Proc Natl Acad Sci USA.* 2000;97:8495-8500.
21. Graham MC, Pentlow KS. An investigation of the physical characteristics of ^{66}Ga as an isotope for PET imaging and quantification. *Med Phys.* 1997;24:317-326.
22. Lövqvist A, Humm JL, Sheikh A, et al. PET imaging of ^{86}Y-labeled anti-Lewis Y monoclonal antibodies in a nude mouse model: comparison between ^{86}Y and ^{111}In radiolabels. *J Nucl Med.* 2001;42:1281-1287.
23. Lambrecht RM, Woodhouse N, Phillips R, et al. Investigational study of iodine-124 with a positron camera. *Am J Physiol Imaging.* 1988;3:197-200.
24. Dejesus OT, Nickles RJ. Production and purification of ^{89}Zr, a potential PET antibody label. *Appl Radiat Isot.* 1990;41:789-790.

chapter

7

Summary and conclusions

SUMMARY AND CONCLUSIONS

Tumor targeting with radiolabeled monoclonal antibodies (MAbs) has shown considerable potential for diagnosis and treatment of cancer. Nowadays, several US Food and Drug Administration (FDA) approved diagnostic radiolabeled MAbs are in use, many radioimmunoconjugates for therapeutic purposes are in advanced clinical trials and recently one therapeutic radiolabeled MAb, Zevalin, was FDA approved (**Chapter 1**). Ongoing developments in the field of MAb modification, increased understanding of tumor physiology, and the identification of promising novel tumor targets, together with the expansion of available radionuclides and advances in radiolabeling chemistry, are all expected to contribute to the successful application of radiolabeled MAbs.

While in the last two decades radiolabeled MAbs have been administered to thousands of patients with various types of tumors, the application of MAbs for detection and treatment of head and neck cancer started relatively late. One of the main reasons for this slow progress has been the lack of MAbs with high specificity for head and neck cancer and a restricted reaction on normal tissues. Just recently, murine MAb (mMAb) U36 and mMAb BIWA 1 were selected at our department as MAb candidates with high potential for detection and treatment of squamous cell carcinoma of the head and neck (HNSCC), which comprises more than 90% of the head and neck tumors. These mMAbs bind to overlapping epitopes in the variable domain v6 of the cell-surface antigen CD44. Radioimmunoscintigraphy (RIS) with these intact mMAbs after labeling with technetium-99m (^{99m}Tc) was found to be as valuable as the conventional imaging techniques X-ray computed tomography (CT) and magnetic resonance imaging (MRI), but the detection of tumor deposits smaller than 1 cm appeared to be a problem [1,2]. Subsequently, chimeric MAb (cMAb) U36 was constructed and tested in clinical phase I dose escalation radioimmunotherapy (RIT) trials. Although not the primary aim in phase I studies, promising anti-tumor effects were observed with rhenium-186-labeled (^{186}Re-labeled) cMAb U36 in inoperable HNSCC patients [3,4]. Variability was observed for ^{186}Re-cMAb U36 pharmacokinetics and tumor absorbed doses for patients treated at the same radioactivity dose level, indicating that individualization of therapy might be desirable. For all three MAbs (mMAb U36, cMAb U36 and mMAb BIWA 1) human anti-mouse or human anti-chimeric antibody responses (HAMA and HACA, respectively) were observed.

The present thesis was aiming the further improvement of RIS and RIT with anti-CD44v6 MAbs by engineering of anti-CD44v6 MAbs as well as by introduction of immuno-positron emission tomography (immuno-PET). Introduction of PET might further improve tumor detection with MAbs because of its high spatial and temporal resolution, and sensitivity. Besides that, imaging of radiolabeled MAb can provide essential information on biodistribution, pharmacokinetics, and dosimetry. This will enable the optimization of MAb therapy, the selection of patients who are eligible for therapy, and provide the means to individualize treatment conditions. When the patient is compared to a black box, imaging can be seen as the ray of light that is enlightening the darkness. Imaging can give insight into biological processes that are otherwise unknown to the clinician. A critical factor in the

assessment of radioactivity distribution in the patient is the availability of accurate noninvasive quantitation methods. For this purpose, immuno-PET promises to be the method of choice.

PET is based on annihilation coincidence detection. For this reason the MAb (or other bio-pharmaceutical) is radiolabeled with a positron emitter. Upon decay, this radioisotope emits, among others, a positron (a positively charged β-particle). After annihilation of the positron with an electron, converting mass into equivalent energy, two photons with an energy of 511 keV are emitted simultaneously in opposite directions. In order to determine the location of a radiation source within a patient, a PET camera is used that consists of a ring of detectors connected in coincidence with each other. After a number of corrections on the PET data, quantitative distribution data can be derived. Besides clinical PET scanners, also several dedicated small animal PET scanners have been developed. A number of positron emitters have been suggested for PET imaging purposes, but physical half-life considerations make only two positron emitters appropriate for intact MAb monitoring: zirconium-89 (^{89}Zr) and iodine-124 (^{124}I). In our research we started exploration of these long-lived positron emitters, because their half-life of 3.27 and 4.18 d, respectively, is compatible with the time needed for intact MAbs to achieve optimal tumor-to-nontumor ratios (2-4 d).

Further optimization of RIS and RIT started with modification of the anti-CD44v6 mMAb BIWA 1 (chapter 2). Two important parameters that exhibit significant influence on MAb pharmacokinetics *in vivo*, MAb form and MAb affinity, were addressed. MAbs of mouse origin are prone to induce HAMA responses, resulting in an increased clearance of the MAb with less efficient tumor targeting, allergic reactions, or even anaphylaxis. For this reason, the use of chimeric and humanized MAbs (hMAbs) is strongly recommended. The construction of the latter MAb forms, however, may result in MAbs with lower affinity and affected tumor uptake. The construction of a chimeric (BIWA 2) and two humanized derivatives (BIWA 4 and BIWA 8) of mMAb BIWA 1 is described in **chapter 2**. These MAbs were evaluated together with mMAb U36 for affinity to the antigen CD44v6 *in vitro* with the use of surface plasmon resonance and competitive cell ELISA. The MAbs bound to CD44v6 with an up to 46-fold difference in affinity (K_d ranging from 1.1×10^{-8} to 2.4×10^{-10} M) with the following ranking: mMAb U36 < hMAb BIWA 4 < hMAb BIWA 8 < cMAb BIWA 2. To evaluate their *in vivo* tumor targeting properties, HNSCC xenograft-bearing nude mice were coinjected with MAbs pairs that were labeled with either ^{131}I or ^{125}I and biodistribution studies were performed. To obtain comparable blood/body clearance of the coinjected MAbs, only MAbs with an identical murine or human isotype were combined. Each pair of MAbs was selected to provide a stepwise decrease in the difference in affinities (from 35.0-fold to 4.0-fold difference). Remarkably, for all three pairs tested, the lower-affinity MAb showed a higher degree and specificity of tumor localization. The difference in tumor localization was more pronounced when the difference in affinity was larger.

On basis of these biodistribution results, it was investigated whether these lower-affinity MAbs would be better suited for RIT. After labeling with the therapeutic radionuclide ^{186}Re, the same MAb pairs showed a more favorable RIT efficacy of the lower-affinity MAbs,

consistent with the tumor localization data of the biodistribution study. We concluded from these studies that a MAb version with intermediate affinity to a given target antigen (e.g. mMAb U36 and hMAb BIWA 4), may show superior tumor targeting in comparison with higher-affinity versions of this MAb. These results are not in line with several studies that have demonstrated improved tumor delivery and therapeutic efficacy in xenograft-bearing nude mice when using MAbs with increased affinity [5-9]. It might be that antibody affinity and tumor uptake demonstrate a bell-shaped relationship, with intermediate-affinity MAbs (e.g. mMAb U36 and hMAb BIWA 4) showing a higher degree and specificity of tumor localization than low-affinity MAbs (K_d below ± 10^{-8} M) and high-affinity MAbs (K_d beyond ± 10^{-10} M). Evidence for such a relationship was also found in *in vivo* studies with scFv and diabodies [10,11]. The less than optimal performance of high-affinity MAbs has been explained by the "binding site barrier" theory. This theory proclaimes that high-affinity MAbs will only bind to the periphery of the tumor, thereby impairing tumor penetration and absolute tumor retention [12].

After the animal studies as described in chapter 2, the intermediate-affinity hMAb BIWA 4 was selected for further clinical evaluation and administered to 48 patients in three parallel RIS/biodistribution studies with HNSCC-, non-small-cell lung cancer-, and breast cancer patients, and in one RIT study with HNSCC patients [13,14]. The overall HAHA response rate with hMAb BIWA 4 appeared 4%, which is significantly lower than the 90% HAMA response rate as observed with the parental mMAb BIWA 1. Furthermore, the phase I RIT trial revealed that ^{186}Re-labeled hMAb BIWA 4 can safely be administered to patients, also in repeated way. Anti-tumor effects were seen in incurable HNSCC patients with bulky disease, which justifies further development of RIT with ^{186}Re-labeled hMAb BIWA 4.

In general, selection, characterization, and optimization of a MAb or MAb construct for RIS and RIT purposes consists of consecutive studies *in vitro*, *in vivo* in animal models, and in patients. The studies as described above illustrates again that careful examination of MAb properties, important for selective tumor targeting, is required for each new MAb or MAb construct. In animal studies, for example biodistribution can be assessed accurately by taking tissue biopsies and measuring radioactivity in these biopsies by use of a γ-counter. Ultimately, clinical studies are needed to confirm the results from *in vivo* animal studies in a noninvasive way. For optimal application of tumor-targeting MAbs in RIS and RIT, it was decided to explore the potential of immuno-PET.

The suitability of a positron emitter for immuno-PET is determined by several factors. Not only a half-life of several days is important, but also availability of the positron emitter and a robust method for its stable coupling to MAbs. The decay properties of the positron emitter are an important factor for obtaining high quality images and accurate quantitative data. When a positron emitter is used in an immuno-PET scouting procedure as a prelude to RIT, the biodistribution of the diagnostic and the therapeutic radioimmunoconjugate should be similar. In the following chapters, several of these considerations were addressed for the positron emitters ^{89}Zr and ^{124}I. In these studies cMAb U36 was used as a model MAb for reasons of availability.

In **chapter 3**, technical protocols for reproducible isolation of highly pure ^{89}Zr and the production of optimal-quality ^{89}Zr-MAb conjugates are provided. Large batches of ^{89}Zr were produced by a (p,n) reaction by bombarding a ^{89}Y-target, an element with a natural abundance of 100%, with 14-MeV protons. After isolation with a hydroxamate column, carrier-free ^{89}Zr with a high radionuclidic purity and high yield was obtained. The use of low-cost target material and the possibility to use a low-energy cyclotron ensures that the procedure can be readily made available, while the high specific activity of the positron emitter facilitates labeling procedures.

For stable coupling of ^{89}Zr to MAbs a new route had to be developed using a novel bifunctional derivative of the chelate desferrioxamine B (Df) and new linker chemistry. To this end, Df was initially succinylated (*N*-sucDf), temporarily filled with Fe(III), esterified by use of tetrafluorophenol, and coupled to MAb. Thus premodified MAb was labeled with ^{89}Zr via a simple postlabeling procedure, resulting in radioimmunoconjugates with preserved integrity and immunoreactivity. The *in vitro* stability of MAb-*N*-sucDf-^{89}Zr was assessed in human serum and its *in vivo* behavior was evaluated by biodistribution and PET imaging studies in HNSCC xenograft-bearing nude mice. For PET imaging a small animal high resolution research tomograph (HRRT) PET scanner was used. These studies demonstrated selective HNSCC targeting with ^{89}Zr-labeled cMAb U36 and visualization of small tumors in the range of 19-154 mg on PET images.

In **chapter 4**, the suitability of ^{89}Zr for immuno-PET was further examined. The applicability of ^{89}Zr-labeled MAb as scouting procedure for ^{90}Y-MAb RIT was studied and the quantitative image performance of ^{89}Zr was evaluated. For this purpose, cMAb U36-*N*-sucDf-^{89}Zr and cMAb U36-*p*-SCN-Bz-DOTA-^{88}Y (as substitute for ^{90}Y) were coinjected into HNSCC xenograft-bearing nude mice and biodistribution was determined up to six days after injection. The radioimmunoconjugates showed similar uptake in tumor, blood, and other organs, except for sternum and thigh bone at later time points. Small differences were found in kidney and liver.

Quantitative image performance of ^{89}Zr was assessed in phantom studies and compared with ^{18}F, the most commonly applied PET isotope in the clinic. Several phantoms were used to determine that ^{89}Zr linearity, resolution, and recovery coefficients approximated that of ^{18}F. In addition, the potential of PET to quantify ^{89}Zr-labeled MAb was evaluated in tumor-bearing nude mice by relating image-derived tumor uptake data (noninvasive method) to ^{89}Zr data derived from excised tumors (invasive method). Millimeter-sized tumors could be visualized with ^{89}Zr immuno-PET and, after correction for partial-volume effects, an excellent correlation was found between image-derived ^{89}Zr tumor radioactivity and γ-counter ^{89}Zr values of excised tumors.

The encouraging results with ^{89}Zr immuno-PET, as presented in **chapter 3** and **4**, opened perspectives for clinical evaluation. Currently, PET with ^{89}Zr-labeled cMAb U36 is being evaluated in a pilot study for its capacity to detect primary tumors and metastases in operable HNSCC patients. In a clinical setting, an additional very important aspect is the radioactivity dose to be administered, as the radiation exposure of the patient is expected to be a limiting

factor. In the animal studies, 3.7 MBq per mouse was administered after which tumors could be visualized in challenging circumstances, that is small tumors in a region with low object-to-background ratio. This injected amount of radioactivity was based on the few articles published concerning PET imaging of mice with positron emitter-labeled MAbs. In these studies clinical PET scanners were used, while the radioactivity injected per mouse ranged from 111 kBq (^{124}I) [15] to 3.7 MBq (^{86}Y, ^{124}I) [16,17]. Since the HRRT camera has a relatively low sensitivity compared to clinically used PET scanners [18], we chose to inject 3.7 MBq per animal. Animal PET studies with lower doses and/or shorter scanning times are planned in the near future. In the preliminary clinical study, tumor deposits were visualized after administration of 74 MBq ^{89}Zr (Fig. 1). This administered dose was selected taking the residence time of cMAb U36 into account. The radiation burden to the patient was estimated to be ± 60 mSv. Guided by the recommendations of the International Commission on Radiological Protection (ICRP Publication 62), such exposure is considered to be acceptable for a diagnostic procedure for this group of patients. The evaluation of the quantitative imaging performance of ^{89}Zr-labeled cMAb U36 in this clinical setting is ongoing. It is of note that corrections for partial volume effects is not common practice in clinical studies, but has been recognized by PET practitioners to be an important factor in improving diagnostic accuracy (position paper EORTC workshop) [19].

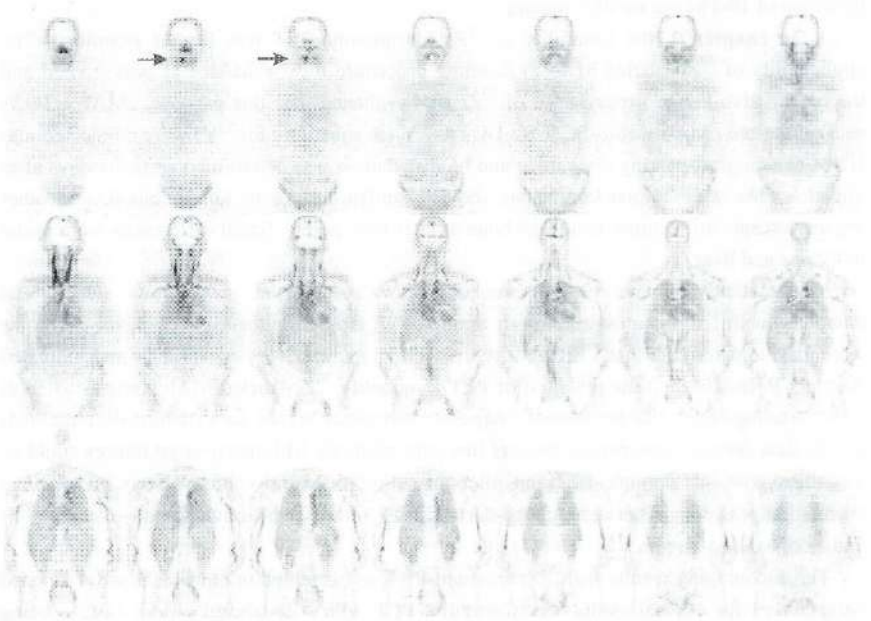

Figure 1. ECAT EXACT HR$^+$ PET coronal images of a head and neck cancer patient (T2N0) 24 h after injection of cMAb U36-*N*-sucDf-^{89}Zr. Increased uptake is seen in the primary tumor at the right side of the tongue (arrow). Note the high blood-pool activity at this early time point.

Chapter 5 is focused on the radiolabeling of MAbs with the long-lived positron emitter ^{124}I. Although radiolabeling with radioiodine isotopes has been a widespread practice for decades, in the past labeling yields with ^{124}I were often lower when directly compared with other iodine isotopes and the quality of the resulting ^{124}I-conjugates did not always meet the quality standards of today. In this study, it was first ascertained that the labeling yield problems were not related to an intrinsic atom characteristic of ^{124}I, but only to radiation induced deterioration of the starting ^{124}I-solution. Labeling of cMAb U36 with a mixture of radioiodide isotopes (^{123}I, ^{124}I, ^{126}I, and ^{130}I) resulted in exactly the same labeling yields for each isotope, excluding a different chemical reactivity of ^{124}I-iodide. Severe deterioration of the ^{124}I-solution at the user site was demonstrated by HPLC analysis and shown to be responsible for the low labeling yields. Subsequently, in this study two regeneration methods were introduced to regain ^{124}I in the iodide form and MAbs were radiolabeled with regenerated ^{124}I. The use of regenerated ^{124}I strongly improved labeling yields, making efficient labeling of MAbs with ^{124}I as straightforward as with ^{131}I. Radiolabeling of cMAb U36 with ^{124}I at patient dose level under conditions that minimize chemical and radiation damage resulted in a radioimmunoconjugate with preserved integrity, immunoreactivity, as well as optimal *in vivo* tumor targeting. The latter was demonstrated with the aid of biodistribution and PET imaging studies in tumor-bearing nude mice. Tumor uptake values of ^{124}I-labeled cMAb were fully concordant with ^{131}I-labeled cMAb U36 and all tumors were visualized with PET.

For the long-lived positron emitter ^{124}I to be applicable for immuno-PET, several factors have to be taken into account. The important first requirement, a reliable radiolabeling procedure that results in radioimmunoconjugates with preserved integrity and immunoreactivity, is provided in **chapter 5**. Other requirements are available production methods and adequate quantitative image qualities. At the moment, production of ^{124}I is too expensive to allow routine clinical application due to high target material and cyclotron costs. For the experiments as described above, ^{124}I was produced in the USA at one of the few sites that is able to supply this radionuclide. Especially, long distance transportation requires methods to counteract radiation induced deterioration of the radioactivity stock solution. Although ^{124}I has a complex decay scheme with relative high energy positrons and prompt single γ-photons, quantitative PET imaging studies have been performed[20-25]. However, additional phantom and animal studies with the small animal HRRT PET scanner need to be performed to determine the quantitative image performance of ^{124}I. An attractive application of ^{124}I immuno-PET is as scouting procedure before ^{131}I-RIT. Whether ^{124}I-labeled MAbs can also fulfil this function for other therapeutic RIT conjugates depends on similarity in biodistribution of the scouting and therapeutic radioimmunoconjugate.

In **chapter 6**, the *in vivo* characteristics of ^{89}Zr-labeled and ^{124}I-labeled MAbs were assessed and compared with MAbs labeled with the therapeutic radionuclides ^{88}Y (as substitute for ^{90}Y), ^{131}I, and ^{186}Re. For this purpose cMAb U36 was radiolabeled with these five radionuclides and the biodistribution of the radioimmunoconjugates was determined in tumor-bearing nude mice. The blood clearance appeared similar for all five conjugates,

despite the fact that different radiolabeling methods were used (direct labeling or indirect labeling with different chelates). This confirms that MAb integrity was preserved and that e.g. the type of chelate did not significantly affect the behavior of the MAb in blood.

Two patterns of biodistribution were observed, one pattern matching for ^{89}Zr- and ^{88}YcMAb U36 and one pattern for ^{124}I-, ^{131}I-, and ^{186}Re-cMAb U36. The most remarkable differences between both patterns were observed for uptake in tumor and liver. In preliminary *in vitro* internalization studies (performed essentially as described by Vrouenraets *et al.* [26]) ^{89}Zr-labeled cMAb U36 exhibited significantly higher total cellular uptake by the HNSCC cell line OE compared to ^{131}I-labeled cMAb U36 (82.2% *vs.* 28.7% after 24 h, respectively). The fact that the biodistribution of ^{89}Zr-labeled MAb is similar to that of ^{88}Y-labeled MAb confirms the residualizing properties of ^{89}Zr, the same as previously described for radiometals such as ^{88}Y, ^{90}Y, and ^{111}In.

In regard to this, the term "residualizing radionuclide", as is commonly used in literature, needs to be used with care. Since it has been reported that ^{111}In and ^{90}Y are retained in cells as low molecular weight catabolites (consisting of the radionuclide and the chelate with probably a peptide residue of the MAb) [27,28], the chemical characteristics of the chelate need to be taken into account as well as the radionuclide used. Illustrative in this respect is the radiolabeling of MAbs with iodine radioisotopes. When directly coupled to MAb, iodine leaves the cell rapidly as iodotyrosine, while indirect iodination of MAb can result in residualization of the radionuclide in the cell. In addition, the linker chemistry as well as the vehicle used can play a role in the retention of the radionuclide in the cell upon internalization.

In conclusion, the long-lived positron emitters ^{89}Zr and ^{124}I hold promise for future application of immuno-PET in the clinic. The difference in individual chemical and *in vivo* characteristics of ^{89}Zr and ^{124}I makes them suitable for a variety of applications. Besides radiolabeling of MAbs, ^{89}Zr and ^{124}I can also be used for labeling peptides and other (bio)pharmaceuticals. Radiolabeling of (bio)pharmaceuticals with positron emitters will enable for instance detection of disease, elucidation of molecular interactions, assessment of pharmacokinetics and biodistribution of the pharmaceutical, and optimization of drug scheduling. ^{124}I has already been used to radiolabel peptides such as insuline [29,30] and annexin V [31]. Another novel application of ^{124}I has been in monitoring a clinical gene therapy trial [32]. PET was used with a ^{124}I-labeled marker substrate to identify location, magnitude, and extent of gene expression. Whether ^{89}Zr is equally suitable for the radiolabeling of small biomolecules, however, remains to be evaluated. The coupling of a radionuclide-chelate complex contributes greatly to the overall size and charge of a small pharmaceutical, possibly influencing pharmacological, biological, and biochemical properties of the molecule.

REFERENCES

1. de Bree R, Roos JC, Quak JJ, den Hollander W, Snow GB, van Dongen GAMS. Radioimmunoscintigraphy and biodistribution of technetium-99m-labeled monoclonal antibody U36 in patients with head and neck cancer. *Clin Cancer Res.* 1995;1:591-598.
2. Stroomer JW, Roos JC, Sproll M, Quak JJ, Heider KH, Wilhelm BJ, Castelijns JA, Meyer R, Kwakkelstein MO, Snow GB, Adolf GR, van Dongen GAMS. Safety and biodistribution of ^{99m}Technetium-labeled anti-CD44v6 monoclonal antibody BIWA 1 in head and neck cancer patients. *Clin Cancer Res.* 2000;6:3046-3055.
3. Colnot DR, Quak JJ, Roos JC, van Lingen A, Wilhelm AJ, van Kamp GJ, Huijgens PC, Snow GB, van Dongen GAMS. Phase I therapy study of ^{186}Re-labeled chimeric monoclonal antibody U36 in patients with squamous cell carcinoma of the head and neck. *J Nucl Med.* 2000;41:1999-2010.
4. Colnot DR, Ossenkoppele GJ, Roos JC, Quak JJ, de Bree R, Börjesson PK, Huijgens PC, Snow GB, van Dongen GAMS. Reinfusion of unprocessed, granulocyte colony-stimulating factor-stimulated whole blood allows dose escalation of ^{186}Re-labeled chimeric monoclonal antibody U36 radioimmunotherapy in a phase I dose escalation study. *Clin Cancer Res.* 2002;8:3401-3406.
5. Colcher D, Minelli MF, Roselli M, Muraro R, Simpson-Milenic D, Schlom J. Radioimmunolocalization of human carcinoma xenografts with B72.3 second generation monoclonal antibodies. *Cancer Res.* 1988;48:4597-4603.
6. Schlom J, Eggensperger D, Colcher D, Molinolo A, Houchens D, Miller LS, Hinkle G, Siler K. Therapeutic advantage of high-affinity anticarcinoma radioimmunoconjugates. *Cancer Res.* 1992;52:1067-1072.
7. Velders MP, Van Rhijn CM, Briaire IH, Fleuren GJ, Warnaar SO, Litvinov SV. Immunotherapy with low and high affinity monoclonal antibodies 17-1A and 323/A3 in a nude mouse xenograft carcinoma model. *Cancer Res.* 1995;55:4398-4403.
8. Kievit E, Pinedo HM, Schlüper HMM, Haisma HJ, Boven E. Comparison of the monoclonal antibodies 17-1A and 323/A3: the influence of the affinity on tumour uptake and efficacy of radioimmunotherapy in human ovarian cancer xenografts. *Br J Cancer.* 1996;73:457-464.
9. Adams GP, Schier R, Marshall K, Wolf EJ, McCall AM, Marks JD, Weiner LM. Increased affinity leads to improved selective tumor delivery of single-chain Fv antibodies. *Cancer Res.* 1998;58:485-490.
10. Adams GP, Schier R, McCall AM, Simmons HH, Horak EM, Alpaugh RK, Marks JD, Weiner LM. High affinity restricts the localization and tumor penetration of single-chain Fv antibody molecules. *Cancer Res.* 2001;61:4750-4755.
11. Nielsen UB, Adams GP, Weiner LM, Marks JD. Targeting of bivalent anti-ErbB2 diabody antibody fragments to tumor cells is independent of the intrinsic antibody affinity. *Cancer Res.* 2000;60:6434-6440.
12. Fujimori K, Covell DG, Fletcher JE, Weinstein JN. A modeling analysis of monoclonal antibody percolation through tumors: a binding-site barrier. *J Nucl Med.* 1990;31:1191-1198.
13. Colnot DR, Roos JC, De Bree R, Wilhelm AJ, Kummer JA, Hanft G, Heider KH, Stehle G, Snow GB, Van Dongen GAMS. Safety, biodistribution, pharmacokinetics, and immunogenicity of ^{99m}Tc-labeled humanized monoclonal antibody BIWA 4 (bivatuzumab) in patients with squamous cell carcinoma of the head and neck. *Cancer Immunol Immunother.* 2003;in press.

14. Börjesson PKE, Postema EJ, Roos JC, Colnot DR, Marres HAM, Van Schie MH, Stehle G, De Bree R, Snow GB, Van Dongen GAMS. Phase I therapy with ^{186}Re-labeled humanized monoclonal antibody BIWA 4 (bivatuzumab) in patients with head and neck squamous cell carcinoma. *Clin Cancer Res.* 2003;9:3961S-3972S.
15. Lee FT, Hall C, Rigopoulos A, Zweit J, Pathmaraj K, O'Keefe GJ, Smyth FE, Welt S, Old LJ, Scott AM. Immuno-PET of human colon xenograft-bearing BALB/c nude mice using ^{124}I-CDR-grafted humanized A33 monoclonal antibody. *J Nucl Med.* 2001;42:764-769.
16. Lövqvist A, Humm JL, Sheikh A, Finn RD, Koziorowski J, Ruan S, Pentlow KS, Jungbluth A, Welt S, Lee FT, Brechbiel MW, Larson SM. PET imaging of ^{86}Y-labeled anti-Lewis Y monoclonal antibodies in a nude mouse model: comparison between ^{86}Y and ^{111}In radiolabels. *J Nucl Med.* 2001;42:1281-1287.
17. Bakir MA, Eccles SA, Babich JW, Aftab N, Styles JM, Dean CJ, Lambrecht RM, Ott RJ. C-erbB2 Protein overexpression in breast cancer as a target for PET using iodine-124-labeled monoclonal antibodies. *J Nucl Med.* 1992;33: 2154-2160.
18. Boellaard R, Buijs F, de Jong HWAM, Lenox M, Gremillion T, Lammertsma AA. Characterization of a single LSO crystal layer high resolution research tomograph. *Phys Med Biol.* 2003;48:429-448.
19. Young H, Baum R, Cremerius U, Herholz K, Hoekstra O, Lammertsma AA, Pruim J, Price P. Measurement of clinical and subclinical tumour response using [^{18}F]-fluorodeoxyglucose and positron emission tomography: review and 1999 EORTC recommendations. *Eur J Cancer.* 1999;35:1773-1782.
20. Pentlow KS and Graham MC. Quantitative imaging of I-124 using positron emission tomography with applications to radioimmunodiagnosis and radioimmunotherapy. *Med Phys.* 1991;18:357-366.
21. Wilson CB, Snook DE, Dhokia B, Taylor IA, Lammertsma AA, Lambrecht R, Waxman J, Jones T, Epenetos AA. Quantitative measurement of monoclonal antibody distribution and blood flow using positron emission tomography and ^{124}Iodine in patients with breast cancer. *Int J Cancer* 1991;47:344-347.
22. Larson SM, Pentlow KS, Volkow ND, Wolf AP, Finn RD, Lambrecht RM, Graham MC, Di Resta G, Bendriem B, Daghighian F, Yeh SDJ, Wang G-J, KCheung N-KV. PET scanning of iodine-124-3F8 as an approach to tumor dosimetry during treatmnet planning for radioimmunotherapy in a child with neuroblastoma. *J Nucl Med.* 1992;33:2020-2023.
23. Herzog H, Tellmann L, Qaim SM, Spellerberg S, Schmid A, Coenen HH. PET quantitation and imaging of the non-pure positron-emitting iodine isotope ^{124}I. *Appl Radiat Isot.* 2002;56:673-679.
24. Collingridge DR, Carroll VA, Glaser M, Aboagye EO, Osman S, Hutchinson OC, Barthel H, Luthra SK, Brady F, Bicknell R, Price P, Harris AL. The development of [^{124}I]Iodinated-VG76e: a novel tracer for imaging vascular endothelial growth factor in vivo using positron emission tomography. *Cancer Res.* 2002;62:5912-5919.
25. Jayson GC, Zweit J, Jackson A, Mulatero C, Julyan P, Ranson M, Broughton L, Wagstaff J, Hakannson L, Groenewegen G, Bailey J, Smith N, Hastings D, Lawrance J, Haroon H, Ward T, McGown AT, Tang M, Levitt D, Marreaud S, Lehmann FF, Herold M, Zwierzina H. Molecular imaging and biological evaluation of HuMV833 anti-VEGF antibody: implications for trial design of antiangiogenic antibodies. *J Natl Cancer Inst.* 2002;94:1484-1493.
26. Vrouenraets MB, Visser GWM, Loup C, Meunier B, Stigter M, Oppelaar H, Stewart FA, Snow GB, van Dongen GAMS. Targeting of a hydrophylic photosensitizer by use of internalizing monoclonal antibodies: a new possibility for use in photodynamic therapy. *Int J Cancer.* 2000;88:108-114.

27. Shih LB, Thorpe SR, Griffiths L, Diril H, Ong GL, Hansen HJ, Goldenberg DM, Mattes MJ. The processing and fate of antibodies and their radiolabels bound to the surface of tumor cells in vitro: a comparison of nine radiolabels. *J Nucl Med.* 1994;35:899-908.
28. Press OW, Shan D, Howell-Clark J, Eary J, Appelbaum FR, Matthews D, King DJ, Haines AMR, Hamann P, Hinman L, Shochat D, Bernstein ID. Comparative metabolism and retention of iodine-125, yttrium-90, and indium-111 radioimmunoconjugates by cancer cells. *Cancer Res.* 1996;56:2123-2129.
29. Glaser M, Brown DJ, Law MP, Iozzo P, Waters SL, Poole K, Knickmeier M, Camici PG, Pike VW. Preparation of no-carrier-added [^{124}I]A_{14}-iodoinsulin as a radiotracer for positron emission tomography. *J Labelled Cpd Radiopharm.* 2001;44:465-480.
30. Iozzo P, Osman S, Glaser M, Knickmeier M, Ferrannini E, Pike VW, Camici PG, MP Law. In vivo imaging of insulin receptors by PET: preclinical evaluation of iodine-125 and iodine-124 labelled human insulin. *Nucl Med Biol.* 2002;29:73-82.
31. Glaser M, Collingridge DR, Aboagye EO, Bouchier-Hayes L, Hutchinson OC, Martin SJ, Price P, Brady F, Luthra SK. Iodine-124 labelled annexin-V as a potential radiotracer to study apoptosis using positron emission tomography. *Appl Radiat Isot.* 2003;58:55-62.
32. Jacobs A, Voges J, Reszka R, Lercher M, Gossmann A, Kracht L, Kaestle Ch, Wagner R, Wienhard K, Heiss WD. Positron-emission tomography of vector-mediated gene expression in gene therapy for gliomas. *Lancet.* 2001;358:727-729.

Samenvatting en conclusies

SAMENVATTING EN CONCLUSIES

Voor de detectie en behandeling van kanker is de toepassing van tumor-selectieve monoklonale antilichamen (MAbs) gelabeld met radioisotopen, veelbelovend. Vandaag de dag zijn er een aantal door de "U.S. Food and Drug Adminstration" (FDA) goedgekeurde diagnostische radionuclide-MAb conjugaten in gebruik. Daarnaast worden er in reeds vergevorderde klinische studies diverse radioimmunoconjugaten voor therapeutische doeleinden getest, en is er recentelijk één therapeutisch conjugaat, Zevalin genaamd, door de FDA goedgekeurd (**hoofdstuk 1**). Verwacht mag worden dat de voortschrijdende ontwikkelingen op enerzijds het gebied van MAb modificatie, het toenemend begrip van tumor fysiologie en de ontdekking van veelbelovende nieuwe tumor-antigenen, en anderzijds vanwege de toegenomen beschikbaarheid van radionucliden en radiolabelingschemie, alle zullen bijdragen aan een succesvolle toepassing van radioimmunoconjugaten.

Terwijl de afgelopen twee decennia reeds aan duizenden patiënten MAbs zijn toegediend, werden MAbs pas in een relatief laat stadium aangewend voor de detectie en behandeling van hoofd-halskanker. Eén van de belangrijkste redenen voor deze trage ontwikkeling is het gebrek aan MAbs met een hoge specificiteit voor hoofd-halskanker. Hoofd-hals tumoren ontstaan in de slijmvliezen van het hoofd-halsgebied, en 90% betreft zgn. plaveiselcelcarcinoom (HHPCC). Onlangs werden op onze afdeling de muizen MAbs (mMAbs) U36 en BIWA 1 geselecteerd als veelbelovende kandidaten voor de detectie en behandeling van zulke HHPCC. Deze mMAbs binden aan overlappende epitopen in het variabele v6-domein van het op het celmembraan gelokaliseerde CD44 antigeen. Radioimmunoscintigrafie (RIS) met behulp van deze mMAbs, gelabeld met technetium-99m (^{99m}Tc), wees uit dat deze diagnostische methode even geschikt is voor tumordetectie als de conventionele beeldvormende methoden CT en MRI. Echter de detectie van tumoren met een diameter kleiner dan 1 cm bleek ook voor RIS problematisch. Nadat de chimere (muis/mens) variant van MAb U36 was geconstrueerd, werd dit cMAb U36 getest in klinische fase I dosis-escalatie radioimmunotherapie (RIT) studies. Hoewel niet de primaire doelstelling van fase I studies, werden veelbelovende anti-tumor effecten waargenomen met rhenium-186 (^{186}Re)-gelabeld cMAb U36 in inoperabele HHPCC patiënten. Uit deze studie bleek bovendien dat binnen een patiëntengroep die met dezelfde hoeveelheid activiteit werd behandeld, de farmacokinetiek en de tumor geabsorbeerde dosis van ^{186}Re-cMAb U36 tussen patiënten onderling varieerden. Dit wijst op de noodzaak van een individuele aanpak per patiënt. Bij alle drie MAbs (mMAb U36, cMAb U36 en mMAb BIWA 1) werd een hoog percentage humane anti-muis en humane anti-chimeer antilichaam reacties (HAMA eq HACA reacties) waargenomen.

Het doel van het onderzoek zoals beschreven in dit proefschrift was de verbetering van RIS en RIT met behulp van anti-CD44v6 MAbs. Dit gebeurde zowel door het maken van nieuwe MAb constructen met behulp van recombinant-DNA technieken, als door de introductie van immuno-positron emissie tomografie (immuno-PET). De introductie van immuno-PET kan, vanwege haar hoge spatiële en temporele resolutie en hoge gevoeligheid,

wellicht leiden tot een verbetering van tumor "imaging" met behulp van MAbs. Daarnaast kan detectie met behulp van radioimmunoconjugaten essentiële informatie verschaffen over distributie, farmacokinetiek en dosimetrie. Dit maakt het mogelijk om MAb therapie te optimaliseren en patiënten die geschikt zijn voor therapie te selecteren. Tevens wordt hiermee de weg naar individualisatie van behandeling geopend. Als op dit moment een medicijn aan een patiënt toegediend wordt, dan is het vrijwel onmogelijk om informatie te verkrijgen over de distributie van het medicijn door het lichaam. In die zin kan een patiënt worden vergeleken met een "black box", waarbij "imaging" de lichtstraal is die enige verlichting kan brengen in het duister. "Imaging" kan inzicht verschaffen in biologische processen waar de arts anders geen weet van heeft. Een heikel punt bij de bepaling van de distributie van radioactiviteit in de patiënt is de beschikbaarheid van non-invasieve methoden waarmee een nauwkeurige kwantificering van de radioactiviteit mogelijk wordt. Immuno-PET lijkt hiervoor bij uitstek geschikt.

PET is gebaseerd op de detectie van annihilatie coïncidentie, en daarom moet in geval van immuno-PET er aan het MAb (of ander bio-farmacon) een positron emitter gekoppeld worden. Een dergelijk radionuclide zendt tijdens zijn verval onder andere een positron (een positief geladen β-deeltje) uit. Tengevolge van de annihilatie van het positron met een elektron, waarbij hun massa wordt omgezet in een equivalente hoeveelheid energie, worden gelijktijdig twee fotonen met een energie van 511 keV in tegengestelde richting uitgezonden. Om de lokatie van het gelabelde farmacon in de patiënt te kunnen bepalen, wordt een PET camera gebruikt. Deze camera bestaat uit een ring van detectoren die in coïncidentie met elkaar zijn verbonden. Na het toepassen van verscheidene correcties op de PET data kunnen nauwkeurige, althans in theorie, kwantitatieve distributie gegevens worden verkregen. Naast klinische PET scanners zijn er ook diverse PET scanners ontwikkeld specifiek voor het scannen van kleine proefdieren. Voor PET "imaging" doeleinden komen een aantal positron emitters in aanmerking. Slechts twee positron emitters zijn echter geschikt voor het monitoren van intacte MAb moleculen: zirconium-89 (^{89}Zr) en jodium-124 (^{124}I). Ons onderzoek richtte zich op deze lang-levende positron emitters omdat hun halveringstijd van respectievelijk 3,27 en 4,18 dagen overeenstemt met de tijd die een intact MAb nodig heeft om een optimale tumor:non-tumor ratio te bereiken (2 tot 4 dagen).

Verdere optimalisatie van RIS en RIT begon met het modificeren van het anti-CD44v6 mMAb BIWA 1 (hoofdstuk 2). Hierbij werden twee belangrijke parameters die van invloed zijn op de farmacokinetiek *in vivo*, namelijk MAb vorm en affiniteit, in ogenschouw genomen. MAbs van muizen-origine kunnen HAMA reacties opwekken, waardoor het MAb sneller uit de circulatie verdwijnt en de "targeting" van tumorcellen dus minder efficiënt verloopt. Bovendien kunnen hierbij allergische reacties opgewekt worden en kan er zelfs anafylaxis optreden. Daarom wordt het gebruik van chimere en gehumaniseerde MAbs (hMAbs) ten sterkste aangeraden. Chimerisering en humanisering van MAbs kan echter tot affiniteitsverlaging leiden, en tot vermindering van de tumorophoping. De constructie van een chimere (BIWA 2) en twee gehumaniseerde varianten (BIWA 4 en BIWA 8) van mMAb BIWA 1 wordt beschreven in **hoofdstuk 2**. Van deze MAbs werd, tezamen met mMAb U36,

de affiniteit bepaald voor het antigeen CD44v6 *in vitro* met behulp van "surface plasmon resonance" en ELISA. De MAbs bonden aan CD44v6 met een tot 46-voudig verschil in affiniteit (K_d variërend tussen $1,1x10^{-8}$ en $2,4x10^{-10}$ M) met de volgende volgorde: mMAb U36 < hMAb BIWA 4 < hMAb BIWA 8 < cMAb BIWA 2. Om de "tumor targeting" eigenschappen van deze MAbs te bepalen werden HHPCC xenograft-dragende naakte muizen geïnjecteerd met mengsels van steeds twee MAbs die gelabeld waren met ^{131}I en ^{125}I. Vervolgens werden met dit proefdiermodel biodistributie studies uitgevoerd. Omdat vergelijkbare bloed/lichaamsklaring van de geïnjecteerde MAb paren werd nagestreefd, werden alleen MAbs met overeenkomstige muize of humane isotypen gecombineerd. Elk MAb paar was zo samengesteld dat een stapsgewijze afname van verschil in affiniteit ontstond (van een 35-voudig tot een 4-voudig verschil). Opvallend was dat bij alle drie MAb paren die getest werden, het MAb met de lagere affiniteit een hogere mate en specificiteit van tumorophoping vertoonde. Hoe groter het verschil in affiniteit tussen de twee MAbs, des te sterker dit effect. Op basis van deze biodistributie resultaten is er onderzocht of lagere-affiniteits MAbs geschikter zijn voor RIT. Na het koppelen van het therapeutische radionuclide ^{186}Re aan dezelfde MAb paren bleek dat de lagere-affiniteits MAbs effectiever waren in RIT, hetgeen overeenkomt met de gegevens van de biodistributie studie. We concludeerden uit deze studies dat een MAb variant met een intermediaire affiniteit voor een bepaald antigeen (zoals b.v. mMAb U36 en hMAb BIWA 4), een superieure "tumor targeting" kan vertonen vergeleken met hogere-affiniteit varianten van dat MAb. Deze resultaten stemmen niet overeen met eerder gepubliceerde studies van diverse andere groepen, waarbij hogere-affiniteit MAbs juist superieur bleken voor wat betreft tumorophoping en effectiviteit in RIT [5-9]. Het is mogelijk dat de relatie tussen MAb affiniteit en tumoropname een optimum heeft, waarbij intermediaire-affiniteit MAbs (zoals b.v. mMAb U36 en BIWA 4) een hogere mate en specifiteit van tumorophoping vertonen dan lage-affiniteit MAbs (K_d van minder dan ca. 10^{-8} M) en hoge-affiniteit MAbs (K_d van meer dan ca. 10^{-10} M). Bewijs voor zo'n relatie werd ook gevonden in *in vivo* studies met scFv en diabodies [10,11]. De suboptimale distributie van hoge-affiniteit MAbs kan verklaard worden aan de hand van de "binding site barrier" theorie. Deze theorie veronderstelt dat hoge-affiniteit MAbs alleen aan de buitenkant van de tumor zullen binden, waardoor tumorpenetratie en absolute tumorretentie worden bemoeilijkt [12].

Na de proefdierstudies zoals beschreven in hoofdstuk 2 werd de intermediaire-affiniteit hMAb BIWA 4 geselecteerd voor verdere klinische evaluatie. Hierbij werd BIWA 4 toegediend aan 48 patiënten in drie parallelle RIS/biodistributie studies met HHPCC -, longkanker-, en borstkankerpatiënten, en in één RIT studie met HHPCC patiënten [13,14]. Het percentage aan HAHA reacties met hMAb BIWA 4 bleek 4%, wat beduidend lager is dan de 90% aan HAMA reacties die met het oorspronkelijke mMAb BIWA 1 werden gevonden. Daarnaast bleek uit de fase I RIT studie dat ^{186}Re-gelabeld hMAb BIWA 4 veilig aan patiënten kan worden toegediend, ook als dit meerdere malen plaatsvindt. Anti-tumor effecten werden gezien in uitbehandelde HHPCC patiënten met relatief grote tumoren. Op basis van

deze gegevens kan gesteld worden dat een verdere ontwikkeling van RIT met ^{186}Re-gelabeld hMAb BIWA 4 gerechtvaardigd is.

In het algemeen bestaat de selectie, karakterisering en optimalisatie van MAbs of MAb-constructen, die bestemd zijn voor RIS of RIT doeleinden, uit opeenvolgende studies *in vitro*, *in vivo* in proefdiermodellen en tenslotte in patiënten. De hierboven beschreven studies illustreren nogmaals dat het raadzaam is om nieuwe MAbs of MAb-constructen nauwgezet te karakteriseren. In proefdierstudies kan bijvoorbeeld de biodistributie nauwkeurig bepaald worden door het nemen van weefselbiopten en het meten van de hoeveelheid radioactiviteit in deze biopten met behulp van een gamma-teller. Uiteindelijk zijn klinische studies noodzakelijk om de resultaten van proefdierstudies op een niet-invasieve wijze te bevestigen. Om MAbs, gericht tegen tumoren, optimaal te kunnen toepassen in RIS en RIT, werd besloten om de potentie van immuno-PET te gaan onderzoeken.

De toepasbaarheid van een positron emitter voor immuno-PET is afhankelijk van verschillende factoren. Niet alleen is een halveringstijd van enkele dagen belangrijk, maar ook de beschikbaarheid van de positron emitter en van een robuuste methode om deze stabiel aan MAbs te koppelen. De vervaleigenschappen van de positron emitter zijn een belangrijke factor voor het verkrijgen van afbeeldingen met een hoge kwaliteit en van nauwkeurige kwantitatieve data. Wanneer een positron emitter in een zogenaamde immuno-PET scouting procedure wordt gebruikt voorafgaande aan RIT, dan moet de biodistributie van het diagnostische en therapeutische radioimmunoconjugaat overeenkomen. In de volgende hoofdstukken worden een aantal van deze punten behandeld voor de positron emitters ^{89}Zr en ^{124}I. In deze studies werd het cMAb U36 als model MAb gebruikt vanwege onbeperkte beschikbaarheid.

In **hoofdstuk 3** werden technische protocollen verschaft voor het reproduceerbaar isoleren van zeer zuiver ^{89}Zr en voor het produceren van ^{89}Zr-MAb conjugaten van optimale kwaliteit. Grote hoeveelheden ^{89}Zr werden geproduceerd door middel van een (p,n) reactie waarbij ^{89}Y, een element met een natuurlijk voorkomen van 100%, werd beschoten met 14 MeV protonen. Met behulp van een hydroxamaat kolom kon carrier-free ^{89}Zr verkregen worden met een hoge radionuclidische zuiverheid en in hoge opbrengst. Het gebruik van ^{89}Y als goedkoop "target" materiaal en de mogelijkheid om een lage-energie cyclotron te gebruiken zorgen ervoor dat de methode eenvoudig op te zetten is, terwijl de hoge specifieke activiteit van de positron emitter koppelingsprocedures vergemakkelijkt.

Om ^{89}Zr stabiel aan MAbs te kunnen koppelen was het nodig om een nieuwe chemische route te ontwikkelen, gebruikmakend van een nieuwe variant van het bifunctionele chelaat desferrioxamine B (Df) en nieuwe "linkers". Voor dit doel werd Df eerst gesuccinyleerd (*N*-sucDf), tijdelijk gevuld met ijzer (Fe(III)), veresterd met behulp van tetrafluorofenol en uiteindelijk gekoppeld aan MAb. Het op deze wijze gepremodificeerde MAb werd gelabeld met ^{89}Zr via een eenvoudige post-labelingsmethode, resulterend in radioimmunoconjugaten die hun integriteit en immunoreactiviteit behouden hadden. De *in vitro* stabiliteit van MAb-*N*-sucDf-^{89}Zr werd bepaald in humaan serum, terwijl het *in vivo* gedrag werd geëvalueerd door middel van biodistributie en PET imaging studies in HHPCC

xenograft-dragende muizen. Voor dit laatste werd een "high resolution research tomograph" (HRRT) PET scanner gebruikt, welke speciaal geschikt is voor het imagen van kleine proefdieren.. Deze studies lieten selectieve targeting van HHPCC door ^{89}Zr-gelabeld cMAb U36 zien, en toonden bovendien aan dat het met immuno-PET uitstekend mogelijk is om kleine tumoren met een grootte van 19 tot 154 mg te visualizeren.

In **hoofdstuk 4** werd de toepasbaarheid van ^{89}Zr voor immuno-PET nader onderzocht. De bruikbaarheid van ^{89}Zr-gelabeld MAb als scouting procedure voor ^{90}Y-MAb RIT werd bestudeerd, alsmede de geschiktheid van ^{89}Zr voor het kwantificeren van weefselopnames aan de hand van images (niet-invasieve methode). Hiervoor werden cMAb U36-*N*-sucDf-^{89}Zr en cMAb U36-*p*-SCN-Bz-DOTA-^{88}Y (^{88}Y als surrogaat voor ^{90}Y) gelijktijdig geïnjecteerd in HHPCC xenograft-dragende naakte muizen waarna de biodistributie werd bepaald op 3, 24, 48, 72 en 144 uur na injectie. De twee radioimmunoconjugaten vertoonden vergelijkbare opname in de tumor, bloed en andere organen, behalve in het borstbeen en dijbeen op de latere tijdstippen. Kleine verschillen in opname werden gevonden in de nier en lever.

De geschiktheid van ^{89}Zr voor kwantificering en beeldvorming met PET, werd bepaald in fantoomstudies. Ter vergelijking werden metingen verricht aan ^{18}F, het meest gebruikte PET isotoop in de kliniek. Verschillende fantomen werden gebruikt om de lineariteit, resolutie en "recovery" van ^{89}Zr-PET vast te stellen, en te vergelijken met die van ^{18}F-PET. Daarnaast werd de mogelijkheid om ^{89}Zr-gelabelde MAb *in vivo* met PET te kwantificeren geëvalueerd in tumor dragende naakte muizen. Daarbij werd de opname van ^{89}Zr in tumoren zowel bepaald met behulp van PET imaging (non-invasieve methode) als door het meten van radioactiviteit in uitgenomen tumoren met behulp van een gamma-teller (invasieve referentiemethode). Tumoren van millimeter-grootte konden worden afgebeeld met ^{89}Zr immuno-PET en er werd, na correctie voor "partial volume" effecten, een uitstekende correlatie gevonden tussen ^{89}Zr tumor radioactiviteit bepaald met behulp van de non-invasieve en de invasieve methode.

De zeer bemoedigende resultaten met ^{89}Zr immuno-PET, zoals gepresenteerd in **hoofdstuk 3** en **4**, openden perspectieven voor klinische evaluatie. Op dit moment wordt PET met ^{89}Zr-gelabeld cMAb U36 geëvalueerd in een pilot-studie om te bepalen wat de mogelijkheden van immuno-PET zijn voor het detecteren van primaire tumoren en metastasen in HHPCC patiënten. Het betreft hier uitsluitend patiënten, die gepland staan voor operatie. Een additioneel aandachtspunt bij klinische toepassing van immuno-PET is de hoeveelheid toe te dienen radioactiviteit, omdat te verwachten valt dat de blootstelling van de patiënt aan straling een limiterende factor zal zijn. In de proefdierstudies werd 3,7 MBq per muis toegediend waarna de tumoren konden worden gevisualiseerd onder ongunstige omstandigheden, dat wil zeggen kleine tumoren in een gebied met een lage object:achtergrond ratio. De hoeveelheid geïnjecteerde radioactiviteit was gebaseerd op informatie uit de enkele artikelen die handelen over PET "imaging" van muizen met positron emitter-gelabelde MAbs. In deze studies werden klinische PET scanners gebruikt, terwijl tussen de 111 kBq (^{124}I)[15] en 3,7 MBq (^{86}Y, ^{124}I)[16,17] per muis werd geïnjecteerd. Aangezien de HRRT camera een relatief lage gevoeligheid heeft ten opzichte van de PET scanners die in de kliniek gebruikt worden[18],

werd er voor gekozen om 3,7 MBq per muis te injecteren. Binnenkort zullen er ook PET proefdierstudies met lagere hoeveelheden radioactiviteit en/of kortere scantijden worden uitgevoerd. In onze klinische pilot-studie konden tumoren zichtbaar worden gemaakt na toediening van 74 MBq ^{89}Zr (Fig. 1). Deze ^{89}Zr dosis was geselecteerd op basis van de verblijftijd van cMAb U36 in het lichaam. De stralingsbelasting voor de patiënt werd berekend op ca. 60 mSv. Volgens de aanbevelingen van de "International Commission on Radiological Protection" (ICRP publicatie 62) is zo'n belasting voor deze groep patiënten acceptabel. De evaluatie van de kwantitatieve gegevens uit deze klinische immuno-PET studie, verkregen aan de hand van de images, loopt nog. Het is opmerkelijk dat correcties voor "partial volume" effecten nog niet algemeen toegepast worden in klinische studies, hoewel PET gebruikers wel inzien dat dergelijke correcties belangrijk zijn voor het verhogen van de diagnostische nauwkeurigheid (EORTC workshop) [19].

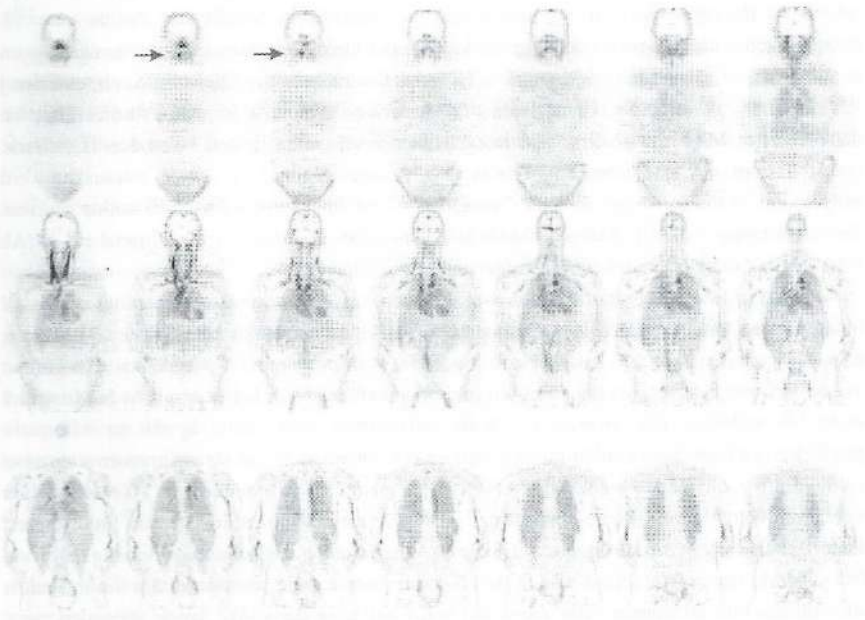

Figure 1. ECAT EXACT HR$^+$ PET coronale afbeeldingen van een hoofd-halskanker patiënt (T2N0) 24 uur na het injecteren van cMAb U36-*N*-sucDf-^{89}Zr. Verhoogde opname is te zien in de primaire tumor aan de rechterzijde van de tong (pijl). Daarnaast valt op dat er op dit vroege tijdstip nog veel radioactiviteit in de bloedsomloop aanwezig is.

Hoofdstuk 5 richtte zich op de koppeling van de lang-levende positron emitter ^{124}I aan MAbs. Hoewel sinds tientallen jaren de koppeling van jodium radioisotopen een algemeen toegepaste methode is, waren in het verleden de labelingsopbrengsten met ^{124}I vaak lager dan met andere jodium isotopen en voldeed de kwaliteit van de resulterende ^{124}I-MAb conjugaten vaak niet aan de eisen die vandaag de dag gesteld worden. In deze studie werd eerst aangetoond dat de problemen met de labelingsopbrengst niet te wijten waren aan de intrinsieke atoomeigenschappen van ^{124}I, maar dat dit puur het gevolg was van stralingsschade. Het labelen van cMAb U36 met een mengsel van jodium radioisotopen (^{123}I, ^{124}I, ^{126}I en ^{130}I) resulteerde in exact dezelfde labelingsopbrengst voor elk isotoop. De mogelijkheid dat ^{124}I-jodide een afwijkende chemische reactiviteit heeft, kan op basis van dit resultaat verworpen worden. Met behulp van HPLC analyse werd aangetoond dat de ^{124}I oplossing gedurende het transport van producent naar gebruiker (USA – Amsterdam) zwaar was aangetast, en dat dit de verklaring was voor de lage labelingsopbrengsten. Vervolgens werden in deze studie twee regeneratiemethoden geïntroduceerd die het mogelijk maken ^{124}I terug in de jodide vorm te krijgen, en werd het op deze wijze geregenereerde ^{124}I aan MAbs gekoppeld. Het gebruik van geregenereerd ^{124}I verbeterde de labelingsopbrengsten aanzienlijk en maakte de koppeling van ^{124}I aan MAbs even eenvoudig en efficiënt als dat van ^{131}I. Koppelingcondities waren zodanig gekozen dat het optreden van chemische- en stralingsschade zo veel mogelijk voorkomen werd. Onder deze condities kon een hoeveelheid ^{124}I aan MAbs gekoppeld worden, die zou volstaan voor gebruik in klinische studies. Behalve dat bleek het MAb na labeling zijn integriteit en immunoreactiviteit behouden te hebben, terwijl het ook nog steeds een optimale *in vivo* "tumor targeting" vertoonde. Dit laatste werd aangetoond in biodistributie en PET "imaging" studies met tumor dragende naakte muizen. Tumorophoping van ^{124}I-gelabeld cMAb U36 was identiek aan die van ^{131}I-gelabeld cMAb U36 en alle tumoren konden worden afgebeeld met PET.

Er zijn meerdere voorwaarden waaraan een lang-levende positron emitter zoals ^{124}I moet voldoen, om geschikt te zijn voor immuno-PET. Aan een eerste belangrijke voorwaarde, de beschikbaarheid van een betrouwbare procedure voor het koppelen van de positron emitter aan MAbs met behoud van integriteit en immunoreactiviteit van het MAb, is in **hoofdstuk 5** voor ^{124}I voldaan. Een tweede en derde belangrijke voorwaarde is dat er effectieve productiemethoden voorhanden moeten zijn en dat het gebruik van de positron emitter moet resulteren in voldoende beeldkwaliteit. Op dit moment is de productie van ^{124}I veel te duur voor routinematige klinische toepassing, dit vanwege de hoge kosten van het "target" materiaal en van het cyclotrongebruik. Voor de experimenten zoals hiervoor beschreven, werd ^{124}I gebruikt dat geproduceerd was in de USA door één van de weinige centra die in staat is dit radionuclide te leveren. Met name het transport over dergelijke lange afstanden vergt maatregelen om de aantasting van de radioactiviteitsoplossing door straling, tegen te gaan. Hoewel ^{124}I een complex vervalschema heeft, met positronen met een relatief hoge energie en "prompt single" gamma-fotonen, zijn er reeds diverse kwantitatieve PET "imaging" studies met ^{124}I uitgevoerd[20-25]. Echter, er moeten nog aanvullende fantoom- en proefdierstudies worden uitgevoerd met de HRRT PET scanner, om de geschiktheid van ^{124}I voor

kwantificering en beeldvorming te bepalen. Een aantrekkelijke toepassing van ^{124}I immuno-PET is als scouting procedure voorafgaand aan ^{131}I-RIT. Of ^{124}I-gelabelde MAbs ook gebruikt kunnen worden in combinatie met andere therapeutische RIT conjugaten, zal afhangen van de overeenkomst in biodistributie van het ^{124}I-scouting conjugaat en het therapeutische radioimmunoconjugaat.

In **hoofdstuk 6** werden de *in vivo* eigenschappen van ^{89}Zr- en ^{124}I-gelabelde MAbs bepaald en vergeleken met MAbs waaraan de therapeutische radionucliden ^{88}Y (als surrogaat voor ^{90}Y), ^{131}I en ^{186}Re waren gekoppeld. Hiertoe werd cMAb U36 met deze vijf radionucliden gelabeld, en werd de biodistributie van de radioimmunoconjugaten bepaald in tumor-dragende naakte muizen. De klaring uit het bloed bleek vergelijkbaar voor alle vijf radioimmunoconjugaten, ondanks het feit dat er verschillende koppelingsmethoden waren gebruikt (directe koppeling of indirecte koppeling met verschillende chelatoren). Dit bevestigt dat de integriteit van het MAb behouden was gebleven en dat bijvoorbeeld het type chelaat dat gebruikt was geen significante invloed had op het gedrag van het MAb in het bloed. Twee verschillende biodistributie patronen konden worden herkend, één patroon deed zich voor bij ^{89}Zr- en ^{88}Y-cMAb U36, terwijl het andere patroon voorkwam bij ^{124}I-, ^{131}I- en ^{186}Re-cMAb U36. De twee patronen verschilden het meest van elkaar voor wat betreft opname in tumor en lever. In preliminaire *in vitro* internalisatie studies (uitgevoerd zoals beschreven door Vrouenraets *et al.*[26]) vertoonde ^{89}Zr-gelabeld cMAb U36 een significant hogere totale cellulaire opname door de HHPCC cellijn OE dan ^{131}I-gelabeld cMAb U36 (82,2% versus 28,7% respectievelijk na 24 uur). Het feit dat de biodistributie van ^{89}Zr-gelabeld MAb overeenkomt met dat van ^{88}Y-gelabeld MAb bevestigt dat ^{89}Zr over residualiserende eigenschappen beschikt, net zoals reeds eerder in de literatuur beschreven is voor de radiometalen ^{88}Y, ^{90}Y en ^{111}In.

In verband met het bovenstaande moet worden opgemerkt dat de term "residualiserend radionuclide", zoals die vaak in de literatuur wordt gebruikt, met enige behoedzaamheid dient te worden toegepast. Er staat beschreven dat ^{111}In en ^{90}Y na internalisatie worden vastgehouden in de cel in de vorm van catabolieten met een laag moleculair gewicht (bestaande uit het radionuclide en het chelaat en waarschijnlijk een peptide-brokstuk afkomstig van het MAb)[27,28]. Daarom moet behalve met het soort radionuclide, ook rekening worden gehouden met de chemische eigenschappen van het chelaat. Illustratief in dit opzicht is de koppeling van jodium radioisotopen aan MAbs. Wanneer deze direct aan het MAb worden gekoppeld, verlaat het jodium vrij snel na internalisatie de cel in de vorm van jodotyrosine, terwijl indirecte koppeling aan het MAb kan resulteren in het residualiseren van het jodium in de cel. Bovendien wordt de retentie van een radionuclide in een cel na internalisatie ook bepaald door de soort "linker" en het transportmolecuul waarvan gebruik wordt gemaakt.

De conclusie is dat de lang-levende positron emitters ^{89}Zr en ^{124}I veelbelovende toepassingsmogelijkheden hebben voor toekomstige immuno-PET studies in de kliniek. Het verschil in specifieke chemische en *in vivo* eigenschappen van ^{89}Zr en ^{124}I maakt hen geschikt voor een scala van toepassingen. Behalve voor het koppelen aan MAbs, kunnen ^{89}Zr en ^{124}I

ook gebruikt worden voor het labelen van peptiden en andere (bio)farmaca. Het labelen van (bio)farmaca met positron emitters maakt het bijvoorbeeld mogelijk om ziekte aan te tonen, moleculaire interacties op te helderen, de farmacokinetiek en biodistributie van het farmacon te bepalen en om het toedieningsschema van een drug te optimaliseren. ^{124}I is reeds gebruikt voor koppeling aan peptiden zoals insuline[29,30] en annexine V[31]. Daarnaast is de monitoring van klinische gentherapie met behulp van ^{124}I een nieuwe toepassing[32]. In een dergelijk onderzoek wordt een ^{124}I-gelabeld marker-substraat gebruikt om de lokatie, mate en omvang van gen-expressie te bepalen. Of ^{89}Zr net zo geschikt is voor de koppeling aan kleine biomoleculen moet nog worden geëvalueerd. Verwacht mag worden dat in het geval van een klein molekuul, het koppelen van een radionuclide-chelaat complex een zekere invloed zal hebben op de uiteindelijke grootte en lading, hetgeen de farmaceutische, biologische en biochemische eigenschappen van het farmacon kan beïnvloeden.

REFERENTIES

1. de Bree R, Roos JC, Quak JJ, den Hollander W, Snow GB, van Dongen GAMS. Radioimmunoscintigraphy and biodistribution of technetium-99m-labeled monoclonal antibody U36 in patients with head and neck cancer. *Clin Cancer Res.* 1995;1:591-598.
2. Stroomer JW, Roos JC, Sproll M, Quak JJ, Heider KH, Wilhelm BJ, Castelijns JA, Meyer R, Kwakkelstein MO, Snow GB, Adolf GR, van Dongen GAMS. Safety and biodistribution of ^{99m}Technetium-labeled anti-CD44v6 monoclonal antibody BIWA 1 in head and neck cancer patients. *Clin Cancer Res.* 2000;6:3046-3055.
3. Colnot DR, Quak JJ, Roos JC, van Lingen A, Wilhelm AJ, van Kamp GJ, Huijgens PC, Snow GB, van Dongen GAMS. Phase I therapy study of ^{186}Re-labeled chimeric monoclonal antibody U36 in patients with squamous cell carcinoma of the head and neck. *J Nucl Med.* 2000;41:1999-2010.
4. Colnot DR, Ossenkoppele GJ, Roos JC, Quak JJ, de Bree R, Börjesson PK, Huijgens PC, Snow GB, van Dongen GAMS. Reinfusion of unprocessed, granulocyte colony-stimulating factor-stimulated whole blood allows dose escalation of ^{186}Re-labeled chimeric monoclonal antibody U36 radioimmunotherapy in a phase I dose escalation study. *Clin Cancer Res.* 2002;8:3401-3406.
5. Colcher D, Minelli MF, Roselli M, Muraro R, Simpson-Milenic D, Schlom J. Radioimmunolocalization of human carcinoma xenografts with B72.3 second generation monoclonal antibodies. *Cancer Res.* 1988;48:4597-4603.
6. Schlom J, Eggensperger D, Colcher D, Molinolo A, Houchens D, Miller LS, Hinkle G, Siler K. Therapeutic advantage of high-affinity anticarcinoma radioimmunoconjugates. *Cancer Res.* 1992;52:1067-1072.
7. Velders MP, Van Rhijn CM, Briaire IH, Fleuren GJ, Warnaar SO, Litvinov SV. Immunotherapy with low and high affinity monoclonal antibodies 17-1A and 323/A3 in a nude mouse xenograft carcinoma model. *Cancer Res.* 1995;55:4398-4403.
8. Kievit E, Pinedo HM, Schlüper HMM, Haisma HJ, Boven E. Comparison of the monoclonal antibodies 17-1A and 323/A3: the influence of the affinity on tumour uptake and efficacy of radioimmunotherapy in human ovarian cancer xenografts. *Br J Cancer.* 1996;73:457-464.
9. Adams GP, Schier R, Marshall K, Wolf EJ, McCall AM, Marks JD, Weiner LM. Increased affinity leads to improved selective tumor delivery of single-chain Fv antibodies. *Cancer Res.* 1998;58:485-490.
10. Adams GP, Schier R, McCall AM, Simmons HH, Horak EM, Alpaugh RK, Marks JD, Weiner LM. High affinity restricts the localization and tumor penetration of single-chain Fv antibody molecules. *Cancer Res.* 2001;61:4750-4755.
11. Nielsen UB, Adams GP, Weiner LM, Marks JD. Targeting of bivalent anti-ErbB2 diabody antibody fragments to tumor cells is independent of the intrinsic antibody affinity. *Cancer Res.* 2000;60:6434-6440.
12. Fujimori K, Covell DG, Fletcher JE, Weinstein JN. A modeling analysis of monoclonal antibody percolation through tumors: a binding-site barrier. *J Nucl Med.* 1990;31:1191-1198.
13. Colnot DR, Roos JC, De Bree R, Wilhelm AJ, Kummer JA, Hanft G, Heider KH, Stehle G, Snow GB, Van Dongen GAMS. Safety, biodistribution, pharmacokinetics, and immunogenicity of ^{99m}Tc-labeled humanized monoclonal antibody BIWA 4 (bivatuzumab) in patients with squamous cell carcinoma of the head and neck. *Cancer Immunol Immunother.* 2003;in press.

14. Börjesson PKE, Postema EJ, Roos JC, Colnot DR, Marres HAM, Van Schie MH, Stehle G, De Bree R, Snow GB, Van Dongen GAMS. Phase I therapy with ^{186}Re-labeled humanized monoclonal antibody BIWA 4 (bivatuzumab) in patients with head and neck squamous cell carcinoma. *Clin Cancer Res.* 2003;in press.
15. Lee FT, Hall C, Rigopoulos A, Zweit J, Pathmaraj K, O'Keefe GJ, Smyth FE, Welt S, Old LJ, Scott AM. Immuno-PET of human colon xenograft-bearing BALB/c nude mice using ^{124}I-CDR-grafted humanized A33 monoclonal antibody. *J Nucl Med.* 2001;42:764-769.
16. Lövqvist A, Humm JL, Sheikh A, Finn RD, Koziorowski J, Ruan S, Pentlow KS, Jungbluth A, Welt S, Lee FT, Brechbiel MW, Larson SM. PET imaging of ^{86}Y-labeled anti-Lewis Y monoclonal antibodies in a nude mouse model: comparison between ^{86}Y and ^{111}In radiolabels. *J Nucl Med.* 2001;42:1281-1287.
17. Bakir MA, Eccles SA, Babich JW, Aftab N, Styles JM, Dean CJ, Lambrecht RM, Ott RJ. C-erbB2 Protein overexpression in breast cancer as a target for PET using iodine-124-labeled monoclonal antibodies. *J Nucl Med.* 1992;33: 2154-2160.
18. Boellaard R, Buijs F, de Jong HWAM, Lenox M, Gremillion T, Lammertsma AA. Characterization of a single LSO crystal layer high resolution research tomograph. *Phys Med Biol.* 2003;48:429-448.
19. Young H, Baum R, Cremerius U, Herholz K, Hoekstra O, Lammertsma AA, Pruim J, Price P. Measurement of clinical and subclinical tumour response using [^{18}F]-fluorodeoxyglucose and positron emission tomography: review and 1999 EORTC recommendations. *Eur J Cancer.* 1999;35:1773-1782.
20. Pentlow KS and Graham MC. Quantitative imaging of I-124 using positron emission tomography with applications to radioimmunodiagnosis and radioimmunotherapy. *Med Phys.* 1991;18:357-366.
21. Wilson CB, Snook DE, Dhokia B, Taylor IA, Lammertsma AA, Lambrecht R, Waxman J, Jones T, Epenetos AA. Quantitative measurement of monoclonal antibody distribution and blood flow using positron emission tomography and ^{124}Iodine in patients with breast cancer. *Int J Cancer* 1991;47:344-347.
22. Larson SM, Pentlow KS, Volkow ND, Wolf AP, Finn RD, Lambrecht RM, Graham MC, Di Resta G, Bendriem B, Daghighian F, Yeh SDJ, Wang G-J, KCheung N-KV. PET scanning of iodine-124-3F8 as an approach to tumor dosimetry during treatmnet planning for radioimmunotherapy in a child with neuroblastoma. *J Nucl Med.* 1992;33:2020-2023.
23. Herzog H, Tellmann L, Qaim SM, Spellerberg S, Schmid A, Coenen HH. PET quantitation and imaging of the non-pure positron-emitting iodine isotope ^{124}I. *Appl Radiat Isot.* 2002;56:673-679.
24. Collingridge DR, Carroll VA, Glaser M, Aboagye EO, Osman S, Hutchinson OC, Barthel H, Luthra SK, Brady F, Bicknell R, Price P, Harris AL. The development of [^{124}I]Iodinated-VG76e: a novel tracer for imaging vascular endothelial growth factor in vivo using positron emission tomography. *Cancer Res.* 2002;62:5912-5919.
25. Jayson GC, Zweit J, Jackson A, Mulatero C, Julyan P, Ranson M, Broughton L, Wagstaff J, Hakannson L, Groenewegen G, Bailey J, Smith N, Hastings D, Lawrance J, Haroon H, Ward T, McGown AT, Tang M, Levitt D, Marreaud S, Lehmann FF, Herold M, Zwierzina H. Molecular imaging and biological evaluation of HuMV833 anti-VEGF antibody: implications for trial design of antiangiogenic antibodies. *J Natl Cancer Inst.* 2002;94:1484-1493.
26. Vrouenraets MB, Visser GWM, Loup C, Meunier B, Stigter M, Oppelaar H, Stewart FA, Snow GB, van Dongen GAMS. Targeting of a hydrophylic photosensitizer by use of internalizing monoclonal antibodies: a new possibility for use in photodynamic therapy. *Int J Cancer.* 2000;88:108-114.

27. Shih LB, Thorpe SR, Griffiths L, Diril H, Ong GL, Hansen HJ, Goldenberg DM, Mattes MJ. The processing and fate of antibodies and their radiolabels bound to the surface of tumor cells in vitro: a comparison of nine radiolabels. *J Nucl Med.* 1994;35:899-908.
28. Press OW, Shan D, Howell-Clark J, Eary J, Appelbaum FR, Matthews D, King DJ, Haines AMR, Hamann P, Hinman L, Shochat D, Bernstein ID. Comparative metabolism and retention of iodine-125, yttrium-90, and indium-111 radioimmunoconjugates by cancer cells. *Cancer Res.* 1996;56:2123-2129.
29. Glaser M, Brown DJ, Law MP, Iozzo P, Waters SL, Poole K, Knickmeier M, Camici PG, Pike VW. Preparation of no-carrier-added [^{124}I]A_{14}-iodoinsulin as a radiotracer for positron emission tomography. *J Labelled Cpd Radiopharm.* 2001;44:465-480.
30. Iozzo P, Osman S, Glaser M, Knickmeier M, Ferrannini E, Pike VW, Camici PG, MP Law. In vivo imaging of insulin receptors by PET: preclinical evaluation of iodine-125 and iodine-124 labelled human insulin. *Nucl Med Biol.* 2002;29:73-82.
31. Glaser M, Collingridge DR, Aboagye EO, Bouchier-Hayes L, Hutchinson OC, Martin SJ, Price P, Brady F, Luthra SK. Iodine-124 labelled annexin-V as a potential radiotracer to study apoptosis using positron emission tomography. *Appl Radiat Isot.* 2003;58:55-62.
32. Jacobs A, Voges J, Reszka R, Lercher M, Gossmann A, Kracht L, Kaestle Ch, Wagner R, Wienhard K, Heiss WD. Positron-emission tomography of vector-mediated gene expression in gene therapy for gliomas. *Lancet.* 2001;358:727-729.

LIST OF ABBREVIATIONS

3D	three-dimensional
BGO	bismuth germanate ($Bi_4Ge_3O_{12}$)
CDR	complementarity determining region
C_H	constant heavy chain
C_L	constant light chain
cMAb	chimeric monoclonal antibody
CSRC	cold spot recovery coefficient
CT	X-ray computed tomography
Df	desferrioxamine B (desferal)
DOTA	1,4,7,10-tetraazacyclododecane-1,4,7,10-tetraacetic acid
DTPA	diethylenetriaminepentaacetic acid
EDC	1-ethyl-3-(3-dimethyl-aminopropyl)-carbodiimide
EDTA	ethylenediaminetetraacetic acid
Fc	constant region
FDA	U.S. food and drug administration
FPLC	fast-protein liquid chromatography
Fv	variable region
FWHM	full width at half maximum
Ge(Li)	germanium(lithium)
GSO	cerium-doped gadolinium oxyorthosilicate ($Gd_2SiO_5(Ce)$)
HAMA	human anti-mouse antibody
HEPES	*N*-2-hydroxyethylpiperazine-*N*'-2-ethanesulfonic acid
hMAb	humanized MAb
HNSCC	head and neck squamous cell carcinoma
HPLC	high-performance liquid chromatography
HRRT	high-resolution research tomograph
HSRC	hot spot recovery coefficient
ICRP	international commission on radiological protection
Ig	immunoglobulin
ITLC	instant thin-layer chromatography
LOR	line of response
LSO	cerium-doped lutetium oxyorthosilicate ($Lu_2SiO_5(Ce)$)
MAb	monoclonal antibody
mMAb	murine monoclonal antibody
MRI	magnetic resonance imaging
N-sucDf	*N*-succinyldesferrioxamine B
NIR	near infrared
p-SCN-Bz-DOTA	*p*-isothiocyanatobenzyl-1,4,7,10-tetraazacyclododecane-1,4,7,10-tetraacetic acid

PBS	phosphate buffered saline
PET	positron emission tomography
PMT	photomultiplier tube
RIS	radioimmunoscintigraphy
RIT	radioimmunotherapy
ROI	region of interest
scFv	single chain variable fragment
SDS-PAGE	sodium dodecylsulfate-polyacrylamide gel electrophoresis
SEM	standard error of mean
SPECT	single photon emission computed tomography
TAA	tumor-associated antigen
TETA	1,4,8,11-tetraazacyclotetradecane-1,4,8,11-tetraacetic acid
TFP	2,3,5,6-tetrafluorophenol
V_H	variable heavy chain
V_L	variable light chain
VOI	volume of interest

DANKWOORD

En dan tenslotte het dankwoord: zonder de hulp van velen had dit proefschrift niet tot stand kunnen komen. Wetende dat woorden altijd tekort schieten, wil ik op deze plaats toch graag een aantal mensen bedanken.

Allereerst wil ik mijn promotor prof. dr. G.B. Snow bedanken voor de gelegenheid die hij mij heeft geboden om op de afdeling KNO, sectie tumorbiologie mijn promotieonderzoek uit te voeren.

Veel heb ik te danken aan mijn promotor prof. dr. G.A.M.S. van Dongen en copromoter dr. G.W.M. Visser. Beste Guus en Gerard, de kennis en vaardigheden die jullie in huis hebben vullen elkaar naadloos aan en maken jullie tot het beste begeleiders-duo dat ik me maar kon wensen. Ik heb geleerd om zowel kritisch naar de details van een onderzoek te kijken, als ook de toepassingsmogelijkheden in de (verre) toekomst niet uit het oog te verliezen. Jullie deuren stonden altijd open. De vele en langdurige artikel-besprekingen eisten soms een zware tol, maar het resultaat is er dan ook naar.

Beste Guus, jouw enthousiasme was aanstekelijk, na anderhalf jaar zag je de klinische studie met ^{89}Zr-gelabeld MAb al binnen handbereik. Dat dit uiteindelijk nog een aantal jaren hard werken heeft gekost, heeft je nooit doen wanhopen. Bedankt voor je inzet en behulpzaamheid, vooral ook op het allerlaatst.

Beste Gerard, we hebben samen menige "^{89}Zr-kop" mogen oplossen. Na het boenwerk van de eerste keer, is de Zr-produktie gelukkig steeds "professioneler" geworden. Bedankt voor alle keren dat je vervolgens samen met mij lange dagen draaide om zoveel mogelijk van de radioactiviteit te kunnen benutten. Ik heb met plezier met je samengewerkt.

Ronald Boellaard van de afdeling Nucleaire Geneeskunde/PET-centrum: beste Ronald, bedankt voor het geduld waarmee je me de principes van PET hebt uitgelegd, het maken van PET opnames en alle hulp bij de PET analyses.

De leden van de leescommissie, dr. O.C. Boerman, dr. M. de Jong, prof. dr. E.P. Krenning, prof. dr. A.A. Lammertsma, prof. dr. C.R. Leemans, prof. dr. W.J.G. Oyen en prof. dr. R.H.M. Verheijen wil ik hartelijk bedanken voor het kritisch doornemen van het manuscript en het zitting nemen in de promotiecommissie.

Al mijn (ex)collega's van afdeling KNO tumorbiologie wil ik bedanken voor de prettige werksfeer. Het "RNC-clubje" wil ik in het bijzonder bedanken voor de goede samenwerking, het verlevendigen van de RNC "bunker" en het vele werk dat jullie voor me hebben verzet: Miranda Siegmund o.a. voor het mij wegwijs maken op het RNC en het uitvoeren van ^{186}Re-labelingen, Maria Vosjan en Liesbet Vervoort voor al het ^{89}Zr- en ^{124}I-werk en de patiënten-labelingen, en Pontus Börjesson voor het uitvoeren van de klinische ^{89}Zr-studie. Marijke Stigter, je hebt mijn onderzoek vanaf het begin meegemaakt. Bedankt voor de *in vivo* studies die we samen hebben uitgevoerd. Zonder een onvertogen woord heb je menig weekend opgeofferd voor het verrichten van biodistributie studies.

Iedereen met wie ik de AIO-kamer heb mogen delen: Pontus Börjesson, Jantien Bremmer, David Colnot, Viola Jansen-van Houten, Ingeborg Klaassen, Eline Nieuwenhuis,

Arnolda de Nooij-van Dalen, Asaf Senft, Serge Smeets, Maarten Tabor en Maarten Vrouenraets, bedankt voor de gezelligheid en levendigheid die jullie boden. Mijn overige collega's van de 4de verdieping, Henrique Ruijter-Schipper, Janny de Vries-Dijkstra, Mireille Snel, Fedor Denkers, Corlinda ten Brink en alle stagiaires die ik in de loop der jaren heb zien komen en gaan, bedankt voor de gezellige lunches en de thee met koekjes. Ruud Brakenhoff, Boudewijn Braakhuis en Jacqueline Cloos, bedankt voor de interesse die jullie in mijn werk toonden en de kritische vragen tijdens de werkbespreking. Fred Snel en Ton Houffelaar wil ik bedanken voor de computer ondersteuning.

Alle medewerkers van het Radionucliden Centrum (RNC) wil ik bedanken voor de wijze waarop jullie me het gevoel hebben gegeven dat ik naast mijn eigen afdeling, KNO, nog een "pleeg" afdeling had. De stralingsveiligheidsdienst, Albert Coops, Jan Boesten en Tjaard Weijer wil ik bedanken voor alle keren dat jullie me hielpen als ik weer iets uit de kluis nodig had of als er afval afgevoerd moest worden. Meneer Coops die me een permanent pasje gaf zodat ik buiten werktijden ongehinderd het RNC in en uit kon en me er 's avonds op wees dat ik wel mijn trein moest halen. De technische dienst van het RNC was onontbeerlijk voor mijn werk. Leo van Rooij, Hans Keus, Fred Buijs, Roy van der Valk, Arjan de Nooij en Peter Schollema, bedankt voor de ondersteuning bij HPLC-, Compugamma-, pH-, pomp-, computer en overige apparatuur problemen, het schilderen van de vele loodstenen, de verhuizing naar G6, de PET opnames, en ontelbare andere zaken. En natuurlijk bedankt voor het bouwen van de half-automaat voor de ^{89}Zr-opwerking, een hele verbetering ten opzichte van het oude "handwerk" en onmisbaar voor de patiënten-labelingen. Daarnaast wil ik graag Rob Klok bedanken voor de HPLC ondersteuning en alle keren dat ik met uiteenlopende vragen bij hem terecht kon. Anton Braker, bedankt voor de Pt/H_2 kolom scheidingen. Iedereen van het RNC die ik nu niet bij naam heb genoemd, bedankt voor de hulpvaardigheid, getoonde interesse en de "wij gaan koffie drinken"-momenten.

De medewerkers van BV Cyclotron, Peter van Leuffen, Roel Mooy en alle overige personeel, bedankt voor het produceren van ^{89}Zr, ook als de aanvraag kort dag was of rond feestdagen. Klaas Pereboom, bedankt voor de vele malen dat je de kop hebt "overgehengeld" in de loodkar en het nauwgezet in het oog houden van het aantal Y-besputterde koppen.

De Nijmegen-groep, met name Otto Boerman en Julliette van Eerd, bedankt voor de prettige en productieve samenwerking.

Arie Kegel wil ik bedanken voor de goede zorgen voor de prooefdieren en Roel van der Schors voor de MS-metingen, ook al staan de resultaten niet in het proefschrift vermeld.

Tot slot wil ik mijn ouders, mijn broer en Sonja, familie en vrienden bedanken voor hun steun en belangstelling. Mijn ouders, die me altijd hebben gestimuleerd en gesteund in mijn keuzes en die met twee kinderen in de wetenschap het altijd maar weer kunnen opbrengen om met interesse naar onze verhalen te luisteren. René, die weet hoe het is om te promoveren en met wie het altijd een genoegen is om van (wetenschappelijke) gedachten te wisselen.

Henk, de laatste maar belangrijkste in het rijtje. Bedankt voor jouw onvoorwaardelijke steun en de duwtjes in de rug die ik zo nu en dan nodig had. Dat proefschrift komt af!

CURRICULUM VITAE

Iris Verel werd geboren op 31 maart 1975 te Willemstad, Curaçao. In 1993 behaalde zij haar gymnasium diploma aan het Stedelijk Gymnasium te Leiden. In datzelfde jaar begon zij haar studie Biologie aan de Universiteit Utrecht. In 1994 werd de propedeuse cum laude behaald. Tijdens de doctoraalfase werden twee stages gevolgd. De eerste stage liep zij gedurende 7,5 maand bij de sectie Immunotoxicologie (dr. R. Pieterse), Onderzoeksinstituut Toxicologie te Utrecht, alwaar zij *in vitro* en *in vivo* studies uitvoerde naar de immunostimulerende effecten van kwikchloride. De tweede stage van een jaar werd gevolgd bij de afdeling Moleculaire Toxicologie (P. Aston), Shell Research and Technology Centre Amsterdam, met als onderwerp biomonitoring van beroepsgerelateerde blootstelling aan industriële chemicalien. Tijdens dit onderzoek stond de ontwikkeling van methoden ter bepaling van mercaptuurzuren en ethyleenoxide-haemoglobine adducten met behulp van monoklonale antilichamen centraal. Het doctoraalexamen werd behaald in maart 1998. Vanaf februari van datzelfde jaar kwam zij als Assistent in Opleiding in dienst bij de afdeling Keel-, Neus-, en Oorheelkunde van de Vrije Universiteit Medisch Centrum te Amsterdam. Onder begeleiding van prof. dr. G.A.M.S. van Dongen, prof. dr. G.B. Snow (afdeling Keel-, Neus-, en Oorheelkunde) en dr. G.W.M. Visser (Radionucliden Centrum, Vrije Universiteit) werd het promotieonderzoek uitgevoerd dat in dit proefschrift beschreven staat. Sinds september 2003 is zij werkzaam als postdoc op the Center for Molecular Imaging Research, Massachusetts General Hospital, Boston, USA.